Morphodynamics of flow through the heart

(The shape of the heart as an organ of flow)

Philip Kilner

PhD Thesis, University of London

1998

Magnetic Resonance Unit,
Royal Brompton and Harefield NHS Trust,
Sydney Street, London SW3 6NP, United Kingdom.

E-mail: p.kilner@rbh.nthames.nhs.uk

LC
UN

Contents

Statement of a problem p 3

Abstract p 5

Chapters

1. Introduction

Scope of enquiry p 7

History of subject p 9

2. Review of forms of vertebrate and invertebrate hearts

Background p 19

Aims and scope of this chapter p 20

Overview of circulatory systems in relation to cell layers p 20

Phylogenetic classification of animals p 22

Supposed origins of circulatory systems p 25

Comparative cardiovascular morphology p 27

Discussion p 34

3. Spontaneously cyclic flows in asymmetric cavities

Objectives p 37

Background p 37

Methods p 39

Results p 41

Discussion p 43

Additional fluid morphodynamic Demonstrations p 48

4. Spatio-temporal patterns of flow through the heart studied by magnetic resonance velocity mapping

Objectives p 55

Background p 55

Temporal patterns of filling and ejection p 57

Methods p 58

Results p 60

Correlation and synthesis of results p 66

Discussion p 68

5. Computation of dynamic differences of pressure in the heart

Objectives p 71

Background p 71

Methods p 73

In vitro flow phantom validation p 74

In vivo results p 76

Discussion p 77

6. Exercise echocardiography of mitral flow and movement

Objectives p 79

Background p 79

Materials and methods p 81

Results p 82

Discussion p 83

7. Interpretation of the heart as a dynamic organ of flow

Purpose p 87

Findings and ideas p 87

8. Strengths, limitations and implications of the work p 93

Acknowledgements p 97

Reprints of papers bound after chapter 8

Three directional magnetic resonance flow imaging of the human heart. Kilner PJ, Wann LS, Firmin DN, Longmore DB. *Dynamic Cardiovascular imaging,* 1989;2:104-109

The application of phase shifts in NMR for flow measurement. Firmin DN, Nayler GL, Kilner PJ, Longmore DB. *Magnetic Resonance in Medicine,* 1990;14:230-241

Helical and retrograde secondary flow patterns in the aortic arch studied by three-directional magnetic resonance velocity mapping. Kilner PJ, Yang GZ, Mohiaddin RH, Firmin DN, Longmore DB. *Circulation,* 1993;88:2235-2247

Computation of flow pressure fields from magnetic resonance velocity mapping. Yang GZ, Kilner PJ, Wood NB, Underwood SR, Firmin DN. *Magnetic Resonance in Medicine,* 1996;36:520-526

Our tortuous heart in dynamic mode - an echocardiographic study of mitral flow and movement in exercising subjects. Kilner PJ, Henein MY, Gibson DG: *Heart and Vessels* 1997;12:103-110

References are listed at the end, after the reprints

Statement of a Problem

As an organ of flow, the human heart has a remarkable shape. In common with hearts of other vertebrate species, its walls accommodate tortuous paths of flow which come about through progressive curvature of the embryonic heart tube. During embryonic development, the human heart loops to form a twisted S-bend which becomes subdivided by septa and valves to form atrial and ventricular cavities of the mature heart. Passing blood is thus made to change direction more than once, notably at ventricular level, but also at the levels of the atria and great arteries. This means that blood is subjected to changes of momentum, not only because propulsive myocardial movements are phasic and streamlines diverge or converge through cavities, but also because of changes of direction. Force exchanges involved in movement of blood through the heart must, therefore, include inertial components, related to both transient and convective changes of momentum. During exercise, when more blood passes, with greater and more rapid changes of momentum, inertial exchanges of force must gain in significance. Similarly, energy exchanges between kinetic energy of blood and elastic/contractile energetics of the myocardium gain importance although, at the same time, elevated fluid kinetic energy means increased susceptibility to dissipation through turbulence.

Knowledge is limited, however, of multi-directional patterns of flow through the four chambers of the living heart, of the importance of overall shape for stability of intracardiac flow, or of the significance of inertial exchanges of force between blood and myocardium, either at rest or during exercise. Looped curvatures of human and other vertebrate hearts are likely to have functional, fluid dynamic implications, but these do not appear to have been considered or investigated.

Abstract

Hypothesis: The tortuous shape of the looped heart has functional significance, particularly on exercise. Chapters as follows:

1. **Introduction.** Scope of enquiry. History of subject.

2. **Review of forms of vertebrate and invertebrate hearts** shows S-shaped curvature, resulting from looping of the ventral embryonic heart tube, to be a feature of all vertebrates, but not of invertebrates.

3. **Spontaneously cyclic flows in asymmetric cavities** are demonstrated *in vitro* in cavities of varied size and effective compliance. Asymmetry and oscillation of flow are considered in relation to forms and functions of heart cavities.

4. **Spatio-temporal patterns of flow through the heart studied by magnetic resonance velocity mapping** show consistency between subjects, with characteristic, coherent movements in each chamber that combine to give sinuous paths of flow, with potential for morphodynamic continuity and interaction between chambers.

5. **Computation of dynamic differences of pressure in the heart.** Differences of pressure associated with changes of momentum, up to 5mmHg from atrium to ventricle, 10mmHg from ventricle to ascending aorta and 10mm from ascending to descending aorta, were computed using the Navier-Stokes equations from resting magnetic resonance velocity data.

6. **Exercise echocardiography of mitral flow and movement.** Early (E) and late (A) diastolic peaks of mitral flow and movement are found to merge, on strenuous exercise, to a single elevated peak, to which diastolic elastic recoil and atrial systole contribute simultaneously. Findings are consistent with an enhancement, with exercise, of dynamic coupling between atrial and ventricular function.

7. **Interpretation of the heart as a dynamic organ of flow.** Correlation of findings leads to an interpretation of the heart as a morphodynamic organ of flow. Shape and movement combine to optimise use of momentum changes, especially on exercise, when transition of function to 'dynamic mode' can be compared to that of the whole body when a walking person begins to run.

8. **Discussion.** Limitations, strengths and implications of the work are discussed.

Chapter 1

Introduction

Scope of enquiry

This thesis presents studies related to morphodynamics of flow through the heart. It considers the overall shape of the heart as an organ of flow.

In this thesis 'the heart' refers mainly to the human heart, studied non-invasively by magnetic resonance and echocardiographic techniques, but morphological comparisons are also made, in Chapter 2, with hearts of other vertebrate and invertebrate species.

The term *morphodynamics* is used to represent the interdependent properties of *form, motion* and *inertial dynamics* that belong to fluids flowing through shaped mobile cavities. Although also used in biology to refer to formative growth processes, 'morphodynamics' has been used previously, as in this thesis, to refer to the dynamic forms and formative dynamics of flow (Abraham 1985).

In flowing fluid, momentum changes are associated with pressure differences and patterns of flow. Cause and effect may be difficult to distinguish. In the case of blood moving through the curved, flexible, elastic, contractile boundaries of the heart, exchanges of force are complex. Analysis of circulatory dynamics might include the following types of force:

- elastic tension associated with passively stretched myocardial and vascular walls
- wall tension of actively contracting myocardium
- diastolic elastic recoil of myocardium after contraction
- hydrostatic pressure resulting from global containment by valves and stressed walls
- gravitational gradients of blood pressure, gravity acting as a 'body' force on the blood
- viscosity resisting flow of blood, particularly through peripheral microvessels
- differences of pressure associated with changes of momentum of blood

The last of these – dynamic differences of pressure – is the aspect of force exchange addressed most directly by the thesis, although, even here, the approach is indirect, via non-invasive velocity measurement. Interaction with the other forces is assumed and

considered, but not measured. In relation to force exchanges involving changes of momentum, overall *shapes* of heart cavities and *timing* of their movements have significance, momentum being a vector, with direction, which can only change at finite rates in relation to finite applications of force.

The heart has evolved as an organ of flow - *the* organ, in all living nature, of sustained, internal propulsion of fluid. As an organ of flow, its shape is remarkable (Figure 1.1). When it is appreciated that tortuous flow paths are a feature of hearts of vertebrate, but not of invertebrate species, the question arises, to what extent does overall heart shape have functional and evolutionary significance?

In literature searches and reading done in the preparation of this thesis, I have failed to find a single statement, discussion or investigation referring specifically to dynamic implications of direction changes of flow path through the tortuous curvatures of the looped heart. A possible reason for failure even to pose the question may have been a tendency in medical science to reduce complex problems to component parts, with more limited appreciation of interactions and interrelations across wholes. In the heart, functions of great veins, atria, ventricles, conducting tissue, valves and arteries have each been studied in detail, but relatively little attention seems to have been paid to dynamic interactions across the curvatures of the heart as a whole.

This is the justification for the relatively broad scope of the thesis. The aim is to appreciate the human heart as a unified organ of flow, capable of transition to a more dynamic mode of action with exercise, considered in relation to hearts found in other species, vertebrate and invertebrate, and in relation to phenomena of flow *in vitro*.

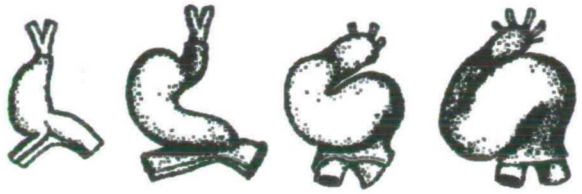
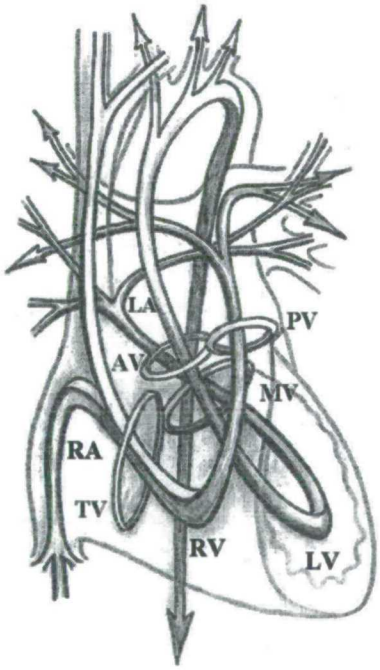


Figure 1.1
Above: Cardiac looping illustrated by curvature of a chick embryo heart, viewed from its ventral aspect between 30 and 48 hours of incubation.
Below: Tortuous paths of flow through the human heart. The drawing is based on anatomical and flow information from post-mortem casts and magnetic resonance imaging. For clarity, principal flow paths are represented by continuous bands; vorticity and phasic variability of flow through chambers and valves are not shown. The rings indicate locations of valve orifices, AV=aortic valve, PV=pulmonary valve, MV=mitral valve, TV=tricuspid valve. Regions of the four heart cavities are indicated by: LA=left atrium, RA=right atrium, RV=right ventricle, LV=left ventricle.



Relevant History of the Subject

This section will consider previous work that is of general relevance to the thesis. Aspects of work relating to contents of chapters will be discussed in the relevant sections.

As stated above, I have not found any publication that addresses specifically the functional significance of overall curvature - the underlying S-shaped tortuosity - of the human and vertebrate heart, although tortuous curvatures of paths of flow must clearly have fluid dynamic consequences. Such a fundamental subject is, however, likely to have been considered from time to time. But it does not seem to have received sustained, focussed attention, and has certainly not been widely recognised as having biological or physiological importance. My own enquiries amongst cardiologists as to the functional significance of cardiac looping have been met with comments on possible morphogenetic origins of looping, for example differential growth of the developing heart tube in relation to surrounding tissues, but never a convincing functional interpretation.

An article in Scientific American by Robinson, Factor and Sonnenblick on elastic myocardial restoring forces (Robinson et al.1986) included two descriptive analogies that are relevant to the subject of this thesis. The first was comparison of the ejecting ventricle with the body of an octopus or squid, moving itself in one direction by ejection of fluid in the opposite direction - by jet propulsion. This was related to the thrust of the cardiac apex against the chest wall in systole that gives rise to the 'apex beat'. The second analogy compared action of the ventricle with that of an automatic rifle, using part of the energy from one discharge to bring in and load its next round. These analogies were not, however, considered in relation to cardiac looping and resultant direction-change at ventricular level, a pre-requisite for *inertial systolic* ventricular recoil to work advantageously for subsequent diastolic filling (see Chapter 6). The article was primarily concerned with the different but related subject of elastic diastolic myocardial recoil.

Numerous separate aspects of blood flow, contractility and elasticity of the heart have been investigated separately and in detail, but the morphodynamic overview - theoretical and investigative - has been neglected.

In western medical science, the work of William Harvey (Harvey 1628/1976) was of crucial importance in the development of understanding of the heart and circulation. His dissertation *De Motu Cordis et Sanguinis,* reveals the breadth and thoroughness of the

first-hand studies on which he based his circulatory theory. Few individuals can have gained broader direct experience of comparative cardiology, acquired, in Harvey's case, through dissection of a variety of creatures, often with the heart still beating. But it is hardly surprising that Harvey did not concern himself with questions of curvature and inertial dynamics. Harvey had to address the most basic anatomical and physiological questions - where and how did vessels and chambers connect to one another? And, in what sequence did they contract or distend? He did not have access to hearts of exercising animals, but, on the contrary, deliberately observed hearts when they were cooled, failing, and beating abnormally slowly. This would not have been conducive to appreciation of inertial cardiovascular dynamics.

In Italy, less than a generation before Harvey, the diverse interests of Leonardo da Vinci embraced, among many other things, cardiovascular anatomy and patterns of fluid flow. Leonardo's notes and sketches, dating from about 1513 (Figure 1.2), include instructions for casting in wax the shape of the cavity above the aortic valve of a bull's heart. Having cast the shape of the blood space, Leonardo described how a replica aortic sinus may be blown in glass for visualisation of flow through it, using small seeds suspended in water (Keele 1952). It is not entirely clear whether Leonardo carried out the experiment in this way, but his drawings show that he correctly deduced that flow must curl back on itself in the sinuses above the valve cusps. He wrote to the effect that *'the purpose of this revolution* (vorticity) *of blood is to shut again the open gates of the heart, with primary flow turned back to make a perfect closure.'*

The experiment, much as Leonardo described it, but using Perspex and latex rather than glass, was carried out in Oxford University more than four hundred years later. Brian Bellhouse, working with his father, found that fluid did indeed curl back above the cusps of his replica aortic valve, contributing to efficient valve closure (Bellhouse and Bellhouse1968, Bellhouse et al, 1968). He went on to make a model of the mitral valve in a simulated ventricular cavity of latex, contained by fluid in a chamber with a piston at its lower end. He observed and filmed back-curling, vortical patterns of flow in the latex cavity which apparently contributed to efficient closure of the valve (Bellhouse and Bellhouse 1969, Bellhouse 1972). Since then, many researchers have studied in vitro and computational fluid dynamic models of heart

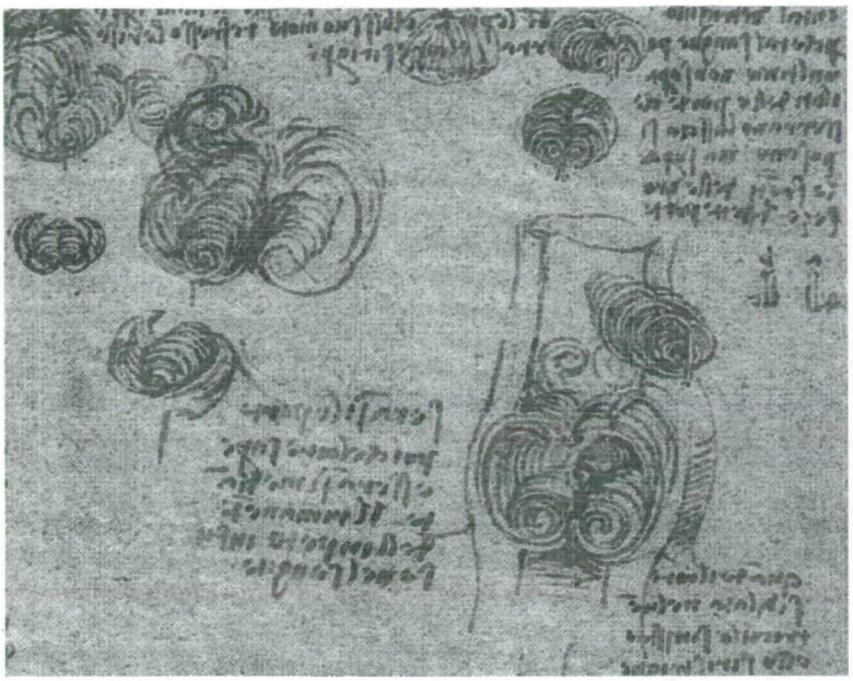
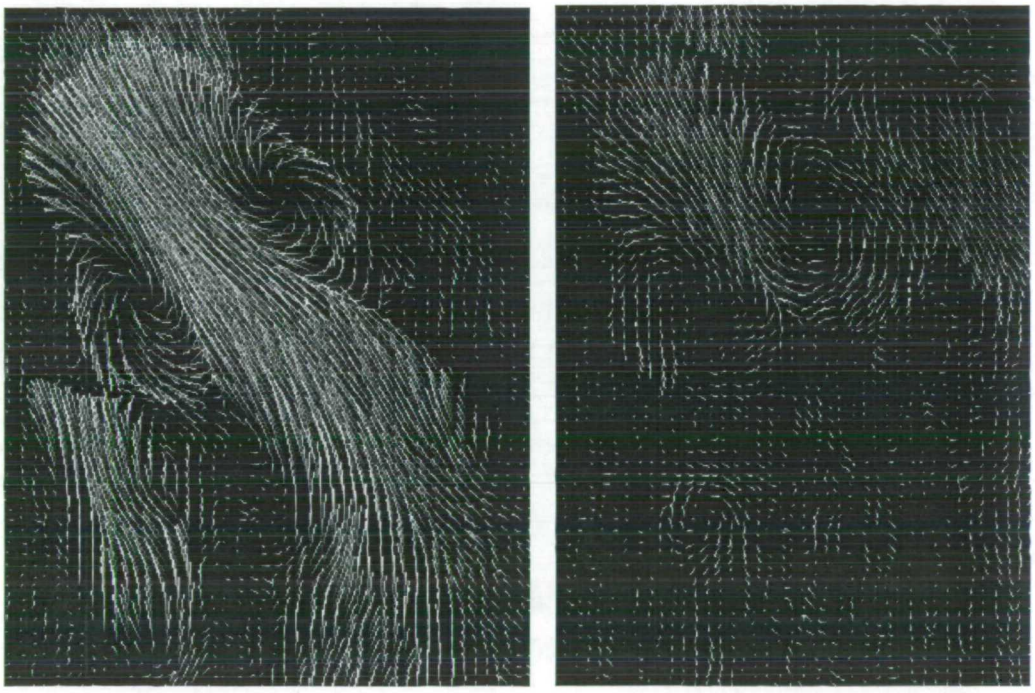


Figure 1.2 ***Above:*** Part of a page from one of the sketchbooks of Leonardo da Vinci, c.1513, illustrating vorticity in the sinuses above aortic valves.
(From document C II 13v in the collection of the Royal Library at Windsor).
Below: Systolic and end-systolic flow vectors of a living human aortic valve, from magnetic resonance flow velocity data (see Chapter 4).



chambers and their valves, particularly with respect to questions of surgical replacement of valves (Taylor and Whamond 1977, Steen and Steen 1994, Garitey et al. 1995, Taylor and Yamaguchi 1995, Peskin and McQueen 1995). In relation to the scope of this thesis, these attempts at modelling have been subject to two kinds of limitation: Firstly, they tend to treat cavities individually, without adequately modelling interaction with structure and fluid dynamics of neighbouring cavities and vessels. This is understandable, given the extreme difficulties of modelling combined elastic, contractile and fluid dynamic properties in 3-dimensional space. Secondly, as far as I know, little attention has been paid, through modelling approaches, to altered cardiovascular dynamics with exercise.

In the early 1970's, soon after Bellhouse's flow modelling experiments, DE Taylor and colleagues carried out *in vivo* flow visualisation experiments in dogs. One of their approaches relied on visualisation of particles in clear blood-replacement fluid by means of endoscopy. They drew attention to the stability and coherence of flow through the mitral valve, with back-curling of flow paths in the ventricle (Taylor and Wade 1973). Taylor also collaborated with JE Malcolm, a former Royal Airforce surgeon who had interests in fluid dynamics and radio telecommunications. Malcolm had previously postulated a model of heart function in which he compared the rhythmic action of heart chambers to that of a reflex clystron, an electromagnetic device used for production of oscillating current and radio transmission (Malcolm 1960). He also constructed a spontaneously oscillating system of flow through lengths of rubber and glass tubing (Malcolm 1961, Malcolm 1962). Elastic segments propagated and reflected waves of expansion and contraction, with spontaneous, periodic deceleration and local reversal of flow. This type of phenomenon was later studied by Pedley and Kamm (Pedley 1980, Kamm and Pedley 1989). Malcolm's comparisons of heart function with passive oscillators have features in common with oscillatory flows illustrated and discussed in Chapter 3. Malcolm's models do not seem to have received widespread attention. They may have appeared limited and remote from the morphology and function of the heart, their possible relevance being inadequately demonstrated or explained. Nevertheless, Malcolm remains one of few to have suggested that inertial/elastic oscillation could play a part in heart chamber function.

There had, however, been a comparable suggestion nearly a century earlier. In 1892 Karl Shmid published a paper in *the Wiener Medicinische Wochenschrift* in which he likened heart function, and the pulse it produced, to the action of a hydraulic ram pump (Schmid 1892). The hydraulic ram is a device, dependent on inertial dynamics of flow, that was widely used for raising water before the advent of more convenient electrically driven pumps. The ram was a fluid dynamic oscillator capable of generating high peaks of pressure by periodic interruption of the momentum of water streaming through a long iron pipe. Its cycle of operation, with interruption of flow caused *by* flow (through a self-occluding outlet valve), is loosely comparable with the cyclic action of Malcolm's elastic tube model, though the materials used were different (iron pipe, metal valves, and an attached air chamber or *'Windkessel'*, for compliance).

Schmid's comparison of heart function with the rhythmic action of a water ram seems even more marginally relevant than Malcolm's elastic tube model. It would almost certainly have been forgotten were it not for another Austrian who, in the early 20th century, drew attention to Schmid's paper. Rudolf Steiner was a philosopher who, in the 1890's, edited Goethe's scientific writings for the centenary edition. His interpretation and development of Goethe's phenomenological approach to natural science subsequently influenced a number of medical and natural scientists. In 1922, Steiner emphasized a responsive aspect of heart function, using Schmid's hydraulic ram model as an analogy, suggesting that the heart is 'set in motion by the currents' (Steiner 1922/1976). This view was taken up by Leon Manteuffel-Szoege, a Polish heart surgeon (Manteuffel-Szoege 1960) and Theodor Schwenk, a fluid dynamicist (Schwenk 1962/1996). Schwenk had particular interest in spatio-temporal patterns of flow. His work, also influenced by Goethe's scientific/artistic approach, lies behind my own interest in the subject.

I was introduced to practical flow visualisation and flow modelling by John Wilkes, an English sculptor who, since collaborating with Theodor Schwenk in the 1960's, had specialised in shaping patterns of streaming flow. In 1970, John Wilkes discovered and later patented his 'Flowform' method of inducing cyclic, spontaneously rhythmic patterns of flow by allowing water to stream over appropriately shaped surfaces (Wilkes 1977). Chapter 3 contains descriptions of my own flow modelling

experiments, which were developed out of John Wilkes' work and teaching.

From the early 1980's I became interested in patterns and dynamics of flow through heart cavities. In medical scientific literature, studies of spatio-temporal patterns of flow through heart cavities (as opposed to studies of temporal variation of velocity or pressure at selected locations) were, at that time, scarce. A practical challenge is posed by the multidimensional/multidirectional nature of flow through the heart. This challenge applies not only to acquisition and presentation of data, but also to conceptualisation. Relatively few medical researchers have had the opportunity to observe and manipulate multidirectional patterns of flow. It is easier to conceptualise flow as linear and uni-directional, for example along a tubular vessel or through the centre of a heart valve.

Contrast x-ray ventriculography and angiography was the first technique to provide images of flow in the heart and vessels, but because contrast medium is usually injected as a turbulent jet, mixing diffusely with blood, it provides only limited information on velocities and patterns of flow.

Use of Doppler ultrasound, able to measure components of velocity directed to or from the transducer, may have tended to foster over-simplified conceptions of flow. In echocardiographic usage, 'flow pattern' generally refers to temporal rather than spatial variation of flow. A few researchers nevertheless made painstaking but limited attempts to map multidirectional flow vectors in heart cavities by pulsed Doppler ultrasound. A technique that might have been expected to provide more comprehensive information on intracardiac flow was 2-dimensional colour Doppler flow mapping. But limited acoustic access, limited quantitative accuracy, and uni-directionality of velocity acquisition all compromise the effectiveness of the approach (Miyatake et al. 1986, Kim et al. 1994).

This is the background against which I made inquiries, and identified magnetic resonance phase contrast velocity mapping as potentially the most comprehensive available approach for investigation of spatio-temporal patterns of flow in the heart and great vessels. I was fortunate to encounter the technique at the Magnetic Resonance Unit of Royal Brompton Hospital, which was one of the first units to develop effective magnetic resonance cardiovascular velocity mapping (Nayler et al.1986, Firmin et al.

1987, Firmin et al. 1990 – bound at end). In 1988, I was able to join the Magnetic Resonance Unit of the Brompton and National Heart Hospitals.

In several respects, magnetic resonance velocity mapping has capabilities beyond those of Doppler echocardiography. It is able to measure velocities in voxels throughout a plane or volume of acquisition. No contrast agent or flow marker is needed. Data can be acquired in oblique planes in any orientation, unrestricted by windows of access. It also allows choice of the direction in which velocities are measured. This may be either in or through the image plane, or both. Magnetic resonance is the only imaging modality with the potential to acquire comprehensive, that is to say 4-dimensional (space-time) and 3-directional (3 orthogonal vector components) velocity information (Firmin et al. 1990). At the present stage of development, however, constraints of time, software and hardware mean that choices have to be made regarding acquisition of velocity data. In most of the studies used for illustration in this thesis, data was acquired from selected planes, with 16 cine frames representing the time course of the cardiac cycle, and velocity encoded in all three orthogonal directions. Our group was probably the first to publish 3-directional cine velocity map data (Kilner et al.1989 and 1993 ii). This approach provides the basis for investigations reported in Chapter 4. A group working in Aarhus, Denmark, has published comparable data relating to pulmonary artery and left ventricular flow (Sloth et al. 94, Kim et al. 95).

Gaining relatively comprehensive information on velocities and velocity changes of blood within the heart is a step towards appreciating morphodynamics of flow through the heart, but questions of *dynamics* associated with changes of velocity remain. Newton's three laws of motion, which underlie the Navier-Stokes flow equations (See Chapter 6), are particularly pertinent to flow through the contractile, tortuously curved chambers of the heart:

1. *A mass continues in a state of rest or uniform motion in a straight line unless it is acted on by an external force.*
2. *The rate of change of momentum of a mass is proportional to and in the same direction as the (net) force applied to it.*
3. *To every action there is an equal and opposite reaction.*

Blood is subjected to changes of momentum because propulsive forces are intermittent (resulting in transient acceleration) *and* because streamlines diverge, converge or change direction (convective acceleration).

Reactions of the whole body to the effects of acceleration and deceleration of blood in the heart and great vessels are detectable externally by the technique of ballisticardiography (Starr et al. 1950 and 1953). Although developed for cardiovascular research and clinical investigation, the technique has been superseded by more clinically applicable investigative approaches such as those of electrocardiography and echocardiography, and has been virtually forgotten. Ballisticardiography involves placing the whole body on a mobile, light-weight table top. Movements of body and table, caused by *net* changes of momentum in heart and great vessels with each beat of the heart, are recorded graphically. Because only net inertial changes are recordable, the approach affords only limited, encrypted information regarding cardiovascular dynamics. But the fact that net inertial changes are recordable at all in resting subjects, in spite of damping effects of the remainder of the body, is telling. Transient inertial effects during ventricular systole are forceful enough to have proved difficult to match by mechanical acceleration of fluid into the aorta during post-mortem simulation. In attempting post-mortem simulation, Starr resorted, somewhat bizarrely, to use of a 58lb mallet, suspended and swung from a scaffold to accelerate fluid from a piston into the aorta of a human cadaver (Starr et al. 1953). Only by this extreme approach could he induce intra-vascular momentum changes equivalent to those of the living circulation. It may be significant that this set-up did not attempt simulation of flow direction-changes through the heart itself, the piston being connected to the ascending aorta. Nevertheless, *in vivo* ballistocardiographic findings, such as those recorded and analysed by Starr, leave no doubt that heart function, even at rest, involves inertial exchanges of force which should not be neglected.

It must be with exercise, however, that rates of change of intracardiac momentum take on real significance. Although difficult to measure, more blood is thought to pass with each beat (Daley et al. 1985 and 1987, Rassi et al. 1988, Nonogi et al. 1988), it attains higher velocities, and those velocities change direction, from inflow to outflow, in shorter periods of time. During exercise, therefore, for each filling of a heart chamber or

vessel, there is not only more momentum to change, but it changes more extremely and more rapidly.

The importance of blood velocity increase with exercise was considered by the Canadian physiologist, AC Burton (Burton 1965). He used measurements of blood velocity, derived from previous investigations in animals and humans, to calculate the kinetic energy per unit volume of blood in different parts of the vascular system. Kinetic energy per unit volume gives a term with the same dimensions as pressure, which can be expressed in mmHg for convenient comparison with measurements of blood pressure. His calculations indicated kinetic energy per unit volume to be negligible, ie less than 1% of measured pressure, in capillaries and smaller venous and arterial branches, but to have the following percentages of measured pressure in different regions at rest and exercise:

	Rest	Exercise (3 x cardiac output)
Caval veins and atria	12%	52%
Pulmonary artery, systole	13%	52%
Aorta, systole	3%	17%

Burton concluded that:

- In the aorta, the kinetic energy factor is small for the resting cardiac output, but it may be of considerable importance in conditions of exercise and increased cardiac output.
- In the smaller arteries, capillaries and small veins, kinetic energy is negligible.
- In the caval veins, kinetic energy is important on exercise, but less so at rest
- In the atria and in the pulmonary artery, the kinetic energy factor is by no means negligible at rest and is of major importance when the cardiac output is increased.

Although Burton's approach may be criticised in a number of ways, it perhaps gives a preliminary guide to levels of kinetic energy in different vascular regions and states.

Problems with the approach include the following: For the caval veins and atria, Burton simply took pressures of 2 and 3 mmHg, at rest and exercise. This is a gross simplification as trans-mural pressures in these regions vary markedly, with position,

cardiac phase and physiological state, dipping close to or below zero at certain phases. The calculations, based kinetic energy associated with a certain velocity, treat blood flow as if it were steady. They give no access to dynamics associated with momentum change in the system. Ambrosi and Starr had, in 1965, commented challengingly on this subject, but perhaps with over-emphasis in relation to dynamics of the heart in the resting state:

"So many of our colleagues continue to think of the function of the heart as the Greeks thought of motion in general, e.g., the sun is drawn by Apollo's chariot because, like a wagon on earth, if not continually worked upon, its motion would stop. Similarly, many think that the heart must keep pushing out the blood up to the end of ejection. That this is not necessary has been clearly demonstrated by Spencer and Greiss (1962)*; the data of Rushmer and associates* (1964) *also supports this view. The blood, once set into motion, will continue in motion because of its inertia until resistance stops it. So, after positive acceleration is over and maximum velocity has been attained, little if any cardiac effort will be required and this effort may cease well before the end of ejection."* (Ambrosi and Starr 1965, quoted in Noble 1968)

Modelling, either physical or computational, of flow through the whole heart is almost prohibitively difficult, so investigative approaches to inertial effects via in vivo measurements of pressure or velocity are of particular importance. Mark Noble recorded instantaneous pressure differences along the left ventriclular outflow tract during systolic acceleration and deceleration phases in dogs. He found evidence of differences of pressure of the order of 15mmHg, and up to 26 mmHg, across accelerating or decelerating blood of the left ventricular outflow tract and proximal ascending aorta in conscious animals (Noble 1968). Laniado and Yellin made similar dual catheter recordings across mitral and aortic valves in dogs and humans (Laniado et al. 1973 and 1975, Yellin et al. 1981), although these approaches were limited by uncertainty regarding precise location of catheter tips.

In 1995, Fujimoto took a different approach, using multi-gated pulsed Doppler to record velocities along the axis of flow from left atrium to left ventricle. He calculated, in healthy volunteers, early diastolic differences of pressure of the order of 4mm Hg associated with acceleration of blood into the left ventricle through the open mitral valve (Fujimoto et al. 1995). This order of magnitude agrees with our own computations of

resting inertial pressure difference, reported in Chapter 6. This pressure difference is by no means insignificant in relation to diastolic atrio-ventricular function, and is a pointer to greater significance during exercise. Hermann Lauboeck (Lauboeck 1980) has attempted an analysis of intracardiac dynamics during exercise, basing his calculations on flow and pressure data published by Laniado and co-workers (Laniado et al. 1975) together with original echocardiographic studies in a single volunteer. These studies purport to show that isovolumic contraction and relaxation periods were not only eliminated during strenuous exercise, but that mitral and aortic valves were momentarily open simultaneously at the beginning and possibly the end of systole. This suggests that exercising inertial pressure gradients may be sufficient, momentarily, to account for considerable differences of pressure between left atrium and aorta. Our own exercise echocardiographic studies (Chapter 6), though they did not provide precise data on timings of opening and closure of valves, gave evidence of gradual elimination of isovolumic periods, with marked increases of rates of change of momentum during exercise.

In conclusion, others have done work in many areas that are relevant to aspects of this thesis, although the question of functional significance of the looped overall curvatures of the heart does not appear to have been addressed.

Chapter 2

Review of forms of vertebrate and invertebrate hearts

Background

Vertebrates attain unrivalled combinations of size, complexity and sustained dynamic activity which rely on a heart capable of vigorous flow. Outward forms of air-borne and aquatic vertebrates show unmistakable structural adaptation for fluid dynamic function, and it would be surprising if hearts were not also shaped in relation to dynamics of fluid propulsion.

Vertebrate hearts have remarkable form in relation to flow, with sinuous changes of direction that arise from looping. My hypothesis is that patterns of flow and dynamic exchanges associated with looping have functional significance. Two distinct, potentially co-acting functional interpretations of looping are addressed later in the thesis. They are briefly introduced here as they should be borne in mind in relation to this chapter's comparative review of heart shapes:

Firstly, asymmetry of cavities arising through looping may predispose to accommodation of relatively stable, inherently cyclic patterns of flow which lend themselves to efficient, phasic interaction with myocardial cycles of movement. This concept is illustrated and discussed in chapter 3, and considered in relation to patterns of flow through the human heart in chapter 4.

Secondly, direction change at ventricular level allows inertial recoil of a forcefully ejecting ventricle to enhance rather than inhibit atrio-ventricular valve movement, and hence atrio-ventricular coupling, especially when rates of change of momentum increase with exercise. This concept is investigated and discussed in chapter 6.

Combining the two, the interpretation proposed is that through looped curvature the vertebrate heart adopts a form suited for cyclic exchange of energy - *morphodynamic* interaction - between fluid and its elastic/contractile walls. The looped, atrio-ventricular arrangement can thus function not only as a valved displacement pump, but also as a morphodynamic pump capable of dynamic interaction, enhanced on exercise, between movements of myocardium and blood.

Aims and scope of this chapter

Recognition that looped curvatures - a feature of vertebrate rather than invertebrate hearts - could have functional significance raises several questions which are addressed in this chapter:

- does cardiac looping occur in *all* vertebrates?
- Does it occur *only* in vertebrates?
- What major variants of heart shape occur amongst vertebrate and invertebrate classes?
- What are the supposed evolutionary relationships among circulatory systems and hearts across animal phyla?

A number of publications provide information relevant these questions, without addressing them specifically (Robb 1965, Bourne 1980, Young 1981, Wilbur 1983, Nielsen 1995, Hamlett et al. 1996, Ruppert and Barnes 1994). With reference to these and other sources, this chapter reviews forms and supposed evolutionary origins of animal circulatory systems and hearts, with functional interpretation of cardiac looping in mind. The review gives perspective against which remarkable features of our mammalian cardiovascular system can be appreciated afresh.

The review begins with an overview of animal circulatory systems, and clarification of what is meant by 'blood vascular systems' and 'hearts'. Classification of animal phyla and supposed evolutionary relationships between them are then considered with particular attention to cardiovascular similarities and differences. Forms and locations of animal hearts are then reviewed phylum by phylum, and discussed in relation to functional interpretation of vertebrate cardiac looping.

Overview of circulatory systems in relation to cell layers

In their review of comparative morphology of circulatory systems, Ruppert and Carle focused attention not on specific forms, but on relationships between circulatory systems and the layers, cavities and segments of animal structure (Ruppert and Carle 1983). They drew a distinction between *coelomic* circulatory systems, on the one hand, and *haemal* or *blood vascular* systems, on the other. The majority of relatively large, active animals with coelomic cavities have both coelomic *and* blood vascular circulatory systems, although, of the two, the blood

vascular system generally fulfils more differentiated and widespread circulatory functions. Both types of circulation may become confluent in a mixed system, for example in arthropods.

Coelomic circulatory systems do not have hearts. Coelomic fluid can be circulated either by the ciliary action of mesothelial cells that line coelomic cavities, or by general movements of body musculature. Coelomic systems tend to be bilaterally symmetric and relatively capacious, generally partitioned by the 'bulkheads' of inter-segmental septa. There are, however, exceptions, for example in sipunculans (peanut worms) in which coelomic channels penetrate a septum, or leeches, a type of annelid, in which body septation appears to have been relinquished and coelomic channels adapted for circulatory function (Nielsen 1995).

Blood vascular systems are systems of internal fluid transport that arise in the extracellular matrix between the basement membranes of cell layers of triploblast animals. They do not, in their primitive form, have a cell lining. Vascular endothelium develops secondarily in two phylogenetically separate groups of animals: the cephalopod molluscs and the vertebrates. Blood may be circulated by contractility of certain regions of vessel wall, by movements of body musculature, or by rhythmic contraction of a distinct muscular region - a heart.

A heart may be defined, for the purposes of this review, as a localised, contractile region of a blood vascular system, moved by contraction of overlying muscle in a pericardium. Heart muscle is generally derived from myoepithelial cells of the modified coelom which forms the pericardium.

Although it tends to be assumed that blood must be propelled by the action of a heart or heart-like vessel segment, it is also possible that short-range physico-chemical interactions predispose to directional fluid movement in microscopic vessels. Metabolism, active substrate transport, respiration and excretion are associated with concentration gradients that might exert localized and subtle directional forces on passing blood elements. But if any such mechanisms exist, they do not appear to be sufficient to sustain large-scale circulatory flow. Hearts or contractile/compressible vascular regions of various types are found in blood vascular systems of triploblast animals above a certain size.

In these animals, major blood vessels develop dorsally and ventrally, in the sagittal plane, which is the plane of mesenteric folds. It is generally part of one of these major vessels that takes on heart function, although there may also be

subsidiary contractile or compressible vascular regions elsewhere. Information and further references relating to microstructural relations of invertebrate vascular systems can be found in relevant volumes of the treatise edited by FW Harrison (Harrison 1990-1998). Ruppert and Carle refer to publications that describe histological origins of vessels and hearts in a number of animal groups (Ruppert and Carle 1983). They emphasise that blood vascular systems, because they develop through extracellular matrix, fulfil a requirement for communication and exchange between separate specialised tissues, readily extending between body segments or compartments. It is intriguing to realise that this primitive communicative potential seems to be retained in humans, even into adulthood. For example, if lung tissue is deprived of blood by valvar or arterial obstruction, new systemic-pulmonary vascular connections may develop across pleural or pericardial spaces, particularly if there is a bridging matrix of scar tissue following inflammation or surgical intervention (Matsunaga et al.1993).

Phylogenetic classification of animals

To compare blood circulations and hearts between phyla, phylogenetic classification needs consideration. The system of classification and nomenclature proposed and refined by Linneus between 1735 and 1758, presumably based largely on observations of outward forms and appearances, remains broadly acceptable to the present time. Through the work of Darwin, Haeckel and others in the 19th century, biological classification came to be interpreted in relation to evolution. A phylogenetic tree is thus generally regarded as a chart of evolutionary descendence, although the reality of this cannot be demonstrated directly. Origins and relationships between species remain open to interpretation and debate. Although clear and widely used, the simplified concept of an evolutionary tree, progressively branching from a shared stem, without confluence, influence or mutual interaction among stems, should not be accepted without question. Nevertheless, it provides a convenient plan in relation to which relationships among living phyla may be considered.

Approaches to phylogenetic classification have taken account of information from fossil records (Skelton 1993, Valentine 1994), morphology, including larval and embryonic morphogenesis (Nielsen 1994 and 1995), and data from genetic and biochemical analysis (Pendleton et al. 1993, Wada and Satoh 1994, Harvey 1996).

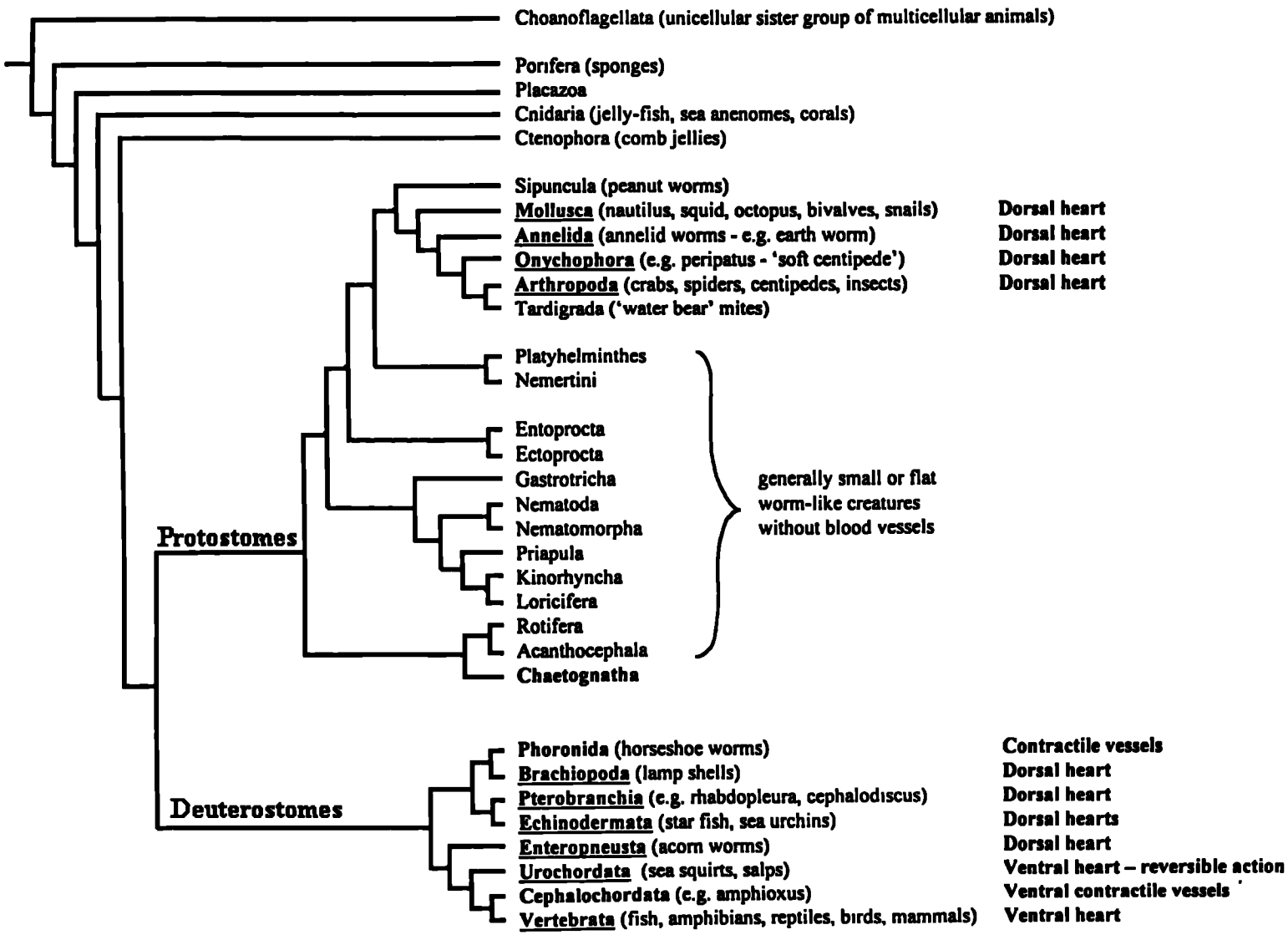


Figure 2.1 Animal phylogenetic tree based on computational analysis of morphological features by Nielsen, 1996. Phyla considered to have representatives with blood circulatory systems are named in bold text, and those considered to have hearts are underlined.

The phylogenetic tree shown in Figure 2.1 (opposite) is based on Claus Nielsen's work, which has the advantage of being clearly documented in a single book, describing morphological - including developmental and ultrastructural - similarities and differences between animal groups (Nielsen 1995). In a subsequent paper, Nielsen re-analysed his morphological data (presence or absence of features in different phyla) using computational analysis (Nielsen *et al.* 1996). This resulted in a diagram on which Figure 2.1 is based, differing only slightly from the phylogenetic tree that Nielsen had previously arrived at by 'manual' analysis. For the purposes of this paper, phyla which are known to have living representatives with blood circulatory systems (bold text) and hearts (underlined) are distinguished.
Different biologists might name and arrange branches of the tree differently; there is not necessarily one correct way of representing on a two-dimensional diagram all the multi-dimensionally interwoven relationships among animals. There seems to be broad agreement on relationships between major phyla possessing cardiovascular systems, although placement of certain phyla such as chaetagnatha, entoproct and ectoproct bryozoans, and phoronids remains controversial (Nielsen 1995).

Certain features of the illustrated phylogenetic tree may need explanation. One phylum of unicellular organisms is included - the choanoflagellates, which Nielsen considers to be the protozoan group from ancestors of which *all* living multicellular animals have descended, including sponges (porifera), jellyfish (cnidaria), comb jellies (ctenophora) and the many phyla of bilaterally formed, triploblastic animals. Nielsen, apparently in accord with other biologists, believes that the step to animal multicellularity (as opposed to mere clusters of potentially autonomous single cells) happened only once in the evolution of animals now living.

Our own phylum, the vertebrates, are classified as just one amongst some 30 or more animal phyla (the number varies according to interpretation). Division of animals into 'vertebrates' and 'inverterbrates' is therefore considerably off-balance, but, from our human perspective, understandable. There is, however, a more fundamental divide that should be considered. This is the division between *protostomes* and *deuterostomes.* Although there is no single characteristic that can be relied upon to distinguish members of the two groups, there is generally a difference in early stages of larval morphogenesis through which guts form from the preliminary, cup-like gastrula. In protostomes, opposite rims of the cup opening - the blastopore - fuse to enclose the gut tube, with mouth and anus arising from different

parts of the blastopore (Figure 2.2). In contrast, the deuterostome gut forms by secondary penetration of tissue, apart from the blastopore, giving rise to a tube with mouth at one end and blastopore (which generally becomes the anus) at the other.

The parting of evolutionary ways between protostome and deuterostome lines is presumed, from fossil evidence, to have taken place more than five hundred million years ago in the precambrian period. According to Nielsen, it probably occurred at a stage when multicellular, polyp- or cup-like animals were beginning to form tubular guts, with the beginnings of interventions of mesoderm and coelomic cavities between ectoderm and endoderm layers. It is by no means clear when and through what organisms protostome and deuterostome lines divided, but recent finds of exquisitely preserved precambrian fossils raise hopes of future paleantological clarification (Xiao *et al.* 1998). What is widely accepted is that there are fundamental differences of development and adult body plan between major living protostome and deuterostome phyla. Strangely enough, urochordates (which include sessile, bag-like sea squirts) and echinoderms (which include pentagonally arranged star fish and sea urchins) appear to be genetically and developmentally closer to ourselves than fellow crawlers, creepers and grabbers such as lobsters and insects (arthropods) or octopus and squid (cephalopod molluscs). The humble sea squirt is a deuterostome, whereas arthropods and molluscs with eyes, limbs, brains and quite sophisticated cardiovascular systems are much more distantly related protostomes.

Early separation of protostome from deuterostome branches explains or is supported by (depending on your point of view) different arrangements of major body structures. Both groups typically have a mouth opening into a tube-like digestive cavity, and both, in larger species at least, develop nervous, respiratiory, excretory and circulatory systems, but there are important variations of location and arrangement of these. Whereas vertebrates have their major nerve tract located dorsally and heart ventrally, the reverse is generally true of protostomes. This might almost suggest that some primitive worm rolled on its back to give rise to the chordate-vertebrate line, but this idea does not stand closer scrutiny. The neural tube of vertebrates forms by ectodermal invagination, dorsally, separate from the more ventral enclosure that forms the gut. The ventrally located neural tissue found amongst protostomes, however, arises in the region of fusion of blastopore lips.

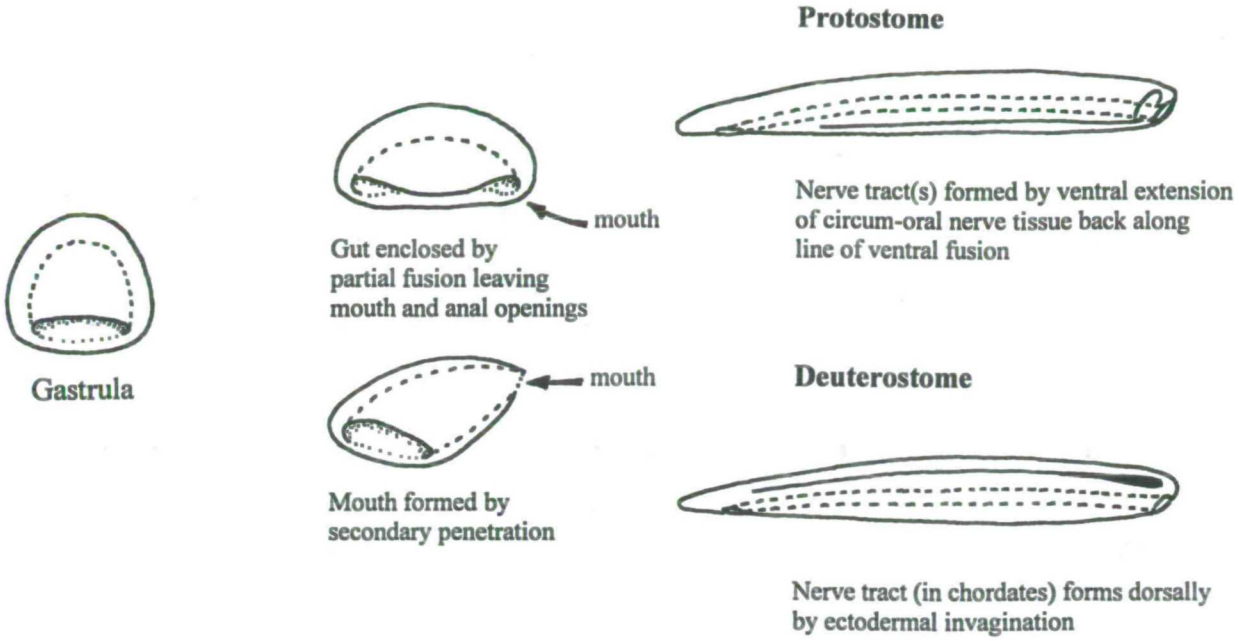


Figure 2.2
Diagram of gut formation in protostomes and deuterostomes. Hearts generally develop from mid-line longitudinal vessels, dorsal to the gut in protostomes and 'lower' deuterostomes, but ventral to the gut in urochordates and vertebrates.

Supposed origins of circulatory systems

According to Nielsen, the common ancestor of protostomes and deuterostomes had no blood vascular system, and blood vascular systems evolved separately in protostome and deuterostome lines (Nielsen 1995). Without adequate fossil records of vascular structures, however, uncertainty remains. Valentine, interpreting indirect fossil evidence in relation to a review of genetically based cladistic analyses, suggests that the common protostome/deuterostome ancestor may have had a blood vascular system, inherited by both lines (Valentine 1994). He draws attention to dimensions of fossilised worm burrows, apparently large enough to suggest that pre-cambrian worms are likely to have been large and active enough to have required blood circulatory systems. This argument seems questionable, however, as relatively large living sipunculans and leeches have coelomic but not blood circulatory systems.

Although all living deuterostome phyla have blood vascular systems, protostomes include a number of approximately worm-like phyla, bracketed in Figure 2.1, without blood vascular systems. This might be accounted for by secondary loss of blood vessels in organisms that have undergone reduction in size or complexity, for example where parasitic existence has been adopted. But it is more widely held that blood vascular systems arose independently, on the one hand in protostome ancestors of molluscs, annelids, arthropods (grouped by Nielsen as articulata) and, on the other hand, in forebears of living deuterostome phyla. Our vertebrate circulatory system is thus not regarded as homologous with the circulatory systems and hearts of arthropods and molluscs. But the concept of homology - unique evolutionary origin of a shared organic feature or complex - is not clear-cut, and is open to interpretation.

Harvey has pointed out that the gene known as 'tinman', of the phylogenetically ancient NK-2 homeobox group, appears to be homologous between the insect Drosophila and vertebrates, with comparable roles in relation to heart development in each (Harvey 1996). He questions, therefore, whether hearts might, after all, be homologous between the two widely separated groups. But this illustrates difficulties in deduction of homology. An alternative interpretation could be that hearts emerging independently in two lines drew on similar genetic/biochemical substrates in relation to similar functional requirements.

Because hearts of vertebrates arise in a quite different anatomic location from those of protostomes, these organs can hardly be said to be homologous with one another.

Although cardiovascular systems and hearts of protostomes and deuterostomes are thought to have evolved separately, features *predisposing* to their development were presumably inherited from the common ancestor. And shared environmental/ecological conditions must, in the course of evolution, have presented organisms of both lines with comparable opportunities and challenges. Factors predisposing to cardiovascular development and influencing its progress may be sought (and apparently found) in ecological conditions, group or individual behaviour, body dimensions, structural features, functional requirements and genetic make-up. Several authors have commented on the apparent convergence of cardiovascular features found in cephalopod molluscs and vertebrates (Martin 1980, Wells 1983, Nielsen 1995). The convergence does not, however, extend to looping of the heart, which only vertebrates seem to manifest, although both groups appear, independently, to have evolved endothelial lining, valved atrio-ventriculo-arterial connections, myogenic rhythmicity and elasticity of arteries.

An interesting interpretation of morphogenetic paralellism or convergence between different phylogenetic groups has been put forward by biologists who have studied the formative dynamics of complex, interactive systems (Goodwin 1995). Mathematical modelling of complex, non-linear, potentially chaotic systems offers insights into the emergence of order out of complexity. Certain typical biological forms may emerge as they do, perhaps in separate evolutionary lines, because that is the way they *tend* to emerge, given the interactive dynamics (not *necessarily* the specific biochemical substrates) of complex systems. As Brian Goodwin expressed it: *"Biologists deal with systems (cells, organisms) that are hideously complex, with thousands of different types of gene and molecule interacting in different ways. Or so it seems at the molecular level. However, what is being recognized within the 'sciences of complexity' is that there are characteristic types of order that emerge from the interactions of many different components. Despite the extreme diversity of genes and molecules in organisms, their interactions are limited so that distinctive types of order arise, especially in relation to the large-scale aspects of structure or morphology."* (Goodwin 1995)

Morphogenesis of the heart, in which various molecular, structural and fluid dynamic factors have been implicated (Olson 1996, Icardo 1996) must be a

candidate for emergence of order through complex interaction. As JM Icardo put it: *"Whether attention is focused on gene expression or shape changes, it is important to recognise that the heart, like any other organ, results from the assembly of concatenated levels of organisation. The levels are concurrent, and each one is necessary for others to be adequately expressed so that they establish a back and forth interrelationship. Although the developmental picture that emerges is of increasing complexity, it is hoped that new techniques (and new approaches) will help us unravel the mysteries of heart development."*(Icardo 1996)

Comparative cardiovascular morphology

Protostome phyla

Molluscs

Cephalopod molluscs such as octopus and squid include the largest living invertebrate animals. Molluscs appear to have separated early from the annelid-arthropod line, and are the only invertebrate phylum to have evolved hearts that come near, in terms of structural dimensions and haemodynamic performance, to those of vertebrates. Molluscan vascular sytems also approach those of vertebrates in other ways. They have a low blood to body volume ratio, closer to that of vertebrates than to that of any other invertebrate phylum (Martin 1980), and their systemic ventricle delivers relatively high systolic pressure, probably up to about 90mmHg, to elastic walled arteries with endothelial linings. But unlike vertebrates or other invertebrate phyla, the predominant blood pigment in higher molluscs is haemocyanin, a blue copper-based respiratory pigment, transported in plasma rather than cells.

Unlike annelids and arthropods, adult molluscs lose obvious signs of multi-segmented body plan. But morphology of larval forms (Nielsen 1994 and 1995), and of fossilized and living examples of monoplacophora, a primitive class of mollusc that retains seven or eight body segments (Martin 1983, Ruppert and Barnes 1994) point to the phylogenetic proximity of molluscs to annelids and arthropods.

This gives a clue to interpretation of the progression of circulatory arrangements and hearts found in different classes of mollusc. Monoplacophora have seven or eight pairs of gills, each draining by branchial veins to the median dorsal vessel that forms the heart, an arrangement not unlike that of certain annelids. In nautilus, an ancient order of cephalopod mollusc, gills are reduced in number to two on

either side, each draining via an expanded vessel segment (atrium) to the dorsally located systemic ventricle of the heart. In octopus and squid, gills are further reduced to one on each side. In some species, an additional contractile chamber referred to as a branchial 'heart' (Figure 2.3) augments flow to each gill.

In bivalve molluscs such as oysters or clams, there appears to have been even further reduction of gills. While in some species flow from paired gills converges via two atria to the ventricle, others have one gill leading to one atrium and ventricle, an arrangement with a degree of non-linearity of flow path. This non-linearity appears, however, to relate to lateral origin of the one retained gill rather than the result of cardiac looping.

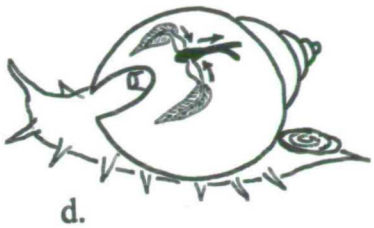
Gastropods such as slugs and snails are the only class of mollusc to have taken to the land. As in bivalves, bilaterally paired gills of more primitive representatives are reduced to a single respiratory organ, the lung or cnetidium, in most land snails. Flow from this organ, via an atrial cavity, has come to lie almost in-line with the axis of the ventricle, although the axis of the whole heart, contained by pericardial cavity, has become displaced by torsion from its original position dorsal to the gut (Martin 1983).

Figure 2.3 (opposite)
Examples of protostome hearts. In all of these, the systemic heart (black) originates dorsal to the gut. The feather-like regions drawn in molluscs represent vessels of gills, or of the cnetidium in the land snail. All animals drawn have valves, generally in and out heart cavities and sometimes in other vessels.

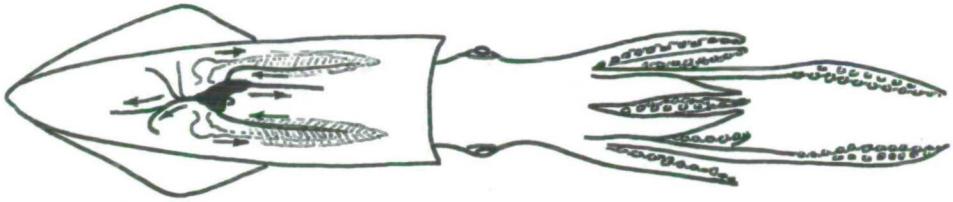
a. Earth worm, *Lumbricus terrestris*, an annelid, has a dorsal, contractile, valved vessel flowing forward to connect with five pairs of valved pseudo-hearts lateral to the pharynx. (redrawn after Martin 1980)
b. *Nautilus pompei*, a mollusc. (redrawn after Wells 1983)
c. Squid, a mollusc, and part of its circulatory system (c') with branchial (white) and systemic (black) contractile chambers. (redrawn after Wells 1983)
d. *Scutibranchia*, a relatively primitive aquatic snail, has two gills, two atrial expansions and adorsal heart chamber (redrawn after Golikov in Martin 1983)
e. *Helix pomatia*, a land snail, has a single respiratory organ, a single atrium, atrio-ventricular valve, ventricle and valved aorta(s). (redrawn after Martin 1983, Somerville 1973 and Dale 1973)
f. Insect (bee), with a linearly arranged heart suspended dorsally in abdomem. Blood is received via segmental ostia from a pericardial blood pool, and propelled forwards to thorax, limbs and head.
g. Spider, with dorsal, segmented heart comparable to those of insects.
h. Lobster, with dorsal heart, accepting blood via ostia from pericardial blood, with arterial outlets in several directions.



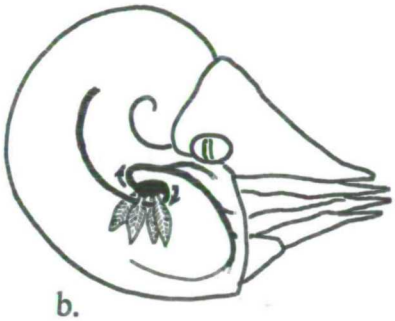
e.



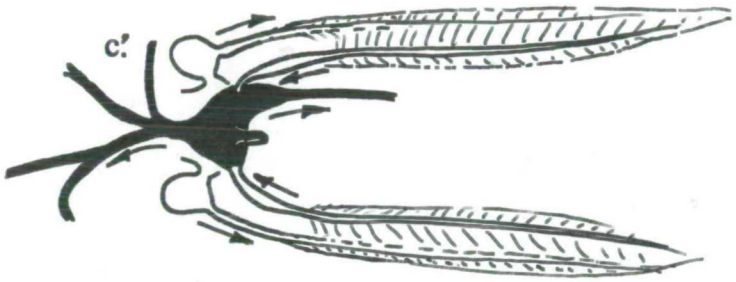
d.



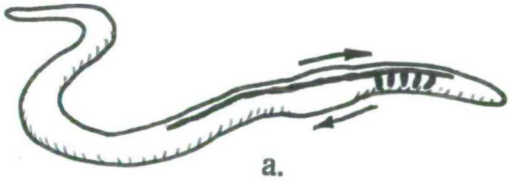
c.



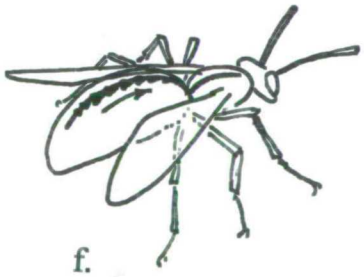
b.



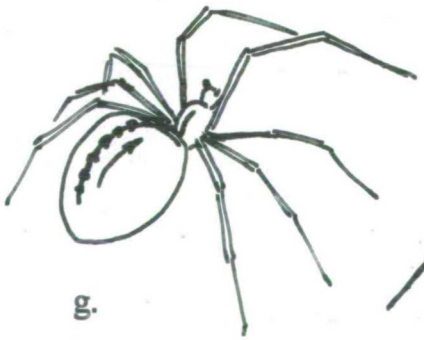
c'.



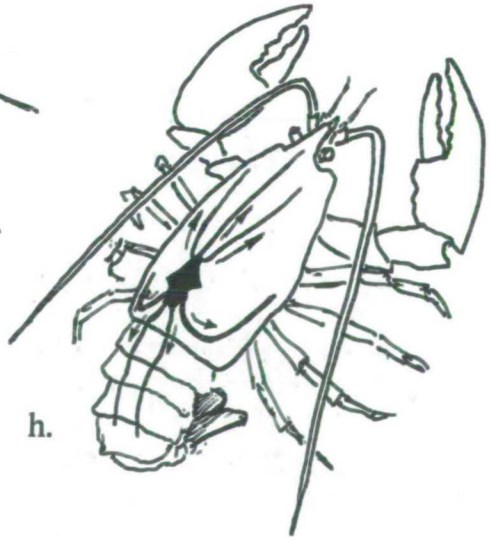
a.



f.



g.



h.

As in vertebrate hearts, atrial and ventricular chambers of hearts of snails have been shown to work reciprocally on one another, contraction of one inducing expansion of the other through exchanges of wall tension and hydrostatic pressure within a pericardium of relatively constant volume (Somerville 1973, Dale 1973, Jones 1983).

Annelids

Annelid worms have a basic circulatory pattern which can probably be regarded as close to the underlying pattern from which both molluscan and arthropod circulations have evolved. It consists of vascular networks absorbing nutrients from the intestine, converging on a contractile dorsal vessel which conveys blood forwards to a neural ganglion and other tissues anteriorly, with branches passing round either side of the pharyngeal intestine to flow back ventrally (Martin 1980). It is a relatively closed system of vessels, in contrast to a more open circulatory system, with blood vessels opening into wider intercellular spaces, found in arthropods.

Circulatory systems of polychaetes show peristaltic, generally forward-directed contractility in the main dorsal vessel. More expanded, localized, contractile segments, sometimes referred to as hearts, are found dorsal and lateral to the oesophagus in certain species, as illustrated by drawings reproduced by Martin (Martin 1980).

In the earthworm (*Lumbricus terestris*), an oligochaete, the contractile dorsal vessel contains valves that direct blood forward. There are also five pairs of expanded, valved, contractile lateral vessels, referred to pseudo-hearts, which propel blood from the main dorsal to the main ventral vessel around the pharynx. In larger specimens that have been investigated, contractile frequencies are of the order of 20per minute have been recorded, with pressures up to 20cm of water in dorsal vessels, and up to 70cm of water in ventral vessels (Martin 1980).

Amongst annelids, an exceptional circulatory arrangement is found in leeches, consisting of a modified coelomic system, with vessel-like connections running either side of the mid-line. Movements of fluid in the system are brought about movements of body musculature, perhaps supplemented by ciliary action, but there is no heart (Ruppert and Carle 1983)

Onychophorans

Onychophorans are a small phylum of soft-bodied centipede like creatures that have characteristics intermediate between annelids and arthropods. Their blood circulatory system, like that of arthropods, is formed by a confluence of coelomic and haemal systems, with a spacious blood-filled body cavity or haemocoel. In part of this, the

pericardial space, dorsal to the gut, runs the longitudinal heart vessel. This linear, tubular heart receives blood via a pair of ostia in each segment, propelling it forward to an anterior opening which returns blood back to the haemocoel (Nylund 1988).

Arthropods

The majority of arthropods have articulated, chitinous exoskeletons which support and protect softer body parts. Their circulatory systems, like those of onychophorans, are myxocoels formed by a fusion of coelomic and haemal systems, with large amounts, relative to body mass, of blood-like fluid consisting of haemolymph with leucocytes. The heart, which is tube-like, bag-like or tent-like in form, is suspended dorsal to the gut in a pericardial space, receiving blood from around itself via paired ostia (Figure 2.3). Numbers of in-flowing ostia vary from one pair to pairs in each of numerous body segments, each one functioning as an inflow valve. Ejection is through a cranially directed dorsal aorta and through additional arterial outlets. A pair of arteries, valved at their origins, may emerge in each segment, although numbers of arteries arising from the heart tend to be fewer in larger crustaceans such as crayfish, crabs and lobsters. Blood moves out through arterial branches back to capacious intercellular spaces before returning to the pericardial region (Clarke 1979, Scram 1986).

In adult crustaceans the dorsal heart is located towards the back of the thoracic region whereas in in the insects and arachnids it is in the abdominal region, with an aorta passing forward through the thorax to the head. Insect hearts are generally subdivided by indentations to give a series of compartments which are moved by suspending alary muscles and by overall abdominal movements, as well as by contractility of the heart itself. In addition, there can be contractile or compressible vessel segments outside the heart, augmenting flow through wing or limb muscles. Many insects also have hollow tracheal systems conducting air directly to metabolising tissues, relieving the blood of gas transfer requirements (Clarke 1979, Tjonneland *et al.* 1987).

Chaetagnatha

Phylogenetic placement of the delicate worm- or fish-like marine organisms known as chaetagnatha is awkward. Some biologists place them amongst deuterostomes (Harrison 1990-1998, Skelton 1993), whereas Nielsen places them with protostomes (Nielsen 1995). The presence of a haemal vascular system, which is transparent, escaped notice until recently. It consists partly of peri-intestinal sinusus, presumably moved by intestinal movements, and is not known to contain a heart (Shinn 1993 and 1997).

Protostome phyla without blood vascular systems

According to Nielsen, sipunculans, an apparently primitive surviving sister group of articulata, have coelomic canals but no blood vascular system (Nielsen 1995). Tardigrades, placed on the other side of the mollscan/arthropod grouping in Figure 2.1, are mite-like organisms closely related to arthropods, but they remain very small in size and are not known to have blood circulatory systems.

Bracketed in Figure 2.1 are a collection of protostome phyla that lack blood vascular systems or hearts. Most of these are small or flat-bodied, worm-like organisms, some of which may be grouped as aschelminthes. As they lack blood vascular systems, these phyla do not concern us directly, but their existence, in appreciable numbers, has bearing on the question of origins of protostome and deuterostome circulatory systems, giving credence to independence of circulatory origins.

Deuterostome phyla

I will begin with brief consideration of the basic vertebrate cardiovascular system as it appears in fishes, comparing it with cardiovascular systems of protostome and non-vertebrate deuterostome phyla before returning to describe developments of heart form in the vertebrate line.

In fishes, a ventrally located, looped heart with atrial and ventricular cavities propels blood forwards via gills to the head and body (Satchell 1971). Blood moves caudally in a dorsal vessel or vessels, returning, via vasculature of caudal muscles and nutritive organs (generally in parallel), to veins that drain through the sinus venosus to the heart. The general direction of circulation is thus the reverse of that of protostomes. Gills are also located differently, generally being upstream of the (systemic) heart in protostomes such as molluscs, but downstream of the heart in fishes.

Cephalochordates (amphioxus or lancelets) are morphologically (Nielsen 1995) and genetically (Turbeville *et al.* 1994) the closest living sister group of vertebrates. The general layout of blood vessels in amphioxus appears to be broadly similar to that of vertebrates (Rahr 1979). Directions of flow are also similar, i.e. forward in ventral vessels and back in dorsal, assisted by several peristaltically contractile but valveless ventral vessel segments: the intestinal vein, hepatic vein, sinus venosus, and the endostylar artery which gives rise to gill branches (Randall 1980, Young 1981, Ruppert 1997). Muscle cells of these contractile vessels are said to be part of the surrounding peritoneum, without any distinct heart or pericardium (Ruppert 1997). Blood circulation is slow, and generally

constant directions, although occasional reversal of contractility has been reported (Ruppert 1997). Amphioxus remains limited in size and motility compared with vertebrates. It seems reasonable to suggest that the ventral heart now found in the vertebrates arose in a circulatory system such as that of present-day amphioxus. The region from sinus venosus to endostylar artery appears to be equivalent to the location of the looped vertebrate heart.

Remaining lower deuterostomes do not so obviously share the vertebrate pattern of blood flow, although *Urochordates* such as sea squirts have a ventrally located heart. This tubular heart extends in its pericardial cavity in a location that originates ventral to the gut, although orientation becomes more difficult to interpret after the tadpole-like larva settles to the sessile existence of the sea squirt. The heart tube, which is bent to a V-shape in some species, lacks valves, and propels blood peristaltically, first in one direction and then the other, in periodic alternation (Randall 1980).

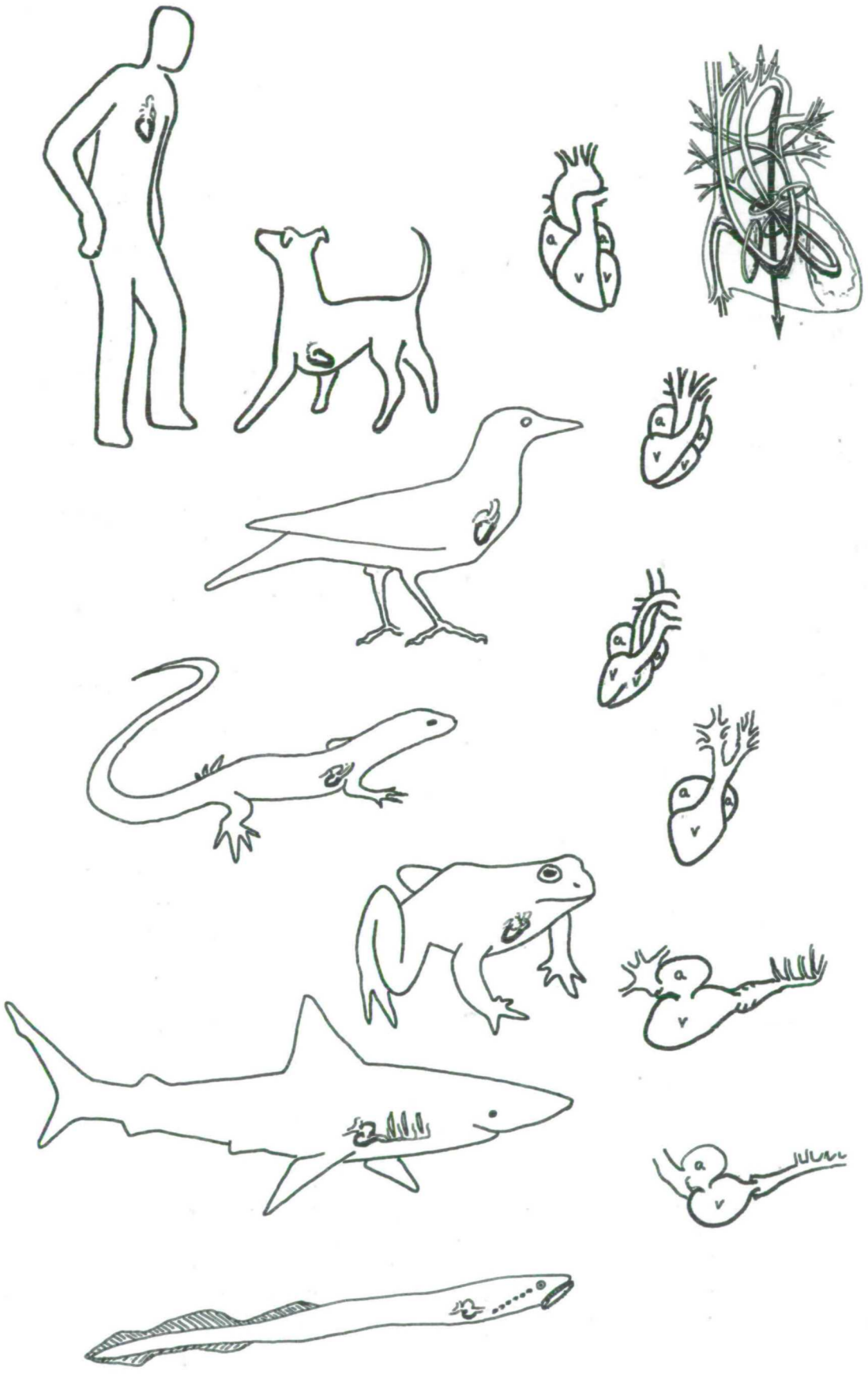
This peculiar arrangement seems to mark a certain 'watershed' between chordate (including vertebrate) circulatory patterns and those of non-chordate deuterostomes, which, on the whole, flow more in the protostome manner - anteriorly in dorsal vessels and posteriorly in ventral. A heart-like region, with pericardial cavity, is located dorsal to the pharyngeal region in pterobranchs and enteropneusts (Young 1981, Ruppert and Barnes, 1994).

Echinoderms and brachiopods also have heart-like regions with pericardium, originating dorsally, although departures of adult forms from more familiar worm- or fish-like body plans make circulatory comparisons awkward (Ruppert and Barnes 1994, Harrison 1994). Phoronids have blood circulatory systems with contractile vascular regions but without pericardium. They are not considered to have hearts (Harrison 1994).

Vertebrate circulatory systems and hearts

Cyclostomes - the jawless fishes including lampreys and hagfish - are regarded as the most primitive living vertebrates. Vertebrate classes may be ordered in the sequence: cyclostomes - jawed fishes - amphibians - reptiles - birds – mammals (Figure 2.4). Through these classes, there is generally a progressive increase in organic and behavioural complexity, and emancipation from aquatic environments (except where aquatic existence has been adopted secondarily). The ventral heart shows increasingly marked looped curvature, with septation of atrial and ventricular chambers associated with development of a pulmonary circuit as lungs supplement and replace gills.

Hearts of fishes, both jawless and jawed, have cavities arranged in series, developing embryonically by differential growth of an initially relatively straight tubular vessel in a



pericardial cavity. Cavites of the fish heart are known as sinus venosus, atrium, ventricle, and conus arteriosus (from which the aorta, with its branchial branches, arises). There are valves between each of the four contractile cavities (Satchell 1971, Hamlett et al. 1996). In higher vertebrates, sinus venosus and conus arteriosus tend to lose their separate identity, becoming incorporated in atrial and ventriculo-arterial regions, respectively. The atrial inflow valve is also lost in higher vertebrates.

Apart from the ventral heart shared by all vertebrates, various peripheral 'hearts' occur in lower vertebrates (not regarded as true hearts because they lack pericardium). Examples include a portal venous and caudal hearts of hagfish, which is a cyclostome (Yamauchi 1980), and numerous contractile, valved lymph hearts that have been identified in fish, amphibians, reptiles and birds (Satoh and Nitatori 1980). There are reported to be more than a hundred pairs of lymph hearts draining to veins in *Caecilia*, a primitive amphibian. Valved, contractile lymph hearts seem to have been relinquished in mammals, although compression of valved veins and lymphatics remains an important subsidiary circulatory mechanism, especially during locomotion.

In the ventral heart of vertebrates, ventricular and atrial cavities function reciprocally in a pericardium of fairly constant volume, which is cartilagenous and relatively rigid in elasmobranch fishes. Ventricular contraction tends to induce atrial expansion, and vice-versa, through essentially static forces of wall tension and hydrostatic pressure, as already described for the snail heart.

If cardiac looping is defined as "secondary curvature causing changes of direction of paths of flow through developing atrial and ventricular cavities", then a degree of looping occurs in cyclostomes, becoming more marked, with increasing angulation between ventricular inflow and outflow, through jawed fishes, amphibians and reptiles to birds and mammals.

Figure 2.4 (opposite) Examples of vertebrates and their hearts. All have looped ventral hearts with juxtaposed atrial and ventricular cavities. From below: A cyclostome (lamprey) and jawed fish (shark). Both have sinus venosus, single atrium and ventricle, conus arteriosus and aorta leading to gill arches. An amphibian (frog) has two atriums and one ventricle. A reptile (lizard) has two atriums, two communicating ventricles, pulmonary trunk, and two aortas, one of these from the sub-pulmonary ventricle. A bird (raven), has two atria, two ventricles, pulmonary trunk and aorta, as do mammals (human and dog). The hearts of the jawless and jawed fish are drawn as viewed from the right, whereas those of higher orders are viewed from the ventral aspect. With increasing tortuosity and entwinement, flow paths through hearts of higher vertebrate are difficult to represent. The drawing above right indicates principal paths of flow through chambers and vessels of the human heart (see Chapter 4).

In adult bird and mammalian hearts, where septation between left and right ventricular cavities is complete, it is the systemic, left ventricle that shows the most acute change of direction between inflow and outflow. Looping, with direction change at ventricular level, may allow inertial forces to enhance coupling between ventricular and atrial function during exertion (Chapter 6). Flexibility of the pericardium in higher vertebrates presumably allows a certain freedom of heart movement during exertion.

There is progressive septation of atrial and ventricular cavities through ontogenetic and phylogenetic development of higher vertebrates. Ventriclar septation is partial, with residual communication, in most reptiles. Ventricular septation is complete in crocodilians, although one of two aortas arises from the sub-pulmonary chamber. Birds and mammals have only one aortic outlet, and complete separation of systemic and pulmonary flow paths (Young 1981).

Solomon Victor has studied progressive division of the single atrioventricular valve of fishes, giving rise to the two atrioventricular valves of reptiles and higher vertebrates (Victor and Nayak 1995), and has drawn attention to spongy, asymmetric trabeculation and partial division of ventricular cavities in lower vertebrates, comparable with that of higher vertebrates during embryonic development.

Although there is variability of outer and inner forms of ventricles among different vertebrate classes, and even among members of single classes (Hamlett et al. 1996, Rowlatt 1980) change of flow direction between ventricular inflow and outflow remains a consistent characteristic of the vertebrate heart. This can be observed, for example, in the contrast x-ray angiograms of vessels and cavities of amphibian and reptilian hearts published by Johansen.(Johansen and Burggren 1980). Rowlatt observed that slow moving members, such as the sloth, of the edentates tend to have more rounded hearts than the relatively narrow, elongated hearts of the more active armadillos and ant-eaters (Rowlatt 1980). The narrower form, with more acute direction-change between ventricular inflow and outflow, and presumably greater long-axis mobility of the atrio-ventricular valve plane, may be better suited for dynamic atrio-ventricular coupling during exertion.

Discussion

This review of circulatory systems and hearts underlines both the diversity of animal life, and, at the same time, the recurrence of certain organic themes, appearing in various forms and relationships in different phyla. There seems to be a deep-seated propensity for vascularisation in triploblast animals that achieve a certain size and mobility. In blood

vascular systems, and also in lymphatics draining to them, non-return valves seem to form readily in relation to contractile or compressible vessel segments. Around particular dorsal or ventral vessel segments, part of a coelomic cavity may become modified so as to enhance the mobility and contractility of the vessel, contributing to the pericardium and musculature of a heart, which acquires different forms in different animal groups.

Looping

From information available, cardiac looping appears to occur in *all* vertebrates, and *only* in vertebrates. The cephalochordate amphioxus is not considered to have a heart, though its general circulatory layout is close to that of vertebrates. In amphioxus there are changes of direction between vessels draining to the sinus venosus and the endostylar artery emerging from it (Rahr 1979, Ruppert 1997). These are not equivalent to curvatures arising through looping, but rather to the direction changes at sinus venosus level observable in fishes. U- or V-shaped curvatures of tubular hearts of Cephalodiscus, a pterobranch (Nielsen 1995) and of certain urochordates (Randall 1980) raise the possibility that there may be a tendency for emerging hearts to adopt curved forms in deuterostomes. But these tubular structures do not give rise to juxtaposed atrial and ventricular cavities characteristic of the looped vertebrate heart.

Potential protostome candidates for cardiac looping might include bivalve molluscs, where the single atrium and ventricle do not lie in-line with one another, but this non-linearity appears to be a relic, resulting from retention of one of the more primitive pair of laterally placed atria. The same goes for snails, except that cavities of certain snail hearts have progressed to an almost linear arrangement - arguably the opposite tendency from looping.

Although there are direction-changes of flow path where vessels enter and leave heart chambers of cephalopod molluscs, for example nautilus and squid (Figure 2.3), these can hardly be described as cardiac looping. The systemic ventricle receives blood from contractile vessel segments or atria on either side, and ejection is generally in more than one direction, an arrangement which appears unsuited for dynamic atrio-ventricular coupling.

Postulated evolutionary significance of cardiac looping

Vertebrates achieve unrivalled combinations of size, complexity and sustained dynamic activity. The largest invertebrates are cephalopod molluscs such as octopus and giant squid. Their cardiovascular systems, although evolved independently, approach those of vertebrates in several respects. But without looping, invertebrate hearts lack potential for

dynamic atrio-ventricular coupling, which may have limited their ability to support sustained, strenuous locomotion. Cephalopods move rapidly by jet propulsion, but this tends to be transient and evasive rather than sustained and predatory. As hunters, they are inclined to lurk, stalk, and seize with extendable, suckered tentacles (Boucard-Camou 1983). In contrast, the one known predator of the giant squid is an air-breathing mammal with a looped, four-chambered heart similar to our own. The sperm whale - Moby Dick of Melville's novel - is phenomenal in its size and its capacity for sustained locomotion. It roams oceans, and can dive from the surface to depths where giant squid lurk.

Vertebrates seem to show remarkable propensity for adaptation of form to fluid dynamic function. Outward forms of fast vertebrate swimmers appear to have reached several separate but comparable peaks of refinement - in elasmobranch fishes such as sharks, in teleost fishes such as tuna, in the extinct reptilian Icthiosaurus, and, with horizontally oriented flukes, in the mammalian dolphins and whales (Young 1981). The looped form of the ventral heart appears to have been retained and gradually refined through all these vertebrate classes. If, as postulated, looped curvature is a dynamically efficient arrangement for atrio-ventricular propulsion of blood, then it is not surprising that it should have been retained once established, the heart fulfilling broadly similar fluid dynamic function regardless of environment.

In biological processes, however, cause and effect are not necessarily distinguishable. It may not be possible to determine to what extent dynamic efficiency of a looped heart gave scope for the vigour and complexity of vertebrates, or, conversely, to what extent evolution of backbone, jaws and associated developments of neural, muscular and excretory systems demanded dynamically efficient heart action. Either way, cardiac looping may have a more significant place in relation to vertebrate evolution and performance than has previously been recognised.

Chapter 3

Spontaneously cyclic flows in asymmetric cavities

Objectives

The main purpose of this chapter is to present in-vitro experiments that demonstrate spontaneous oscillations of flow in asymmetric cavities. Results are considered in relation to the hypothesis that curvatures and asymmetries arising through cardiac looping predispose to relatively stable, inherently cyclic patterns of flow which lend themselves to dynamic interaction with cyclic myocardial movements through certain stages and states of heart development and function.

In a separate section at the end of the chapter (p48-53), further examples of coherent, multi-directional patterns of flow (a ring vortex, trains of vortices, and flows in symmetric and asymmetric cavities) are illustrated. Fluid dynamic analysis of these examples, the first two of which are well known and have been studied previously, is not attempted. Their inclusion is intended to illustrate characteristic phenomena of secondary flow for consideration in relation to patterns of flow in heart cavities, to be studied in Chapter 4.

Background

My interests in flow and form, which lead to the work of this thesis, arose through an unusual path of study. After medical qualification, I studied sculpture and flow at Emerson College in Sussex with John Wilkes, an English sculptor who had previously collaborated with Theodor Schwenk. Schwenk was a German fluid engineer who, in the 1950's and 60's, investigated forms and rhythms of transitional states of flow. He published a beautifully illustrated book on flow phenomena, presciently titled *das Sensible Chaos,* later translated as 'Sensitive Chaos' (Schwenk 1962/1997), at least a decade before the burgeoning of modern chaos theory.

After he had worked with Schwenk, John Wilkes discovered, in 1970, that he could induce rhythmic oscillations in a stream of water by appropriate shaping of boundaries. His initial discovery came about through observation of flow in an open channel with bilaterally symmetric dilatations and strictures. Water streaming forward between paired dilatations set up back-curling recirculation zones either side of the mid-line. These, if shaped appropriately, could break symmetry,

deflecting the forward stream first to one side and then to the other in rhythmic alternation. Working interactively with streams in clay boundaries, John Wilkes shaped and reshaped containing surfaces, streamlining them to accommodate recirculating vortices so that fluid momentum was smoothly redirected and oscillatory cycles optimised. An example of a cascade of forms, shaped in this way is shown in Figure 3.1, opposite. In 1975, John Wilkes patented what he called the 'Flowform' principle, which has subsequently been used widely for mixing and aeration of fluid, for example in waste-water treatment systems. The satisfyingly rhythmic sounds and appearances of Flowforms have been used in sculptural water installations throughout the world. Through the 1970's John Wilkes and collaborators produced variants of Flowforms, all with two or more cavities, and all inducing alternate formation of more than one vortex so that swirls and counter-swirls alternated either side of the mid-line.

While studying with John Wilkes in 1980, I sought and discovered the single-cavity Flowform variant (Figure 3.2, opposite), which is to be discussed and illustrated further in this chapter. It is an interesting variant for several reasons:

- It is apparently the simplest case of the Flowform phenomenon, involving only one vortical recirculation zone.
- Unlike paired- or multiple-cavity Flowforms, it can, when suitably shaped, give rise to intermittent outflow, its flow cycle mediating between continuous inflow and phasic outflow.
- Its asymmetric form is of interest both aesthetically and in relation to asymmetric forms of heart cavities.
- It may be seen as the liquid-gravity-wave counterpart of air oscillations in a whistle, flute or organ pipe.
- Its asymmetric form and rhythm have apparent similarities with those of cavities of looped hearts of more primitive vertebrates such as the fish.

These points have occupied me in the years since discovery of the single cavity Flowform. Recognition of its somewhat tantalising apparent likeness to primitive heart cavities led to enquiries that led me back into medical work, in the fields of cardiac imaging and research, including studies described in the rest of this thesis.

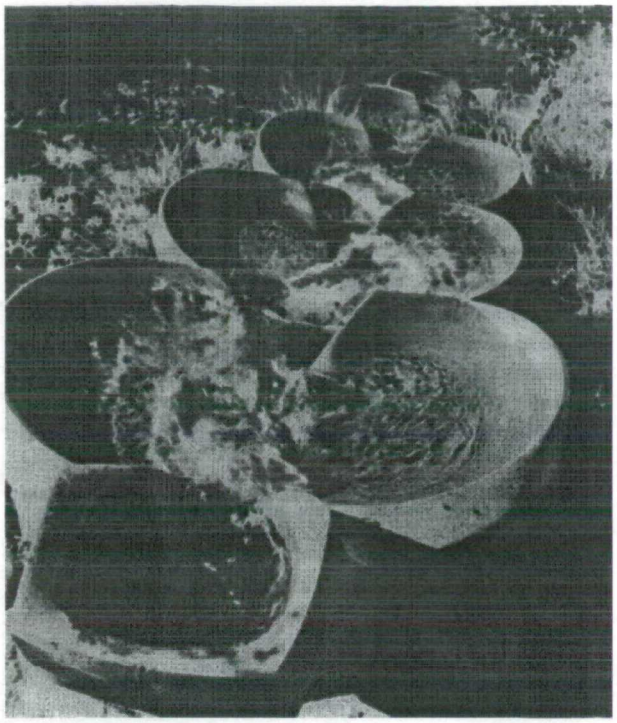


Figure 3.1 A cascade of Flowforms designed by John Wilkes (1974). Flow from the inlet in the foreground is continuous, but in each of the paired cavities, flow swings from side to side in repeating figure-of-eight movements. Oscillation is related to cyclic wave propagation and rhythmic deflection of the inflow stream.

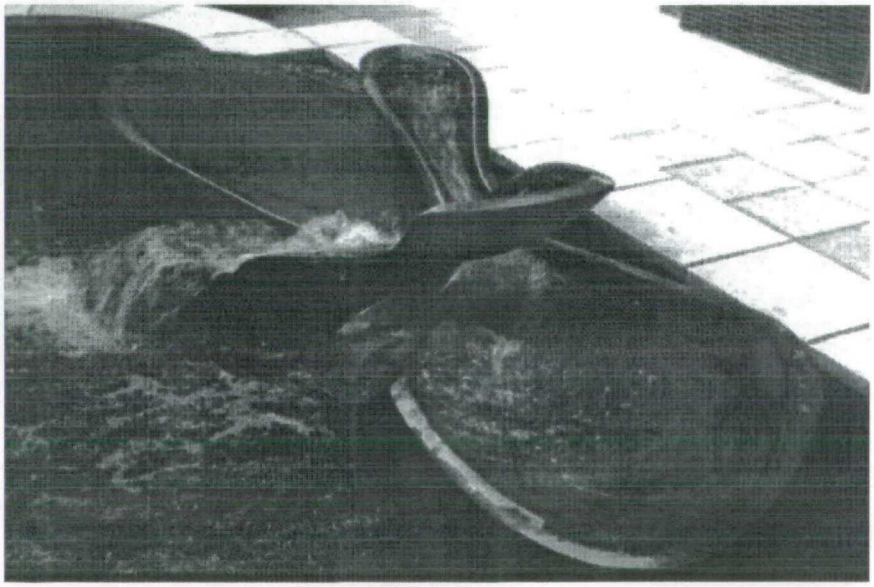


Figure 3.2 A pair of single-cavity Flowforms by Philip Kilner (1989) at Royal Brompton Hospital, London. Each receives continuous inflow, but delivers intermittent surges of flow to the pool. The nearer form is in its filling phase, while the further one is emptying. See figure 3·4.

Methods

General approach to establishment of asymmetric cyclic flows

Using continuous inflow of water from a tubes, channels or trickles, the containing boundaries of single, asymmetric cavities were adjusted interactively, by trial, observation and modification, until, in each case, a unilateral, recirculating region of back-flow impinged on the in-flowing stream in a way that deflected it periodically. The asymmetric cavity would then fill and empty alternately, its contained cycle of flow and wave propagation mediating between continuous inflow and phasic outflow.

This type of self-sustaining fluid oscillation was established in cavities over a range of sizes. Most of the examples shown required some skill and patience to shape appropriately, but the cyclic flow phenomenon can be set up relatively easily as follows:

A readily constructed flow model

Flexible plastic tubing, 10mm internal diameter, delivered a continuous stream of water of a rate of 3 l/min (Figure 3.3, opposite). The tube was fixed so as to give a stream issuing horizontally across the surface of a sloping plane board, angled at 15° to the horizontal so that the water flowed in a curve to escape down the slope of the board. A flat, rigid slat was placed on edge to form an oblique wall, beginning 8-10 cm beyond the tube outlet, located so as to deflect most of the stream on an up-hill path until it lost momentum. Adjustments were made to the position and angle of the wall (about 35° from a horizontal contour) until a self-sustaining, repeating cycle of fluid build-up and escape was achieved.

Shaped open cavities

Observation of the above flow cycle gave a basis for establishment of similar flow cycles contained by appropriately curved surfaces, shaped in malleable materials (clay, wax or sheet copper) through a process of trial, observation and modification. Surfaces were curved and streamlined in relation to flows of the recirculation zone, optimising the oscillatory cycle until intermittent outflow from continuous inflow was achieved. The examples shown in Figures 3.2 and 3.4 were both shaped initially in beaten copper, over which water was allowed to stream at intervals during the shaping process to establish cyclic flow. For magnetic resonance imaging, the smaller form was then cast in a non-metallic plastic material and sprayed black to provide photographic contrast (Figure 3.4, overleaf).

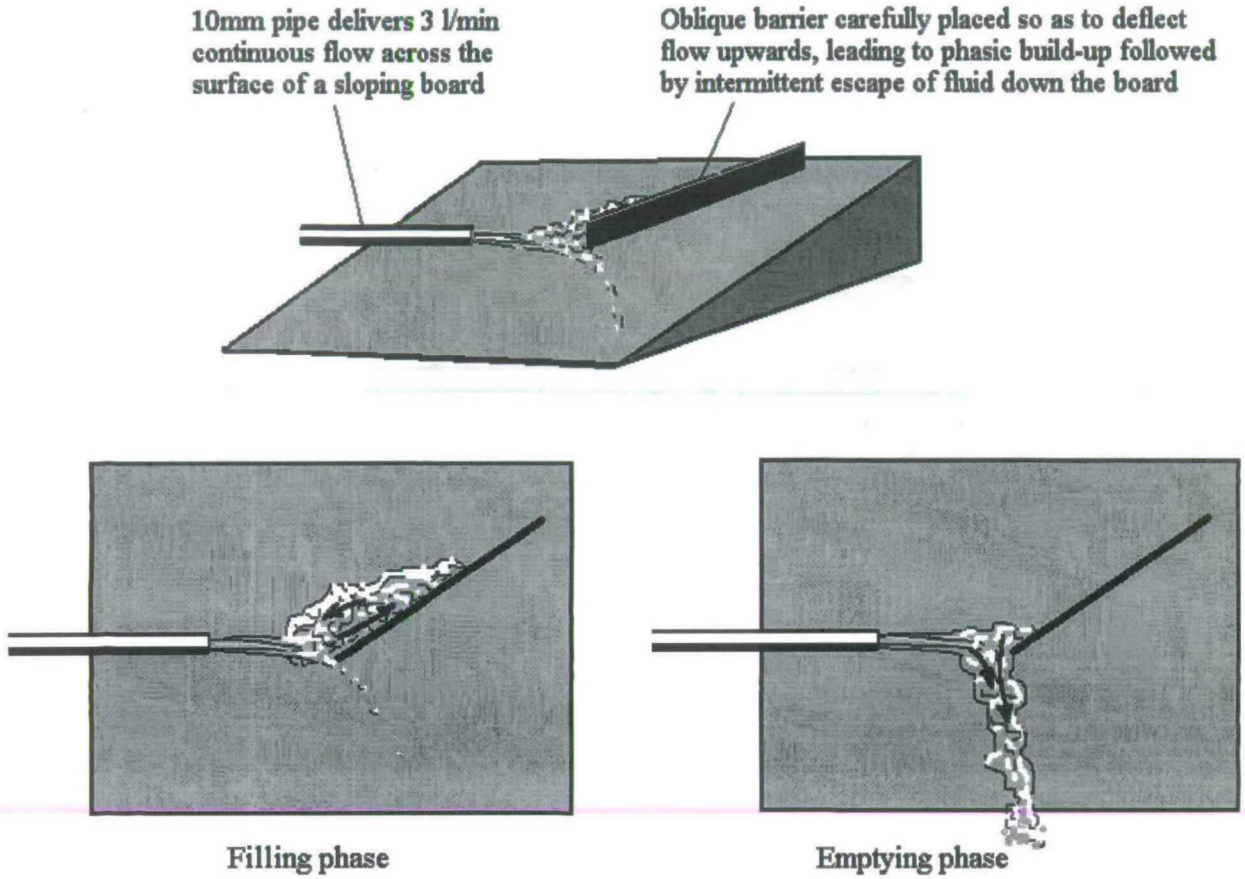


Figure 3.3
A demonstration of spontaneous oscillation of flow, with cyclic accumulation and escape of fluid on a sloping board. This is the liquid, gravity-wave equivalent of acoustic oscillation in an organ pipe or whistle.

Magnetic resonance flow velocity mapping

Cyclic flow in the small open-cavity form, 15cm in length and 7cm across, was studied by magnetic resonance phase velocity mapping (see Chapter 4). A constant head tank gave continuous inflow of a copper sulphate solution in at a rate of 5.4 l/minute to the form located in the bore of a 0.5Tesla Picker imaging magnet. All three electrodes of an ECG gating system were placed in the intermittent outflow, which poured to a catching vessel before escaping to a reservoir outside the magnet. Arrival of flow in the magnet caused a voltage spike sufficient for gated acquisition of cine phase velocity maps, TE=6ms, at ten gating delays spaced evenly through the 998ms flow cycle. Velocity was encoded in both phase and read gradient directions in a slice 16mm thick, aligned horizontally so as to image water movements in the curved floor of the cavity. The field of view was 30x30cm. Two repetitions of 128 phase encoding steps were performed. Flow vector maps were computed through correlation of X and Y velocity components in a manner that was also used for mapping patterns of blood flow in heart cavities (Chapter 4). A gated cine gradient echo acquisition in a plane cutting vertically through the length of the cavity allowed measurement of vertical amplitude of surface waves, to be used as an indicator of pressure fluctuations associated with the flow cycle.

Pulsating trickle experiment

On a smaller scale, a comparable cyclic flow phenomenon was set up by shaping the outline of a trickle of water running over a plane waxed surface (Figure 3.5, opposite, overleaf). The trickle flowed steadily at a controlled rate of 75 ml/minute over an inclined plastic board, 5° from horizontal, coated with a layer of paraffin wax. The angle of attachment between free surface and waxed surface was 80-90°. This gave an approximation of hemi-cylindrical flow, contained by tension of the curved free surface above (radius of curvature between 3 and 6 mm) and by the wax surface beneath. Steady streamlines were demonstrated by introduction of small crystals of potassium permanganate, just large enough to lodge on the floor of the trickle without appreciable disturbance of flow. The tip of narrow stick was used to re-shape the trickle to a bend and swelling, by re-attaching its free surface along curved lines. As curvatures of the lines of attachment were adjusted, dye from potassium permanganate crystals located upstream allowed visualisation streamlines, which now showed marked secondary curvatures, with flow separation and recirculation in the shaped region. When an asymmetric recirculation zone of

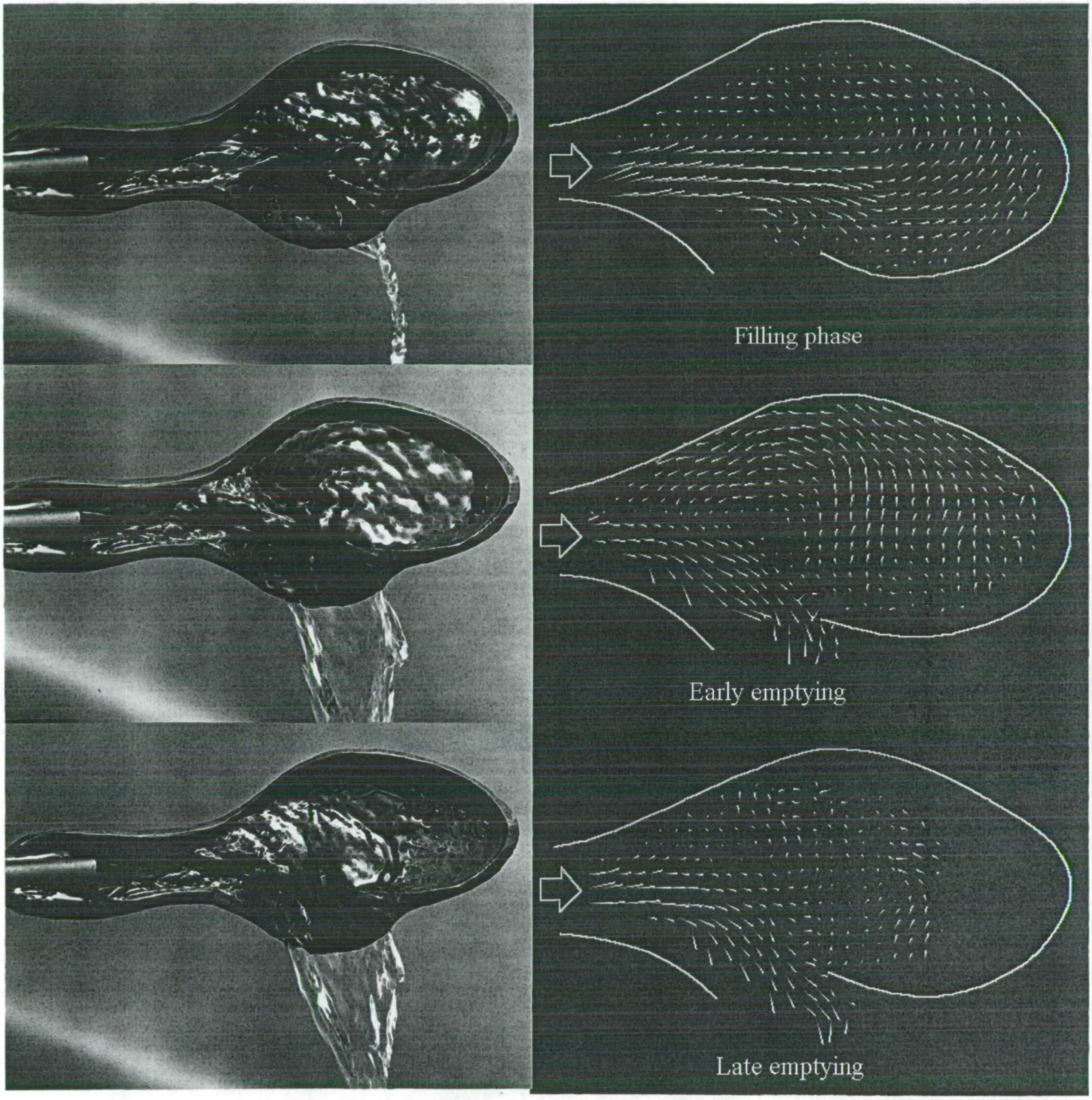


Figure 3.4

Cyclic flow in an open cavity, three phases photographed (left) with corresponding flow vectors recorded by magnetic resonance velocity mapping (right). Inflow from the tube on the left is constant at 4 l/min, but outflow is pulsatile, with almost complete interruption during the filling phase.

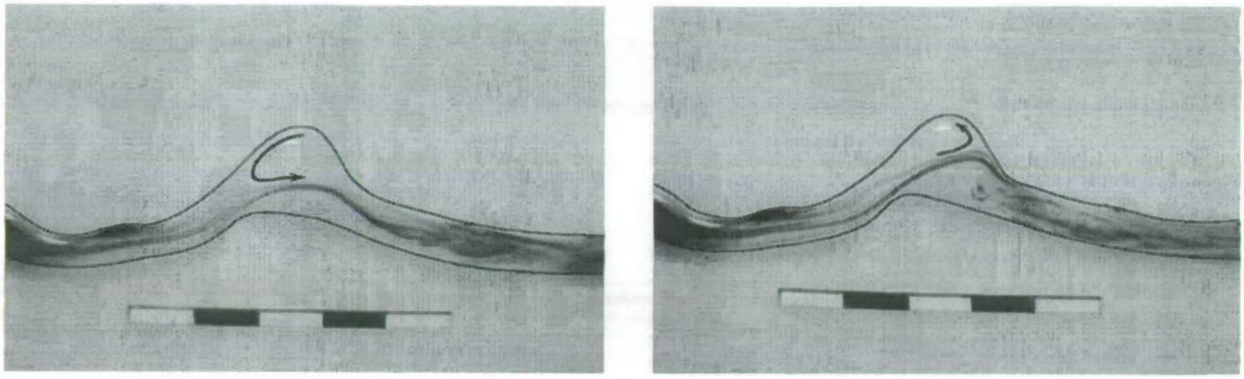
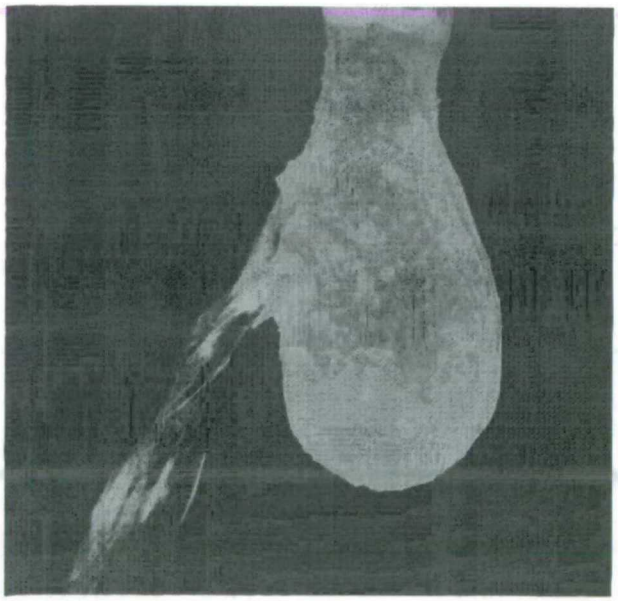


Figure 3.5 (above) A steady trickle of water, flowing left to right over a plane waxed surface, streamlines marked by potassium permanganate crystals lodged up-stream. When photographed, in 'emptying' and 'filling' phases of its cycle, the bulge was pulsating spontaneously at 41 cycles per minute. Notice that streamlines upstream are similar in both phases, but not those downstream. Each black or white mark on the scale = 1cm.

Figure 3.6 (below) A hollow silicone rubber cavity, 9cm in length, oscillating spontaneously at 3.4 Hz. Inflow from above is continuous at 5.4 *l*/ minate, but outflow fluctuates with cavity oscillation.



appropriate proportions was formed, self-sustaining oscillation was apparent though regular fluctuation of streamlines. Two distinct phases of the cycle of oscillation were photographed (figure 3.5).

Hollow compliant cavity

To test whether a comparable oscillatory flow cycle could be established within compliant, fully 3-dimensional boundaries, a bulb-like form, 9cm in length and 5cm across, its outline shaped to accommodate cyclic flow as illustrated in Figure 3.4, was modelled in wax. Around this, the hollow rubber cavity shown in Figure 3.6 (opposite) was cast. The wax former had a tapering extension above, around which the inlet was cast, and an oblique extension on one side to form the outlet. A layer of translucent, air-curing silicone rubber (clear silicone rubber bathroom sealant) was applied to the surface to a thickness of about 2mm. When set to a rubber coat, the model was warmed and the wax removed from the lumen. The resulting hollow compliant cavity, with inlet above and oblique outlet to one side, was attached beneath an adjustable, continuous supply of water.

Results

Figures 3.2 and 3.4-3.6 all show asymmetric cavities that contained spontaneously oscillating cycles of flow when photographed.

This type of flow cycle was most easily set up using the simplified tube-and-board arrangement illustrated in Figure 3.3. The other examples illustrated, with containing cavities curved to conform to patterns of flow, required some skill and patience to shape effectively. Figures 3.2 and 3.5 show examples that are among the largest and smallest that have been made by the author to date.

Shaped open cavities

Figure 3.2 shows a pair of large open-cavity forms, overall length of each being 2.6m, rates of oscillation being 0.36 and 0.24 Hz respectively. Similar forms have been made in a range of sizes and proportions. Reduction of cavity size was generally associated with increased frequency of oscillation, although shallow, flatter cavities, with slower intra-cavity wave propagation, showed relatively low frequencies. Though inflow was continuous in all cases, spontaneous, cyclic interruption of outflow was achievable through appropriate adjustment of cavity shape.

Figure 3.4 shows an example made on a scale comparable with that of a

human heart cavity. The photographs show three phases of the flow cycle, with almost complete interruption of outflow during the filling phase, in spite of continuous inflow. Curvature of the cavity deflected momentum of inflow round and back on itself. Arrival of the back-stream/wave caused deflection of inflow, leading to escape of both to the outlet, until initial conditions recurred. The cycle, in this case, repeated regularly at a frequency of 0.99±0.02 Hz.

MRI flow vector mapping

Images on the right of Figure 3.4 show magnetic resonance flow vector maps corresponding to the three phases photographed. Frame b, showing early emptying, was gated immediately after the voltage spike caused by arrival of outflow. Frames c and a were at 400 and 700ms gating delays, respectively. The "ECG" voltage trace recorded during acquisition demonstrated regularity of cycle lengths, which remained between 987 and 992ms over 50 cycles. Changing patterns of flow through the cycle can be appreciated from the vector maps. Peak velocity in the direction of inflow was 0.7m/s. Velocity of recirculating flow, in a direction opposite to that of inflow, peaked at 0.4m/s during early emptying. The vertical amplitude of surface fluctuations in the cavity was 1.8cm, representing cyclic pressure fluctuations in the cavity of the order of 1.3mm Hg.

Pulsating trickle

Through many attempts to set up oscillations in small trickles on waxed surfaces, a range of types of intermittency or oscillation have been observed. These include periodic fragmentation into drops, partial fragmentation with sinuous, almost peristaltic movements of lines of attachment between free surface and wax, sinuous, meandering realignments of the whole trickle, and development of more complex oscillations with two or more interacting recirculation zones. Cyclic oscillation can be established at frequencies spanning a range, from 10 Hz or more (too rapid to count by direct observation) to 0.5 Hz or less.

The example illustrated in Figure 3.5 represents the simplest type of oscillation observed, with a single, asymmetric bulge accommodating cyclic flow. When photographed, this example showed distinct oscillation of streamlines in the curved region, with to-and-fro displacement of the point of re-attachment of streamlines near the outlet of the bulge. Oscillation was regular at a frequency of 0.68 Hz (41 pulsations counted in 1minute). Patterns of secondary flow were sinuous but not turbulent. The two photographs, at different phases of the cycle,

show alteration of streamlines in the cavity in spite of near-identical streamlines on the upstream side. Oscillation originated in the cavity, with propagation of pulsation downstream and, to a lesser extent, upstream.

Hollow compliant cavity

When attached to a continuous supply of water flowing at 5.4 l/min, the hollow rubber form did not oscillate immediately, but only after interactive adjustment. This was achieved by realignment of the flexible inlet until spontaneous oscillation of cavity and outflow occurred, at 3.4 Hz when photographed. When flow was increased to 10 l/min, the cavity showed more vigorous, pendular oscillation with phasic indentation of cavity walls, in this case at a lower frequency of 2.8 Hz, probably related to involvement of gravitational (pendular) as well as elastic restoring forces in this mode of oscillation.

Discussion

Models and observations have been described which, though requiring patience to set up, do not rely on complex equipment. They could have been shaped and considered in relation to heart function at any time in the last several hundred years. Osborne Reynolds, the 19th century pioneer of fluid dynamic research, may have inadvertently contributed to the relative lack of attention paid to transitional and cyclic flows through the first two thirds of this century. Although his work was wide ranging, Reynolds is remembered for experiments whose clear findings and mathematical interpretation relied on strict limitation of conditions. For example, he observed and measured *continuous* flows through *straight, rigid, cylindrical tubes* (Reynolds 1883). In these conditions, he noted relatively abrupt transition from laminar flow to turbulence at a certain rate of flow beyond which resistance tended to rise steeply. Measurement of certain parameters (diameter, fluid velocity, density and viscosity) allowed Reynolds to identify a dimensionless numerical relationship, now known as the Reynolds number, which allowed prediction of transition to turbulence. His studies gave a basis for applied industrial fluid dynamics in which rigid boundaries and continuous flows are typical. Where boundaries, such as those of the heart, are curved, compliant and of variable diameter, oscillatory modes of flow can be maintained, passively and/or actively, more readily than in rigid tubes, although such conditions, even today, remain difficult to interpret and model mathematically (Pedley 1980, Peskin and McQueen 1995).

From an engineer's point of view, spontaneous oscillation of flow can be problematic, giving rise to vibration, stress, noise and, in certain situations, increased drag between structures and fluids. For wind musicians, or for anyone who whistles, sings or speaks, fluid oscillations are a source of sound. Rockwell reviewed a range of self-sustaining oscillations in both gases and liquids flowing asymmetrically in relation to cavities, describing parameters, mainly deduced from empirical research, that modify them (Rockwell and Naudascher 1978). He distinguished 'fluid dynamic', 'fluid resonant' and 'fluid elastic' examples. 'Fluid dynamic' referred to intra-fluid oscillation that is not coupled with movements of free surface or compliant walls, 'fluid resonant' referred to fluid oscillations coupled with surface wave effects, and 'fluid elastic' referred to fluid oscillations coupled with displacements of compliant walls. Examples described in this paper fall in the last two categories. Cardiovascular fluid-boundary interactions would relate most closely to the last (fluid-elastic) category, although in the heart, active myocardial contractility is an inseparable aspect of fluid-elastic interactions, modifying them to such an extent that their role in cardiac function is not easy to appreciate.

Liquid such as water or blood is practically incompressible, and boundary compliance takes on particular importance in relation to oscillatory cycles. In most examples illustrated (figures 3.1-3.5), displacements of free surfaces, restored either by gravity or surface tension, allowed cyclic wave propagation, the free surface providing effective compliance. It has been recognised in industrial flow modelling that open channel systems, with surface wave propagation, can behave as analogues of systems where compliant walls interact with unsteady flows. This was borne out by establishment of oscillation in both open and enclosed versions of the single cavity form (Figures 3.4 and 3.6). The open channel format allowed ease of flow visualisation and interactive modification, which were crucial for discovery and development of the particularly effective mode of oscillation described – effective enough, in open forms, to convert continuous inflow to intermittent outflow through a non-occlusive cycle of movement.

Described like this, it is not difficult to see that the principle might be incorporated at atrial level in the heart-like pump, enabling blood to pass intermittently through the atrio-ventricular valve without interruption of momentum of venous return. But consideration of the phenomenon in relation to heart action is by no means straightforward. In humans and other mammals, atrial cavities have



Figure 3.7 Simplified diagram of developmental stages of a simple vertebrate heart, showing atrial and ventricular cavities arising from curvature of the primitive heart tube. In relation to spontaneous flow oscillations illustrated in Figures 3.4, 3.5 and 3.6, the form can be interpreted as that of a fluidic oscillator/amplifier.

several inlets, with additional asymmetry in the lateral direction. Venous return, in the resting state at least, is modulated by atrial and ventricular systole, with two peaks of flow and pressure per beat. Atrioventricular flow is also biphasic at rest (Figure 4.2, opposite p. 57), only becoming monophasic with strenuous exercise (see Chapter 6). Any fluid-elastic oscillatory effects are clearly modified and dominated by several interacting physiological and mechanical factors. These include pacemaker function, myocardial conductivity, contractility, neuro-hormonal influences, valve action and arterial impedance. It is pertinent that myocardial movement may itself be described as passive-active-passive, with initial stretch predisposing to forceful contraction, which is followed by elastic diastolic recoil. Cardiac fluid-boundary interactions are thus complex. They have presumably arisen through progressive stages of phylogenetic and ontogenetic development, and they are modified during different physiological states.

Fluid morphodynamics and heart form

Flow cavities described in this chapter compare most readily with simpler, more primitive forms of heart such as those of present day fishes, or those of vertebrate embryos through early stages of looping. The comparison is interesting. The outline of the open cavity form (Figure 3.4), shaped to optimise the spontaneous filling and emptying, shows correspondence with the outline of the *atrial* cavity of a fish heart, viewed from one side (Figure 3.7, opposite). The ventricular cavity also shows similar overall form, but in this case with apparent reversal of orientation in relation to flow. This suggests an intriguing interpretation: that the looped, atrio-ventricular heart might be shaped as a "fluidic" oscillator-amplifier in relation to flow, the term fluidic referring to the use of channelled flow in fluid control devices (Holbrook 1984). Form and oscillation of the shaped trickle (Figure 3.5) lend support to the idea by showing that the passive oscillatory cycle can occur on a small scale (albeit not as small as an embryonic heart tube) in the bend and swelling of a tube-like surface boundary. Vertebrate heart cavities, in the early stages of looping, emerge through forms and movements provocatively similar to those of the shaped, passively pulsing trickle (Figure 1.1, opposite p8). But, again, the comparison is not straightforward. Origin of heart pulsation in living vertebrates appears to be myogenic (Icardo 1996) and, in higher orders at least, endocardial cushions apparently contribute to occlusive or semi-occlusive action at an early stage. In spite of these objections, it is appealing to consider the basic form of the looped

vertebrate heart as that of a fluidic oscillator-amplifier, an arrangement elegantly suited for deployment of responsive-active myocardial action in which contractile force increases with initial stretch (Noble 1978 and 1979).

It is hardly possible to confirm or disprove this hypothesis in relation to evolutionary origins. Existing hearts, particularly of higher vertebrates, show additional refinements and modifications. Lateral asymmetry, in addition to antero-posterior asymmetry, results in a helical twist which may allow recirculating or out-flowing streams to pass inflows without collision (see Chapters 4 and 7). Collision, with resultant deflection of inflow, appeared to be a necessary aspect of cyclic flows in models illustrated (Figures 3.2 and 3.4), but it was associated with increased intensity of flow disturabance or turbulence in the region where recirculating flow impinged on the inflowing stream. The phase of emptying was initiated by this interaction. In hearts however, where a contractile cycle is initiated by specialised myocardial tissue of the sino-atrial node, this type of fluid interaction is not necessary. This being the case, avoidance of collision between inflowing and out-flowing streams, for example through overall helical asymmetry, could help to minimise dissipation of kinetic energy. Co-ordination and coupling between fluid and myocardial cycles of movement nevertheless retain importance as accelerations, decelerations and turns of flow each require finite periods of time and involve force exchanges that are directional and phasic. The curvatures and movements of human heart cavities may thus be adapted for fluidic or morphodynamic function, but in a way that departs from the fluidic oscillator-amplifier model outlined above.

Interpretation of heart function is, understandably, dominated by ventricular systolic considerations. Atrial systolic and ventricular diastolic function, particularly early diastolic elastic recoil (Sonnenblick 1980, Strobeck and Sonnenblick 1981, Robinson et al.1986) have also received considerable attention. But fluid-inertial-elastic interactions, especially at atrial level, have been relatively neglected. In terms of pressure and energy, their importance, at rest, might seem to be minor, but gauge pressures remain low in this region, and through stretching of myocardial filaments for subsequent contraction, with possible influences on initiation and conduction of the action potential, their role may be amplified. Dynamic force exchanges gain importance during exercise when rates of change of momentum rise, and passive and active movements of the myocardium follow one another in rapid alternation. This is the state in which morphodynamic function of the heart may reach a peak of

effectiveness, with cyclic flows contained by curved walls propagating, redirecting and exchanging momentum in relation to myocardial cycles of movement (see Chapter 6).

Even at rest, the myocardium not only acts on the blood, but presumably responds to its dynamics. Atrial myocardium is displaced by streams arriving from various parts of the body before its action potential initiates the contractile cycle that gives rise to the arterial pulse that then propagates back through arteries to the brain and other organs. Fluidic-elastic-contractile interactions of the heart may play roles in transfer of information, as well as in transfers of fluid, gases, metabolites and energy in the living body.

In conclusion, phenomena of cyclic flows in shaped cavities suggest fresh interpretations of origins, asymmetries and functions of vertebrate hearts. The simplicity of the models described is both a limitation and strength of the approach taken. The models provide clear demonstration of a particular type of cyclic fluid-cavity interaction. Demonstration of comparable flow cycles in a range of sizes and types of model, which can also be compared with acoustic oscillations in organ pipes and flutes, shows the principle to be relatively universal and transferable. It would be surprising if structures of the evolving looped heart, approaching so close, at least, to forms capable of accommodating spontaneous fluidic oscillation, had not incorporated the phenomenon in relation to pulsatile function. It is not surprising, however, that the principle should have been modified in relation to further elaboration of cardiac form and function through the course of vertebrate evolution.

The interpretation proposed is that cavity asymmetry arising through cardiac looping predisposed to cyclic patterns of flow, which lent themselves to cyclic interaction with myocardial cycles of movement. Through looping, the primitive vertebrate heart may have adopted forms of a fluidic oscillator/amplifier. This principle appears to have been modified, however, through refinements of heart form and function in higher orders. In more complex hearts, tortuously asymmetric curvatures may contribute to the effectiveness of morphodynamic interaction between fluid dynamic, elastic and contractile forces, and to avoidance of flow instability, especially on exertion.

Additional fluid morphodynamic demonstrations

In this section, examples of relatively well-known fluid morphodynamic phenomena are illustrated for consideration in relation to patterns of intracardiac flow recorded by magnetic resonance velocity mapping in the next chapter.

Ring vortex

Method

A tall rectangular glass tank, 16x16x40cm, was built. It was filled with water and allowed to stand overnight to equilibrate with room temperature to eliminate convection currents. The barrel of a 60ml syringe was used to provide a plastic cylinder, 25mm in diameter, 12cm in length, partially closed at one end, provided with a nozzle of internal diameter 1.5mm. A supporting framework was made which allowed this cylinder to be supported in a vertical position, and lowered or raised while penetrating the water surface at the top of the tank. Using this, the open end was lowered, the nozzle occluded, and the whole cylinder raised to lift a column of water 8cm above the surrounding free surface. Occlusion of the nozzle was then released, allowing entrance of air through the nozzle and steady descent (at about 50cm/s) of contained water into the tank. This resulted in formation of a ring vortex moving down into the tank from the cylinder – but invisibly unless a suitable marker was introduced. Two types of marker were used:

Black ink (diluted with an equal quantity of water and kept at room temperature). This was introduced carefully, via a slightly bent hypodermic needle, to the edges of the water contained by the cylinder before it was raised and released. The resulting ring vortex was photographed from one side against a white background (Figure 3.8a, opposite).

White polystyrene spheres, 0.2mm in diameter, were wetted and attached by moisture to the inner walls of the cylinder before positioning in the tank. These particles, then suspended in fluid that formed the ring vortex, were photographed (at a shutter speed of $1/30^{th}$ sec) against a dark background (fig 3.8b).

Results

The ring vortex containing ink appears as a multi-veiled doughnut. It is generated beneath the lower rim of the cylinder as ink layers move in relation to the relatively still fluid of the tank. As it does so, fluid curls back on all sides to generate the doughnut form that separates from the cylinder to travel down the tank. Ink-marked

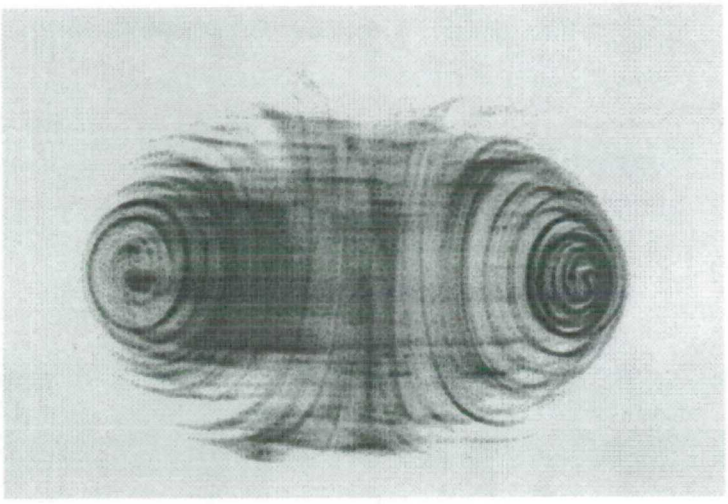
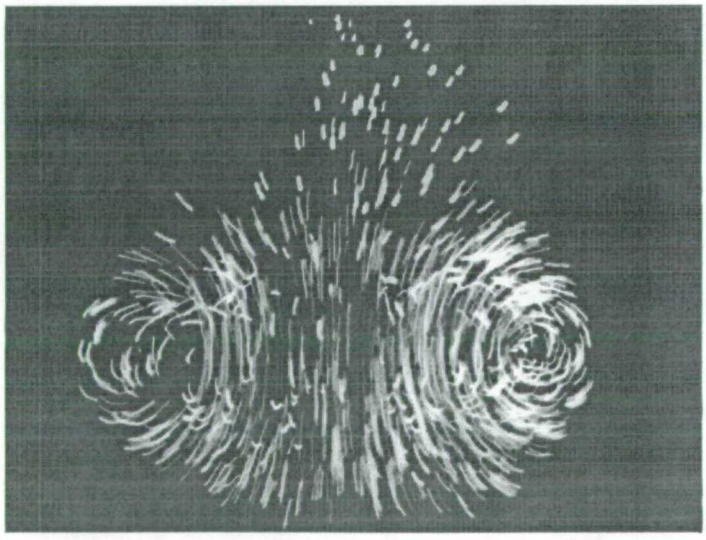


Figure 3.8
Above: **(a)** A ring vortex, 6cm across, marked with ink., photographed from one side.
Below: **(b)** A similar ring vortex marked with suspended particles.



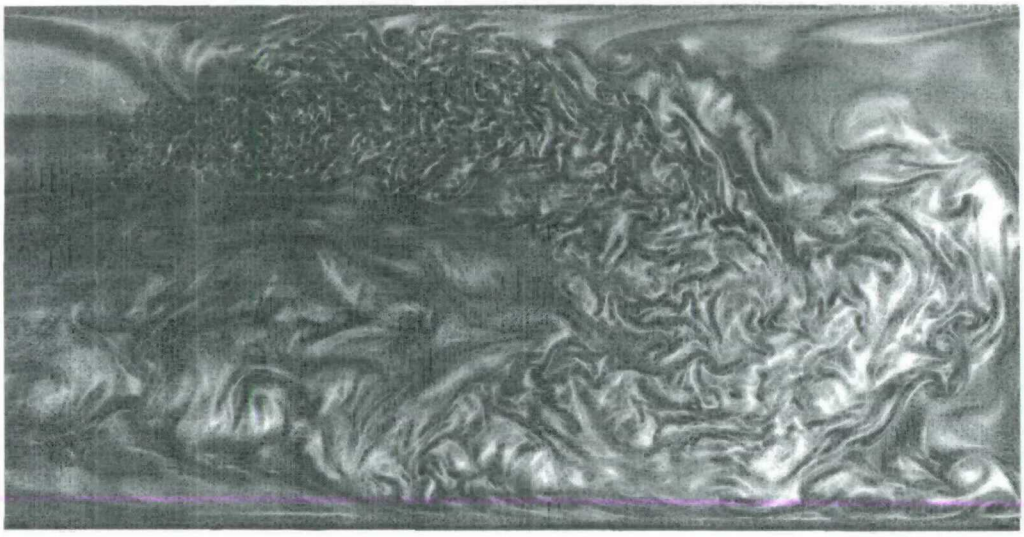


Figure 3.9 Turbulent flow, visualised using a suspension of fine, light-reflecting flakes. Flow from a tube, top left, into a shallow trough is photographed from above.

fluid makes up part of the ring vortex – but clear water, entrained from adjacent layers, also becomes wrapped in as the whole progresses downward, thus gaining steadily in total volume. The ring vortex, if generated at a suitable rate, conserves momentum remarkably efficiently, progressing steadily down the tank.

The ring vortex marked with particles and photographed at a $1/30^{th}$ sec exposure (fig 3.8b) gives insight into velocity distributions within the structure. Relative to the camera fixed on a tripod outside the tank, highest velocities pass down the centre, with some reversal of velocity in outermost regions of the ring. (A camera moving down at the same rate as the whole ring vortex would give a different picture, with apparently lower central velocities and higher reversed velocities). Velocity down the middle of the ring, estimated to be about 25cm/sec from lengths of streaks on the photograph, was approximately twice that of progress of the whole structure.

The examples photographed were generated from a rate of fluid descent that gave a relatively stable ring vortex. At a much lower inflow rate (lower Reynolds number), initial momentum may be insufficient to maintain the dynamic structure, and convective and diffusive fluid movements gradually distort the form. At a higher rate (higher Reynolds number) secondary flows within the shear structure of the vortex induce more complex movements. These may initially adopt regular formations with multiple radial symmetry, but they readily deteriorate to more chaotic disorder where velocity gradients are high. A ring vortex that degenerates in this way fails to conserve its (greater) momentum, and both form and forward momentum disperse rapidly.

Comment

The dynamic form of the ring vortex may be relevant to flow through the heart. Passage of blood through all four heart valves into the cavity or sinus beyond gives rise to flow structures akin to that of the ring vortex, though modified in each of these cases by containing boundaries.

Visualisation of turbulent flow

Method

A suspension in water of fine metallic dust-like flakes allows visualisation of turbulent flow (Figure 3.9, opposite). The material used was a metallic paint pigment (Pale Gold Bronze Powder supplied by Cornellisen and Son Ltd, 105 Great

Russell Street, London WC1B 3RY). The metallic flakes, about 0.01-0.1 mm in length, have a tendency to align with planes of shear within the fluid, spending more time parallel to streamlines than not. If illuminated from a single source, reflection of light from surfaces of flakes, and absorption of light where flakes lie edge-on, gives a depiction of patterns of shear.

This type of flow visualisation was used to provide a photograph of turbulence of varying intensity. A hollow trough was set up with flow of the aqueous suspension into it through 12mm tubing at a rate of 4l/min, giving a Reynolds number (Re) of over 5,000 in the tube, and turbulent flow into the trough. A single outlet, at the same end of the trough as the inlet, was adjusted to maintain a depth of about 2cm.

Comment

The intensity of turbulence, as represented by spatial compactness of eddies and counter-eddies, can be seen to diminish from a maximum close to the tube inlet, to larger-scale (slower moving) eddies further down-stream in the trough. The stream itself, though containing numerous eddies and counter-eddies of turbulence, also has large-scale structure and coherence, curving round from the inlet towards the outlet (outside the field of view, to the left).

Trains of vortices in the wake of a cylinder

Method

Fluid, to a depth of 2 cm was allowed to come to rest in a flat trough. The fluid was composed of 40% glycerol and 60% water, giving a viscosity of about 0.005Ns/m^2, with fine metal flakes in suspension, as described above. A narrow vertical cylinder, 10mm diameter, was drawn steadily in a straight line through the fluid using a sliding jig, draw string and rotor turned at adjustable steady rates by an electric motor. Rates of linear movement were adjusted between about 2cm/s (Figure 3.10 a) and 70cm/s (Figure 3.10c), and resulting surface flow patterns in the wake of the cylinder photographed, using an exposure time of 1/125th sec.

Results

Resulting photographs are shown in Figure 3.10 (opposite), with increasing linear velocities of cylinder movement from above downwards. They illustrate a sequence of states or patterns of flow in the wake of the cylinder. Sedimentation patterns in fluid outside the wake are incidental.

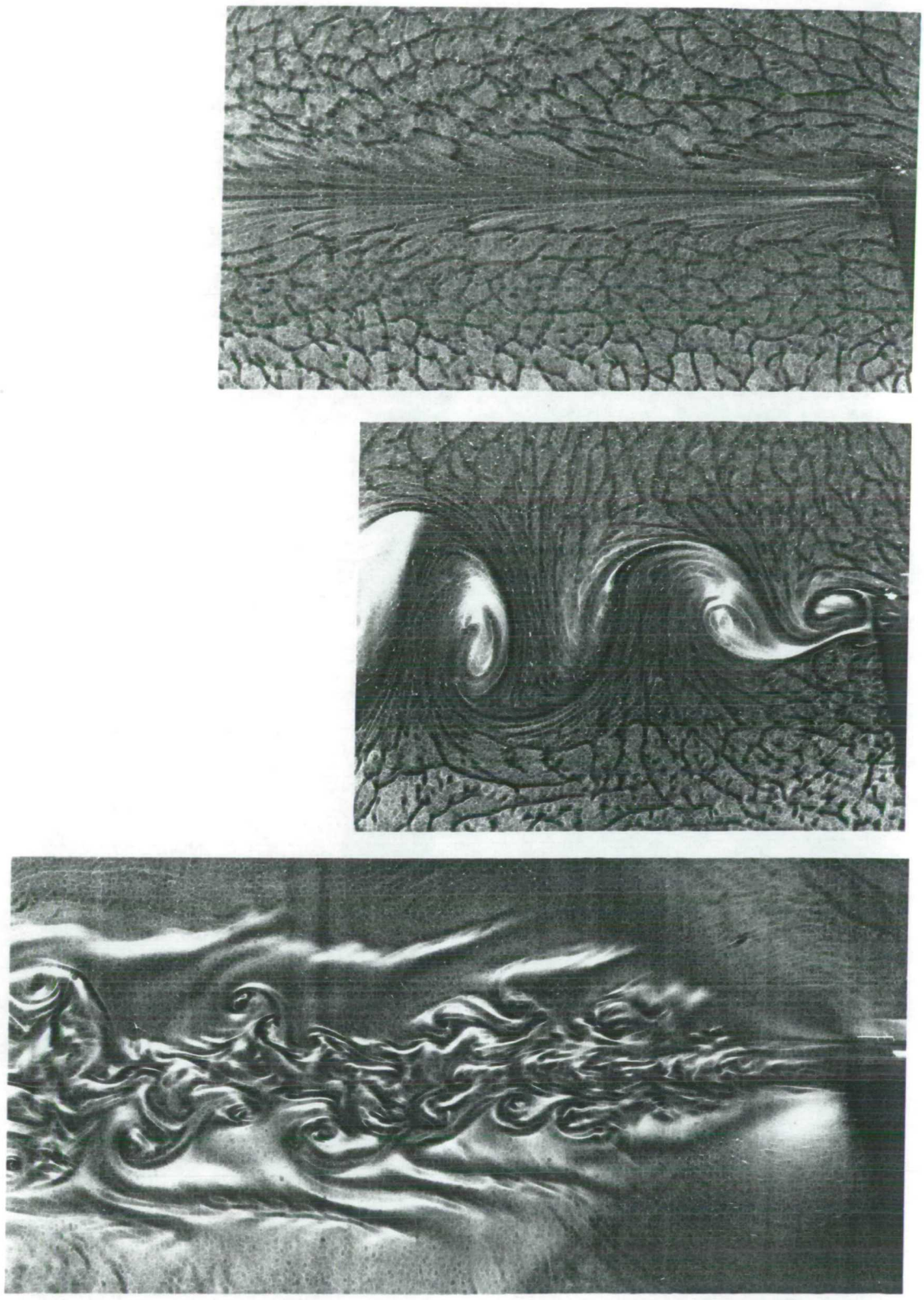


Figure 3.10a-c Patterns of flow in the wake of a cylinder moved at different speeds in a straight line through a trough of fluid marked with suspended light-reflecting flakes. See text.

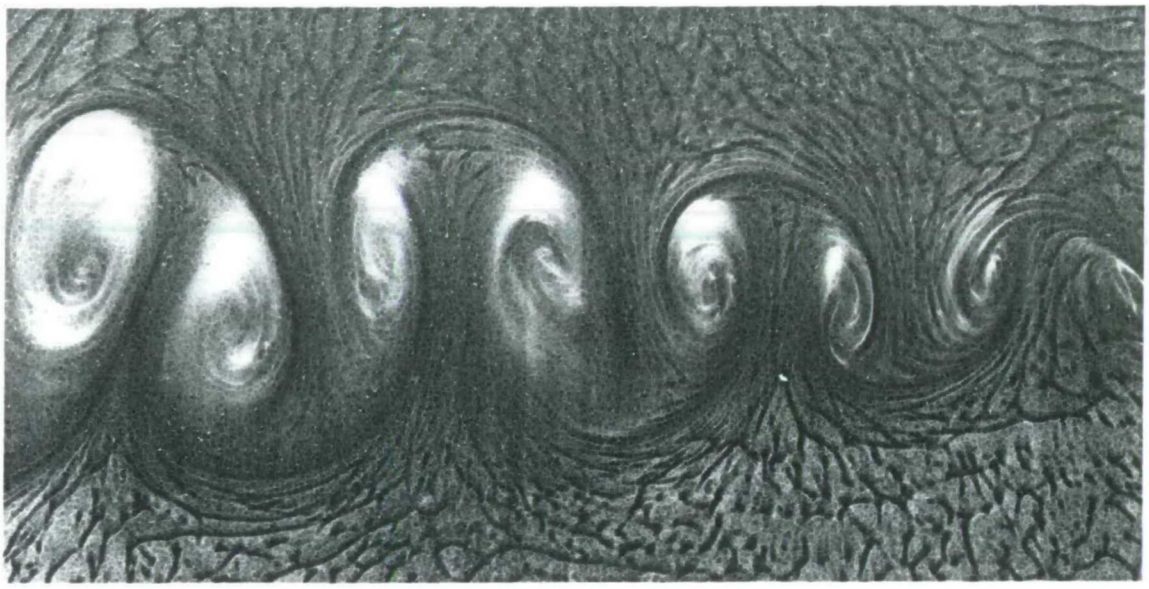


Figure 3.10d Alternating vortices shed in the wake of a cylinder moved steadily in a straight line, as in Figure 3.10b on the previous page.

Figure 3.10a shows a nearly laminar fluid wake. There is stable, localized separation of streamlines bilaterally from trailing curvatures of the cylinder, but symmetry of streamlines is unbroken, and the wake forms in a straight line.

Figure 3.10b shows an intermediate state in which trailing vortices oscillate regularly, with periodic shedding that leaves expanding, alternating vortex systems in the wake of the cylinder. A further photograph of this type of wake is shown in Figure 3.10d, overleaf.

Figure 3.10c shows a complex pattern of eddies in the wake of the rapidly moving cylinder. The linear velocity of the cylinder was approximately 1.5m/s, giving a Reynolds number of the order of 3,000.

Comment

The sequence of photographs illustrates a series of progressively complex flow patterns between laminar and turbulent states. Analysis of the fluid mechanics involved in transitional steps or 'bifurcations' - from laminar flow, through flow separation, symmetry-breaking, vortex shedding, onset of chaotic complexity and turbulence - is beyond the scope of this chapter. What can be seen is that there is an intermediate state of coherent and, in this case, temporally and spatially *rhythmic* flow between laminar and turbulent states. In contained flow systems, appearance and persistence of this type of coherent, large-scale secondary flow structure tends to be excluded by straight, rigid boundaries such as those of Reynolds' tube, described on P 43. Appropriately curved and compliant boundaries, however, such as those of Flowform variants, (Figures 3.1-3.7) and perhaps those of heart cavities, may accommodate and stabilise vortical flow structures so that coherent, cyclic topologies occur, even where there may also be turbulence within the larger-scale flow structure (Figures 3.1 and 3.2). Flow through heart cavities may characteristically occupy this intermediate state. The central vortex pair in Figure 3.10d, opposite, formed through relatively free, unconfined fluid movement, can be compared with patterns of flow through the mitral valve in diastole (see Figure 4.14, opposite p61). Forms of heart valves and cavities may be streamlined not for laminar, but for coherent, multi-directional secondary patterns of flow.

Flow in symmetric and asymmetric cavities.

Method

Two hemi-hour-glass forms, each 10cm in length, were shaped in beaten copper, each designed to contain 20ml of water when half filled. Both forms could be rocked in see-saw fashion about a horizontal axis passing through their narrow points (the axis passes horizontally across the middle of the photograph in Figure 3.11) so that water flowed back and forth through the central stricture, filling cavities in rhythmic alternation. Both double-forms were designed to have similar dimensions, and a similar size and shape of orifice between cavities, except that one was symmetrically shaped about its long axis, whereas the other was asymmetric, as shown in Figure 3.11. White polystyrene spheres, 0.2mm in diameter were sprinkled as markers on the water surfaces, and photographed from above with an exposure of 1/30s while water was flowing from one cavity to the other during steady rocking.

Result

The photograph in Figure 3.11, opposite was taken while flow was passing from cavities seen above to those below. Flow through the symmetric opening appears more disordered, with irregular velocity vectors (up to about 50cm/s) close to the orifice. Although induced by the same rocking movement, higher velocities are distributed more widely and coherently in the asymmetric form, with a single dominant swirl in the receiving cavity. There was less lingering of particles in extremities of the asymmetric form during rocking. After cessation of rocking, swirling movement continued for at least a second in the asymmetric form, whereas fluid movements ceased more rapidly, through turbulent dissipation of kinetic energy, in the symmetric form.

Comment

This simple model gives visual demonstration of a principle that has been recognised in relation to flows in natural and artificial heart chambers and ventricular assist devices. It has also been considered in relation to orientation of atrio-ventricular valves: asymmetry of inflow with respect to a chamber fosters relatively stable intracavity flow that minimises residence times and tends to conserve the momentum and energy of inflow. Rotational momentum resulting from asymmetric inflow, if conserved until outflow, contributes to asymmetry and stability of flow in the following cycle.

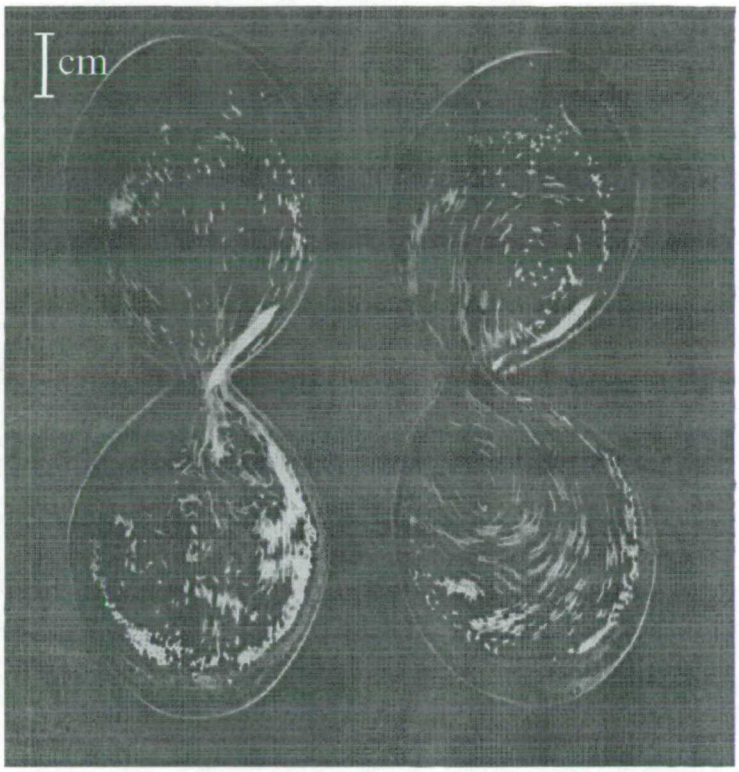


Figure 3.11 Flow between symmetrically and asymmetrically shaped cavities induced by rocking. Movements of suspended particles show more coherent, swirling flow in the asymmetric form.

Attention is drawn to the potential relevance of these observations to cavity asymmetry that arises through looping of the vertebrate heart. Flow patterns in cavities of the human heart are illustrated in the next chapter. Cavity asymmetry could contribute to stability of flow, minimising dissipation of energy through turbulence, especially in more rapid flows and phase changes of the exercising heart.

Papers bound at end of thesis –content in relation to Chapter 4

1) Kilner PJ, Wann LS, Firmin DN and Longmore DB (1989) Three directional magnetic resonance flow imaging of the human heart. *Dynamic Cardiovascular Imaging* **2**, 104-109.

This paper introduces three-directional velocity measurement by magnetic resonance. It illustrates an *in vitro* validation study of velocity mapping using a rotating disc phantom.

2) Firmin, D.N., Nayler, G.L., Kilner, P.J. and Longmore, D.B. (1990) The application of phase shifts in NMR for flow measurement. *Mag. Reson. in Med.* **14**, 230-241.

This paper gives background to magnetic resonance velocity measurement. It describes and illustrates factors effecting the accuracy of phase velocity mapping and reports results of an *in vitro* validation study using continuous tube flow.

3) Kilner, P.J., Yang, G.Z., Mohiaddin, R.H., Firmin, D.N. and Longmore, D.B. (1993) Helical and retrograde secondary flow patterns in the aortic arch studied by three-directional magnetic resonance velocity mapping. *Circulation* **88**, 2235-2247

This paper reports use of three-directional phase velocity mapping for study of multi-directional patterns of flow in the aortic arches of healthy volunteers.

4) Yang GZ, Kilner PJ, Wood NB, Underwood SR and Firmin DN (1996) Computation of flow pressure fields from magnetic resonance velocity mapping. *Magnetic Resonance in Medicine* **36**, 520-526.

This paper relates to studies reported in chapter 5. It includes *in vitro* phantom studies in which results of velocity mapping were used to derive differences of pressure.

5) Kilner PJ, Henein MY and Gibson DG (1997) Our tortuous heart in dynamic mode - an echocardiographic study of mitral flow and movement in exercising subjects. *Heart and Vessels* **12**, 103-110.

This paper relates to echocardiographic studies reported in chapter 6.

Chapter 4

Spatio-temporal patterns of flow through the heart studied by magnetic resonance velocity mapping

Objectives

The aim of this chapter is elucidation of large-scale spatio-temporal patterns of flow through all four chambers of hearts of resting volunteers using magnetic resonance phase velocity mapping.

Background

The peculiarly tortuous arrangement of streams through the human heart can be appreciated by comparison with hearts of invertebrates, described in chapter 2. Potential functional implications of curvatures and asymmetries of heart chambers have been considered in chapter 3, and a further important aspect will be addressed in chapter 6. Relatively little in vivo research has been done, however, on spatio-temporal patterns of flow through chambers of the heart, particularly with chambers studied in relation to one another as a functional unit.

Compared with other available techniques, magnetic resonance phase velocity mapping is capable of providing, non-invasively, remarkably comprehensive flow velocity data. As long as care is taken to control or eliminate potential artefacts (Firmin et al. 1990, Buonocore and Bogren 1992), the technique allows measurement of blood velocity in vitro and in vivo (Firmin et al. 1987, Kilner et al. 1991, 1993 and 1996, Kim et al. 1995). Phase velocity mapping can measure X, Y and Z components of velocity, with good spatial and reasonable temporal resolution, cine frames typically being 30-60ms apart, in voxels throughout a plane or volume of acquisition. The information is not acquired in real time, but phasic variations of velocity are recorded by acquisition of data over many cardiac cycles at a series of different delays after the R-wave of the ECG. An average cardiac cycle is thus represented by a sequence of cine frames.

Data can be acquired in oblique planes in any orientation, unrestricted by windows of access, with measurement of components of velocity in and/or through the image plane. Magnetic resonance is the only imaging modality with the potential to acquire comprehensive, that is to say 4-dimensional (space-time) and 3-directional (3 orthogonal vector components) velocity information (Firmin et al.1990). At the present

stage of development, however, constraints of time, software and hardware mean that compromises have to be made. For example, in most of the studies presented in this chapter, data was acquired in selected planes rather than volumes, with 16 to 20 cine frames per cycle. Velocity was encoded in all three orthogonal directions.

A preliminary study, describing use of magnetic resonance to record all three directional components of velocity in a through planes cutting right atrium and left ventricle, was published in 1989 (Kilner et al.1989 - bound at end). A more thorough study of flow in the aortic arch (Kilner et al.1993 - bound at end) correlated velocity information in and through several planes, establishing the general approach taken in this chapter. In-plane velocity distributions were displayed as flow vector maps, computed from vertically and horizontally directed velocity measurements in the image plane. Through-plane velocity components were displayed as grey-scale images. On the basis of velocity data acquired in several planes, typical multidirectional flow patterns in the aortic arch at different phases of the cycle were illustrated (figure 4.1) – not by computation, but by graphic interpretation of mentally correlated velocity and vector map data. This approach requires facility for 3-D conceptualization together with appropriate experience and training. My own preparation included practice in representational drawing and sculpture, and studies of cardiovascular anatomy and experimental fluid dynamics, including design of water sculptures. The aortic flow data was studied repeatedly before attempts were made to represent principal features of what is effectively 7-dimensional flow (3 spatial, 1 temporal and 3 velocity 'dimensions') on the 2-dimensional page. The drawings depicting flow through the whole heart at the end of this chapter are similarly based on mental assimilation and correlation of data from cine velocity map acquisitions.

A group working in Aarhus in Denmark undertook 3-directional magnetic resonance velocity mapping of left ventricular flow (Kim 95 et al.). The study is relevant to this chapter. It showed vortex formation in the left ventricle during both early and late diastolic filling phases, and demonstrated repeatability of this type of flow study. The study provided time curves of velocities recorded at pulmonary venous, mitral inflow and aortic outflow locations. But only a single, oblique long-axis plane was investigated, aligned with mitral and aortic valves and the long axis of the left ventricle, as illustrated in Figure 4.12. This plane revealed a single dominant vortex developing during diastolic filling, rotating beneath the anterior mitral leaflet towards the outflow tract, with a smaller vortex curling back, in some cases, beneath the



Figure 4.1
Drawing of patterns of flow in the aortic arch, based on magnetic resonance flow studies (Kilner 1993, bound at end). During early systolic acceleration (left) vectors are axially directed, with highest velocities near the inside of the arch. By late systole (centre) helical secondary flows have developed, with reversal of direction in the separation zone beyond the arch. In early diastole (right) rotational and retrograde blood movements persist, with little mean flow.

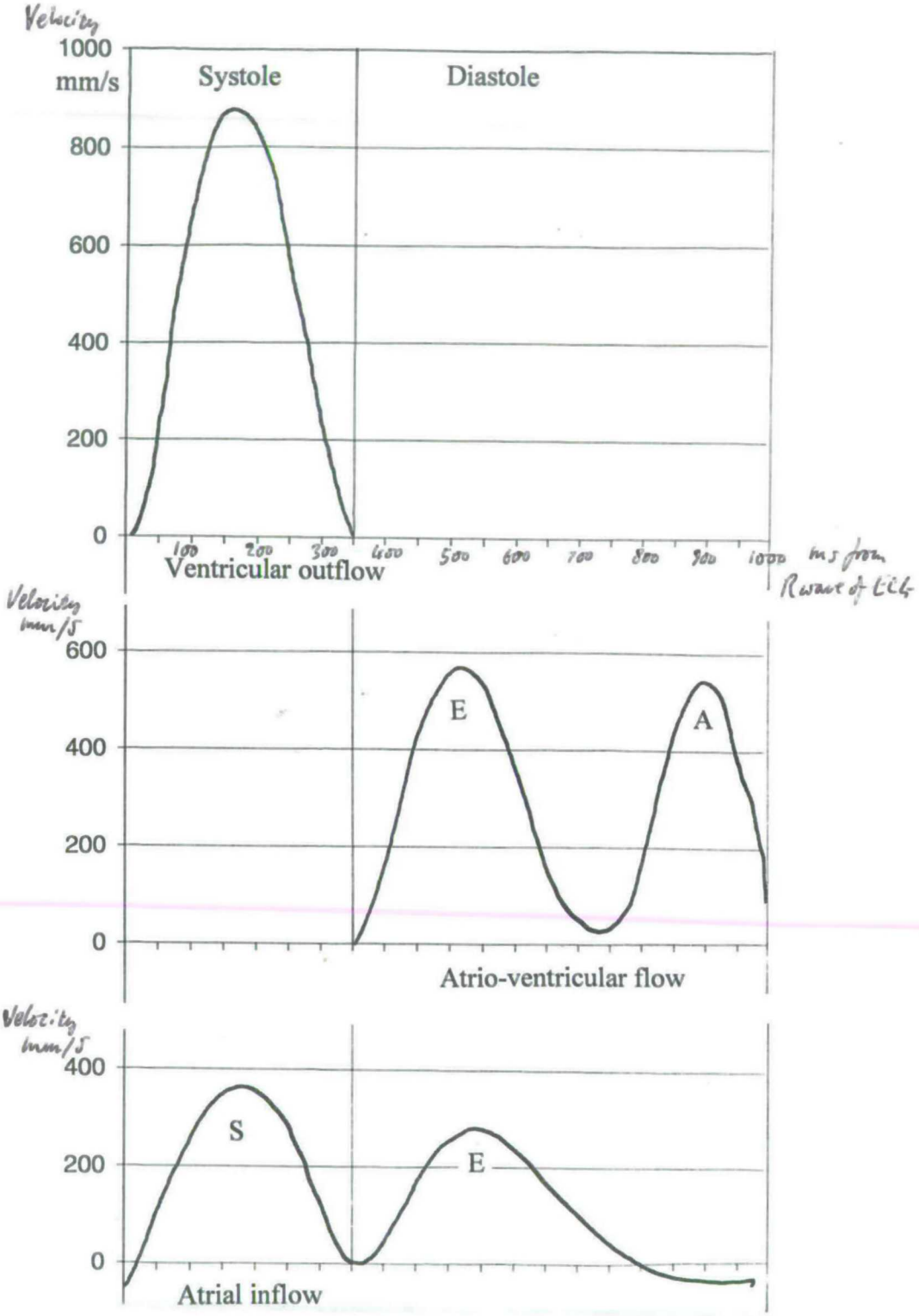


Figure 4.2
Diagram of flow curves in and out of heart chambers at rest

posterior leaflet. The maximal kinetic energy of rotational movements of the anterior vortex, in the plane studied, was calculated to be $4.3x10^{-4}\pm7.1x10^{-5}$J. This small amount of energy was concluded to be insignificant in relation to the total stroke work output of the left ventricle (~1 J/beat) Furthermore, the vortex was found to have lost most of its limited kinetic energy by the time of isovolumetric contraction, just before ventricular ejection.

The study confirmed the presence of vorticity during filling of the left ventricle, with its potential contribution to efficient mitral valve closure. The calculations dispelled any illusion, however, that the anterior vortex carried significant energy between inflow and outflow in the resting heart. But the study measured flow in only one plane of the 3-dimensional volume of the chamber, and did not consider altered timings and dynamics with exercise. Furthermore, the approach of calculating only vortical (rotational kinetic) energy from velocities in a single plane is inherently limited. Kinetic energy of mitral inflow presumably also contributes to distension of the ventricle. It thus contributes to outflow, not only through conservation of kinetic energy and interchange with myocardial elastic potential energy, but also, according to Starling's law (Noble 1978), by priming myocardial fibres for their systolic contraction. This potentially important aspect of inflow dynamics, which would take on greater importance with exercise, was not considered.

The present chapter does not attempt to go so far either, but rather attempts to elucidate large-scale spatio-temporal patterns of flow through the four heart chambers. Pressure differences associated with momentum changes will be considered in chapter 5. In the present chapter, flow fields of the four chambers will be studied one at a time, and in relation to one another as a functional whole.

Temporal patterns of filling and ejection

Before illustrating spatial flow patterns through different phases of the cycle, it will be helpful to clarify temporal patterns of inflow and outflow of each heart chamber. These flow curves have been studied previously by Doppler ultrasound and magnetic resonance velocity mapping, and can be useful diagnostically as the curves change with ventricular and pericardial disease (Appleton *et al.* 1987-1988, Mohiaddin *et al.* 1991). Figure 4.2, opposite, displays typical healthy atrial and ventricular inflow, and ventricular outflow curves. The illustration is based data from the magnetic resonance and Doppler ultrasonic studies described in this and the next chapter, which show general agreement with data published by others (Appleton *et al.* 1987-1988, Mohiaddin *et al.* 1991, Kim *et al.* 95).

At atrial inflow level, a first peak coincides with ventricular systole (the 'S' peak) – atria expand as ventricles contract - and a second peak coincides with early ventricular diastole (the 'E' peak). The E peak coincides with the E peak of atrio-ventricular flow, induced, in part at least, by elastic recoil of ventricular muscle in early diastole. The S peak tends to be more dominant on the right side of the heart, and the E-peak on the left.

At ventricular inflow level, there is no flow through the atrio-ventricular valves during ventricular systole, although some movement of blood up- and down-stream accompanies movement of the valve rings. Flow through the valves begins with the E peak of early diastole. There is decline of velocity in mid diastole (mid diastolic diastasis), followed by a second peak of flow in late diastole, at the time of atrial contraction (the A peak). The atrio-ventricular valve rings move back towards the atria in diastole, as ventricles relax. This means that slightly more blood passes relative to each valve, particularly the tricuspid, than might be registered by diastolic measurement of velocities relative to the chest. Left atrio-ventricular flows and movements, recorded echocardiographically, are illustrated and measured in Chapter 6, with attention drawn to important changes of their magnitude and time course with exercise.

The magnetic resonance acquisitions reported in the present chapter were prospectively gated from the R-wave of the ECG, with frames spanning systole and most of diastole. The phase of atrial systole is not well demonstrated by this approach, although after-effects of atrial contraction are generally visible in the first frame after the R-wave, which falls during the isovolumic contraction phase of the ventricles, prior to ejection.

Chamber geometry

The geometry and spatial relations of blood spaces of the four heart chambers were studied by means of post-mortem casts (Tompsett 1970, Kilner 1988), and magnetic resonance tomographic and 3-D angiographic data. A brief description of the shape of each chamber will be given before results of flow studies.

Magnetic resonance velocity mapping

Magnetic resonance phase velocity mapping was used to acquire data on blood flow velocities in three orthogonal directions (Kilner 1989, 1993 ii, Kim 1995) in- and through planes selected to cut each chamber of the heart. Data were acquired in 22 healthy adult volunteers, listed in Table 4.3a, in planes listed in Table 4.3b.

Table 4.3

a) Subjects studied

No.	m/f	age
1	m	34
2	m	46
3	f	32
4	m	34
5	f	29
6	m	31
7	m	35
8	m	36
9	f	26
10	m	34
11	m	49
12	m	56
13	m	51
14	f	26
15	m	31
16	m	39
17	m	37
18	m	38
19	f	42
20	f	32
21	m	35
22	m	26

b) Planes studied by velocity mapping		Subjects
Coronal, 5 contiguous (all chambers)	(n=2)	1,2
Sagittal, 5 contiguous (right atrium +)	(n=1)	1
Sagittal, mid right atrium	(n=6)	1,2,3,5,16,22
Transaxial, mid right atrium	(n=2)	1,9
Oblique coronal, right atrium-ventricle	(n=3)	1,2,7
Coronal, left atrium	(n=4)	1,2,10,20
Straight sagittal, left atrium	(n=1)	1
Oblique sagittal, aortic arch plane	(n=10)	1,3,4,7,16,17,18,19,20,21
Left ventricle – vertical long axis	(n=8)	3,4,6,8,11,12,13,14
Left ventricle – horizontal long axis	(n=9)	2,3,4,6,8,11,12,13,14
Left ventricle – oblique long-axis	(n=7)	1,2,3,6,9,10,15
Left ventricle – short axis, below mitral v.	(n=9)	1,2,3,4,6,8,9,12,13

Velocity maps in selected planes are illustrated and described in the following pages. Due to limited space, velocity data from one subject only will be illustrated for most planes. To give visual comparison of intra-cavity flow between subjects, right atrial filling patterns in four different subjects are illustrated in Figure 4.8, and planes through the left ventricle can be compared between subject 3 (Figures 4.12 and 4.13) and subject 9 (Figure 4.14). Major flow features illustrated can be taken as representative, although detailed features and proportions varied between subjects, probably about as much as anatomical features and proportions vary between individuals.

Two magnetic resonance systems were used, both capable of phase contrast velocity mapping. Most studies were acquired using a 0.5 Tesla Picker magnet with modified gradient coils and a surface receiver coil, operated by a Surrey Medical Imaging Systems (SMIS) computer with software written in-house. A 1.5 Tesla Picker Edge system with commercially available cardiovascular imaging software was used for studies later in the series. All data were acquired with subjects at rest, lying supine in the magnet

Three-directional cine velocity mapping was performed using gradient echo sequences with echo times of 14ms in the 0.5T magnet, (Firmin *et al.* 1990, Kilner *et al.* 1993 i and ii) or 4.4ms in the 1.5Tmagnet (Kim *et al.* 1995). Slice thickness was 8-10mm, field of view 40cm, with 2 averages of 128 phase encoding steps. On the 0.5T system, reference and (x/y/z) velocity encoded data were acquired in successive heart beats over the acquisition period, which was relatively prolonged, taking 15-20 minutes for all 3 velocity components in a single plane, depending on heart rate (Kilner *et al* 1993, ii). The 1.5 Tesla Picker Edge system, allowed sequential acquisition of reference and velocity data within about within 15ms of each other in each heart beat. This allowed complete velocity map acquisitions (x and y, or z) in about 4 minutes per plane (Kim *et al* 1995). Velocity maps were generated by subtraction of reference from velocity encoded phase images. Each directional velocity map consisted of sixteen or more cine frames gated prospectively from the R-wave of the ECG, distributed through systole and most of diastole, successive cine frames being at 40-60ms intervals, depending on heart rate.

Data Analysis

Flow data were stored and studied in three forms:

1) Original magnetic resonance velocity map format, with velocity in each direction displayed as grey-scale images (as in Figure 4.6). These were viewed at the console in cine mode, or analysed frame by frame, using a cursor to interrogate pixel values in different regions. Standard software allowed profiles of velocity along any chosen line to be drawn, or temporal variations of velocity in a selected region to be plotted.

2) Software written by GZ Yang (Yang et al. 1992) was used to combine x and y velocity data in a given plane to produce cine vector maps displaying magnitudes and directions of flow in an image plane (Figures 4.6 - 4.14). Local vectors are depicted as tapered streaks, the thick end pointing in the direction of flow, extending from points distributed in a rectangular matrix. The length and direction of each streak represents in-plane velocity at the point of origin. Vector maps can be viewed frame by frame or in cine mode at a computer console.

3) Software was also written by GZ Yang for viewing 3-directional velocity vectors aquired in 5 contiguous slices through the heart. Vectors in and through all 5 planes were displayed as tapered streaks extending appropriately from a 3-dimensional rectangular matrix. The whole display was viewed using 3-D paralax spectacles which allowed images with slightly different rotations to be admitted to each eye in rapid alternation. The whole vector matrix, viewed a frame at a time, could also be rotated at will, and viewed in cine mode in any chosen orientation (Figure 4.4).

Results

Figure 4.4 shows a single photographic exposure which captures both left- and right-eye views of the sagittal multislce 3-dimensional study of right atrial flow. Figures 4.6-4.14 show selected frames form in-plane (x-y) velocity vector map or through-plane (z) velocity map acquisitions. Where multiple phases of the cardiac cycle are displayed, they are arranged with systolic frames from left-to-right in the upper row, and diastolic from right-to-left in the lower row. Images representing a similar phase and similar plane in four different subjects are shown in Figures 4.8. The four chambers are illustrated and then described in the following sequence: right atrium - right ventricle - left atrium - left ventricle. Overall cardiac flow patterns, deduced from correlation of different studies, are illustrated at the end of the chapter, in Figures 4.15 and 4.16.

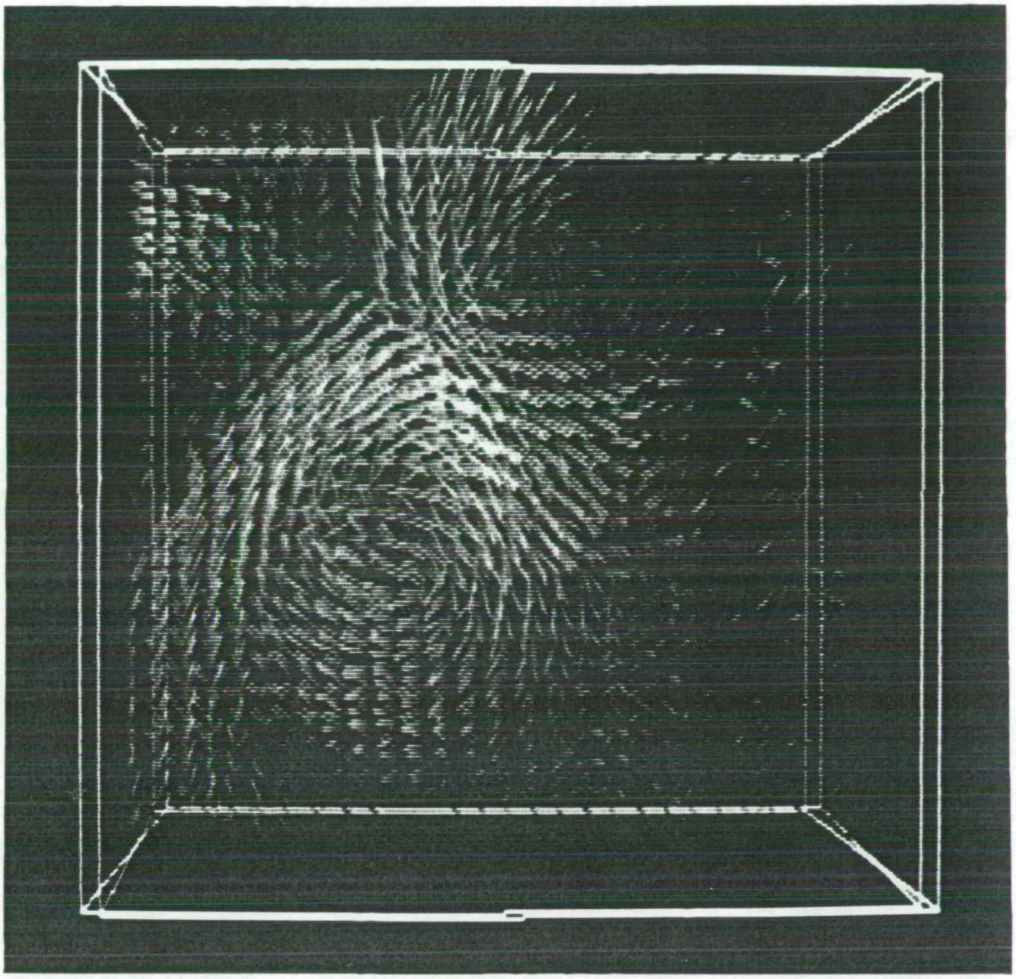


Figure 4.4 Three-dimensional view of flow in the right atrium, viewed from its right side (subject 1). This photographic exposure shows both left- and right-eye views of a three-dimensional display of flow vectors in 5 contiguous slices through the right atrium. At the computer console, with parallax viewing spectacles admitting different images to each eye in rapid alternation, rotational movement of blood in the right atrium, and helical passage through the tricuspid valve, were visible. Flows in both ventricles and their outflow tracts, mapped in 5 contiguous coronal slices, were similarly studied three-dimensionally. Vectors are displayed as tapered streaks, the thick end to the direction of flow.

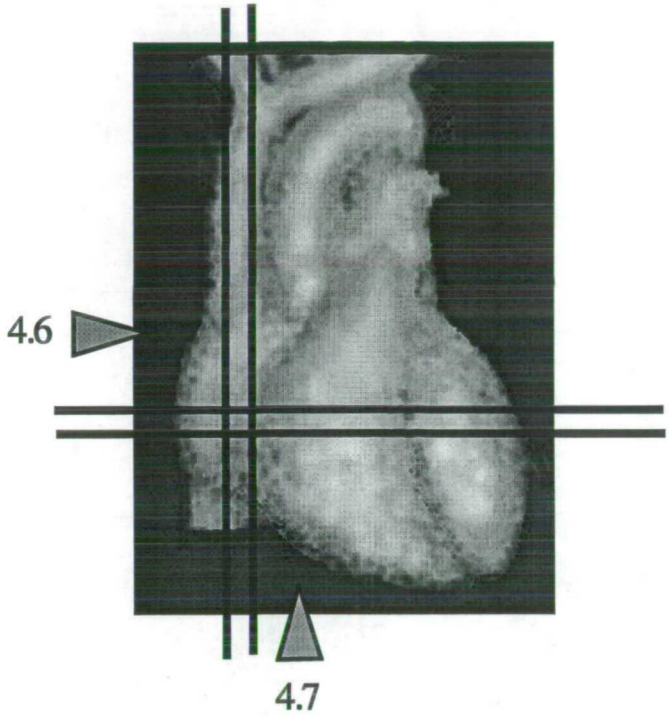


Figure 4.5
View points of sagittal and transaxial planes through the right atrium studied by velocity mapping in Figures 4.6 and 4.7

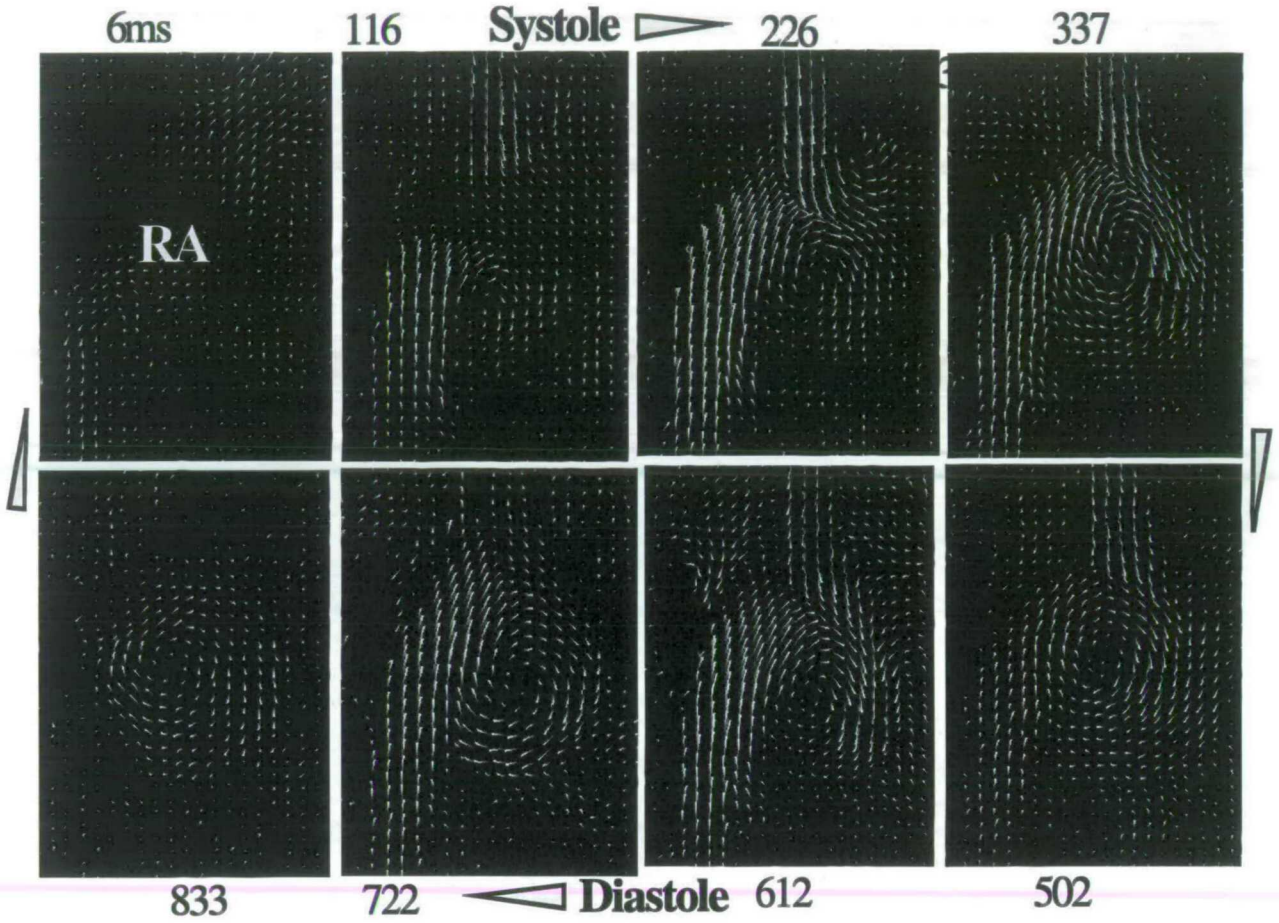
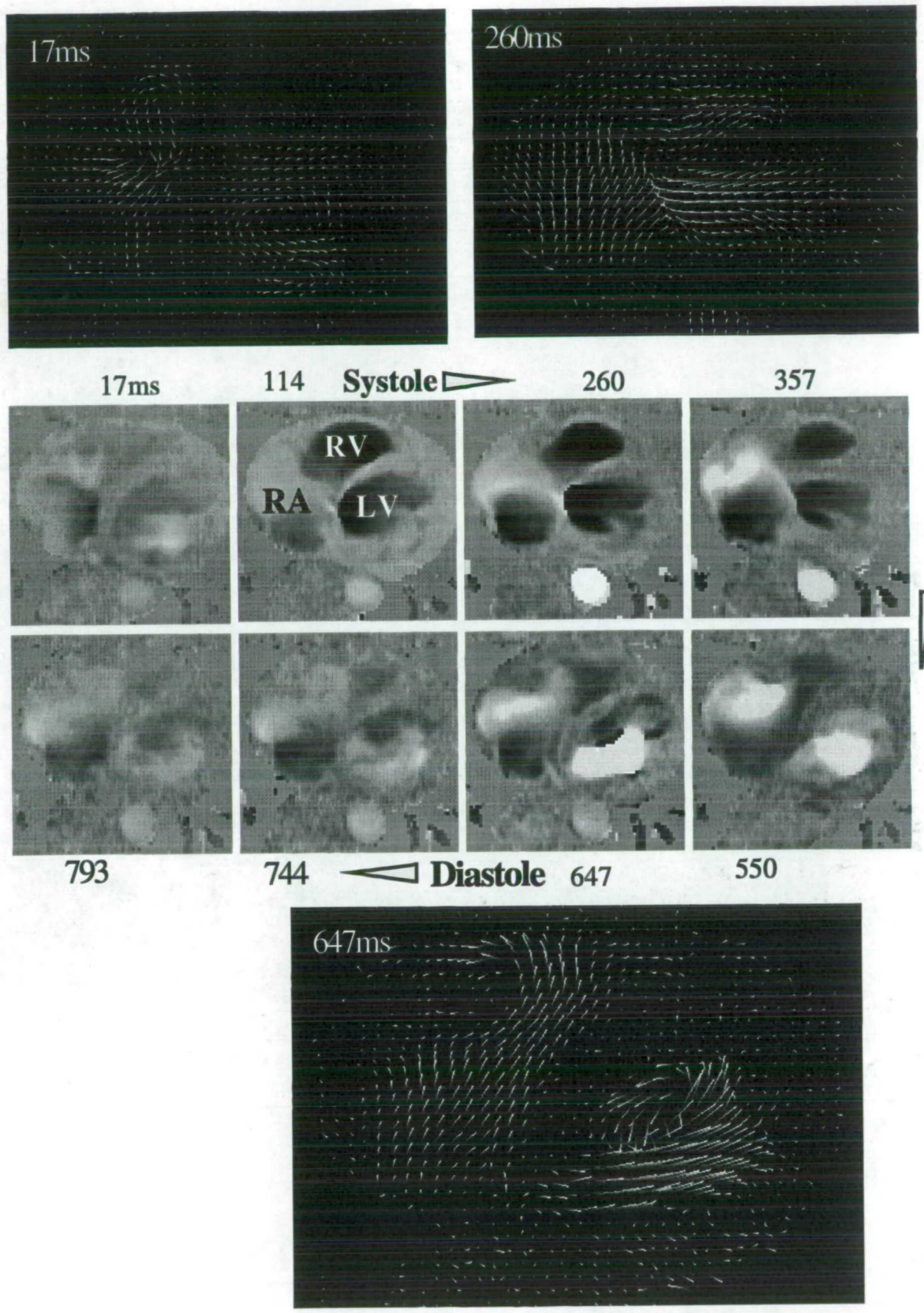


Figure 4.6 (above) Right atrial flow viewed from the right side (subject 1).
The velocity vector maps (8 of 16 frames) show filling of the atrium during ventricular systole (top row) and during ventricular diastole from the superior and inferior caval veins do not collide head on , but turn forward to feed a large forward rotating movement of blood that fills most of the right atrium in both phases of the cycle. Numbers represent the timing in ms from the R- wave of the ECG.

Figure 4.7 (opposite) Right atrial and ventricular flows in a transaxial slice viewed from below. (Subject 1). The velocity maps show through-plane velocities - black towards the head, (e.g. up the back of the right atrium) and white towards the feet (e.g . down the front of the right atrium). Vector maps at 3 phases show ventricular swirls persisting from the preceding atrial systole that contribute to atrio-ventricular valve closure (at 17ms), movements associated with ventricular systole (260ms) and early diastolic filling of both ventricles with vortices turning forward around anterior leaflets of both inflow valves (at 647ms).

60c


17ms
260ms
17ms
114
Systole
260
357
RV
RA
LV
793
744
Diastole
647
550
647ms

60d

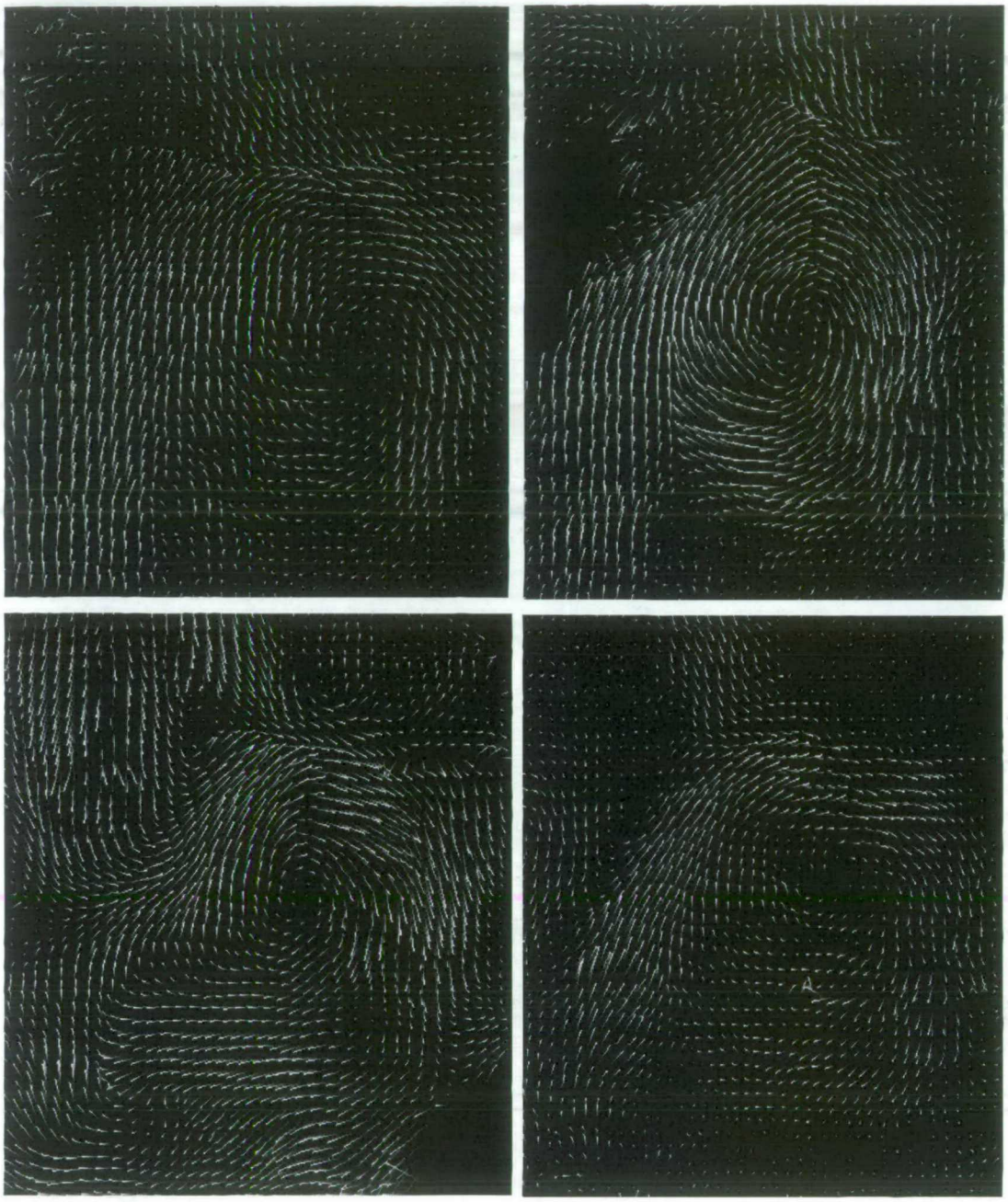


Figure 4.8 Right atrial filling patterns during late systole in four different subjects (2,1,5 and 16), all viewed in a sagittal plane from the right side. All show a forward-rotating swirl of blood in the chamber.

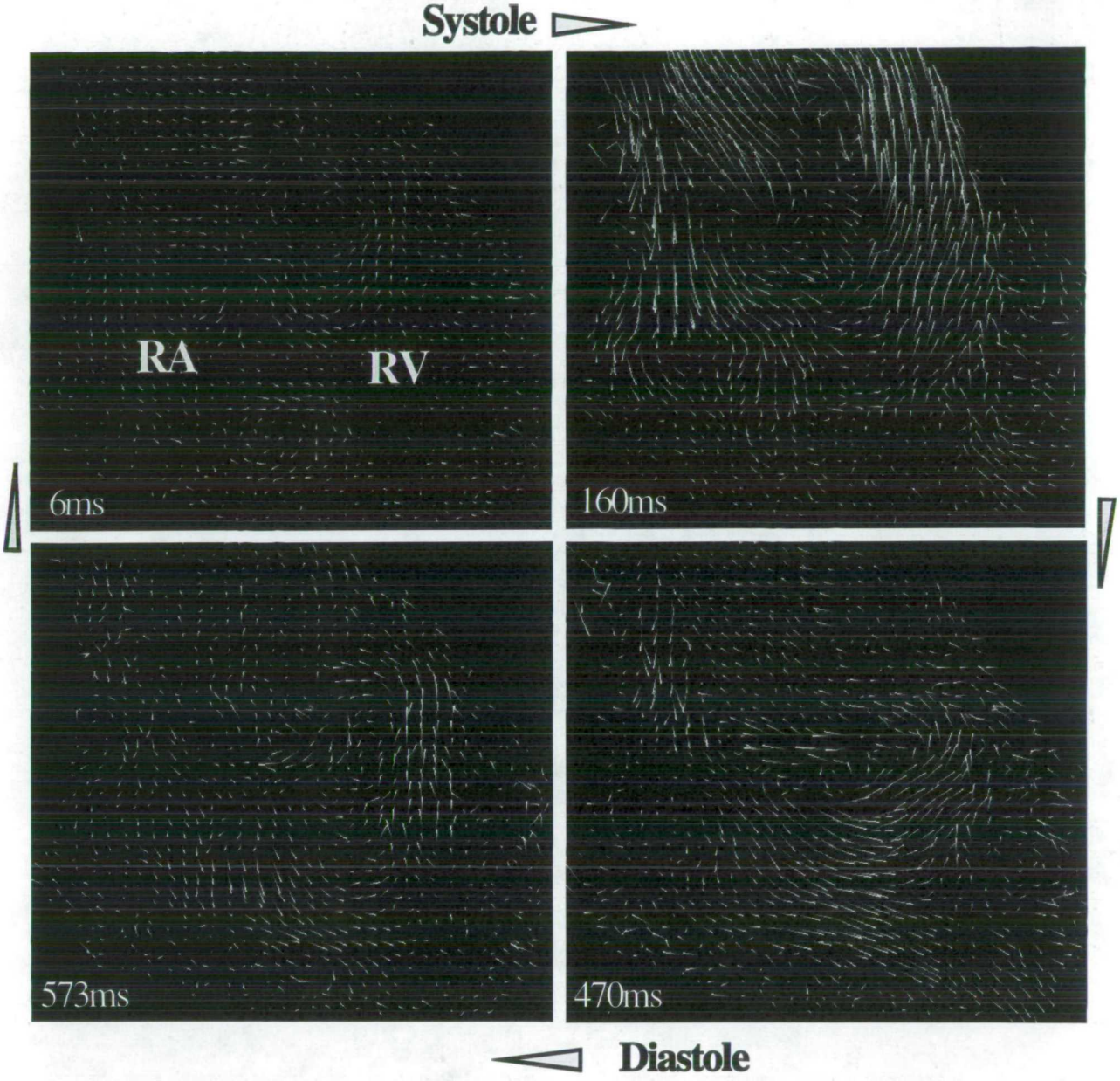


Figure 4.9 Right atrio-venricular flows viewed in an oblique coronal plane from front and right of the chest (subject 1). In the first frame (6ms), there is some flow in the right ventricle following atrial systole, with clock-wise vorticity close to the lower part of the recently closed tricuspid valve, and movent up towards the pulmonary valve. During systolic flow, at 160ms, there is inflow to the right atrium from the superior caval vein and ejection up from the right ventricle. Part of the ascending aortic flow is seen between the two. In early diastole, at 470ms , flow through the tricuspid valve turns up towards the outflow tract, and some of this movement persists in the mid-diastolic diastasis (573ms).

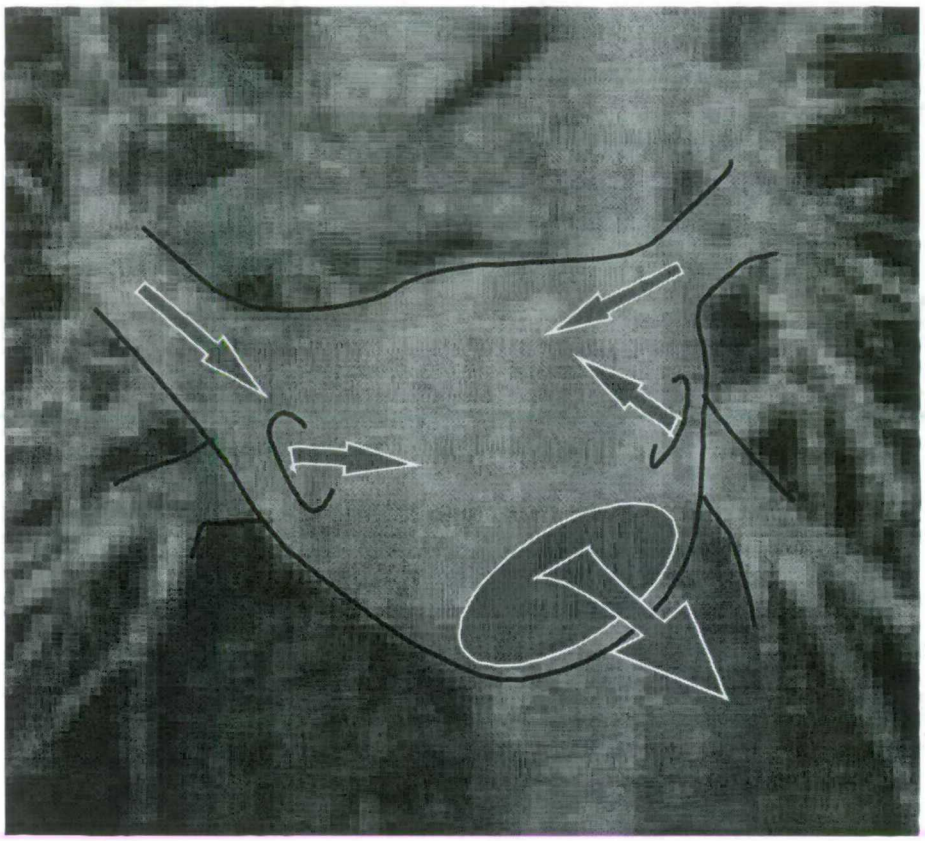


Figure 4.10 The shape of the left atrium: outlines and arrows are drawn on a magnetic resonance contrast angiogram, showing right and left pulmonary veins returning asymmetrically to the left atrium of a patient with no known cardiac abnormality. The large ellipse represents the position of the mitral valve.

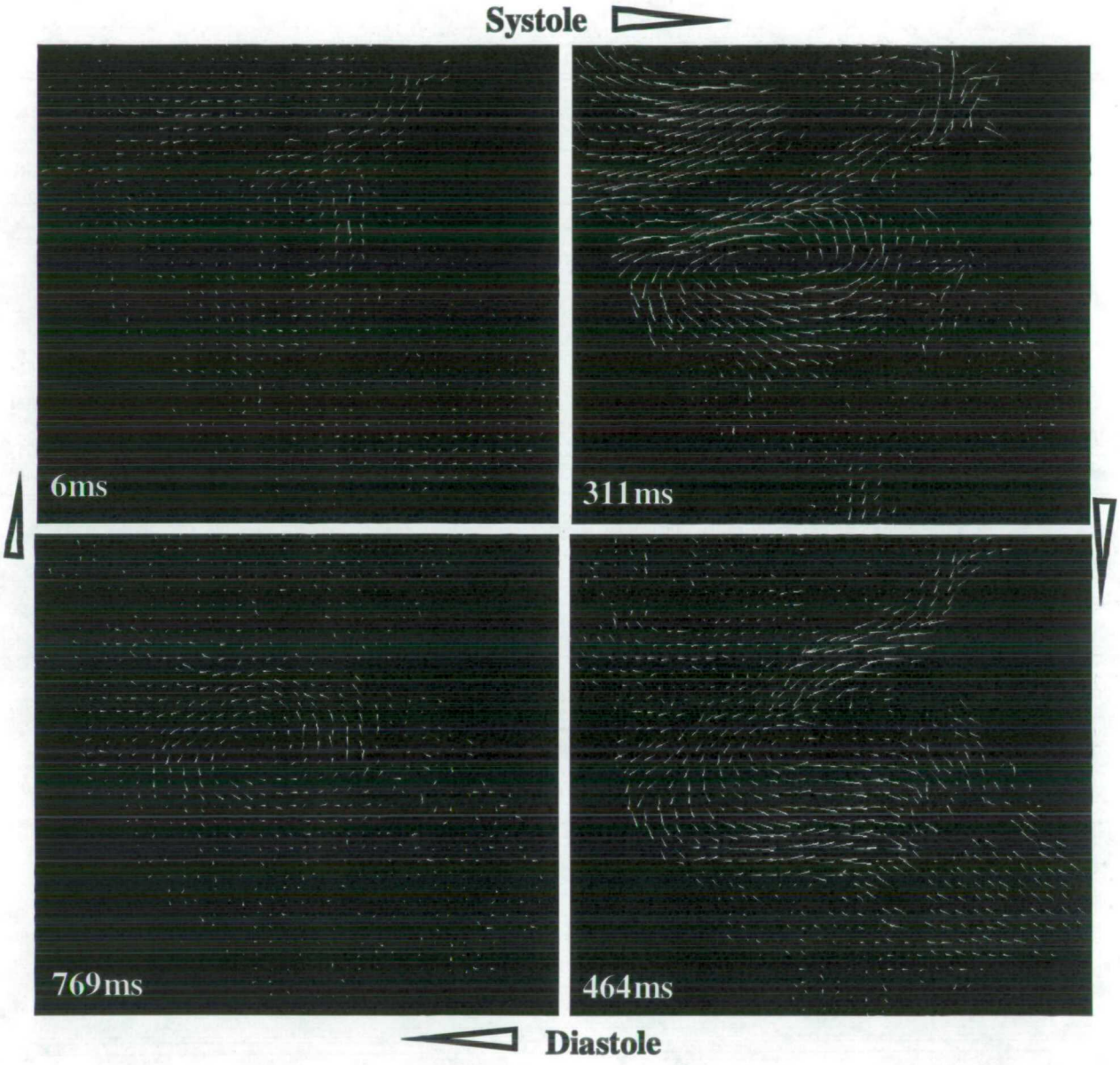


Figure 4.11 Left atrial flow viewed from front (subject 1).
This coronal plane is aligned with the left upper pulmonary vein which can be seen flowing down and left into an anticlockwise swirl of blood in late systole (311ms). Flow in the right pulmonary artery can be seen in the upper part of this frame. Flow passes on through the mitral valve, in front of the plane, in diastole (464ms).

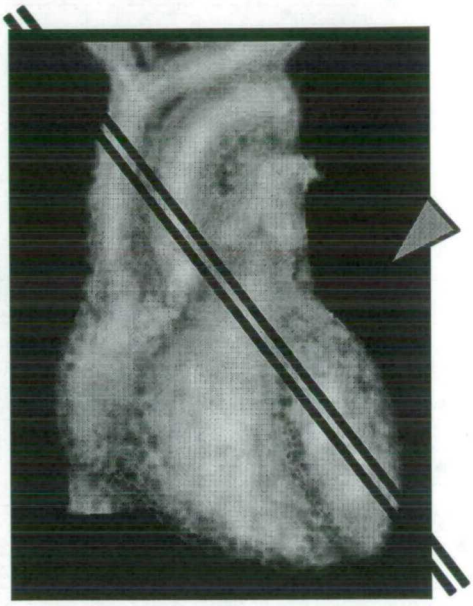
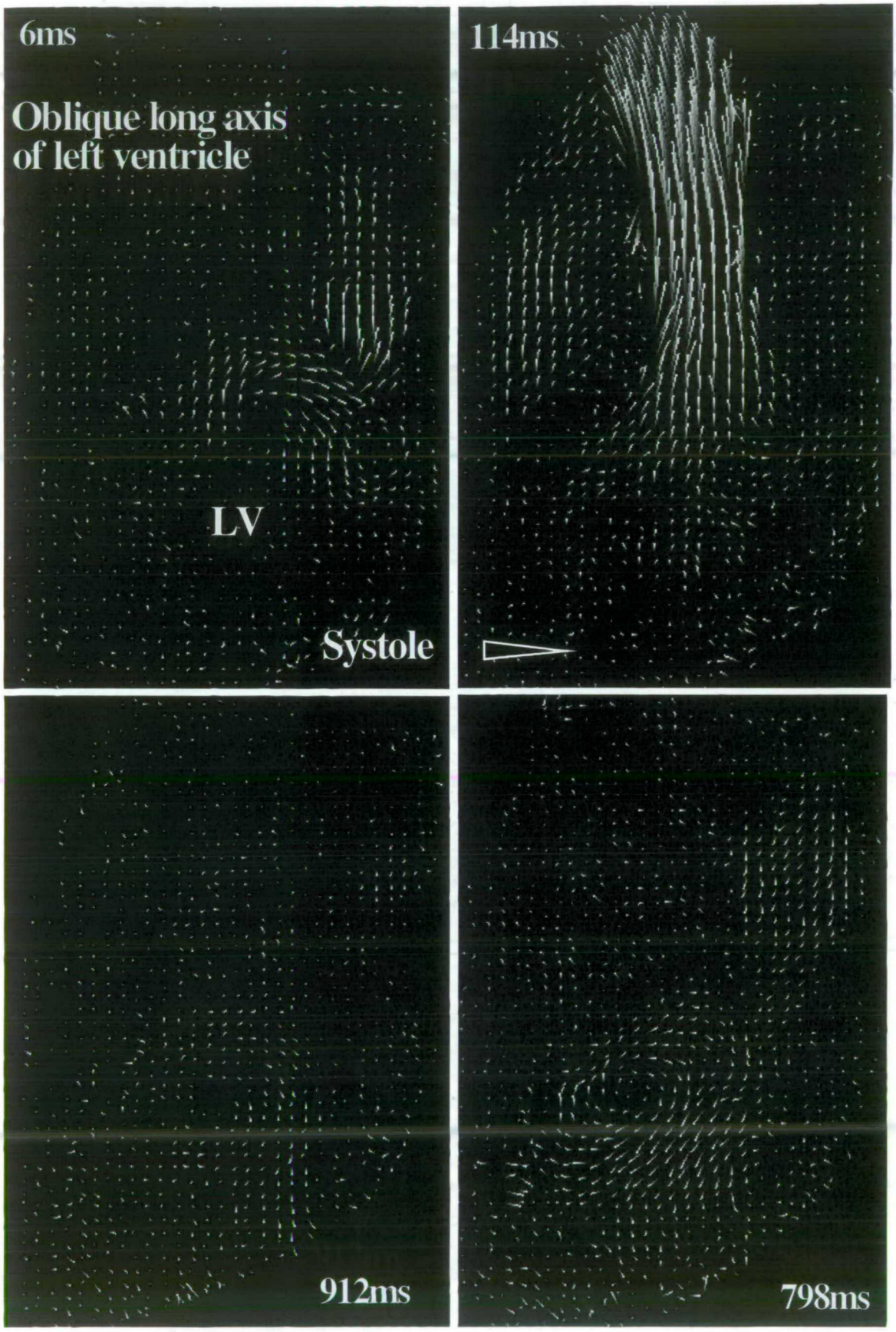
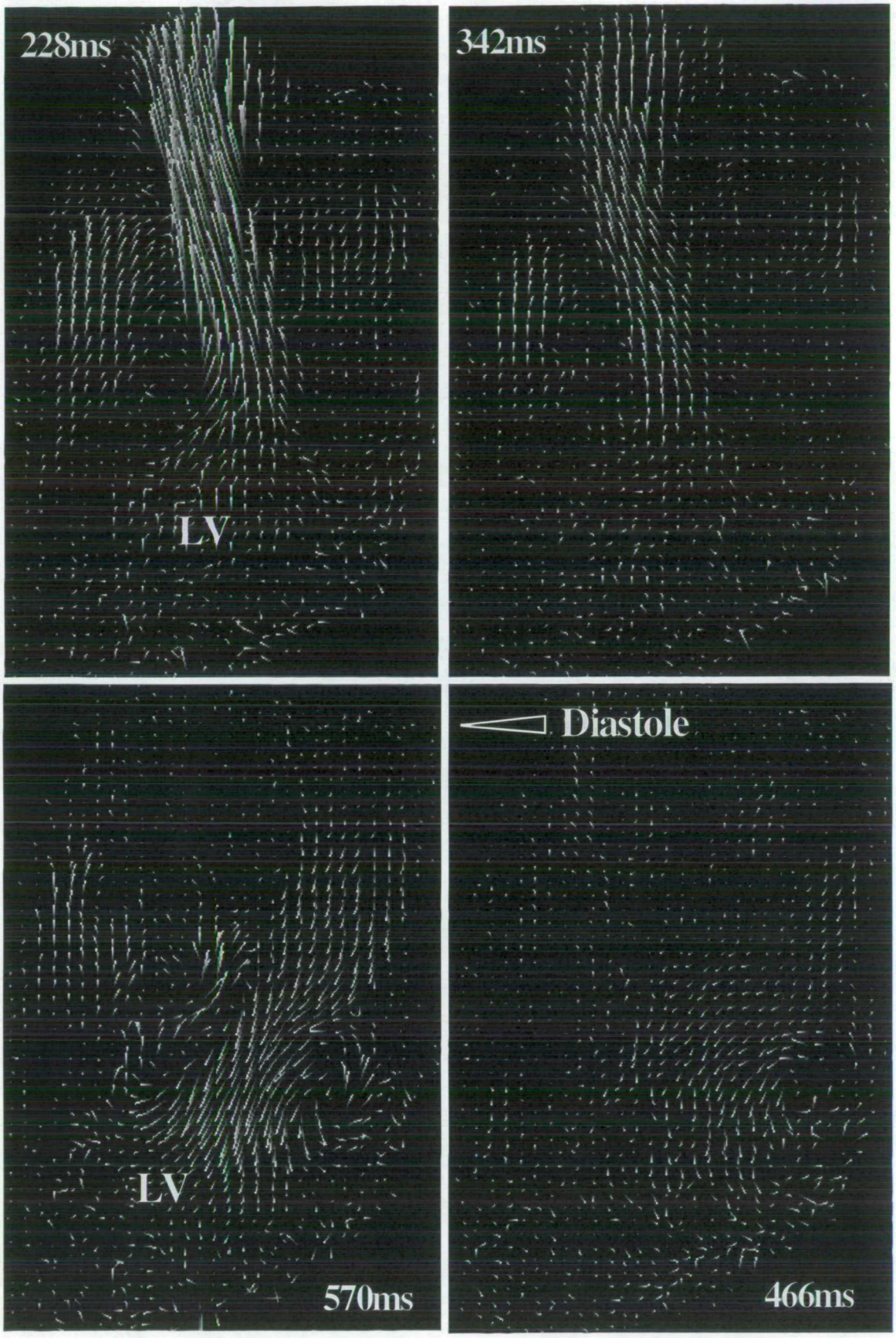


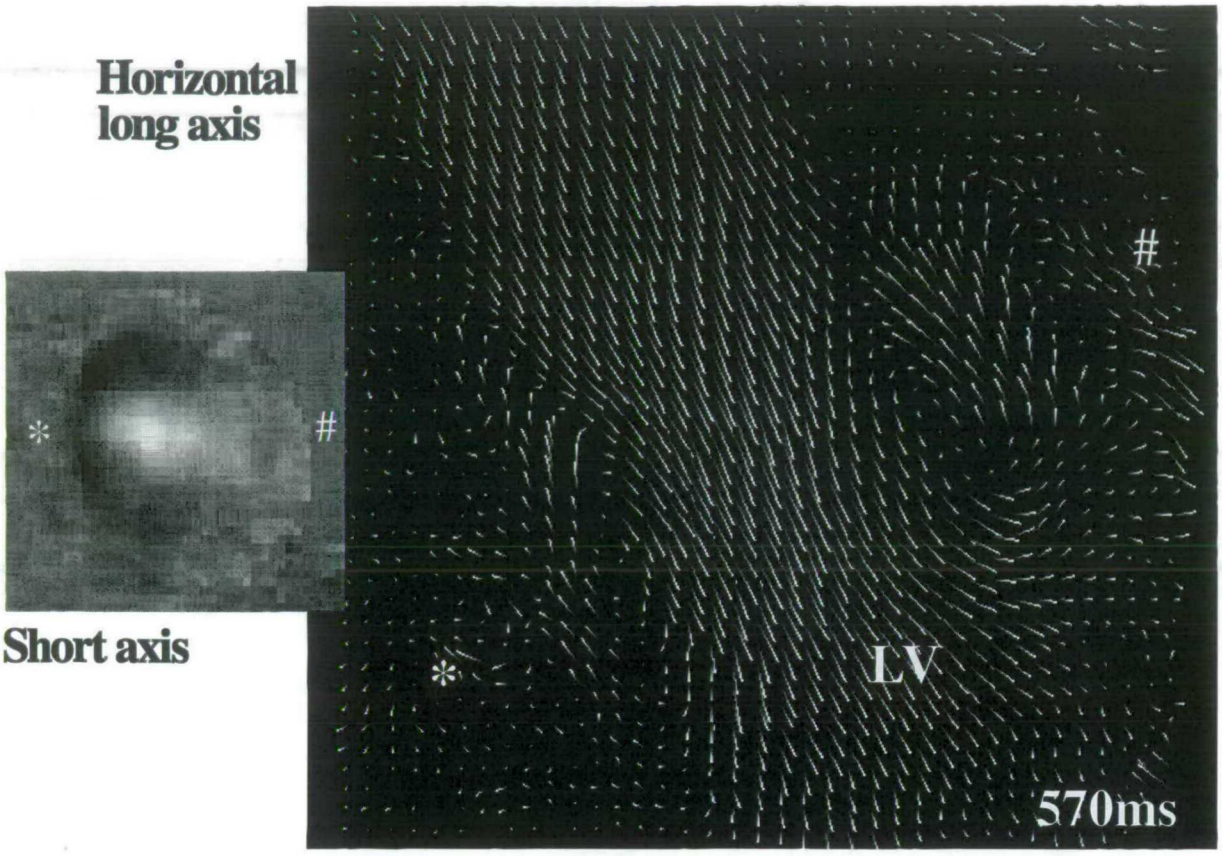
Figure 4.12
Above: Location of the oblique long axis left ventricular plane, to be viewed from above left, overleaf.
Overleaf: Velocity vector maps in the oblique long axis plane. Four systolic and four diastolic frames (from a total of 18 frames)are displayed. In the first frame, 6ms after the R-wave, vorticity persists beneath the closed mitral valve following atrial systolic inflow. Systolic flow into the aorta is seen from 114-342ms. In the left atrial region, vectors towards the mitral valve are present before it opens. Vortical back-flow beneath the mitral valve leaflets is seen most clearly at 570ms. Slight residual swirling, mainly beneath the anterior leaflet, persists at 912ms.

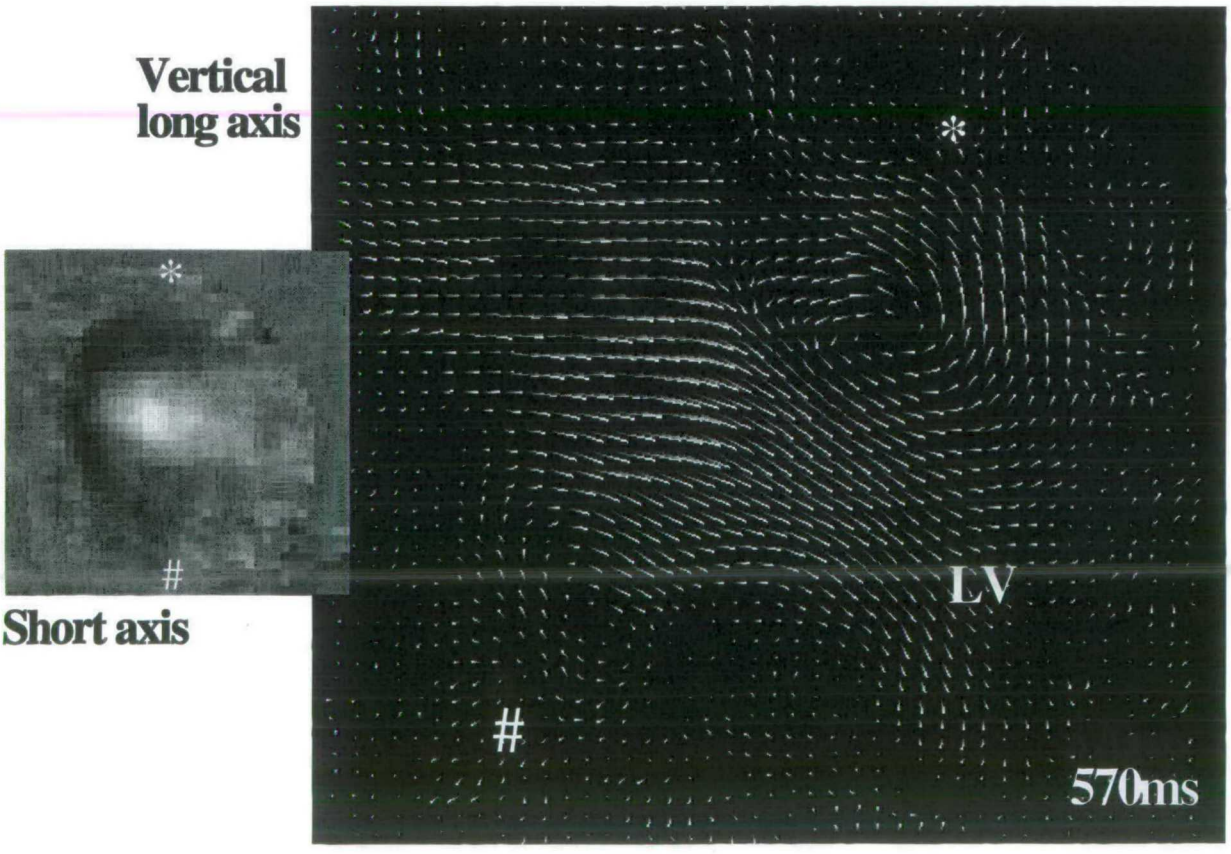

6ms
Oblique long axis
of left ventricle
LV
Systole
114ms
912ms
798ms

60j



60K


Horizontal
long axis
Short axis
LV
570ms


Vertical
long axis
Short axis
LV
570ms

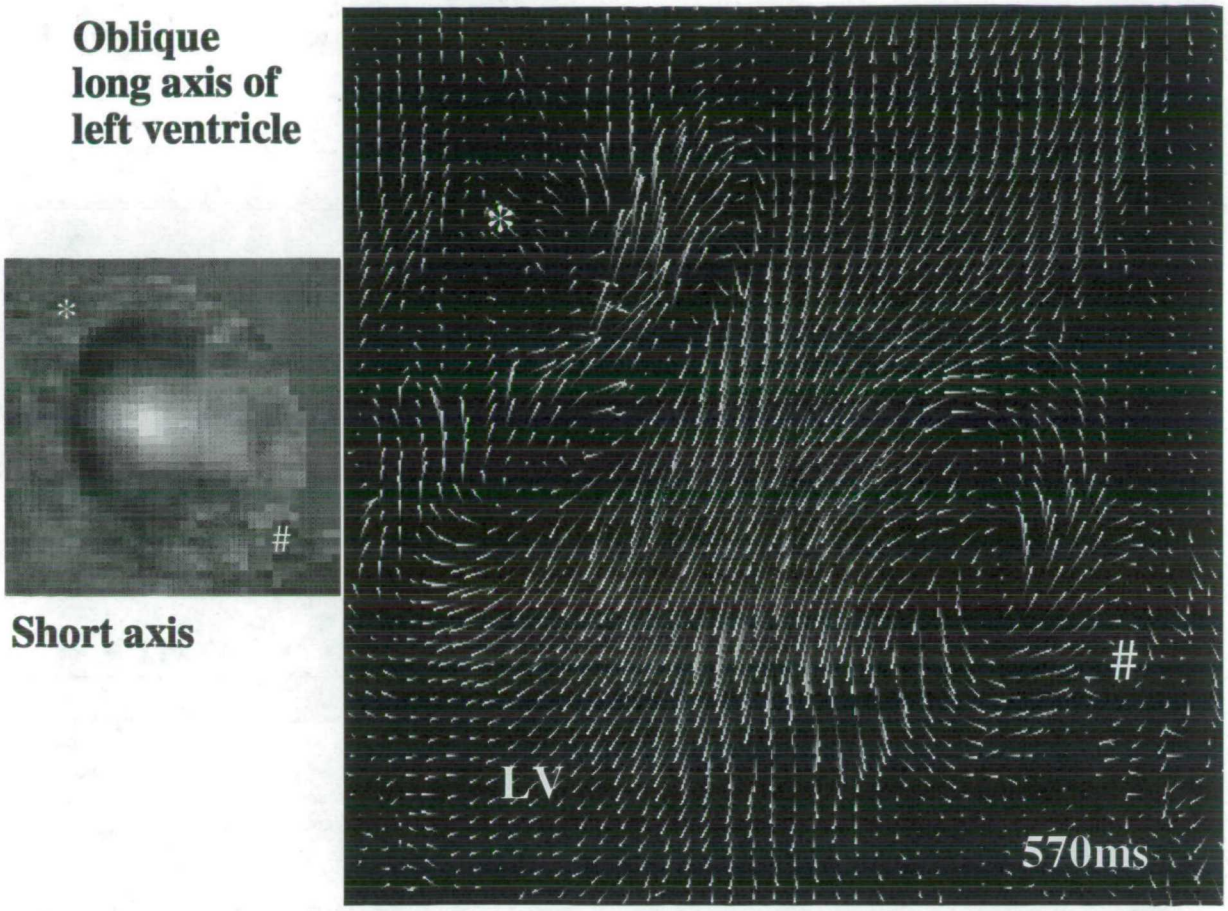


Figure 4.13 Ealy diastolic filling patterns of left ventricle (subject 3) cut in different planes. The short axis views show through-plane velocities, white = towards the apex, dark = back towards mitral valve. The marks represent points marked on adjacent vector maps in long axis planes. In the oblique long axis plane (above) the asterisk is close to the outflow tract. Correlation of information from these views indicates flow topology during early diastolic filling to be that of a somewhat constrained and asymmetric ring vortex. This is illustrated in another subject overleaf.

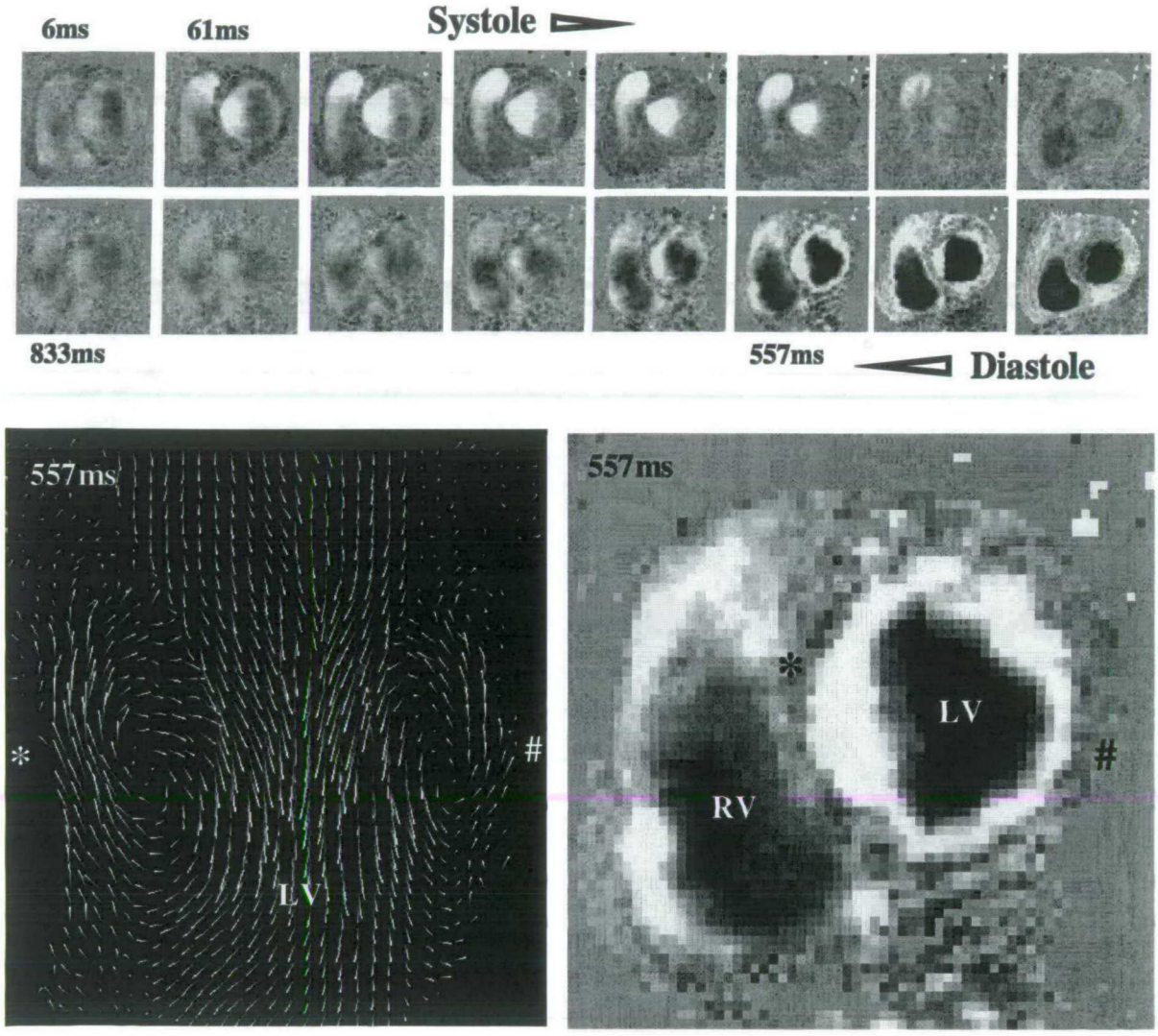


Figure 4.14 Left ventricular flows in subject 9. All 16 short axis velocity map frames are shown (above). Velocities away from the viewer (e.g. systolic outflows) appear white, those towards the viewer (mitral inflow), dark. One early diastolic velocity map and corresponding oblique long-axis vector map (below) show evidence of ring-vortical recirculation back towards the mitral valve, particularly on the side of the outflow tract (left of the images). In the right ventricle (RV), back-flow beneath the tricuspid valve occurs mainly in regions towards the outflow tract (above)and free wall (left).

Right atrium

Geometry

The right atrium is the most rounded of the four heart cavities. Flow enters via the superior vena cava (SVC) from above and inferior vena cava (IVC) from below. A third, smaller vein - the coronary sinus - drains blood from the heart's coronary vessels through an orifice to the left of the inlet of the inferior vena cava.

Flow leaves the right atrium through the tricuspid valve, the widest of the four heart valves, to the right ventricle, located anterior, slightly inferior, and left of the right atrium (left and right refer to the subject's anatomy, not to the image). The right atrial appendage, a flattened pyramidal diverticulum of little volume extends above/anterior/left of the right atrial cavity to lie in front of the aortic root.

The IVC and SVC, flowing up and down, respectively, open into the posterior part of the atrial cavity, the IVC slightly more posterior than SVC, with a slight anterior indentaion of posterior wall between the two, accommodating passage of the right pumonary veins to left the atrium, which is located behind and left of the right atrium.

Velocity mapping planes

With both caval veins almost vertically orientated, and the rounded right atrial cavity placed forward relative to them, the form of the chamber and its flows are relatively easily demonstrated. Straight sagittal, transaxial and coronal planes through mid-cavity all show evidence of a single large-scale flow feature.

A straight sagittal plane located through SVC and IVC (n=6) shows a large forward rotating vortex or swirl of blood developing to occupy almost the whole chamber through the course of (ventricular) systolic and early diastolic phases of atrial filling. This feature was observed in all 6 subjects studied. The two caval streams do not collide head on, but turn forward in a confluence that feeds the upper part of the forward rotating vortex. In the sagittal view, a second, smaller, up-turning vortex may appear transiently in front of the superior caval stream in early systole, curling up towards the right atrial appendage. This was distinguishable in only 2 of the 6 subjects.

Following the time course of right atrial flows, as seen in the sagittal plane, there is transient back-flow into both SVC and IVC orifices, visible only in the first frame, which, being immediately after the R-wave, follows shortly after atrial systole (Fig 4.6, 6ms). From the second frame to about the sixth, the effect of

ventricular systole, pulling the tricuspid ring towards the ventricle and so expanding the atrium, can be seen, giving the systolic filling phase of the right atrium. Streams from both caval veins turn forward in the cavity, even before they meet (Fig 4.6 116ms), then flow together until, by late ventricular systole (Fig 4.6 337ms), the forward swirl is well developed. There is then a generalized decrease of velocities until a second phase of inflow occurs (Fig 4.6 612ms), coinciding with diastolic opening of the tricuspid valve, when the atrium simultaneously fills and discharges.

A straight transaxial plane (n=2) located through the middle of the right atrial cavity and tricuspid valve give another view of the forward-rotating right atrial swirl. Components of velocity *through* the transaxial plane are shown in Fig. 4.7. They appear as distinct dark and light regions which represent velocities to and from the head, located predominantly anteriorly and posteriorly, respectively. The light region extends back beside the dark on both sides in late systole, (Fig 4.7 337ms) an appearance that is clarified by study of vectors in the coronal plane, described below. As the tricuspid valve opens (Fig 4.7 550-647ms), rotational momentum is conserved as a right-handed helical twist to flow through the tricuspid valve. Although this is not easy to determine in any single plane, it was apparent through binocular vieiwing of 3-dimensional-3-directional flow data on computer screen (Figure 4.4).

A straight coronal plane through mid right atrium (n=2) shows topology of the right atrial swirl to be more complex than a simple rotational movement. During filling phases, vectors in the coronal plane pass up the middle of the cavity from the IVC, but downwards on either side. They indicate that the swirl has 3-dimensional form somewhat like a *croissant* or hemi-annular vortex, thickest anteriorly (seen in sagittal plane), with some vorticiaty on either side (coronal plane) and absence of vorticity posteriorly (sagittal plane).

Right ventricle

Geometry

The right ventricle is the least rounded of the four heart cavities. Its posterior wall (inter-ventricular septum) and anterior wall each have forward convexity. This leaves a cavity that has the shape, in cross section, of a curved wedge or crescent, dépending on how it is cut. Inflow and outflow regions are not adjacent to one another, as in the left ventricle, but separated at slightly less than a right angle. The

inner muscular surface is coarsely trabeculated, particularly towards the apex, with muscular bands, notably the moderator band, traversing parts of the cavity.

The tricuspid valve is not clearly tricuspid. It has a septal leaflet, and a rather longer non-septal 'skirt' which may appear pleated and partially slit to give the appearance of two or more additional leaflets (Victor 1994). The leaflets are supported by chordae attaching to trabeculae of the septal and free walls, without distinct papillary muscles. The tricuspid is the widest opening of the four heart valves, and its 'ring' is also the most mobile, with considerable baso-apical excursion during systole.

Velocity mapping planes

A straight transaxial plane (n=2) the same as described for the right atrium, passes through the tricuspid valve and right ventricle. Flow vector maps in this plane show the stream of flow into the ventricle in early diastole passing close to the septal wall. In this plane, there is a back-curling, vortical movement around the non-septal leaflet of the valve, in the direction of the free wall, but little or no vorticity towards the septum. Systolic ejection to the pulmonary valve is away from this plane, and not well demonstrated.

An oblique coronal plane (n=3) orthogonal to the transaxial and aligned with the stream through the tricuspid valve shows the vertical breadth of this stream - 3-4.5 cm - and vortical curvature of it up towards the (pulmonary) outflow tract during both early and late diastolic ventricular filling phases (Figure 4.9).

The basal short axis plane (n=9) cutting the short axis of the left ventricle also cuts across right ventricular inflow. Maps of velocities through this plane show the vertically elongated cross section of the stream through the valve, with the most dominant reversal of flow above, turning towards the outflow tract, and reversal anteriorly, adjacent to the free wall, and, to lesser extents, posteriorly and inferiorly (Figure 4.14).

The horizontal long axis plane (n=9) described for the left ventricle also passes through the ventricular inflow and apical regions. Flow vector maps in this plane, also show some vorticity in diastole, mainly forwards, around the non-septal leaflet.

Left atrium

Geometry

With oblique inflows from four pulmonary veins, and discharge forward, down and left through the mitral valve, geometry of the left atrium is not easy to grasp. It is illustrated in Figure 4.10 which shows a projection, viewed from the front, of a 3-D Gadolinium contrast magnetic resonance angiogram of the left atrial region in a patient with no known cardiac abnormality. Right and left upper and lower pulmonary veins are asymmetrically placed. Those on the left lie slightly higher than those on the right. On both sides, inferior pulmonary veins flow obliquely forward from behind the left atrium, whereas superior veins flow in and down, almost in the coronal plane of the main cavity.

The left atrial appendage is a narrow diverticulum, shaped like the finger of a small glove, extending anteriorly from an opening just in front of the left lower pulmonary vein.

From back to front, the left atrium is flatter than the right atrium. It may be considered as a skewed rectangular pyramid, its apex toward the mitral valve. It has slightly less volume, and less volume-change than the right atrium, thus acting partly as a conduit for blood, and less fully as capacitant chamber than the right atrium.

Velocity mapping planes

A straight coronal plane (n=4) aligned with upper pulmonary veins passes down through the left atrial cavity. Mapping of vectors in this plane (Fig 4.11) shows development, perticularly in late ventricular systole, and again in diastole, of a rotating or turning flow that passes to the right superiorly and to the left inferiorly. In other words, the left atrium also fills with a swirling movement, in this case rotating anti-clockwise, as viewed from the front of the chest.

With entry of blood from four different oblique directions, three-dimensional flow topology must be more complex than described. Viewing components of velocity *through* the same coronal plane (not illustrated) shows streams moving obliquely forward from both inferior pulmonary veins. Towards the end of systolic and diastolic filling phases, however, all four inflow streams appear to contribute to the single, large-scale rotational movement.

A straight sagittal plane passing through left atrial cavity (n=1) and an oblique sagittal plane aligned with the aortic arch (n=10) both substantiate the general pattern described above. Maps of velocities through these planes

consistently showed predominance of flow to the right in the upper half, and predominance of flow to the left in the lower half of the left atrial cavity during systolic and diastolic phases of filling.

Left ventricle

Geometry

The shape of the left ventricular cavity changes from a slightly bulging ellipsoid at end diastole to a more sharply pointed cone at end systole. In both phases, the apex points down, left and slightly forward, and the base (mitral valve plane) lies superior-posterior-right, with the narrower outflow tract curving forward, up and right, anterior to the base. During contraction, the apical point moves little, whereas the circumferential walls and basal (mitral) plane move in and out, decreasing and enlarging the volume.

Looking back up the barrel of the ventricle towards the base, with the subject's head above, the aortic valve appears above-left, at 10-11 o'clock, with the anterior mitral leaflet opening towards it. The posterior mitral leaflet opens in the opposite direction. The two papillary muscles, aligned with commisures of the mitral valve, appear above right and below left, from this point of view.

Also from this point of view, the oblique long axis plane (see below) appears as a diagonal line, sloping from above-left to below-right, cutting both mitral leaflets almost at right angles, whereas the horizontal long-axis plane appears as a horzontal line, oblique to the leaflets, and the vertical long axis plane as a vertical line, also oblique to the leaflets (Figure4.13).

The inner surface of left ventricular muscle is composed almost entirely of trabeculations. The two papillary muscles, giving rise to the chordae that prevent prolapse of the mitral leaflets, emerge like fingers from the apical third, pointing back to the mitral valve.

Trabeculations and papillary muscles move together in systole, expelling blood from their interstices, and move apart in diastole. Their mechanical role is probably mainly related to freedom of contractile and expansile movement, although their presence, aligned slightly oblique to the long axis in a right-handed helical twist, may have bearing on dynamics of flow in and out of the cavity.

Velocity mapping planes

Oblique long-axis planes (n=7) were aligned either from coronal pilots to pass

through mitral and aortic valves and the axis of the left ventricular cavity, as used by Kim (Kim 1995) (n=2). A very similar plane was located in other cases (n=5) by identification of 3 points - mitral orifice, left ventricular apex and aortic orifice on transaxial pilot images. Either of these oblique planes allow visualisation of both inflow and outflow streams of the left ventricle. As described by Kim, they show vortex formation, with a more dominant anterior vortex turning beneath the anterior mitral valve leaflet towards the outflow tract, and a smaller counter-rotating vortex curling back beneath the posterior mitral leaflet, clearly identifiable in five of the seven subjects studied.

A basal short axis plane (n=9) was located orthogonal to the axis of the left ventricle, one third of the way from base to apex. The inflow stream from the mitral valve passes through this plane, and display of through-plane components of velocity (Figures 4.13 annd 4.14) shows not only apically directed flow, but around it on most sides, transient basally directed back-flow can be seen. The distribution of this back-flow is not confined to the line of the oblique long-axis cut, but appears to be almost circumferential, suggesting an almost complete ring vortex. Back-flow, after both early and late phases of diastolic filling, is maximal towards the outflow tract, in accord with appearances in the oblique long-axis plane, but is also identifiable in other regions around the circumference.

A vertical long-axis plane (n=8) was located in the long axis of the left ventricle from straight transaxial multislice pilots. Velocity vector maps in this plane showed generation of two counter-rotating vortical regions during filling phases (in 7 subjects out of 8) compatible with ring vortex formation described above, and dominance of a single vortical region (1 subject out of 8), apparently another view of the dominant anterior vortex, turning towards the outflow tract.

A horizontal long axis plane (n=9) was located in the long axis of the left ventricle orthogonal to the vertical long axis plane. Velocity vector maps in this plane showed generation of two counter-rotating vortical regions during filling phases, also compatible with incomplete annular vortex formation described above.

Correlation and synthesis of results.

In order to appreciate spatio-temporal relations between flows of chambers and vessels of the heart, illustrations have been prepared, based on information obtained from the studies presented above.

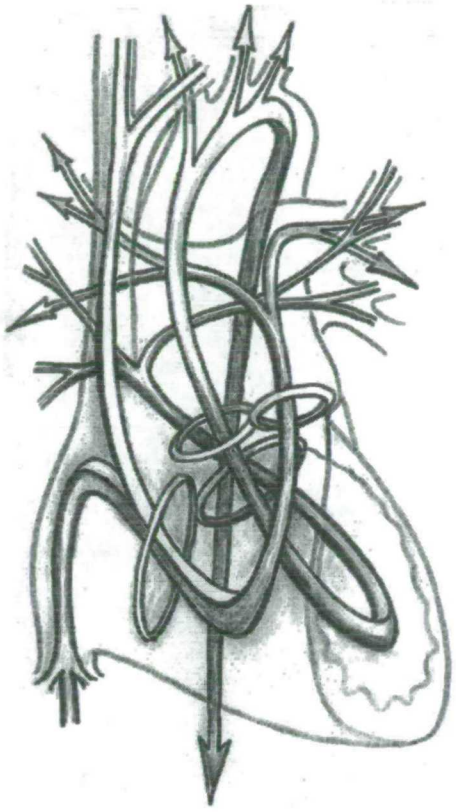
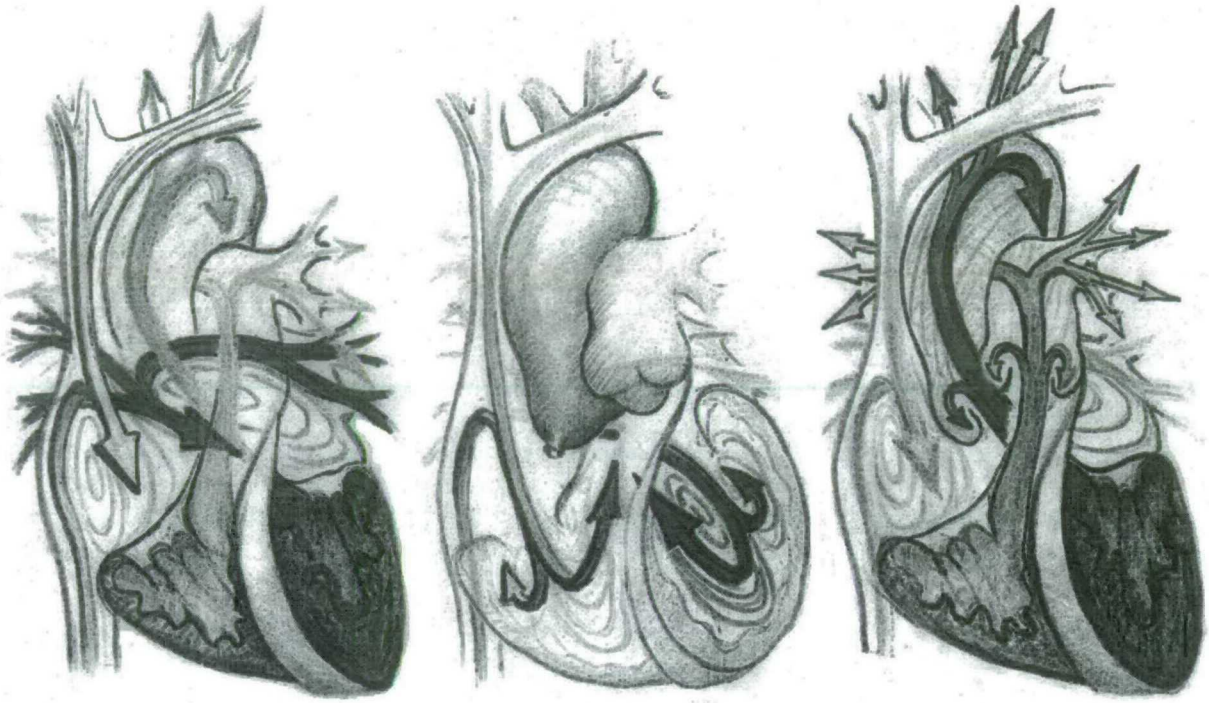


Figure 4.15 Drawing of main streams of blood through the heart. For clarity, principal flow paths are represented by continuous bands; vorticity and phasic variability of flow through chambers and valves are not shown.



Systole (inflows) **Diastole** **Systole** (outflows)

Figure 4.16 Drawing of main streams through the whole heart in systolic and diastolic phases. Vorticity has been emphasized, and late diastole omitted, to give an impression of the potential continuity of momentum -between chambers and between phases - that may gain importance during exercise (see Chapter 6).

Figure 4.15 illustrates spatial relations of *main streams* of blood through the heart and adjacent vessels. For the sake of clarity, main streams have been drawn as continuous bands, their curvatures appearing like those of catheters passing through cavities of the heart. This representation is accurate in that the bands pass through connecting vascular and cardiac regions in appropriate sequence and direction, but the drawing is a simplification in that blood flows are obviously not continuous – they varying in different regions through different phases of the cycle.

Figure 4.16 illustrates two key phases - mid systolic ejection and (early) diastolic filling. At rest, late diastolic filling gives rise to similar spatial patterns of inflow in more expanded ventricles. On exercise, early and late diastolic filling phases merge (chapter 6), so Figure 4.16 may be considered as a representation of the rapidly alternating systolic and diastolic phases of exercise, each dynamically coupled with the other through tensions of tissues and via conservation of momentum between one compartment and another.

This drawing reveals the potential continuity of atrio-ventriculo-arterial flows. Momentum of flow in one compartment can either be redirected to the next, or decelerating, it can contribute energy to elastic expansion of the receiving chamber. And contraction of a chamber not only gives force to ejection of blood, but pulls adjacent tissues, notably of the atrio-ventricular valve ring. Velocity map data can be interpreted in relation to these interactions. Attention is drawn to the following:

- The extent to which atrial filling is dominated by two ventricular events - systolic contraction and early diastolic recoil.
- The tendency in all chambers for entering streams to turn spontaneously in the direction of outflow, providing a certain amount of momentum (limited in the resting heart) towards the outflow valve before its moment of opening
- Through atrio-ventricular valves, there is almost circumferential, quasi ring-vortical back-curling beneath tricuspid and mitral leaflets. The relatively limited velocity of these, however, compared with vectors of a free ring vortex (see Figure 3.8b, opposite p 48) suggests that at least some of the kinetic energy of inflow may not be conserved, but rather is transferred to elastic potential energy of stressed ventricular fibres.

Discussion

Comprehension of the asymetrically tortuous geometry of the heart, and patterns of flow through it, requires time and effort. Patterns of flow are not only asymmetric in the space of each chamber, with 'right' and 'left' chambers asymmetric with respect to each other, but, in the resting condition, there is also 'temporal asymmetry', with two phases of inflow to each chamber, but only one phase of ventricular ejection. Attempts to demonstrate inertial (Noble 1968, Laniado et al.1975, Fujimoto et al. 1995) or kinetic (Burton 1965, Kim et al.1995) components of force/energy exchanges seem to have shown this aspect to be of minor importance relative to forces and work delivered by myocardium contracting against closed inflow valves. To begin to appreciate the potential role of coordinated inertial/elastic/contractile morphodynamics of the heart, however, a more integrated view is needed, giving due consideration to the relatively gentle dynamics atrial as well as ventricular filling, and the relation of these to each other. Studies presented in this chapter aim towards this.

It becomes clear from study of relative positions and timings of blood movements that atrial inflows are dominated by the dynamics of ventricular contraction and recoil, and that ventricular inflow cannot be separated from the dynamics of atrial flow. Ventricular ejection is clearly powered overwhelmingly by ventricular contraction, and pressures generated in this region are high. Acceleration into the aorta and around the aortic arch also involves greater rates of change of momentum, and hence inertial exchanges of force, than any other region of the cardiovascular system. These inertial exchanges of force, together with changing wall stresses and strains, effect movements of adjacent boundaries, including those of low-pressure veins and atrial cavities. Thus ventricular function works back on atrial function, which, in turn feeds ventricular function. The tight, tortuous formation of chambers and vessels lends itself to coupled interaction. Furthermore, the vortical, cyclic movements of blood in right and, to a lesser extent, left atrial cavities, bear resemblance to spontaneously cyclic flows in asymmetric cavities illustrated in Chapter 3. At rest, however, they remain biphasic, and presumably not as strongly coupled with myocardial action as they might become on exercise.

It is the resting condition that has been studied both because that may be regarded as the basic state of the heart, and because it is amenable to magnetic resonance investigation. Computational analysis of dynamic pressure differences

associated with velocity changes is presented in the next chapter. Magnetic resonance study during exercise is problematic due to movement artefacts, difficulties in obtaining ECG traces for gating and because of the narrow confines of magnets. It is clear, however, that the relative importance of dynamic, inertial forces must increase with exercise. For this reason, an approach was sought for study of the changes of timing and magnitudes of flow velocity during exercise. The resulting Doppler echocardiographic studies are reported in Chapter 6.

Chapter 5

Computation of dynamic differences of pressure in the heart

Objectives

The aim is to reveal dynamic differences of pressure associated with changes of momentum of blood flowing through the heart chambers and great vessels.

Background

Chapter 4 showed changing, multi-directional patterns of flow through the heart, but the question remained - how might forces associated with changes of fluid momentum be recognized and quantified?

In collaboration with Guang-Zhong Yang, who undertook the computational work of this chapter, the Navier-Stokes equations were used to derive maps of dynamic differences of pressure from cine velocity map data. In theory, at least, this allows dynamic components of pressure to be isolated, so that their magnitude can be appreciated in relation to familiar blood pressure measurements recorded either externally by pressure cuff, or internally by catheterization.

Several distinct but interacting fluid mechanical factors contribute to pressures of blood recorded at locations and instants in the system. In small peripheral vessels, the effects of viscous friction predominate, and blood pressure gradients result largely from energy dissipation associated with fluid shear. In larger arteries and veins, and in heart cavities, additional factors must be considered where greater distances, fluid masses and momentum changes are involved. Firstly, gravity - a body force - imposes a uniform pressure gradient up and down the fluid mass. Secondly, fluid contained in an effectively closed system may be globally pressurised or released, so that pressures are modified. This applies to fluid in a ventricle during iso-volumetric contraction or relaxation. But as soon as valves open, interaction with the inertia of fluid comes into play. According to Newton's laws of motion, fluid can only change momentum through application of force, manifesting as a gradient of pressure, decreasing towards the direction of acceleration. It is this aspect of pressure that is addressed in this chapter.

Relationships between momentum change and pressure difference can be appreciated from observing displacements of fluid surfaces against gravity. Forms and movements of the surface of tea or coffee can be observed while stirred or swung from side to side in a cup. On this basis, two flow models were devised - a rotating vertical cylinder of water with a free surface above, and a tank containing an oscillating standing wave - in which displacements of free surfaces could be imaged and velocity fields measured by magnetic resonance. Knowing the magnitude of the gravitational pressure gradient, these models allowed validation of algorithms for computation of dynamic gradients of pressure from spatial and temporal changes of momentum. If computed pressure differences agreed in direction and magnitude, without evidence of errors exceeding 10%, with those deduced or measured directly in the phantoms, it seemed reasonable to apply the approach to intracardiac cine velocity data.

Newton's laws of motion were applied to elements of fluid volume by Navier in 1827, and by Stokes in 1845. Their equations, derived from considering conservation of momentum in a certain volume, are now recognised as a full description of the mechanics of simple fluids. In their basic form for an incompressible fluid, they can be represented as:

$$-\frac{\partial p}{\partial x_i} = \rho\frac{\partial u_i}{\partial t} + \rho\left(u_1\frac{\partial u_i}{\partial x_1} + u_2\frac{\partial u_i}{\partial x_2} + u_3\frac{\partial u_i}{\partial x_3}\right) - \mu\left(\frac{\partial^2}{\partial x_1^2} + \frac{\partial^2}{\partial x_2^2} + \frac{\partial^2}{\partial x_3^2}\right)u_i - f_i \quad (i = 1,2,3) \quad (1)$$

with x_i $(i=1,2,3)$ representing the three orthogonal axes in space, u_i their corresponding velocity components, μ the coefficient of viscosity and ρ the density of the fluid. Variables f_i $(i=1,2,3)$ represent the body force components along x_i. The equations represent the contribution to the momentum balance of four constituents of force, namely the pressure force, transient and convective inertia, viscous resistance, and body force, *i.e.*,

Pressure Force** = **Transient Inertia** + **Convective Inertia** - **Viscous Resistance** - **Body Force.

In the computations of dynamic pressure difference that follow, the only body force present is gravity. It represents an essential component in relation to surface waves of the flow models, but it is not included in representations of flow pressure within the

heart and vessels. Viscous forces are neglected in computations pressure differences in both the models and in the heart and large vessels.

Methods

Cine flow velocity data was acquired, in the 0.5Tesla magnet, by methods described in Chapter 4. Prior to calculation of flow pressures, flow fields in selected compartments (left atrium, left ventricle and aortic arch) were identified and delineated manually, and computation applied to these regions only.

Computation of Pressure Distribution

It can be seen from Eq. [1] that the pressure gradient

$$\nabla p = \left(p_{x_1}, p_{x_2}, p_{x_3}\right) \tag{2}$$

where $p_{x_i} \equiv \frac{\partial p}{\partial x_i}$ $(i = 1,2,3)$, can be calculated directly from cine velocity data. Thereafter, integration is required over the whole flow region to derive relative pressure contours from ∇p. A numerical algorithm, based on the least squares method and pressure Poisson equation, was derived so that potential inaccuracies arising from noise within the velocity data were minimised (Yang et al.1996 – bound at end).

In Vitro Flow Phantom Validation

Prior to computation of flow pressures from *in vivo* data, two *in vitro* experiments were performed to validate the technique. The first consisted of an open-topped rotating cylinder containing water, as illustrated in Figure 5.1a. The steady angular velocity of the cylinder and its contained fluid, which was allowed to reach hydraulic equilibrium (*solid body rotation*), was controlled by a rotary motor. In this case, the pressure at any given point within the fluid should be proportional to its vertical distance below the surface. In other words, if we measure the pressure distribution in a horizontal cross section of the cylinder, the result expressed in mmH_2O should match the surface shape of the fluid. This relationship was used to evaluate the accuracy of our proposed numerical method. Figure 5.1b shows the calculated relative pressure distribution within the image plane, and 5.1c shows the central horizontal pressure profile of the calculated result and its correlation with the surface shape of the fluid. An close match was achieved, with only slight discrepancies amounting to less than 10% of overall pressure differences. Discrepancies in voxels close to the wall of the cylinder may reflect inaccuracies in the velocity data where voxels span the fluid boundary.

Although the rotating cylinder phantom provided a convenient way of assessing pressure results calculated from magnetic resonance data, its velocity field, and hence the calculation, involved spatial but not temporal acceleration. As the fluid had reached hydraulic equilibrium, *i.e.*, $\partial u_i/\partial t = 0$, transient inertia played no part in balancing Eq. (1). We therefore devised a phantom with transient motion. This consisted of a glass tank in which a relatively large-scale standing wave was induced, as shown in Figure 5.2, overleaf.

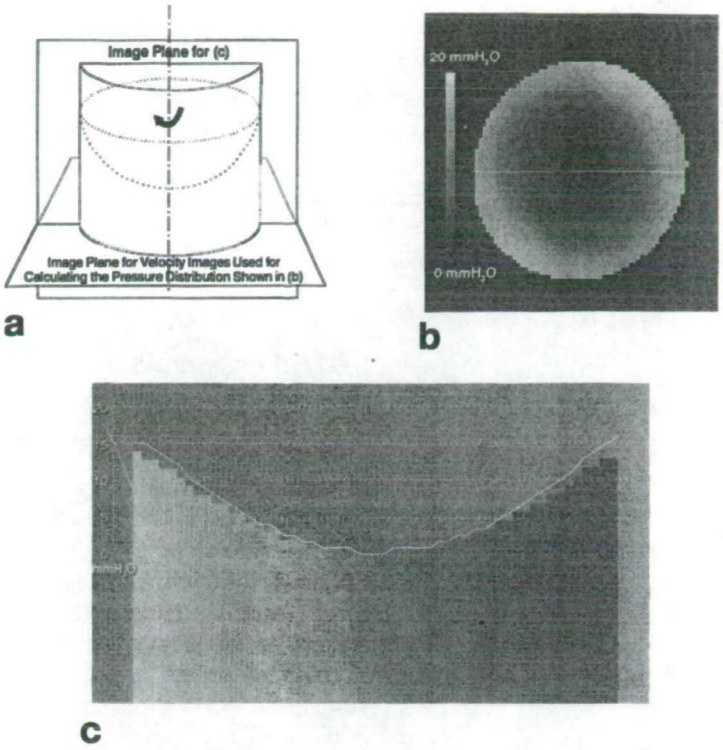


FIG. 5.1 (a) Schematic drawing of a phantom that contains water in a steadily rotating open-topped cylinder. (b) The calculated relative pressure distribution expressed in millimeters of water (mm H_2O) within a horizontal image plane as shown in Fig. 1a. (c) The central horizontal pressure profile of Fig. 1b and its correlation with the surface shape of the fluid determined by a through-plane velocity encoded image aligned with the axis of the phantom. Because the fluid had reached hydraulic equilibrium, a match between the surface shape of the fluid and the pressure profile (expressed in mmH_2O) should be expected. The imaging field of view used for this experiment was 30 cm.

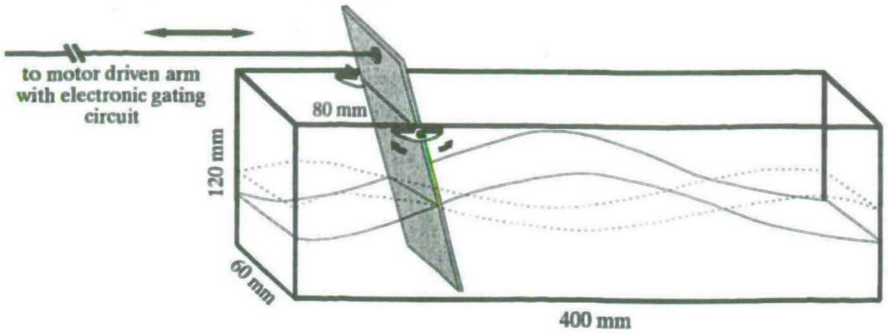


FIG.52 A schematic diagram showing the configuration of the wave phantom. The glass tank is 400 mm in width, 120 mm in height, and 60 mm in depth. The water was filled to a level of 50 mm. A motor driven pivoted flap was used to generate large scale standing waves. A gating circuit was attached to the arm of the motor to allow acquisition of cine velocity data.

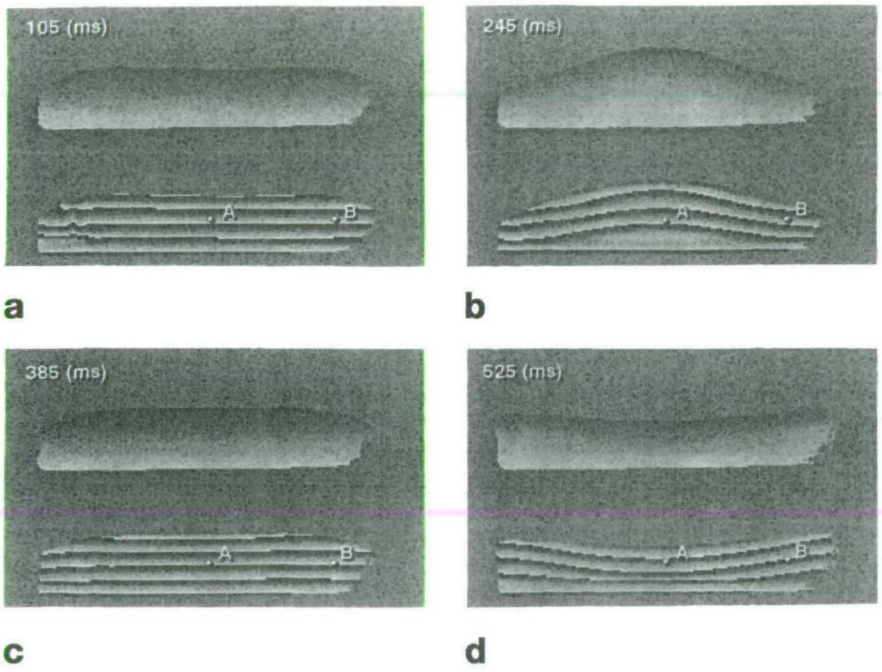


FIG. 53 The reconstructed pressure distribution for an *in vitro* flow phantom. The wave timed at (a) 105 ms, (b) 245 ms, (c) 385 ms, and (d) 525 ms after the onset of the electronic gating pulse. The top picture in each subfigure shows the overall pressure distribution with white for high pressure and black for low pressure. In the bottom subfigure the pressure values are wrapped around at 1 mm Hg intervals to provide a convenient visual assessment of pressure, pressure gradient, and isopressure contours. Catheter-tip pressure measurements were performed at positions marked as A and B, and the results were used to compare with MR measurements. Distortion of the wave tank outside the central 30-cm region of the field of view in image data was caused by nonlinearity of magnetic gradients.

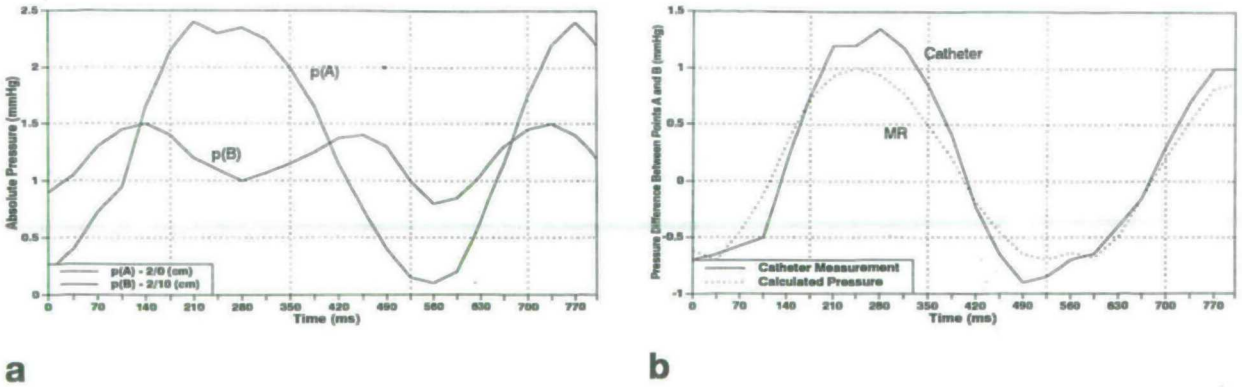


FIG. 5.4 (a) The pressure measured at positions A and B of Fig. 3 using a high-fidelity catheter-tip pressure transducer. (b) A comparison of the pressure difference curves calculated from the catheter measurements (solid line) and that derived from the MR technique (dotted line).

A pivoted flap driven by a motor located outside the magnet was used to generate wave motion in the tank. A gating circuit was attached to the arm of the motor to allow interleaved data acquisition similar to that of *in vivo* studies. A total of 24 time frames were acquired in each cycle, the time interval between frames being 35 ms.

Figures 5.3a-d show calculated pressure at four phases, 105, 245, 385, and 525 ms after the gating pulse. In each sub-figure, the top picture shows the overall pressure distribution with white for high and black for low pressure. In the bottom sub-figure, the pressure values are wrapped around at 1 mmHg intervals, each occupying a complete grey scale range, so that a semi-quantitative visual assessment can be made. This display scheme depicts pressure contours at 1mmHg intervals and the pressure gradient is proportional to the number of bands crossed in a given distance, as in the *in vivo* studies that follow

The viscous terms in Eq. [1] were neglected in the calculations. The viscous boundary layer adjacent to tank walls was estimated to be only a few mm in thickness (Yang 1996 - bound at end), and viscous effects therefore negligible through most of the volume of the tank. The actual pressures within the wave phantom were subsequently measured using a 2F Millar SPR 524 catheter-tip pressure transducer which provides high-fidelity pressure readings. The transducer of the probe was set parallel to the main direction of fluid motion. Possible errors due to deflection of the flow around the probe are likely to have been relatively small, given the small size of the catheter and limited velocities of flow.

Figure 5.4a shows the local temporal pressure variations measured at points A and B as marked in Figure 5.3. In Figure 5.4b, the temporal pressure difference between A and B is plotted as a solid curve, whereas the corresponding pressure difference calculated from velocity data is delineated as a dotted line. It can be seen that a good correspondence between the measured and calculated results was achieved. Some under-estimation of the pressure difference, however, is evident for results derived from velocity data. This may be attributed to the use of velocity data averaged over many cycles which may have had a smoothing effect on velocity changes, and the 35 ms time interval between successive frames which may have accounted for under-estimation of transient velocity changes.

In Vivo Results

Flow pressure fields computed from *in vivo* magnetic resonance cine velocity map data are shown in figures 5.5 and 5.6. The subjects were studied at rest in a supine position, and the force of gravity was neglected. The viscous terms in Eq. [1] were neglected in the calculations. Figure 5.5a, opposite, uses the oblique long axis velocity map acquisition that was illustrated in Figure 4.12 of the previous chapter. Selected frames are enlarged overleaf. The plane is aligned with left atrium, left ventricle and aortic root. Dynamic pressure maps are displayed between systolic (upper row) and diastolic (lowest row) maps of vertically directed velocity. Dynamic pressure differences are displayed in 1mmHg pressure bands which graduate to white on the edge towards high pressure and black towards low pressure, and then wrap to the next band. Gradients of pressure associated with accelerations and decelerations of flow are shown.

Appearances can be understood as follows: the mass of contained blood is almost at rest at the start of the cardiac cycle. In early systole, acceleration of blood from left ventricle to aorta is associated with relatively tightly packed 1 mmHg pressure bands, with higher pressure proximally. A maximum dynamic pressure difference of 10mmHg is computed from ventricle to mid-ascending aorta, beyond which the arch passes out of plane, and velocity or pressure measurements become unreliable. In late systole, the direction of the gradient reverses with deceleration of flow. The reversed pressure gradient appears moderately steep in the aorta, but not in the outflow tract, presumably because, as long as flow continues, convective acceleration associated with convergence of streamlines counteracts effects of temporal deceleration in this region.

In diastole, pressure differences in left atrial as well as left ventricular blood have been computed. Early diastolic acceleration from atrium to ventricle is associated 5 mmHg computed pressure difference (*), but in the very next frame (**) the slope of the gradient reverses in the ventricle as entering blood decelerates. Here effects of divergence of streamlines (convective deceleration) and temporal deceleration combine to contribute pressure to the ventricle. In the next diastolic frame, deceleration extends further back in the atrium, suggesting backward propagation of a ventriculo-atrial expansion wave (Macrae 1997). The remainder of

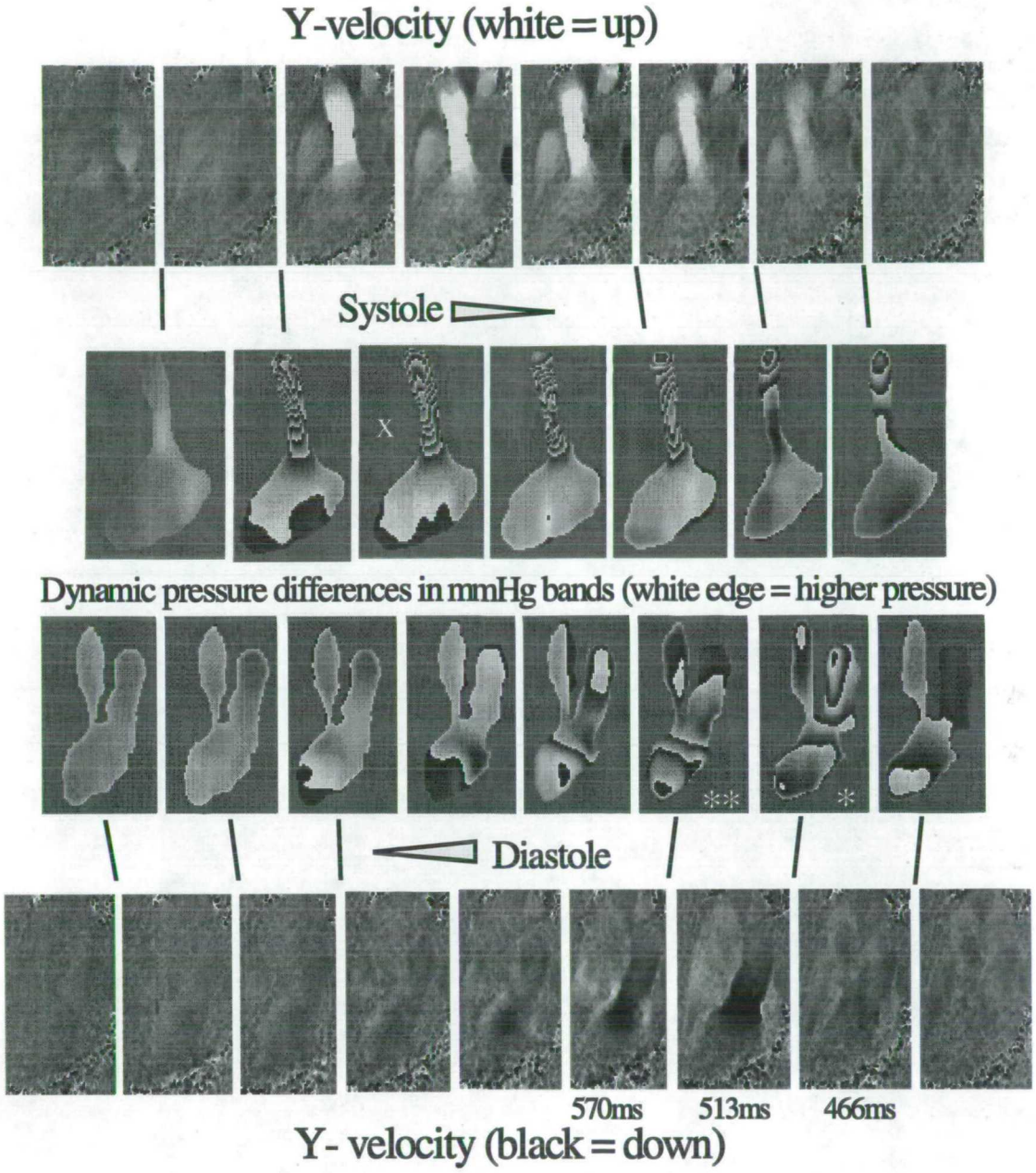


Figure 5.5a Dynamic pressure differences (middle rows) in the left heart and ascending aorta of subject 3, computed from cine velocity data (top and bottom rows). Pressure differences up to 10mmHg during peak systolic acceleration into the aorta are computed (x). In early diastole, a pressure difference of 5mmH is computed during acceleration from atrium to ventricle (*) and, in the following frame, a reversed pressure difference of 3-4mmHg is associated with deceleration in the ventricle (**). Enlargements of selected frames, with associated flow vector maps, are shown overleaf.

Figure 5.5b Onset of early systolic acceleration into the aorta

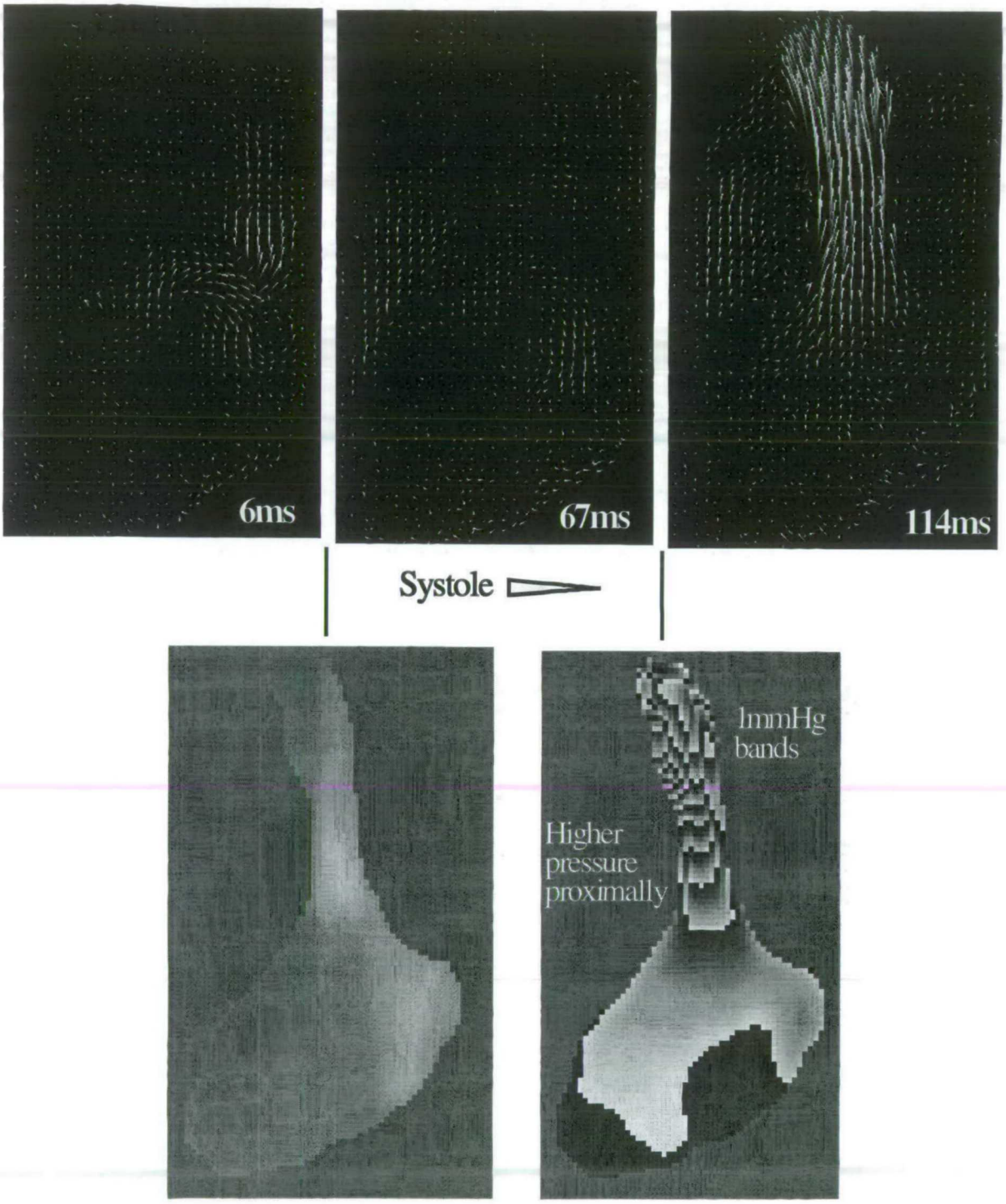
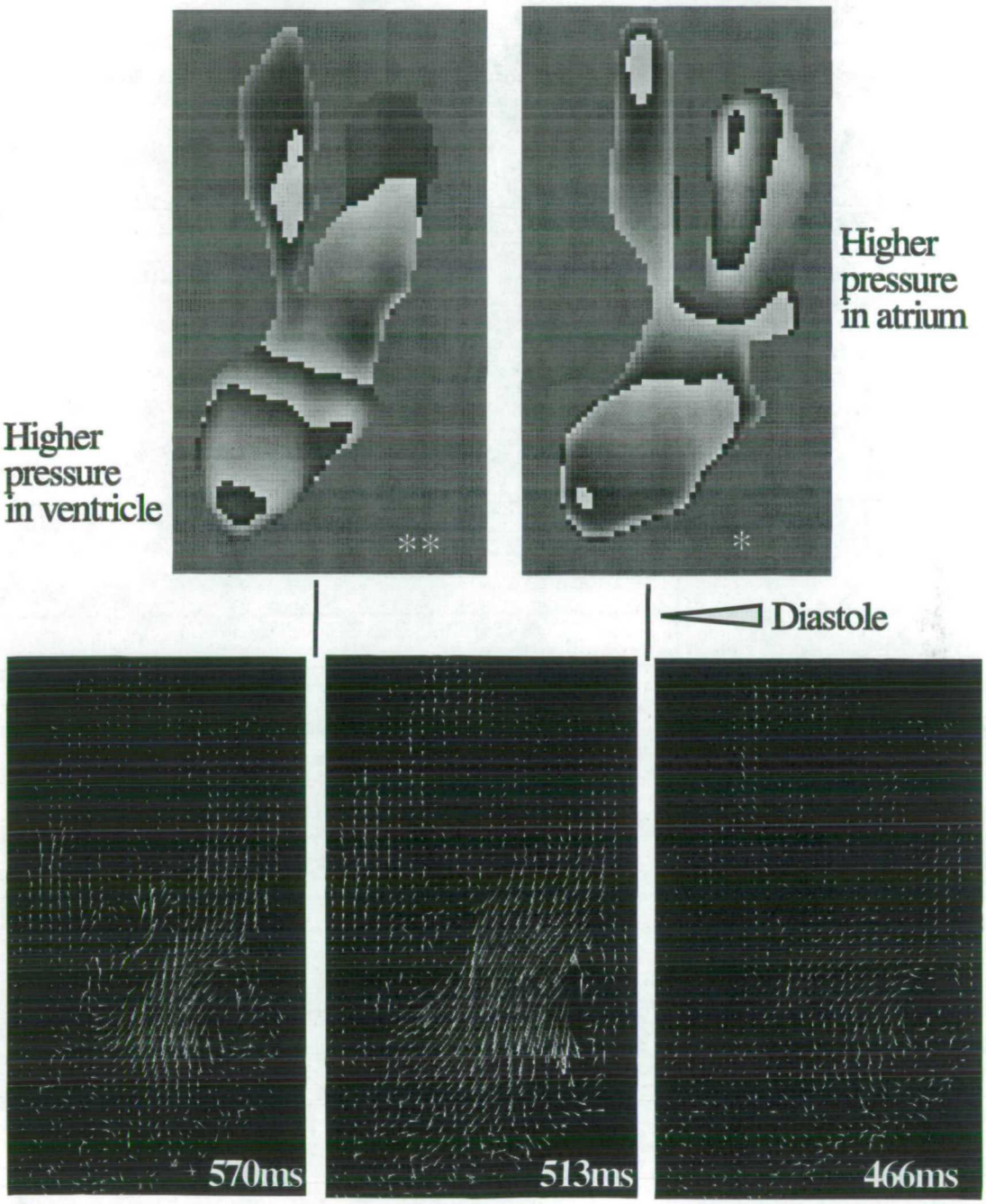


Figure 5.5c Early diastolic acceleration (right) immediately followed by deceleration (left)



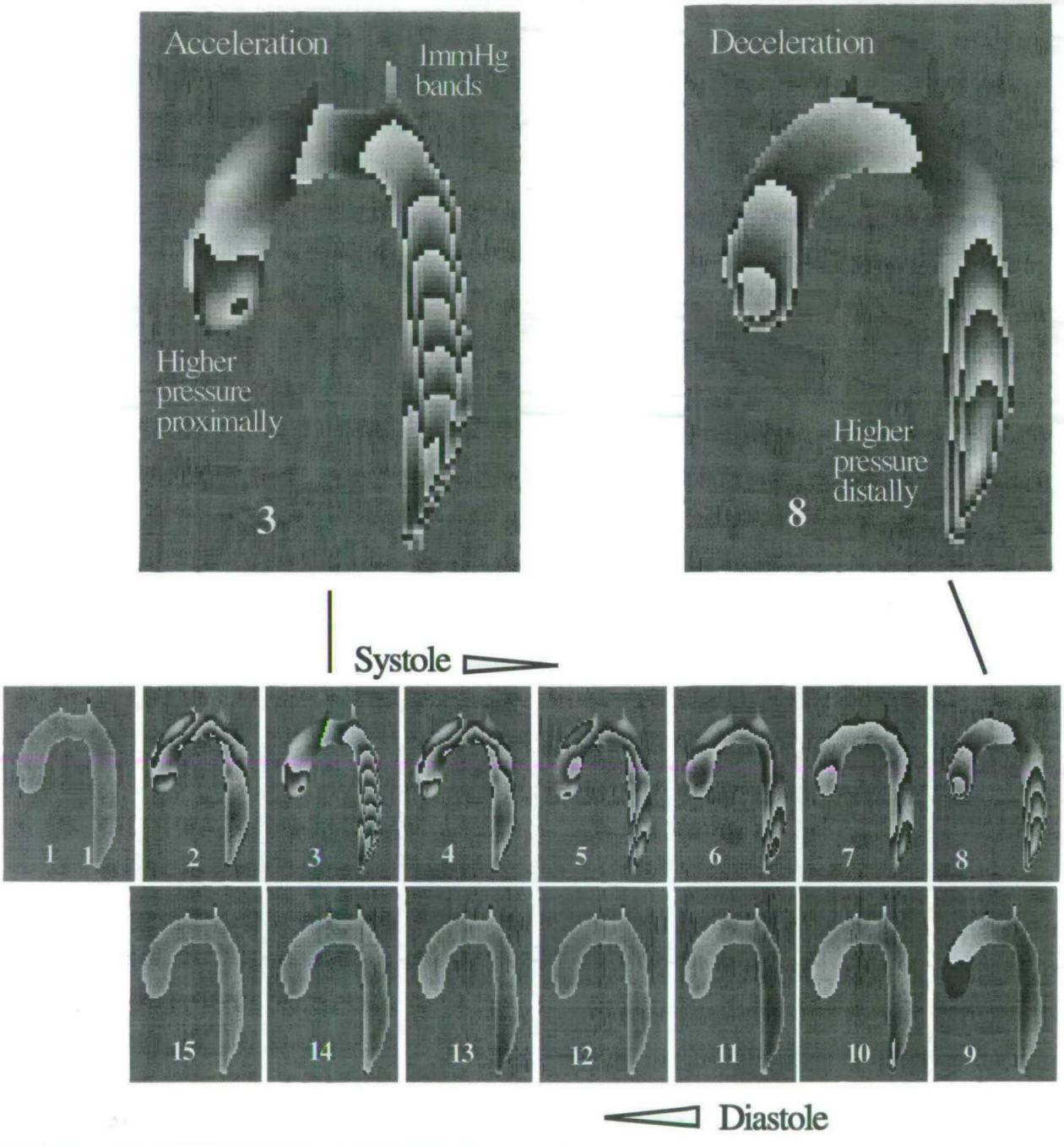


Figure 5.6 Dynamic pressure differences in the aorta (subject 18) computed from cine velocity data. Pressure differences of 10mmHg during peak acceleration (3), and reversed pressure differences of 6mmHg during deceleration (8) are computed in the thoracic aorta of this healthy subject at rest. A centrifugal pressure gradient towards the outer curvature of the arch is shown during peak systolic flow (4-6).

the diastolic frames, which do not cover atrial systole, show little pressure difference, although the first (pre-ejection) systolic frame shows minor variations of pressure, under 1mmHg, associated with residual vorticity following atrial systole.

The second *in vivo* study analyses magnetic resonance velocity data acquired in the plane of the aortic arch in subject 18, (described in Kilner *et al.* 1993, and Yang *et al.* 1996, both bound at end). During peak early systolic acceleration, a dynamic pressure difference of about 10 mmHg is computed in the length of thoracic aorta studied, although velocities and pressure differences in proximal and distal region, which pass out of plane, may be under-estimated. A reversed pressure difference of 6mmHg is computed at end systole. During systolic flow, a slight centrifugal pressure gradient is apparent in the arch.

Discussion

In early diastolic atrio-ventricular flow fields, rapid reversal of pressure gradient from one frame to the next suggests that temporal resolution of the velocity map data was barely adequate for computation of flow pressures in this region and this part of the cycle. The computed pressure differences do, however, accord reasonably well with those measured at catheterisation by Laniado (Laniado *et al.* 1976) and with those estimated from Doppler ultrasound measurements by Fujimoto (Fujimoto *et al.* 1995). Our computations probably tend towards under-estimation of pressure difference for the reasons noted in relation to the second *in vitro* study. And, during the acceleration phase at least, gradients might have been slightly steeper if viscous terms were included. Viscous retarding forces, however, are likely to be small in relation to inertial forces in the relatively large spaces of heart and aorta (Yang *et al.* 1996).

This indirect approach to cardiovascular dynamics, via differences of pressure derived from changes of velocity, gives an assessment of the dynamic relative to 'viscous-occlusive-hydrostatic' contributions to blood pressure. The results suggest that, at certain phases of the cycle, a by-no-means-negligible fraction of local aortic blood pressure, and a major part of diastolic atrio-ventricular pressures are associated with dynamic differences of pressure, even at rest. Potential enhancements of dynamic factors with exercise are considered in the next chapter.

Chapter 6

Exercise echocardiography of mitral flow and movement

Objectives

Studies in this chapter aim to record and measure changing interactions, with exercise, between left atrium, left ventricle and blood moving through them. The objective was to find out whether changes of mitral flow and movement with exercise were compatible with transition of the heart to a 'dynamic mode', in which inertial exchanges of force play a major role. In particular, clarification was sought as to whether and at what stage the relatively prolonged, biphasic diastolic mitral flow curve of the resting heart would became monophasic with exercise, and whether atrio-ventricular interaction, represented by long-axis movement of the mitral valve ring, increased with exercise.

Background

Studies of this chapter arose from the hypothesis that changes of flow direction help to optimise dynamic coupling, *particularly on exercise*, between ventricular and atrial function. A distinct functional interpretation of cardiac looping, compatible with, but not the same as the 'fluidic oscillator/amplifier' model introduced in Chapter 3, is being considered here. Change of direction at ventricular level is important for the following reason: if systolic ejection is to become rapid and forceful, with appreciable momentum imparted to out-flowing blood, then, according to Newton's laws, the ejecting chamber, like the body of a squid or the barrel of a gun, must recoil in the opposite direction. If systolic recoil pushed back towards the atrium, it would tend to impair or even reverse motion of the atrioventricular valve, with consequent impairment of atrial filling. The direction change at ventricular level allows inertial recoil of a contracting ventricle to pull rather than push on the atrium, enhancing atrial filling and inducing intra-atrial momentum towards the ventricle prior to opening of the atrio-ventricular valve – particularly on exertion.

That paths of flow through hearts are not necessarily tortuous can be appreciated from study of invertebrate hearts (Chapter 2). A telling example is the

heart of a snail such as *Helix pomatia.* Although thought to have evolved independently of vertebrate hearts, this particular molluscan heart shows major components surprisingly similar to those of vertebrate hearts, with atrial and ventricular cavities juxtaposed in a pericardial space. But, in distinction from vertebrate equivalents, the cavities and main vessels are linearly arranged. Atrium, ventricle and aorta lie in-line, so inertial recoil of the contracting ventricle, were it to occur, would push back on blood in the atrial cavity. Snails, though, are not noted for dynamic vigour.

Vertebrate species, on the other hand, achieve unrivalled combinations of size, complexity and mobility. When a terrestrial vertebrate runs, mechanics of the whole body operate in a distinct dynamic mode. Rapid locomotion is achieved through cycles of force and energy exchange that differ from the statics-dominated mechanics of walking. Inertial forces increase to match and overcome gravitational forces, with powerful, transient interactions between myo-contractile, inertial and elastic forces.

The looped heart could also undergo transition to dynamic mode on exercise, coming to operate as a flexible, pulsatile, tortuous, dynamic pump, for which there is no close mechanical equivalent. In this state, there could be tight coupling between contractile, inertial and elastic forces of atria, ventricles, great vessels and their passing blood masses, the whole heart functioning as a unit to achieve sinuous, sling-like redirection and enhancement of fluid momentum. Aspects of this dynamically coupled state, amenable to investigation by echocardiography, would be patterns and timings of atrio-ventricular interactions.

Pulsed Doppler and M-mode echocardiography, unlike magnetic resonance velocity mapping, are suitable for use during exercise, displaying flow and movement of selected cardiac regions. With the expert help of Michael Henein, who caried out the echocardiographic studies in this chapter, mitral flow (by pulsed Doppler) and long-axis mitral ring motion (by M-mode echocardiography – Jones et al. 1990) were recorded, from rest to strenuous exercise in healthy volunteers. Flow in the left ventricular outflow tract was also studied in selected subjects. Although studies of mitral flow during exercise have been published (Rassi et al. 1977, Turkevich et al. 1988), we could not find data presented in ways that revealed the progress, timing and extent of

changes of atrio-ventricular interaction from rest to strenuous exercise. That is what this chapter and its publication (Kilner *et al.* 1997 – bound at end) aim to contribute.

Materials and methods

Subjects

Sixteen volunteers, 15 male and 1 female, aged 24 - 57 (mean ± sd: 38 ± 10), without symptoms or history of cardiovascular disease, were studied.

Exercise

Echocardiographic studies were performed before and during exercise on a semi-recumbent exercise cycle, starting at 75 watts, increased in steps of 25 Watts at 2 minute intervals. Final work levels achieved varied with strength and tolerance of subjects. Peak work rates between 100 and 225 Watts were reached (146 ± 30 Watts). The aim was to record echocardiographic traces at rest, during at least one intermediate stage of exercise, and at strenuous exercise. Subject 1 (Figure 6.1, overleaf) went through a more extended exercise protocol than other subjects: exercise was commenced at 25 Watts, and increased in 25 Watt steps to 175 Watts over a period of 25 minutes. This allowed investigation at a series of stages of exercise, four of which are illustrated in figures 6.2, 6.4 and 6.5.

No subject reported chest pain or other unexpected symptom during investigation. The subjects varied in physical fitness. Subjects 1, 2 and 4 had exercised regularly over a number of years, subjects 2 and 4 being competitive athletes. None of the other subjects were in the habit of exercising regularly, and subjects 6 and 14 and 15 were overweight for their height. Subject 11 was the only female.

Echocardiography

A Hewlett Packard 77020 Sonos 1000 system was used with a 2 MHz transducer. Electrocardiographic and phonocardiographic traces were recorded.

Mitral flow velocities were recorded from the apical four chamber view by pulsed Doppler echocardiography with frequency shift calibration (Henein 1994). In addition to mitral studies, left ventricular outflow tract (LVOT) flow velocities were recorded at rest in ten subjects, at intermediate exercise in six of these, and at strenuous exercise in four.

M-mode echocardiograms showing long-axis movements of the atrioventricular valve plane were recorded in all subjects from an apical window using the same equipment (Jones 199). Movements of left lateral and septal regions of the mitral ring, and of the tricuspid ring to the right of the valve, were recorded. M-mode traces shown in Figures 6.2 and 6.4 are from the septal region of the mitral ring.

Doppler and M mode studies were recorded at a paper speed of 100mm/s. Measurements were made either direct from the paper recording, or by analysis of a digitised record traced from the original. Measurements made from the traces were as follows: R-R interval was measured as an average of five ECG cycles. The systolic period was measured from the ECG Q wave to onset of A2, the aortic component of the second heart sound identified on the phonocardiographic trace. Diastolic period was taken as R-R interval minus systolic period. The isovolumic relaxation time was measured from the onset of A2 to the onset of mitral flow, located by linear extrapolation of the early diastolic upstroke back to the base-line. Total valve ring excursion and, at lower heart rates, its late diastolic, atrial systolic component, and peak rates of systolic shortening and diastolic lengthening were measured from the digitised traces as were times to peak shortening and peak lengthening, from the Q-wave and A_2, respectively.

Results

Figures 6.1 – 6.4 display patterns and amplitudes of Doppler and M-mode curves at rest and during exercise. Figure 6.1 gives an overview of mitral flow curves in all 16 subjects. Figure 6.2 correlates mitral and aortic Doppler and mitral M-mode traces at rest and exercise in subject 11. Figure 6.3 shows progressive changes of Doppler and M-mode mitral curves from rest through intermediate stages to peak exercise in subject 1. Outlines of these are traced and superimposed, using the R wave of the ECG for temporal registration, in figure 6.4. The table, 6.5, presents values of selected measurements.

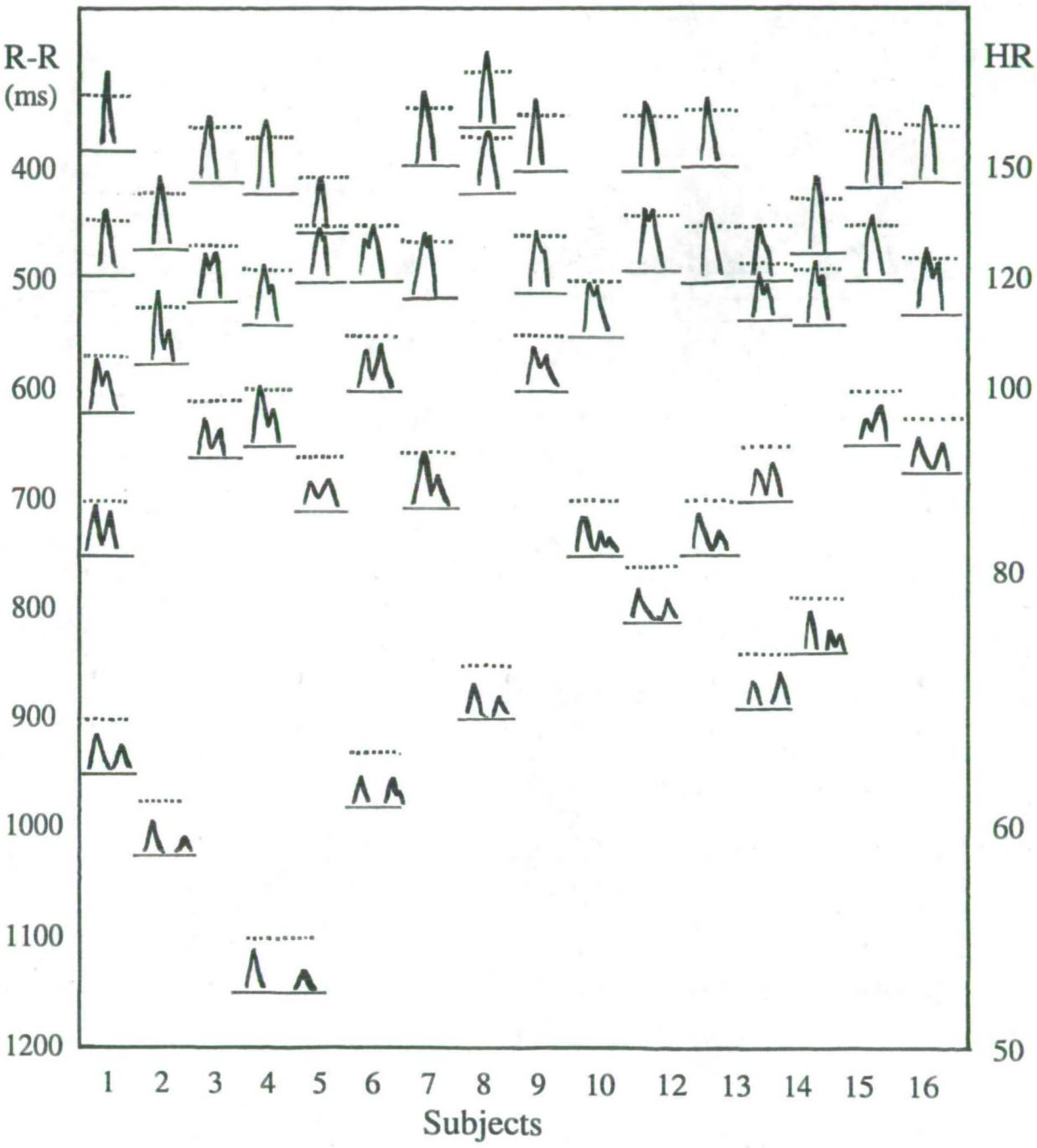


Figure 6.1. Doppler mitral flow curves in all subjects, from rest to strenuous exercise displayed with respect to R-R interval and heart rate (*HR* in beats per min). *Dotted lines* mark 1m/s levels. Transition to single-peak mitral inflow occurred at approximately 120 beats/min. *Y-axis values* should be read off at the baseline under each curve.

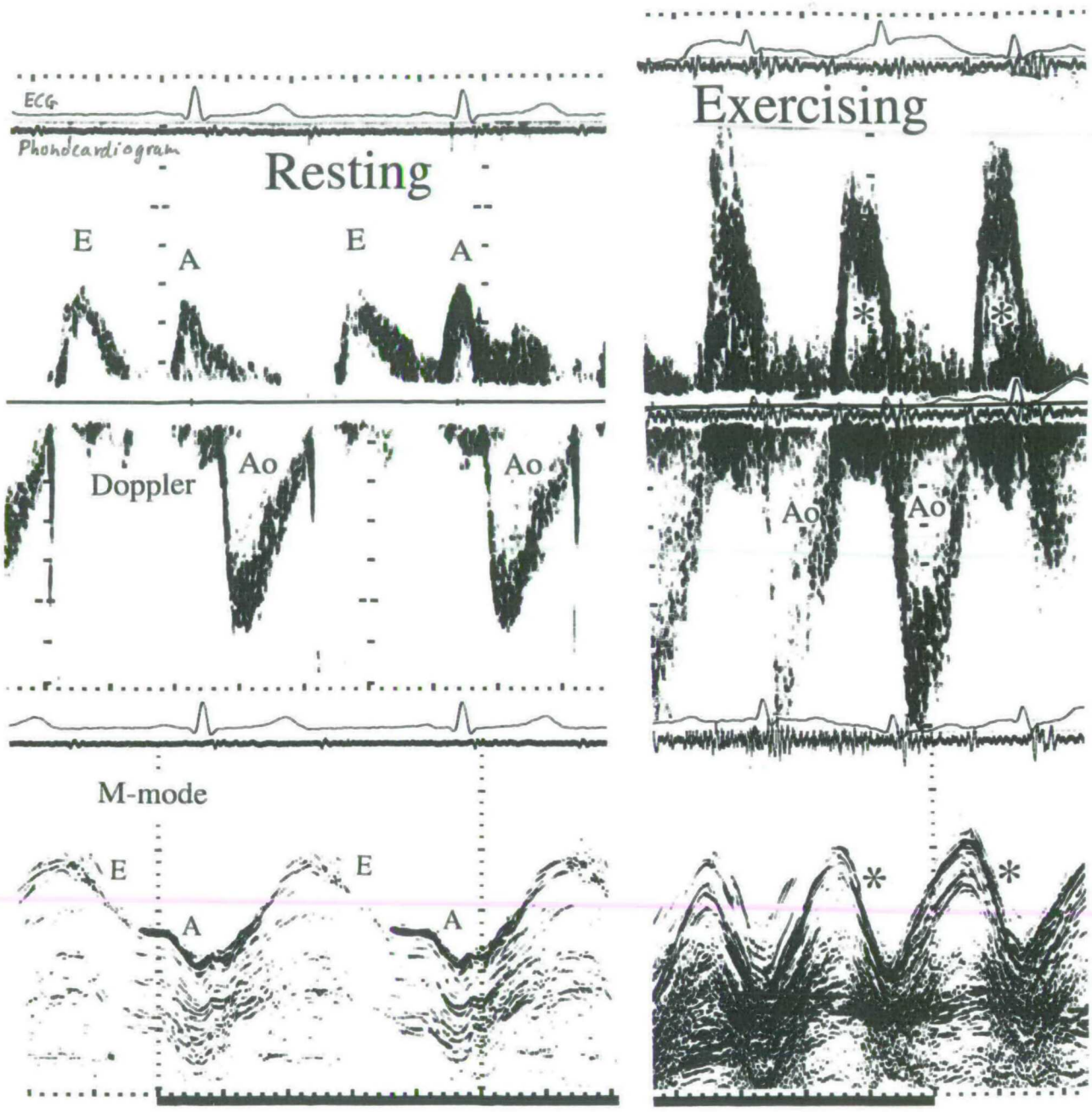


Figure 6.2 Pulsed Doppler traces of mitral and aortic flow, M-mode traces of long-axis movement of the septal part of the mitral ring, and corresponding ECG traces, at rest (*left*) and during exercise (*right* – subject 11 exercising at 125W). Phases of corresponding traces are temporally registered, as far as possible, although they were not recorded simultaneously. Upward deflexions of Doppler and M-mode traces represent velocities or displacements towards the apically located transducer. On exercise, notice the short diastolic period with a single elevated peak of mitral flow , reaching about 1.3m/s, coinciding with a single., rapid downstroke on the M-mode trace, to which elastic diastolic recoil and atrial systole contribute simultaneously (*asterisks*). *Ao*, Aorta; *E*, E-wave; *A*, atrial systolic wave.

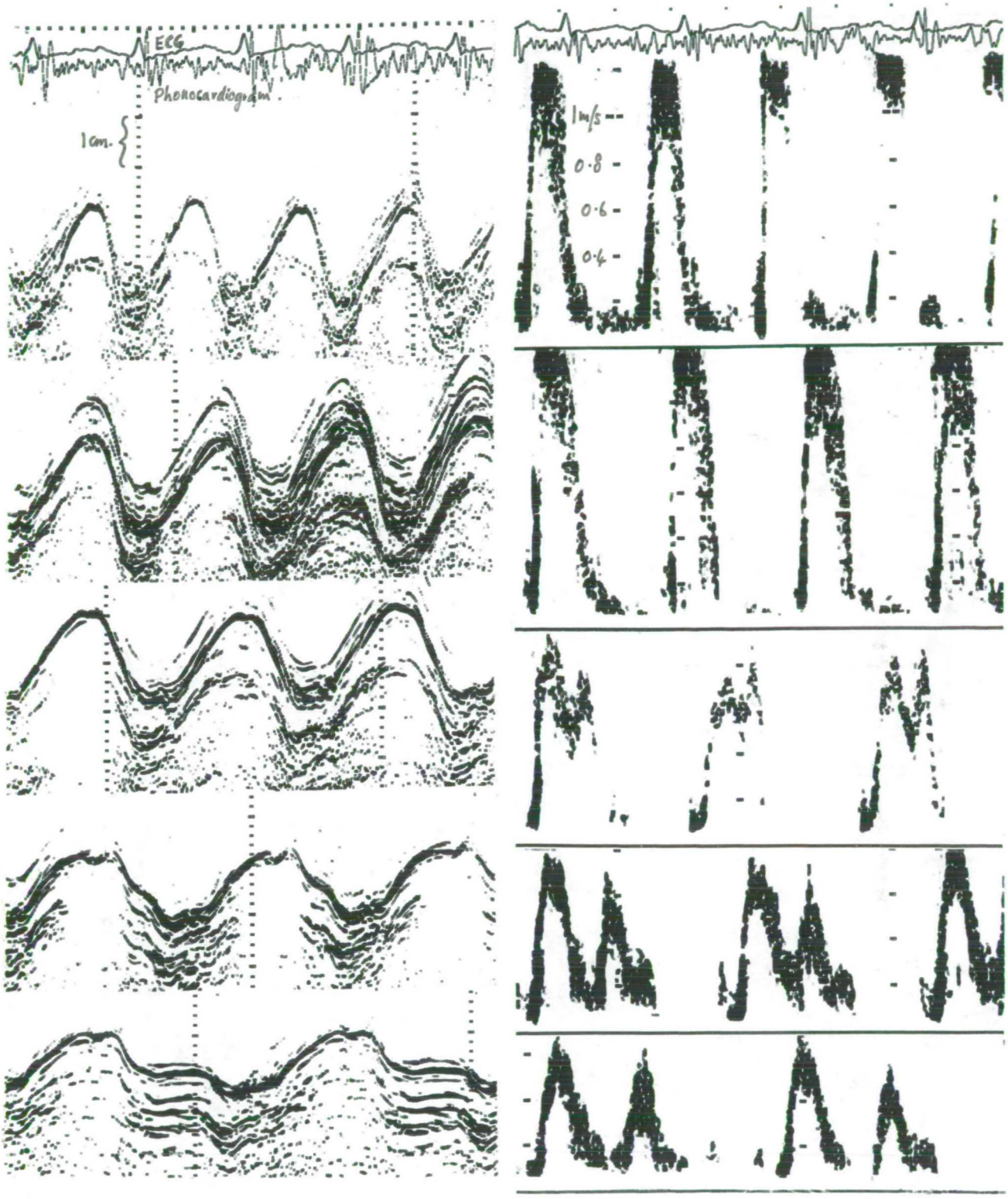


Figure 6.3 Progressive changes from rest (*below*) to exercise (*above*) of M-mode long-axis mitral ring motion (*left*) and Doppler mitral flow (*right*) in subject 1.

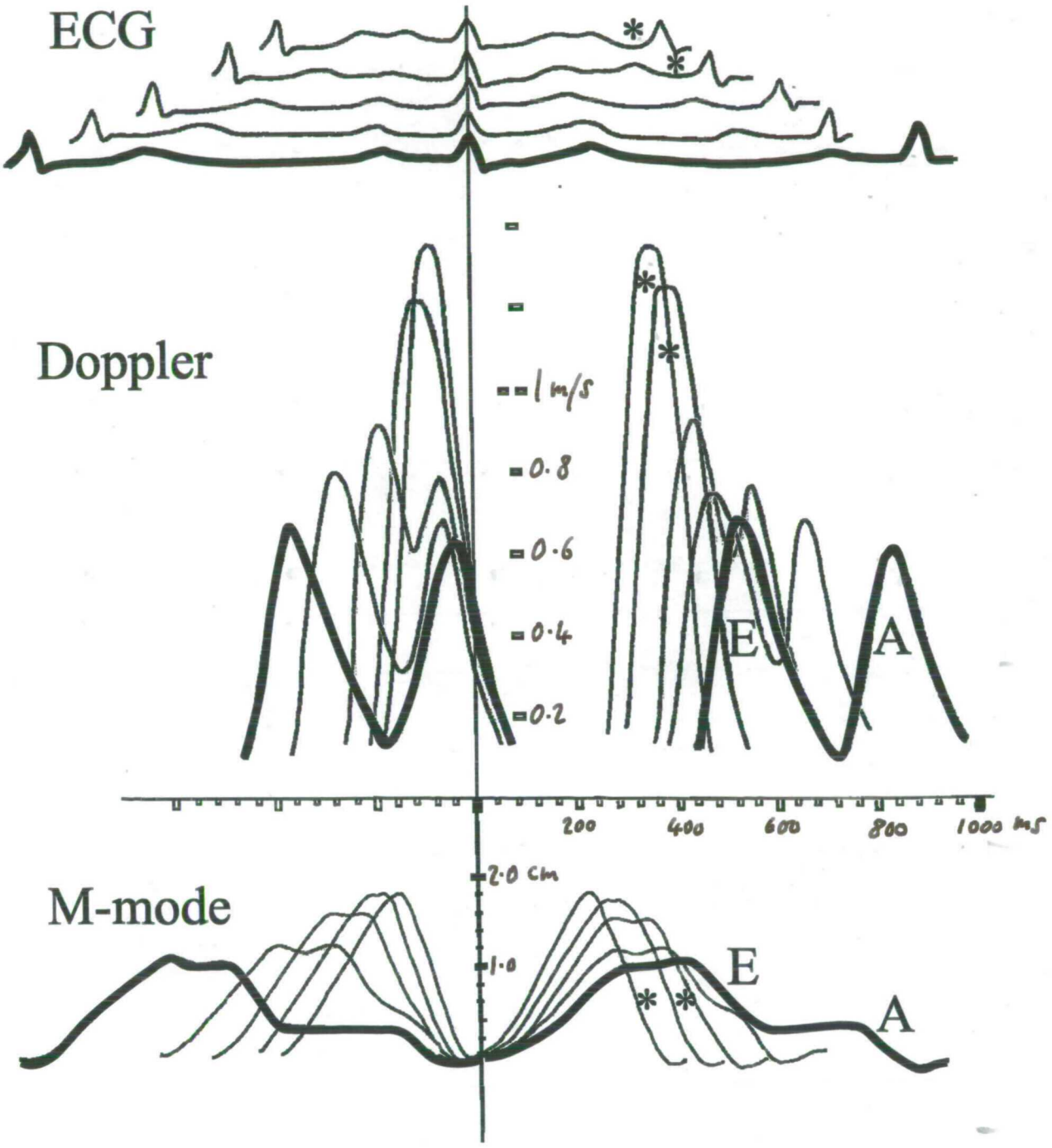


Figure 6.4 Superimposed outlines of Doppler and M-mode traces (from *Figure 6.3*), showing progressive changes from rest to strenuous exercise, together with corresponding ECG traces. All Doppler curves share the same base line and velocity scale. *Asterisks* mark atrial systole on two sets of exercise traces.

	Rest	Moderate exercise	Peak exercise
Work rate (W)	–	75–125 (103 ± 19)	100–225 (146 ± 30)
R-R interval (ms)	600–1160 (821 ± 151)	420–620 (527 ± 51)	355–530 (437 ± 51)
Systolic period (ms)	320–405 (362 ± 27)	255–340 (294 ± 28)	240–320 (268 ± 22)
Diastolic period (ms)	310–780 (458 ± 134)	190–310 (233 ± 48)	115–230 (169 ± 33)
Isovolumic relaxation time (ms)	65–90 (71 ± 11)	10–55 (29 ± 10)	0–35 (12 ± 10)
Mitral flow velocities (m/s)			
E peak	0.4–1.0 (0.68 ± 0.17)		
Summation peak		0.9–1.3 (1.09 ± 0.15)	1.0–1.50 (1.27 ± 0.16)
A peak	0 4–0.8 (0.54 ± 0.13)		
LVOT velocity (m/s)			
Peak velocity	0.8–1.1 (n = 10)	1.2–1.5 (n = 6)	1.4–2.0 (n = 4)
Displacements of valve rings (mm)			
Lateral mitral	9–20 (13.8 ± 3.3)	13–24 (18 ± 2.8)	15–24 (19.3 + 3.4)
Septal mitral	11–18 (13.7 ± 2)	15–20 (17.4 ± 2.2)	14–25 (18.6 ± 3.6)
Tricuspid	20–32 (23.8 ± 3.9) (n = 13)	22–34 (n = 4)	20–32 (n = 3)
Peak shortening rate (mm/s) and time to peak shortening from Q wave of ECG (ms)			
Lateral mitral	50–100 (73 ± 13)	70–130 (99 ± 20)	70–170 (125 ± 24)
Q-PS	60–230 (157 ± 47)	50–200 (127 ± 47)	50–200 (96 ± 33)
Septal mitral	50–100 (70 ± 13)	60–120 (87 ± 19)	60–170 (109 ± 35)
Q-PS	100–150 (137 ± 33)	100–180 (137 ± 40)	70–170 (108 ± 32)
Tricuspid	70–170 (115 ± 30) (n = 13)	110–200 (n = 4)	120–210 (n = 3)
Q-PS	80–170 (134 ± 28) (n = 13)	70–130 (n = 4)	60–110 (n = 3)
Peak lengthening rate (mm/s) and time to peak lengthening from A2 heart sound (ms)			
Lateral mitral	50–140 (92 + 27)	120–210 (154 ± 30)	90–230 (170 ± 42)
A2-PL	80–150 (122 ± 18)	90–230 (102 ± 17)	70–130 (86 ± 16)
Septal mitral	50–120 (81 ± 20)	80–190 (135 ± 38)	90–220 (163 ± 56)
A2-PL	90–180 (119 ± 20)	80–180 (99 ± 27)	60–180 (82 ± 20)
Tricuspid	80–170 (106 ± 30) (n = 13)	140–220 (n = 4)	140–380 (n = 3)
A2-PL	80–200 (134 ± 46) (n = 13)	80–100 (n = 4)	50–80 (n = 3)

Subjects: n = 16 (except where fewer indicated), 15 men and 1 woman; age, 24–57 (38 ± 10) Years: Range (mean ± SD)
LVOT, Left ventricular outflow tract; ECG, electrocardiogram

Table 6.5 Measurements from Doppler and M-mode echocardiographic traces

There was a striking increase of peak mitral flow velocity, in the region of 100%, from rest to exercise - a greater proportional increase than that recorded in the left ventricular outflow tract. This was associated with marked shortening of the diastolic period, which, although longer than systole at rest, was shorter than systole in all subjects at peak exercise. At rest and through initial stages of exercise, two peaks of mitral flow, the early diastolic E-wave and late diastolic (atrial systolic) A-wave, were distinct, but they progressively merged with rising heart rate, and fused to a single elevated peak at heart rates above 120 beats per minute, i.e. as R-R interval fell below 500ms (Figures 6.1 – 6.4).

Progressive summation of mitral Doppler E and A waves with increasing heart rate was accompanied by a corresponding changes of M-mode traces of long axis valve ring motion (Figures 6.1, 6.2 and 6.4). Whereas at rest the diastolic phase contained two distinct periods of movement, these merged to one rapid, continuous diastolic movement on exercise, at the same time as the single peak of mitral flow appeared. Peak lengthening rate was consistently greater than the maximum early diastolic value at rest.

There was relatively little difference between M-mode trace changes recorded in the lateral and medial mitral positions. The extent of long axis motion of the tricuspid valve ring was greater than that of the mitral ring at rest, but it showed little increase with exercise in the few subjects studied.

The isovolumic relaxation time progressively shortened, and at peak exercise was effectively eliminated.

Discussion

The patterns and timings of mitral flow and movement change progressively, as illustrated by the traces displayed in the figures. In the much shortened diastolic period of exercise, the entire stroke volume, probably greater than that of the resting heart (Higginbotham et al.1986, Nonogi et al.1988, Salmasi et al.1987), has to pass through the atrioventricular valve. This is accomplished by rapid apical flow of blood coinciding with rapid basal movement of the valve. Correlation of echocardigraphic and ECG traces (Figure 6.4) shows that elastic ventricular recoil, considered to be the principal cause of the early diastolic peak of flow and movement at rest, must come

to coincide with atrial systole in the short diastolic phase of exercise. So, in contrast to the relatively prolonged, biphasic diastolic interactions of the resting heart, the exercising heart develops one-to-one coupling of atrial systolic with ventricular diastolic function (and *vice versa*).

Although these observations of transmitral velocity and ring motion, up to strenuous exercise, may not be surprising to cardiologists familiar with stress echocardiography, we had not been able to find them clearly recorded and displayed. We set out to do this, with the aim of considering the changes in relation to momentum changes of blood as it moves through the curvatures of the heart, postulating that the way in which atria, ventricles and arterial trunks are connected in space gains particular importance on exercise. To appreciate this, the roles of static and dynamic force exchanges between atria and ventricles need to be recognised.

Stresses associated with tension of elastic and muscle fibres, hydrostatic pressures in blood and pericardial fluid, plus any gravitational influences on these, are among the forces or counter-forces of the heart. Atrial and ventricular function are coupled through these types of force at rest and during activity, even in a snail (Dale 1973). Forces associated with changes of momentum, on the other hand, increase and gain significance as rates of change of momentum increase with exercise. When this happens, flow direction-change has twofold bearing on atrioventricular coupling. Firstly it determines the direction in which inertial recoil, away from ventricular ejection, acts. Recoil from rapid ventriculo-arterial ejection would hinder statics-mediated atrioventricular coupling in a linearly arranged heart, but can act as a bonus in the looped vertebrate heart, contributing to increased mitral ring motion during exercise. And secondly, reversal of direction between inflow and outflow means that momentum changes of decelerating inflow and of accelerating outflow are summated. They act in the same direction, swiftly following one another, on exercise, without an intervening pause. The rapidity with which mitral inflow turns to become left ventricular outflow can be appreciated from study of the exercise Doppler traces in Figure 6.2. Flow into the exercising heart does not need to come to rest (it does not need to be stopped by valve closure, given excursions of valve rings and swirling of blood in cavities), but may be redirected fluently from one direction to another, as illustrated in Figure 4.16.

The exercising heart may thus operate as a coordinated unit, propelling blood kinetically as well as by occlusive displacement, through redirection and enhancement of momentum via sinuous paths of flow. It is the combination of looped curvature with alternating contractility of atrial and ventricular loops that makes possible the sling like action and counter-action of the heart's dynamic mode.

Echocardiographic changes illustrated in this chapter accord with this description, but do not, on their own, enable proof or quantitative analysis of it. Because postulated dynamics involve fluid-structure interactions extending across heart chambers and vessels, echocardiographic data remain, on their own, too limited for quantification of the role of inertial force exchanges in relation to other components of cardiovascular mechanics. There is as yet no technique that provides sufficiently comprehensive information on changing cardiovascular geometries, velocity fields and wall mechanics. Magnetic resonance techniques offer relatively comprehensive anatomic and flow information, but are not well suited to investigation during exercise. Development of computational models, incorporating structural and functional information from multiple sources, may provide an indirect approach to the subject, although, even for single heart chambers and valves, such computation is complex, and adequate input data may not be available (Peskin and McQueen 1995). Attention is drawn to the possibility of computer simulation of large-scale dynamic interactions across the exercising heart. The data presented in this chapter could contribute towards appropriate computer simulation.

Clinically, the results may have bearing on management of physically active patients who require reconstructive heart surgery, or who have rhythm or conduction disturbances needing intervention by drugs or pacing. Better understanding of morphodynamic function of the exercising heart could lead to refinement of surgical, pharmacological or electrophysiological approaches, with a view to maintenance of optimal heart function during exercise as well as at rest.

In conclusion, the illustrated patterns of exercise flow and movement accord with the postulated 'dynamic' mode of function in which forces between atria, ventricles and passing blood masses become tightly coupled to achieve sling-like redirection of momentum through tortuous paths of flow. Computation of dynamic pressure differences in the resting heart (Chapter 5) showed inertial

components of pressure to be significant in relation to atrial function and ventricular filling, even at rest. Taking this finding together with those of this chapter, there can be little doubt that momentum changes of blood through tortuous curvatures, and dynamic exchanges between atria and ventricles mediated through tension of walls and momentum of blood, gain crucial importance on exercise. But more extensive data would be needed to adequately model and quantify inertial force exchanges of the exercising heart.

Chapter 7

Interpretation of the heart as a dynamic organ of flow

Purpose

This chapter summarizes principal findings and ideas of Chapters 2 to 6, with the aim of correlating them in a more integrated interpretation of the heart as a dynamic organ of flow.

Findings and ideas

The thesis illustrates and describes a series of conceptually distinct but functionally interrelated concepts. These are briefly recapitulated here, and each given a heading for discussion and correlation.

Vertebrate cardiac looping

In the comparative review of heart shapes (Chapter 2), cardiac looping was not found to occur among the varied hearts of invertebrates, but was found to be a feature common to all vertebrates, with increasing refinement in higher orders. This supports the proposition that looping may have contributed to evolution of vertebrate complexity and dynamic prowess. Or, considered another way, advances of bodily structure such as vertebral column and jaws may have called for corresponding enhancement of cardiac efficiency, met through looping of the ventral heart.

Chapter 3 introduces two key observations regarding fluid dynamic consequences of the asymmetries* of heart cavities – perhaps especially atrial cavities - that arise through looping. There are spontaneous oscillation and stability of flows associated with asymmetries of containing cavities, summarized overleaf:

---

* Animal bodies show asymmetries in three orthogonal directions: cephalo-caudal, dorso-ventral and lateral. It is the second (dorso-ventral) that may be seen as the most characteristic asymmetry of cardiac looping, with the atrial loop displaced dorsal to the ventricular. But lateral asymmetry is also present. Although the fish heart, with one atrial and one ventricular cavity, appears relatively symmetrical laterally, a degree of lateral asymmetry is surprisingly fundamental. Even in jawless fish such as lampreys and hagfish, liver and hepatic veins form asymmetrically, imparting some degree of lateral asymmetry to the developing heart.

Flow oscillation associated with cavity asymmetry

Asymmetry of a (compliant) cavity can be associated with a particular type of spontaneous oscillation of flow, such that continuous inflow is converted to intermittent outflow without occlusion or interruption of momentum within the cavity. This principle might contribute to efficiency of heart function at atrial level.

Comparison of heart cavities of a fish with forms of asymmetric fluid oscillators (Chapter 3) suggests that the looped vertebrate heart might have adopted the form of a fluidic oscillator-amplifier. The oscillating trickle (Figure 3.5), whose form can be compared with initial curvatures of vertebrate hearts in embryonic development (Figure 1.1 and Figure 3.7), lends support to the idea. In the fluidic oscillator-amplifier model, the atrium, with appropriate shape and compliance, accommodates a flow cycle that mediates between relatively continuous venous return and intermittent atrio-ventricular flow. If the latter is boosted by atrial contraction, so much the better. Ventricular form shows apparent reversal with respect to flow (Figure 3.7); it receives flow intermittently and delivers flow to the arteries with amplified peaks of velocity and pressure.

There are problems in application of this model to complex mammalian hearts, however, which have multiple venous inlets and marked lateral as well as dorso-ventral asymmetry.

Stability of flow associated with cavity asymmetry

The second observation raised in Chapter 3 is that asymmetric inflow, with unilateral separation and large-scale recirculation, provides a more stable flow topology than symmetric, bilateral (or multi-lateral) separation and recirculation. Separation of streamlines on entry to a cavity is inevitable with certain inflow rates and cavity dimensions. Unilateral separation allows streamlines to remain attached on one side, stabilised by inward curvatures of walls, so minimising intra-cavity counter-streaming and collision which would predispose to turbulence.

The above two principles work together. One of the methods used in design of 'Flowforms' by interactive flow modelling (Chapter 3) is elimination of unwanted recirculation zones, retaining and stabilizing only large-scale flow structures. In other words, streamlining not for laminar, but for secondary patterns of flow which

show large-scale coherence, and, in this case, spontaneous, flow-mediated rhythmicity of flow.

Ring-vorticity and valvular streamlining

Chapter 3 includes illustrations of the 3-dimensional structure of a ring vortex, and the 2-dimensional surface appearance of a train of vortices shed in a wake, each formed relatively freely through inertial-viscous interaction in a fluid volume. These examples are introduced for consideration in relation flow through heart valves at atrio-ventricular and ventriculo-arterial levels. Topology of flow through a heart valve into the receiving ventricular cavity or sinus may be considered as that of a ring vortex, constrained and modified by the proximity of boundaries. The thin, flexible forms of valve leaflets conform to the separation streamline (stream-surface) of the incipient ring vortex. Flow vectors through the mitral valve into the left ventricle show asymmetric vorticity (Figure 4.14, opposite p61), comparable in long-axis section to a pair of vortices shed in a wake (Figure 3.10d, opposite p51). Lines of shear between vortices correspond in position and form to lines of the valve leaflets. Containing walls of ventricle or sinus may also conform, to some extent, to outermost shear layers of the vortical system.

Clearly, there are deviations from this description, particularly in the right ventricle, but it nevertheless seems to throw light on the topology of flow in relation to heart valves. The occlusive efficiency of the valves relies in part, as Leonardo da Vinci (Keele 1952) and later Brian Bellhouse (Bellhouse 1972) deduced, on dynamics of quasi-ring-vortical flow systems.

Further stability through helical asymmetry

Lateral asymmetry gives a helical twist to the S-bend of the looped heart. Helical asymmetry was not simulated in the Flowform models of Chapter 3 (the models, using gravity waves for compliance, effectively lie on one side, 'dorso-ventral' being simulated horizontally). Their spontaneous oscillatory cycle relied on impingement of recirculating with inflowing streams, and hence collision and turbulence at a certain phase of the cycle. Sino-atrial rhythmicity, however, absolves intracardiac streams of any rhythm-*triggering* role, although inertial mass in relation to finite elastic and contractile restoring forces must still be associated with a natural frequency that would vary according to rate of inflow, and with endocrine and

autonomic influences. The Frank-Starling law fits well in the picture of responsive-active heart action. Given myogenic origin of contractility, however, optimum cavity form may combine dorso-ventral asymmetry with lateral asymmetry to give flow paths that trace sinuously twisted curves without collision.

Intracardiac flow patterns were studied by magnetic resonance velocity mapping in Chapter 4.

Atrial filling patterns

Both atrial cavities, particularly the right, fill (during systolic and early diastolic phases) with large-scale, rotating swirls of blood, forward rotating in the right atrium, and anti-clockwise rotating (viewed from the front) in the left atrium. These swirls are broadly comparable with asymmetric swirls formed *in vitro* during the filling phase of the spontaneous flow cycle in an asymmetric cavity (Figure 3.4) and during rocking of an asymmetric form (Figure 3.11). Patterns of intra-atrial flow accord with the ***"Stability of flow associated with cavity asymmetry"*** and ***"further stability through helical asymmetry"*** theories outlined above, although understanding of ***"Flow oscillation associated with cavity asymmetry"*** is not straightforward in relation to human heart function.

Inertial-elastic-contractile interaction

An interpretation of flow-structure interactions of human atrial cavities could be outlined as follows: moving inertial mass of entering blood interacts with compliant walls, increasing tension and so priming fibres for subsequent contraction, which then boosts the tensile restoring force. The inertial mass and restoring forces are finite, so a certain oscillatory frequency is likely to be associated with this interaction. Its period is probably short compared with cycle lengths at rest, and filling is found to be biphasic in this state, but the oscillatory period may correspond closely on exercise with the time of cavity filing and ejection. On exercise, blood enters the ventricles with more momentum, induced, in part, by work of the preceding systolic contraction, and so contributes more to pre-systolic stretch of the myocardium.

Redirection and continuity of momentum

Correlation of spatio-temporal patterns of flow through chambers of the resting heart (Figure 4.16, opposite p67) suggests that at least part of the momentum of inflow is

turned towards outflow, even if, at rest, little of the kinetic energy of inflow is conserved until the onset of outflow. In the exercising state, however, when momentum of inflows are greater but cycles shorter, redirection and continuity of movement from inflow to outflow, and from one compartment to the next, is likely to gain importance for efficiency of heart action.

Dynamic force exchanges

In chapter 5, computations of 'flow pressures' from measured changes of velocity showed evidence of pressure differences of the order of 5mmHg along atrioventricular, and over 10mmHg along ventriculo-aortic flow paths during phases of acceleration or deceleration. These, particularly the atrio-ventricular pressure differences, are not insignificant. Atrio-ventricular blood, in the diastolic phase, has gauge pressures of this order.

Merging and summation of inflow peaks with exercise

The exercise echocardiographic studies of Chapter 6 demonstrated enhancement of mitral movements, flow velocities and rates of change of velocity with exercise. The relatively prolonged, biphasic diastolic flows of the resting heart become short, swift and monophasic with exercise. These changes are likely to have significance for the dynamics of flow, although data on spatial distributions of velocity were not obtainable by the echocardiographic methods used.

Inertial recoil of the looped ventricle

Direction change of blood at ventricular level, a consequence of looping, is a prerequisite for inertial recoil of the forcefully ejecting ventricle to exert pull rather than push in relation to the atrial cavity. Without looping, inertial systolic recoil on exertion would tend to impair ventriculo-atrial coupling. With looping, ventriculo-atrial coupling can become enhanced with exercise, as seen in the studies of Chapter 6.

Dynamic mode of the exercising heart

Several of the factors outlined above may combine to transform cardiac fluid-elastic-contractile dynamics into a distinct mode on exercise, analogous with change of mode of whole-body mechanics from walking to running. Velocities and quantities of blood passing are increased, and rates of change of velocity (hence momentum) increase greatly. Rapid alternation and coupling of systolic and diastolic phases of ventricular and atrial cavities, enhanced by inertial recoil of looped ejecting chambers, may

contribute to the effectiveness of the exercising heart. Enhanced inflow velocities would give rise to more marked swirling as chambers fill. With shortened cycle lengths, momentum of inflow, redirected, may not only contribute to ejection, but also, if conserved as a swirl in the remaining fraction of blood, deflect fresh inflow, so maintaining the swirl - a relatively stable form of intracavity flow - from one cycle to the next. Inflow, turn and outflow take finite time, and exert a certain tension on the relaxing wall. Coordination of this fluid-elastic cycle with the myocardial cycle of movement could be functionally advantageous.

Morphodynamic action of the heart as a whole

Combining these effects, what is proposed is that the exercising heart functions morphodynamically, redirecting and slinging blood through its tortuous curvatures, with tight reciprocation of atrial and ventricular function which depends on overall shape as well as on structural, electro-conductive and contractile properties of parts.

Chapter 8

Strengths, limitations and implications of the work

This work has attempted to contribute to understanding of dynamic implications of sinuous curvatures of the heart.

The subject has been approached in several ways - through comparative review of shapes of animal hearts, through in vitro flow modelling, through magnetic resonance and Doppler echocardiographic investigations of blood flow, and through computational analysis of flow data. The approaches relate to several aspects of the subject. In combination, they support the interpretation that flow direction changes and asymmetries of the heart have functional importance, although each approach alone is not, at the present stage of the work, sufficient to confirm or disprove the underlying hypothesis.

It was this problem that motivated me to put the thesis together at this stage, although I do not regard the work as complete. As presented, it calls for imagination on the part of the reader to relate parts and make allowances for limitations of the data. There is relatively little mathematical analysis of fluid dynamic observations and interactions. But in defence, rigorous analysis of limited information may be more misleading than informed semi-quantitative consideration of the complex and extensive interactions that must operate.

Through repeated study of magnetic resonance cine velocity maps in different planes and different subjects, I have had access to more flow information than there has been time or space to analyse and illustrate. The computational analysis of dynamic pressure differences remains more limited than I had intended, being applied to single studies in only two planes. I hope to take this aspect further, in collaboration with GZ Yang, comparing results between subjects, improving temporal resolution of velocity acquisitions, and, if technical difficulties can be overcome, acquiring magnetic resonance flow data in exercising subjects.

Another approach, for which I would like to find collaborators, is computational fluid dynamic modelling of the exercising heart. I have alluded to difficulties of computing interactions between multi-directional flows and

compliant-contractile boundaries of complex geometry. But, as a preliminary step at least, I believe that 2-dimensional simulation of the dynamics of a sinuous atrio-ventricular flow field contained by compliant/contractile boundaries could provide information on the functional implications of transition to the more strongly coupled, dynamic mode of exercise.

Organic complexity

The ideas investigated in this thesis are limited in a way that is shared by any other type of cardiovascular investigation or explanation. In relation to living reality, they deal with no more than incomplete and imperfect fragments. This would still apply if investigations were undertaken at sub-cellular levels, although no attempt was made in this thesis to comprehend cardiac micro-structure or metabolism. Living organic reality is inconceivably complex and in a state of continual change. This can be appreciated though informed imagination, using information from various sources.

Imagine, for example, flows of the heart in relation to the intricate branches of arterial and venous streams, connecting peripherally through systemic and pulmonary capillary beds. Consider the origins and fate of the particular volume of blood taken into the right atrium during a single cardiac cycle. Traced back upstream, it would have gathered, during the preceding seconds and tens of seconds from converging venous streams of the volume of the whole body. Similarly, subsequently and downstream, via pulmonary vasculature and left heart, the volume of atrial blood will again be dispersed and diffused through the volume of the whole body. It will never come together again in the same combination of cells and fluid - each heart-full contains a unique gathering of blood. Also unique, presumably, from one beat to the next, are the intricacies of small-scale flow disturbances within the large-scale order of intracardiac flow.

The heart and the sentient organism

Regarding broader implications of the work, an aspect I would like to raise, even if it might not follow obviously from what has been presented, is role of the heart in relation to sentient experience. Contemporary cardiology and heart surgery treats the heart as little more or less than a muscular, valved pump that maintains circulation of blood for other organs to do their work. Studies in this thesis contribute to

appreciation of responsive aspects of heart function. In relation to flow, the vertebrate heart appears to have the underlying, though modified form of a fluidic oscillator-amplifier, an arrangement that complements responsive-active function at myocardial level (Frank-Starling law). Magnetic resonance flow studies show large-scale, coherent movements of blood that must engage with elastic-contractile function of the thin-walled atrial chambers from which the events of ventricular filling, contraction and arterial pulse proceed. The heart is connected to receive blood from all parts of the systemic and pulmonary circulations, and to deliver arterial blood to all parts of pulmonary and systemic circulations, respectively. Responsive to the dynamics of returning streams, as well as to incoming endocrine and autonomic influences, the heart must variably 'sound' the global organic state, and in doing so, give rise to the pulse which propagates back out to brain and other organs. It can be recognised as one of the richest and most unifying information pathways of the body. Passages and exchanges of biological information are not deterministic, but non-linearly interactive and variable (Goodwin 1995, Williams 1997). Cardiac interactions apparently take place almost entirely sub-consciously, although continually modified, in wakefulness, through activities and breathing patterns (Hildebrandt 1991). The brain, presumed to be our primary organ of awareness, is bathed in the heart's pulse.

Clearly any part played by the heart in relation to sentient experience is not easily defined. It is neither deterministic, nor, apparently, essential. A range of cardiac pathologies, artificial pacing and even mechanical heart replacement remain compatible with continued sentient experience. But this does not exclude the possibility that the heart, in its healthy state, plays a participatory role in the experiences as well as continued viability of our sentient organism.

Clinical implications

Regarding clinical implications of the work of this thesis: although I regard its interpretation of heart form and function to be of fundamental biological importance, and of physiological importance during exercise, its clinical relevance is not obvious. Like other organs, the healthy heart has a great deal of spare capacity in its resting state. It can continue to serve in spite of marked deviations from normal form and function. Heart valve stenosis or incompetence, various degrees and types of

congenital malformation, and ischaemic myocardial dysfunction may all be tolerated for years or decades as long as moderately effective myocardial and valve function, and reasonable vascular connections, are maintained. Refinements of morphodynamic function do not appear to be essential.

There are two possible responses to this observation. One concerns management of patients who wish to remain physically energetic. If such patients require reconstructive heart surgery, cardiac pacing or pharmacological treatments for arrhythmia or other myocardial disease, it may be important to be aware of the morphodynamics of efficient heart action on exercise. Surgery that maintains the mobility and flexibility of valves, for example, may be more appropriate than achievement of absolute competence of valves. In patients with arrhythmias, dual-chamber pacing that allows precise re-adjustment of timing to match the altered dynamic mode of exercise may be advantageous.

The second response concerns length and quality of life. The healthy heart is a remarkably flexible, responsive and reliable organ of flow. It continues to beat second by second, day and night through all the months, years and decades of life. Patients, for example with congenital or valvular heart disease, undergoing surgery with a view to a full remaining life span should expect to have their heart restored as closely as possible to a healthy functional state. Knowledge of that state is a prerequisite for this is to be attempted.

In conclusion, I would like to say that I find the most satisfying aspects of this work to be the biological and aesthetic. The evidence suggests, to me at least, that functional advantages of sinuous curvatures of the heart could have been pivotal in evolution of our vertebrate line. And the studies give insight into the fluent beauty of the heart – its sinuously entwined streams continually responding to and serving the states and needs of the body as a whole.

Acknowledgements

My interest in the shape of the heart as an organ of flow began in 1981 when I was studying form and flow with the sculptor John Wilkes. I would not have found my way to this area of enquiry, or realised the value of combining complementary approaches, without the stimulus of John's teaching. This, in turn, owed much to artistic/scientific approaches that, via Theodor Schwenk and Rudolf Steiner, can be traced back to Johann Wolfgang von Goethe, the great figure of 18th century German literature. It is not so widely known that Goethe was a natural scientist who made highly original contributions to studies of colour and organic form. His lively, perceptive, inclusive scientific approach was different in quality from the analytical, deductive brilliance of Isaac Newton, his English contemporary. As it turned out, Newton was to have far greater influence on 19th and 20th century science, and this thesis relies on his fundamental insights. But the approach taken owes much to Goethe's example as a scientist using artistic faculties.

My re-entry to main-stream medical research was made possible through the support of Marc de Leval and Donald Longmore, both heart surgeons appreciative of my experience designing water sculptures. Through Donald and David Firmin - patient and gently encouraging supervisors of the thesis - I was introduced to cardiac magnetic resonance imaging and velocity mapping. And I would like to thank Raad Mohiaddin, Guang Zhong Yang and Michael Henien for their collaboration. Raad Mohiaddin contributed some of the velocity map acquisitions reported in Chapter 4. Guang Zhong Yang made outstanding image processing contributions, being responsible for computations of flow vector maps and dynamic pressure fields of Chapters 4 and 5. Michael Henein carried out the echocardiographic studies used in Chapter 6.

I appreciate the tolerance of all my colleagues in the Magnetic Resonance Unit at Royal Brompton Hospital who allowed me to pursue studies which may not have appeared to be clinically relevant. I am very grateful for financial support received over a number of years from the Lloyds of London Tercentenary Trust, the Coronary Artery Disease Research Association (CORDA) and, over the last three years, from the British Heart Foundation.

Three directional magnetic resonance flow imaging of the human heart

6

Philip Kilner, M.B., B.S., L. Samuel Wann, M.D., David Firmin, Ph.D. and Donald Longmore, FRCS

We used a modified 0.5 Tesla Picker MR machine and the Field Even Echo Rephasing (FEER) sequence to acquire flow velocity data in three orthogonal directions in and through selected slices of phantoms and human volunteers. Our purpose was to progress towards more comphrehensive mapping of intracardiac patterns of flow than the one directional analysis we have previously used. The machine was programmed to encode MR phase shift velocity data in slice select, phase encode and read gradient directions during a single acquisition period. For validation, we used a uniformly rotating disc phantom containing water with gelatin. Velocity profiles accurately reflected the linear velocity increase from the center to the periphery of the disc for the two directions in the disc plane. For the in vivo study, we acquired, with cardiac gating, 16 consecutive images per cycle for each of the velocity directions in oblique planes through the hearts of four healthy volunteers. We concentrated on two image planes, one transecting the right atrium and the right ventricle, and the other through the left atrium and ventricle. The results, which are shown on videotape, confirm that in the chosen planes there are components of flow in all three directions with coherent streams and eddies identifiable in certain phases of the cardiac cycle. The mass of data acquired, however, even for single slices, is difficult to interpret and present. This powerful technique gives fuller access to a complex and potentially significant aspect of cardiac physiology and pathology.

INTRODUCTION

Flow of blood through the human heart is a highly complex phenomenon which is closely related to cardiac structure and function as well as to the fluid mechanical properties of the blood itself. Pulsatile flow of inhomogeneous blood through the mobile form of the beating heart does not obey simple physical laws. Basic physiological information is per force usually obtained in an empirical manner as a prerequisite to understanding basic hemodynamic relationships.

Since the observations of such early anatomists and hemodynamicists as Erasistratus (300 B.C.), Leonardo da Vinci (1452-1519) and William Harvey (1628), it has been increasingly evident that proper tools for detecting and quantifying blood flow are indispensible if knowledge of cardiac blood flow is to be advanced.[1] The ideal method for measuring blood flow should accurately assess such properties of flow as direction, velocity, and volume and their modulation over time, all with correct spatial localization. These methods should be noninvasive and not interfere with the underlying phenomenon being observed. Magnetic resonance represents one such advance in our ability to study intracardiac blood flow. The purpose of this paper is to describe early applications of magnetic resonance to the measurements of three-directional blood flow within the human heart.

From the Magnetic Resonance Unit, National Heart Hospital, London, England and the Medical College of Wisconsin, Milwaukee, WI.

This work was performed during Dr. Wann's sabbatical at the MR Unit.

Dr. Kilner is the recipient of a Lloyds of London Tercentenary Fellowship.

Address for correspondence: L. Samuel Wann, M.D., Medical College of Wisconsin, 8700 W. Wisconsin Ave., Milwaukee, WI 53226.

Copyright © 1989 by Dynamedia, Inc.

0891-9313/89 $3.50

METHODS

A modified Picker International Vista MR 2055 machine operating at 0.5 Tesla with a special gradient coil and a jacket surface receiver coil was used to measure flow. Multiple spin echo images were acquired using electrocardiographic gating and from these oblique planes were defined, by the three point method, for velocity mapping.

Velocity mapping was performed using the Field Echo Rephasing Sequence (FEER), as previously described.[2-6] Gradient modifications were used for velocity encoding in all three orthogonal directions (Fig. 1). Maps of velocity components in slice select, phase encoding and read gradient directions were obtained separately during a single acquisition period which lasted 20-25 minutes depending on heart rate.

To validate the flow mapping technique, a rotating disc filled with water was imaged. The water was solidified with gelatin to prevent any secondary motion within the disc.

As an initial demonstration of flow in the normal heart, two phases were selected for imaging: a right atrial plane passing through the superior and inferior caval veins and the tricuspid valve, and a left ventricular plane passing through the mitral valve, ventricular apex and aortic root. Each plane was imaged in four healthy volunteers.

RESULTS

Figure 2 shows one of the MR images of the disc phantom rotating at a steady rate inside the magnet, showing velocity components in the read gradient direction (arrows). The speed of any point in the disc is proportional to its distance from the center. Positive and negative velocity components are represented by light or dark shades of grey. Velocity profiles can be plotted along selected lines across the image. Note that the transition from dark to light is smooth, with a near linear velocity profile. The image showing velocity components in the phase encode direction showed a comparable appearance, oriented appropriately, and, as expected, no significant velocities were recorded in the slice select direction which passed perpendicularly through the disc planes.

Flow was also mapped simultaneously in all three directions in a plane through the superior and inferior vena cavae and tricuspid valve of the normal heart. Figure 3 (and the first cine MR sequence of the videotape) shows velocity components in and through a right atrial plane in one of the subjects. Comparable but by no means identical images were also acquired from the other subjects. Anatomic landmarks are shown in the upper left panel. The upper right panel shows flow in the vertical or up-and-down direction with white representing flow downward and black upward. This late systolic frame shows flow down the superior vena cava and up the inferior vena cava.

The lower left panel of figure 3 is an image of flow in the horizontal direction with flow towards the right being black and flow towards the left being white. The two caval streams do not collide head-on but are redirected into a stream moving towards the tricuspid valve. The lower right panel of figure 3 is an image of flow velocities in-and-out of the image plane with light representing flow toward the viewer and dark away from the viewer. Velocity components in this direction are not great but note that the atrial cavity has both light and dark regions indicating fluid rotation through the imaging plane. Integrating information from all three velocity maps leads to the conclusion that as the right atrium fills, there is a circulatory movement of blood, up the posterior part, forward and down toward the tricuspid valve.

Representative images of diastolic flow in the left ventricle are shown on the last section of the videotape. Ventricular filling and ejection can be seen, with evidence of vortical movements of blood in the region of the mitral valve leaflets. This motion is thought to contribute to efficient valve closure.[7]

The images representing velocities through the left ventricular plane show small velocity components within the ventricle, but in the great arteries, which pass through the image plane, patterns of secondary flow are revealed. A channel of reversed flow can be recognized in the pulmonary artery in diastole. In the ascending aorta, which curves towards the viewer through the image slice, a dark region (movement away) is fringed by light (movement towards) in late systole. This implies a double helical pattern of flow, which accords with expected flow dynamics in a curved tube.

DISCUSSION

The MR velocity map and profile depicting movement of the rotating phantom correspond with the predicted velocity distribution. The re-

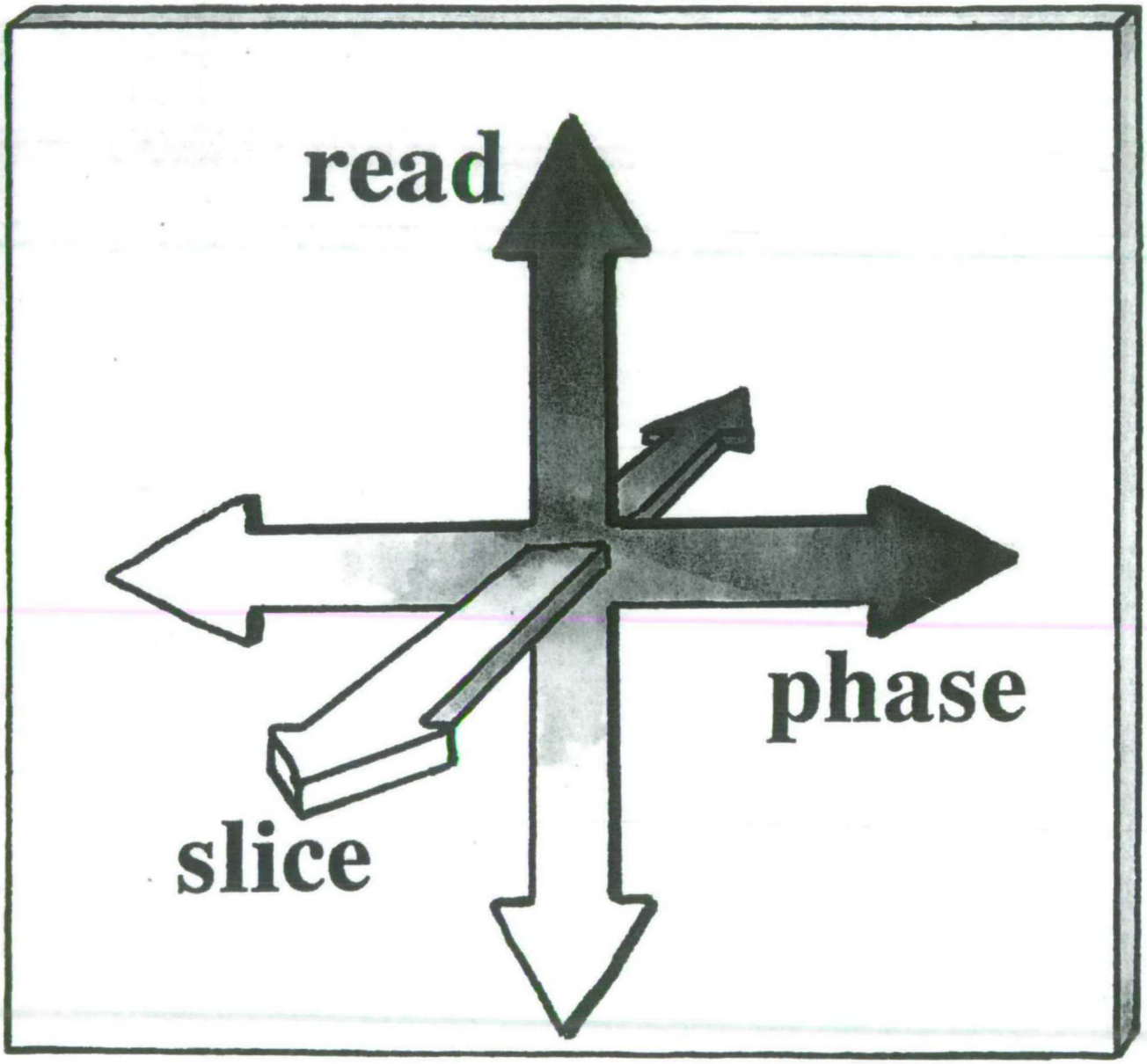


Fig. 1 The three directions in which velocity can be measured. Phase encode and read gradient directions lie in the image plane. The slide select gradient direction passes perpendicularly through the plane. Positive and negative velocities in each direction are represented by lighter or darker shades of grey.

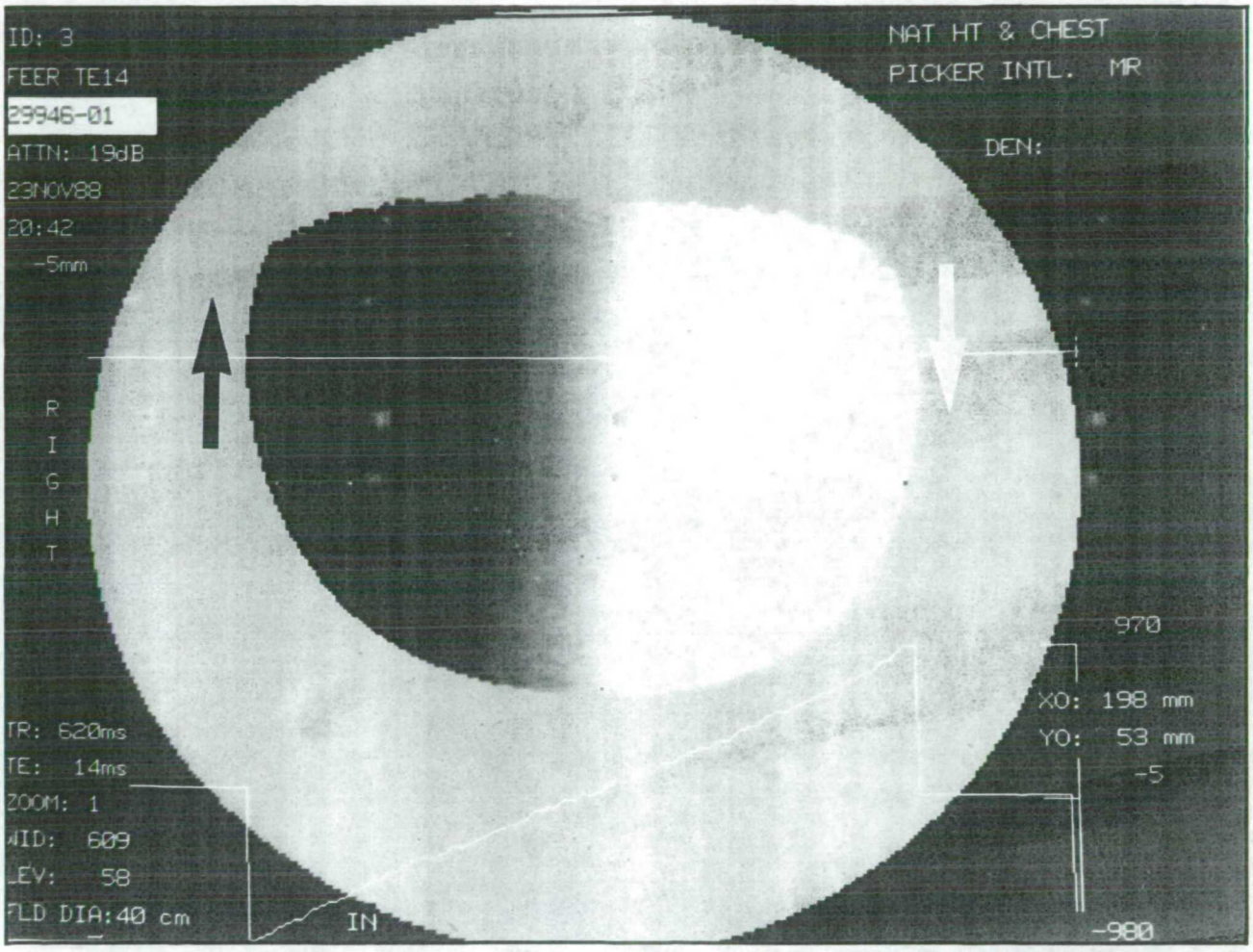


Fig. 2 MR velocity map of a uniformly rotating disc phantom. In this image, velocity components in the read gradient direction (arrows) are mapped. A velocity profile has been plotted for a line across the center of the disc.

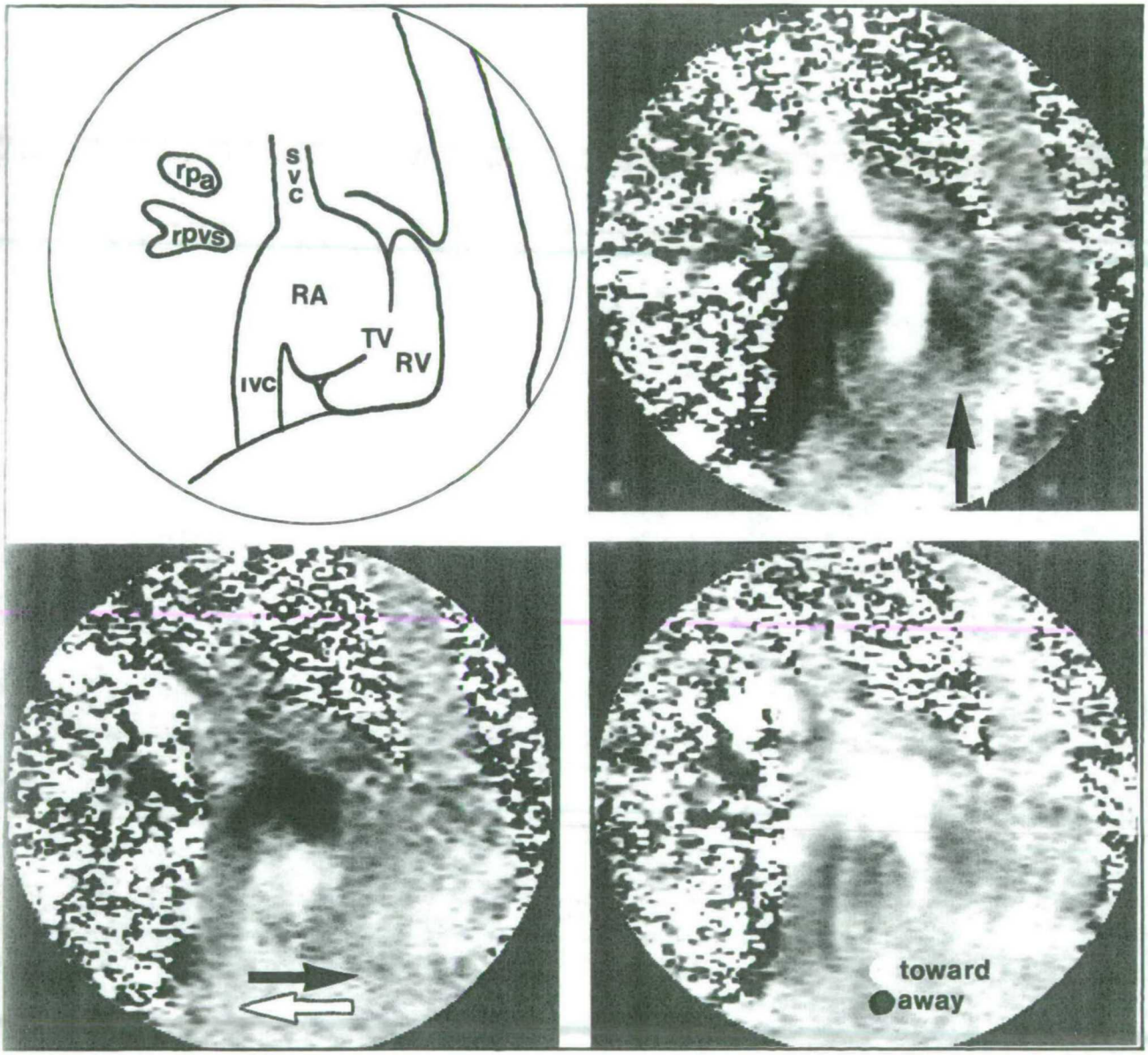


Fig. 3 Right atrial velocity maps in late systole. Velocity components in and through a plane transecting the right atrium are represented by three images, each being one frame of a cine loop. In the absence of signal, background noise gives a speckled appearance. It can be seen that superior and inferior caval streams do not collide head on, but move forward and to the left in this subject, contributing to a rotational movement of blood during atrial filling.

sult supports the accuracy of the method, and illustrates the appearance of rotational flow as represented by a unidirectional velocity map.

The intracardiac velocity map sequences, particularly when viewed in cine mode, reveal patterns of secondary flow within the heart and great vessels. Our results corroborate aspects of earlier studies in hydrodynamic models,[7] in animals,[8] and in humans,[9] from which vortex formation during left ventricular filling and the presence of coherent streams in the right atrium have been inferred. Noninvasive acquisition of velocity data in all three orthogonal directions, however, represents a significant advance over earlier methods. Slight differences between velocity maps acquired from different subjects may be partly due to lack of precision in the location of image planes.

Each of the cycles of flow images contains a tremendous quantity of information which is not easily presented or assimilated. The still-frame images shown here represent only the velocity and direction of flow at a single instant in time. The cine display format adds the dimension of time and more realistically portrays blood flow through the heart. Additional parameters such as acceleration, deceleration and volumetric flow can also be derived from this data. Additional tomographic slices could be acquired to map flow through the volume of the heart, although, at present, this would require a large amount of imaging time.

Magnetic resonance flow imaging is a powerful new tool which can obtain data on patterns of flow traced by blood coursing through the heart. Presentation of multidirectional flow data in a format readily perceived by the human brain is a difficult undertaking, at least in part because the nature and fidelity of the information is unlike any that has been available previously. Work remains to be done on the processing of flow maps into a more readily assimilated form. We draw attention to the potential contribution that understanding of such data may bring to the study of normal and pathologic blood flow.

REFERENCES

1. Milnar WR. Hemodynamics. Baltimore: Williams & Wilkins 1989;1-10.

2. Bryant DJ, Payne JA, Firmin DN, Longmore DB. Measurement of flow with NMR imaging using a gradient pulse and phase difference technique. J Comput Assist Tomogr 1984;8:588-93.

3. Nayler GL, Firmin DN, Longmore DB. Blood flow imaging by cine magnetic resonance. J Comput Assist Tomogr 1986;10.715-22.

4. Underwood SR, Firmin DN, Klipstein RH, Rees RSO, Longmore DB. Magnetic resonance velocity mapping: clinical application of a new technique. Br Heart J 1987;57:404-12.

5. Firmin DN, Nayler GL, Klipstein RH, Underwood SR, Rees RSO, Longmore DB. In vivo validation of MR velocity imaging. J Comput Assist Tomogr 1987;11:751-6.

6. Underwood SR, Gill CRW, Firmin DN, et al. Left ventricular volume measured rapidly by oblique magnetic resonance imaging. Br Heart J 1988;60:188-95.

7. Bellhouse BJ. Fluid mechanics of a model mitral valve and left ventricle. Cardiovasc Res 1972;6:199-210.

8. Taylor DEM, Wade JD. Pattern of blood flow within the heart: a stable system. Cardiovasc Res 1973; 7:14-21.

9. Miyataki K, Izumi S, Shimizu A, et al. Right atrial flow topography in healthy subjects studied with real-time two-dimensional Doppler flow imaging technique. J Am Coll Cardiol 1986;7:425-31.

MAGNETIC RESONANCE IN MEDICINE 14, 230–241 (1990)

The Application of Phase Shifts in NMR for Flow Measurement*

D. N. FIRMIN, G. L. NAYLER,† P. J. KILNER, AND D. B. LONGMORE

Magnetic Resonance Unit, National Heart and Chest Hospitals, London, England; and †Picker International, Wembley, England

Received December 19, 1989

A brief overview of the history of the application of phase shifts in NMR, and in particular NMR imaging, is presented. The imaging methods include direct phase mapping, Fourier flow imaging (where the flow data are Fourier transformed into one dimension of an image), and alternative methods, where flow-related phase shifts are utilized for flow measurement from the magnitude of the signal. A discussion then follows of the principal errors that can affect the accuracy of the various flow imaging techniques, with particular reference to the phase mapping methods that have been used extensively in our institution. The results from a number of experiments are included to illustrate the extent of the errors and methods of removing or minimizing these effects are suggested. © 1990 Academic Press, Inc.

INTRODUCTION

The effect of phase shifts on the NMR signal due to slow coherent motion (flow) was first investigated by Carr and Purcell (*1*) in 1954 when they noted the phenomenon of even echo rephasing of the signal produced from their multiple echo sequences. The first to describe methods of flow measurement utilizing the effect of phase shifts was Hahn (*2*), who described a method in which a magnetic field gradient was applied to introduce a phase shift to the signal from flowing sea water. The basis of Hahn's method is very similar to the phase mapping methods used in combination with imaging today. Another important development was that made by Stejskal and Tanner (*3*) in 1965 when they applied gradient pulses, as opposed to a continuous gradient, to improve the measurement of diffusion. The use of pulsed gradients enabled better definition of the period of the diffusion measurement. The same approach was subsequently applied to velocity phase mapping where the gradient pulses served to mark the position of moving spins at two intervals during the sequence (*4*). Another approach to the use of phase shifts in flow measurement was that described first by Grover and Singer (*5*) in 1971 and later by Garroway (*6*) (1974). In these studies a gradient was applied in the direction of flow and the multiple spin-echo signals were Fourier transformed to give a plot of the distribution of flow velocities.

Despite the considerable knowledge gained from the type of nonimaging studies described above, concerning the effects of flow on the phase of the NMR signal, the

* Presented at SMRM Workshop on MR Imaging of Blood Flow, Philadelphia, PA, March 13 and 14, 1989.

0740-3194/90 $3.00
Copyright © 1990 by Academic Press, Inc.
All rights of reproduction in any form reserved.

early attempts to image flow concentrated on factors that affected the signal intensity as opposed to the phase. It was not until 1982, when Moran (*7*) suggested the introduction of bipolar velocity phase encoding pulses to the three axes of a standard spin-echo imaging sequence, that interest in the use of phase began to be established. The imaging methods that were later developed fell broadly into three categories:

(1) Phase mapping methods that mapped the phase of the signal directly in order to measure the flow.

(2) Fourier flow imaging methods that phase encoded flow velocity so that a number of flow phase encoding steps would separate the different flow velocities present at a particular location.

(3) Alternative methods that, in a variety of different ways, encoded the effect of flow-related phase shifts on the magnitude of the signal.

Phase Mapping Methods

In 1984 both Van Dijk (*8*) and Bryant *et al.* (*4*) demonstrated the use of velocity phase mapping to measure flow velocity directly from the phase of the signal originating from each imaging voxel. These phase mapping methods were made clinically more useful, partly by the use of a field-echo sequence (*9, 10*) and, most importantly, by the introduction of velocity-compensated gradient waveforms (*11*). The improvements enabled the sequence to be repeated rapidly and prevented the characteristic signal loss due to shear flow when uncompensated gradient waveforms were employed. The technique has been validated *in vivo* (*12*) and has already provided useful information in clinical and physiological flow studies (*13, 14*).

Fourier Flow Methods

Redpath *et al.* (*15*) in 1984 were the first to demonstrate experimentally the method of Fourier flow imaging, eight flow phase encoding steps being used to image a circle of fluid-filled tubing rotating in the image plane. Different segments of the circle were seen on the eight resultant images, each corresponding to different velocity ranges in the direction of the flow phase encoding gradient. Feinberg *et al.* (*16*) in 1985 applied the method both *in vitro* and *in vivo* but shortened the acquisition time and simplified the reconstruction by encoding only one spatial dimension and one flow velocity dimension. The phantom results proved the accuracy of the method and the *in vivo* study, while showing the flow in the descending aorta, also highlighted the problem of very high signal from stationary tissue imaged in the spatial dimension. In 1988 Hennig *et al.* (*17*) described a development of this method where the signal from stationary tissue was saturated and the sequence repeated much more rapidly. The main problem with the technique, particularly when pulsatile flow is being studied, is that the time required to obtain a reasonably high resolution in the velocity axis precludes the use of more than one spatial dimension.

Alternative Methods

A number of other methods which use the effect of velocity-induced phase shifts to facilitate flow measurement should be mentioned at this point. Van As *et al.* (*18*)

described an approach that was initially designed for nonspatially resolved measurement of flow through plant stems and involved the application of a string of 180° pulses. Although stationary material did not contribute to the phase sensitive detected signal, material flowing in the direction of a static gradient was phase shifted and contributed a signal with a shape related to the mean flow velocity. Spatial encoding was achieved by applying orthogonal modulated gradients, each with a null plane to define a sensitive line along the length of the flow vessel. One of the main advantages of the above technique was that flow measurements could be made in real time.

Dumoulin and Hart (*19*) described the use of a sequence that included a bipolar flow phase encoding gradient. The sequence was repeated with the bipolar gradient inverted so that flow-related phase shifts were reversed and subtraction of the two data sets resulted in cancellation of the signal from stationary material while a flow signal remained. In theory, the magnitude of the flow signal varies with the sine of the flow-related phase shift, so that over the range of approximately $\pm\pi/3$ radians a reasonably linear relationship should be found between the signal intensity and the velocity. The method proved particularly good for producing angiograms of relatively small tortuous vessels while one disadvantage, in some applications, might be the reliance of the method on a constant magnitude of signal from the flowing blood. Any variations in the flow signal magnitude, due to phase dispersion or flow enhancement effects, will produce errors in the flow measurement.

FACTORS AFFECTING THE ACCURACY OF PHASE VELOCITY MAPPING

(1) Aliasing of Velocity Data

Because phase is cyclic there is a natural limit of 2π radians to the maximum range of phases that can be measured without ambiguity and, therefore, the certainty in phase-related velocity measurement is similarly limited. However, because of the method of phase subtraction normally used where two images are acquired with different velocity phase sensitivities in any designated direction, velocity aliasing is not, in fact, a major problem. The difference in flow sensitivity between the two sequences used can be simply tailored to suit the particular application under study. The range of flow velocities that can be measured by the phase mapping technique covers the complete physiological range from approximately 0.1 mm/s (*20*) to several meters per second (*21, 22*).

All the methods of velocity imaging that use phase shifts are prone to problems similar to that described above. The Fourier flow method, for example, suffers from aliasing in the velocity axis of the image similar, in principle, to the aliasing of material outside the field of view that occurs when spatial phase encoding is employed. Dumoulin's method of MR angiography (*19*) is affected somewhat differently because of the reconstruction method used which results in there being no sudden discontinuity in velocity measurement. This introduces the possibility of hidden errors which enable cleaner angiograms to be produced but could reduce the accuracy of velocity measurements.

(2) Misalignment of Flow Encoding

Misalignment between the direction of flow and the direction of the flow encoding will affect all methods of flow measurement that use the phase of the signal. The relationship between the true flow and the measured flow is

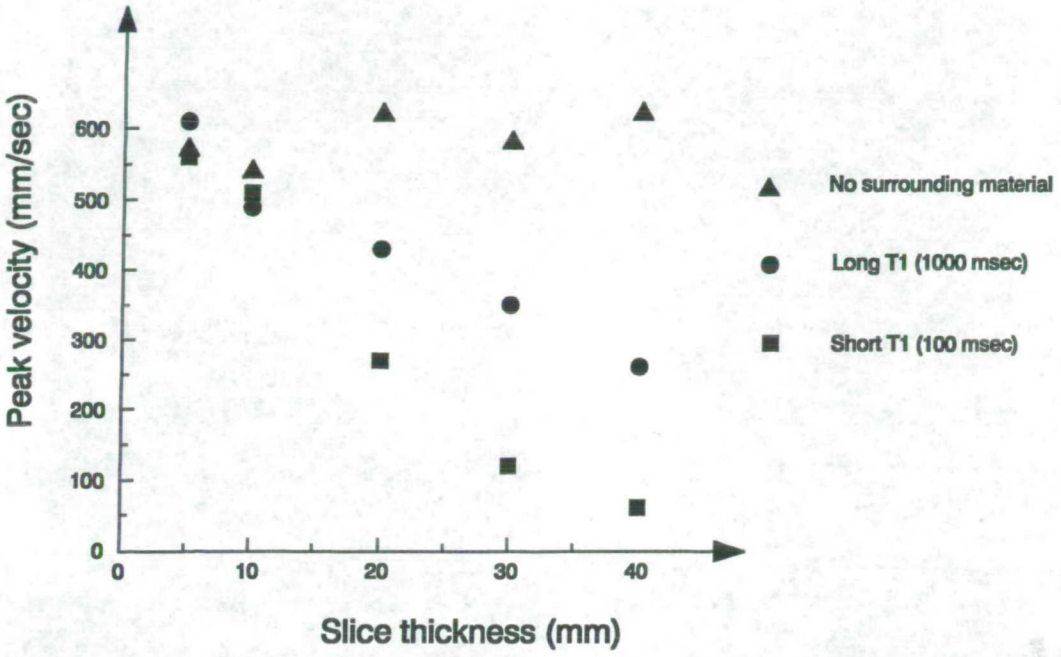


FIG. 1. Plot showing the error in flow measurement due to the partial volume effect. As the slice thickness is increased more signal from surrounding fluid is included in each voxel and the potential error is thus increased. The plot includes results with three different surrounding media: air, a fluid with a short T_1 (100 ms), and a fluid with a long T_1 (1000 ms). With air as the surrounding medium, reasonably constant flow measurements were obtained with increasing slice thickness. However, with a fluid surrounding the tube the partial volume effect resulted in a reduced flow measurement. The error depended on the relative signals between the flowing and stationary fluids; saturation of the surrounding media with a long T_1 resulting in a smaller error than that which occurred when the surrounding media was of a short T_1.

$$F_{meas} = F_{true} \cos \theta, \qquad [1]$$

where θ is the angle of misalignment and F_{meas} and F_{true} are the measured and true flows, respectively. This cosine relationship results in small errors; a misalignment of as much as 20° would produce only a 6% error while a more realistic misalignment of 5° would cause an error of less than 1%.

(3) Partial Volume Averaging of Flow Data through the Slice

A potential problem, particularly where in-plane flow is being studied in vessels which are relatively small, is that of averaging of flow phase data through the slice. The extent of the error in flow measurement depends on the amplitude of the signal contribution from the surrounding tissue which, in turn, depends on a number of factors such as the T_1 and T_2 of the tissue, and the T_R, T_E, and excitation pulse angle of the imaging sequence. To demonstrate this error and the effect of altering the signal from the surrounding medium, a constant mean flow velocity of 45 cm/s was measured through a 10-mm-diameter tube surrounded by three different media: air, a solution of long T_1 (approx 1 s), and a solution of short T_1 (approx 100 ms), respectively. Flow images were acquired with slice thicknesses of 5, 10, 20, 30, and 40 mm. Figure 1 shows a plot of the measured mean flow velocity versus slice thickness for the three different surrounding media.

These partial volume effects described do not affect the flow measurements made using the Fourier flow imaging techniques (*15–17*); by its very nature the velocity

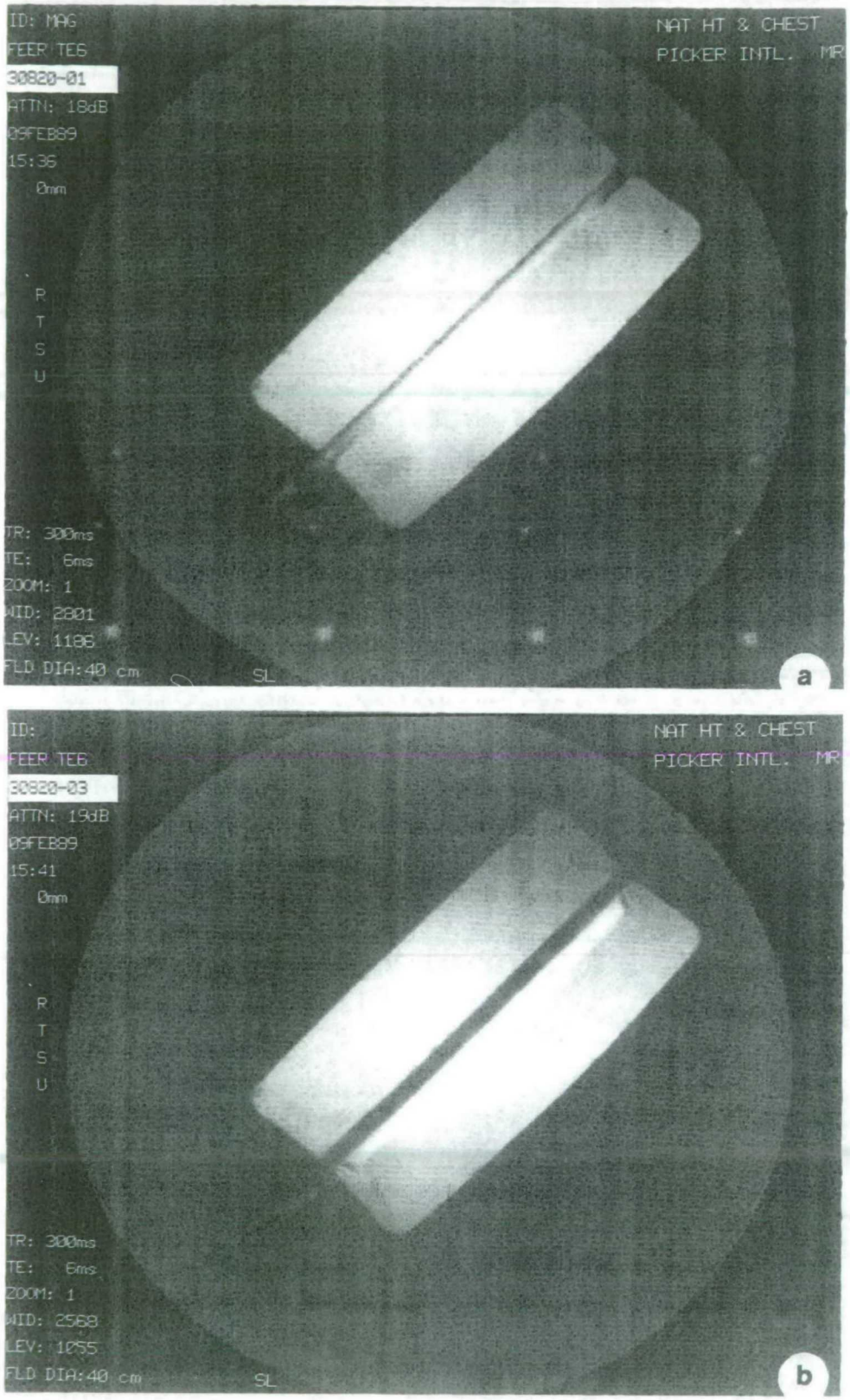


FIG. 2. Demonstration of the effect of in-plane misregistration. (a) and (b) are magnitude images acquired with short (3 ms) and long (33 ms) intervals between phase encoding and reading, respectively. In (b) the signal from the fluid, which is flowing at an angle of 45° to the phase encode and read directions, can be seen to be misregistered over the signal from the stationary fluid surrounding the tube. The corresponding flow images are shown in (c) and (d), the signal averaging present due to the large misregistration in (d) resulting in a mean flow measurement of only 53% of that in (c).

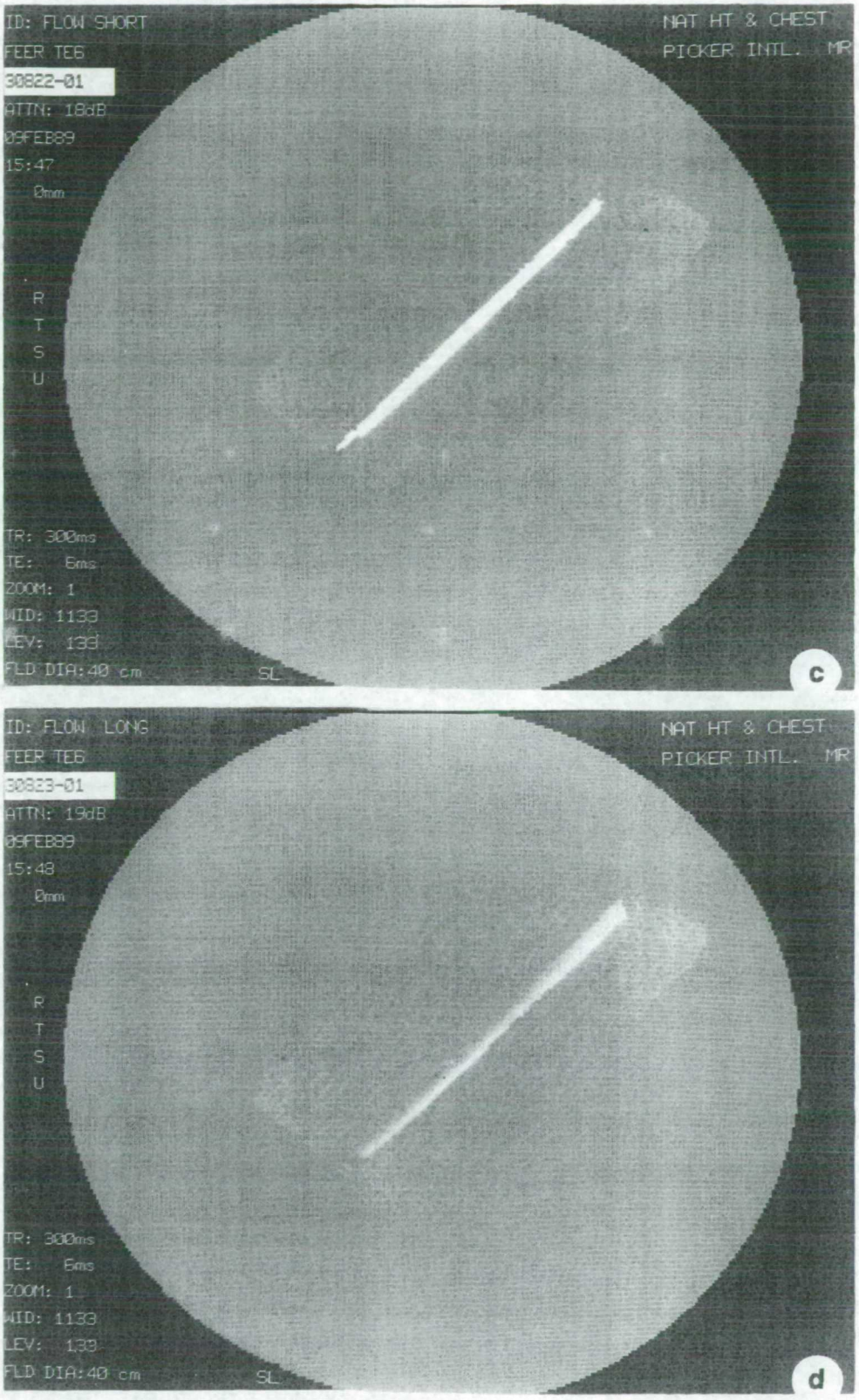


FIG. 2—*Continued*

phase encoding separates out all the different velocity components whatever the proportion of stationary material present. Similarly, the method of MR angiography (*19*) (where complex subtraction of the signals, as opposed to phase subtraction, is

used to produce the flow image) is also unaffected by partial volume errors and it is for this reason that it can be used to produce quantitative projection flow angiograms which promise to be most useful in the study of complex tortuous vascular regions.

(4) Misregistration Effects

Signal misregistration occurs due to movement between the times of slice selection, phase encoding, and frequency encoding. The effect of this is that the signal from flowing material may be mispositioned with respect to any stationary material. Two forms of error result: first, blood flow signal, for example, cannot be compared directly with features on an anatomy image because the blood signal might be out of position and distorted and, second, if the misregistration results in the flow signal overlaying any stationary tissue, a type of partial volume error can result where the phases of the stationary and flowing material are averaged.

Two forms of misregistration were demonstrated by imaging the flow of copper sulfate solution through a fluid-filled tank. In the first experiment the tube was orientated in the image plane at 45° to both the phase encode and the read directions. The mean velocity of flow was 60 cm/s and the velocity was phase encoded in the read direction. A field even echo rephasing (FEER) sequence (*11*) with an echo time of 40 ms was used to acquire two velocity images. On the first acquisition the phase-encode-to-echo interval was 3 ms, while on the second this interval was increased to 33 ms. Figures 2a and 2b show the difference in phase-encode-to-read misregistration effects between two different image acquisitions; minimal misregistration occurred when the phase-encode-to-echo time was only 3 ms and maximal misregistration occurred when this time was increased to 33 ms, in the latter case the flow signal completely overlaying the signal from the stationary fluid. Figures 2c and 2d show the corresponding velocity phase maps where, because of phase averaging effects, the flow measurement in Fig. 2d is only 53% of that in Fig. 2c. If the above type of misregistration effect does occur then the degree of flow measurement error depends on the signal intensity from the stationary material in very much the same way as that described for the partial volume errors.

A second experiment was performed in order to demonstrate the measurement error resulting from oblique flow through the plane. The tube was orientated in such a way that it was at 45° to the slice select and read directions. A long echo time (T_E = 40 ms) was again used to accentuate the effect produced. The effect of altering the repeat time was demonstrated; in this case the signal from flowing material (being replenished between excitations) was not affected while that from the stationary surrounding material (T_1 = 300 ms) was affected. Figure 3 shows an example of a magnitude reconstruction of the misregistered flow signal overlaying the stationary surrounding fluid. The error in mean flow measurement was determined as 5% with a repeat time of 100 ms and 30% with a repeat time of 1000 ms. The magnitude of these errors, in the clinical situation, would depend on the relaxation time of the tissue surrounding the vessel. Many clinical flow studies involve cine acquisitions where short repeat times are used, resulting in partially saturated tissue signals; this, combined with the fact that flow enhancement effects are also often present, should therefore result in a relatively small error.

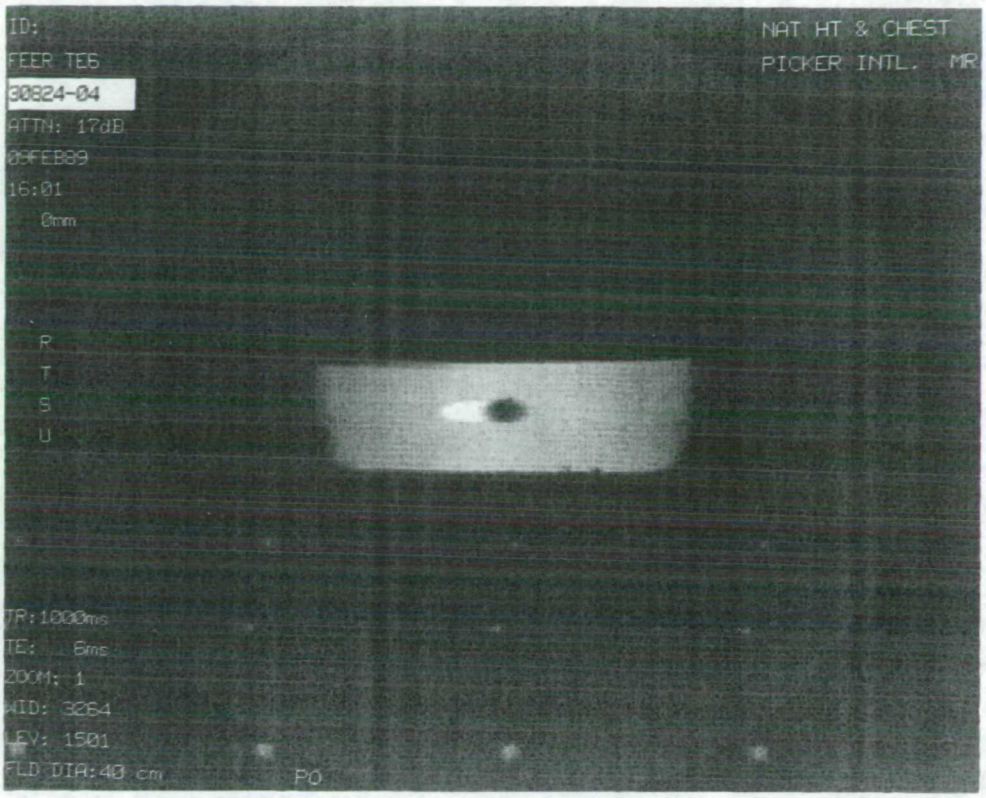


FIG. 3. Magnitude image demonstrating the misregistration due to flow between the slice selection and data collection, when the direction of flow was at an angle of 45° to the slice select and read axes. The deformed, crescent-shaped, flow signal resulting from the velocity profile is seen to overlay the stationary fluid signal.

The error introduced to the quantification of flow where the flow signal overlays stationary signal can be treated as if it were a partial volume error, as described above, and therefore only applies to the phase mapping method. Misregistration effects occur in all flow imaging methods in which there are delay intervals between the different axes of spatial encoding. The effects of misregistration can be minimized in two ways: first, by designing a sequence that is very short and therefore has very short periods between the different spatial encodings and, second, by arranging the image plane such that the flow is perpendicular to the slice and zero motion occurs in the other spatial encoding axes.

(5) Errors Due to Phase Shifts Resulting from Other Orders of Motion

The general equation describing the phase of the signal from a spin isochromat is

$$\phi = \int \gamma G(t)x(t)dt, \qquad [2]$$

where $G(t)$ and $x(t)$ are functions describing the variation in the gradient amplitude and the position of the spin isochromat with time, respectively. The function $x(t)$, which in fact describes the spin motion, is given by

$$x(t) = x(0) + x(0)'t + x(0)''t^2/2! + \cdots + x(0)^{[n]}t^n/n! \qquad [3]$$

assuming that x is continuously differentiable over the interval $[0, t]$. The above

TABLE 1

Error in Velocity Measurement of 1 m/s due to an Acceleration of 10 m/s

Sequence	Error
FEER 22 ms	7.9%
FEER 14 ms	3.9%
FEER 6 ms	1.7%

equation consists of a series of terms initiating with displacement and including increasing orders of motion. If, for example, a velocity measurement is required and a significant acceleration is also present then the resultant phase shift given by Eq. [2] will be a net effect resulting from both orders of motion. The method of phase subtraction normally used in velocity phase mapping (where the phases of signals acquired with a velocity insensitive and a velocity sensitive sequence are subtracted), however, removes most of the error resulting from the acceleration term because the phase shifts introduced by the two sequences are similar. A small error remains, nevertheless, the degree of which depends to a great extent on the duration of the particular gradient profile. Table 1 shows the percentage error introduced to a velocity measurement of 1 m/s due to a typical physiological acceleration of 10 m/s^2 when the measurements are made using three FEER sequences with echo times of 22, 14, and 6 ms, respectively.

Turbulent and other irregular flow types, which contain higher orders of motion that are random in space and time, will tend to produce signal loss; however, errors due to higher order terms should be averaged out over the duration of the study.

(6) Signal Loss

Flow-related signal loss is probably the most significant factor in the accuracy of these flow measurement methods. It may occur due to signal washout or loss of phase coherence within a voxel and eventually results in an inability to detect the phase of the flow signal above that of noise therefore removing any possibility of flow measurement. Partial signal loss alone, however, should not greatly affect the accuracy of the phase mapping flow measurement and, in the case where signal loss is the result of a spread of phase within a voxel, the mean phase will be detected. Any of the flow imaging techniques that use phase shifts to measure flow will be susceptible to signal loss of one form or another, although these can normally be minimized. Signal washout can normally be avoided by employing a field-echo sequence, while loss of phase coherence due to flow in the direction of imaging gradients can be reduced by appropriate gradient profile design.

Two approaches have been suggested for gradient designs to minimize signal loss and the success of each is dependent on the flow type that is present. The first approach is to design complex gradient waveforms that nullify phase shifts due to the first few successive derivatives of position (*23*). A problem with this method is that for every additional successive derivative an additional gradient section is required

and the length of the sequence is thus extended. Probably a better method, particularly where turbulent flow is present with many higher orders of motion, is to use a symmetrical gradient waveform that nullifies phase shifts due to all the odd order derivatives of position (*11*) and then to shorten the sequence as much as possible to reduce the effects of the even order derivatives.

Spatial variation of higher order motion components is thought to be the greatest contributing factor to signal loss and the following theory emphasizes the importance of shortening the sequence in order to reduce these effects.

From eqs. [2] and [3] the phase shift due to the nth order of motion, $x^{[n]}$, can be described by

$$\phi = S_n \cdot x^{[n]}, \qquad [4]$$

where S_n is the sensitivity of the signal phase to the nth term and is given by

$$S_n = G_f \cdot c_n \cdot \tau^{(n+1)}, \qquad [5]$$

where S_n is a factor relating to the gradient waveforms shape and amplitude, c_n is a constant of proportionality relevant to the nth motion term, and τ is the duration of the gradient waveform.

In imaging there is normally a constraint such that

$$G_f \cdot \tau = C, \qquad [6]$$

where C is a constant (i.e., a higher gradient strength is required to produce the same effect in a shorter time). It follows therefore that

$$S_n = C \cdot c_n \cdot \tau^n \qquad [7]$$

which demonstrates that progressively higher motion terms become progressively more significant with longer gradient profile durations. As this duration is reduced so is the signal loss enabling the quantitative study of a wide range of flow types. For accurate flow quantification using the method of Dumoulin and Hart (*19*) signal loss is an even more critical factor and extremely short sequences may be required to study flow in the region of cardiovascular abnormalities, which are known to result in complex higher order flow types.

Slice orientation may also be an important factor, where signal loss is concerned, because of the "tower block" voxel shape that tends to be used in imaging. It may be possible to orientate the slice such that the intravoxel distribution of a particular higher order (phase dispersive) motion term is reduced. In a narrowing vessel, for example, with constant flow, the blood would exhibit an acceleration dependent upon its position along the axis of the vessel, but relatively independent of its position across the diameter. In this situation, therefore, the signal loss may be minimized by imaging the flow in-plane as opposed to perpendicular to it; in this way the longest axis of the voxel will lie across the diameter of the vessel.

VALIDATION OF THE PHASE MAPPING METHOD

An *in vitro* validation of the phase velocity mapping method was made by imaging the flow of doped water (1 mM $CuSO_4$) through two tubes of diameter 12.7 and 6.4

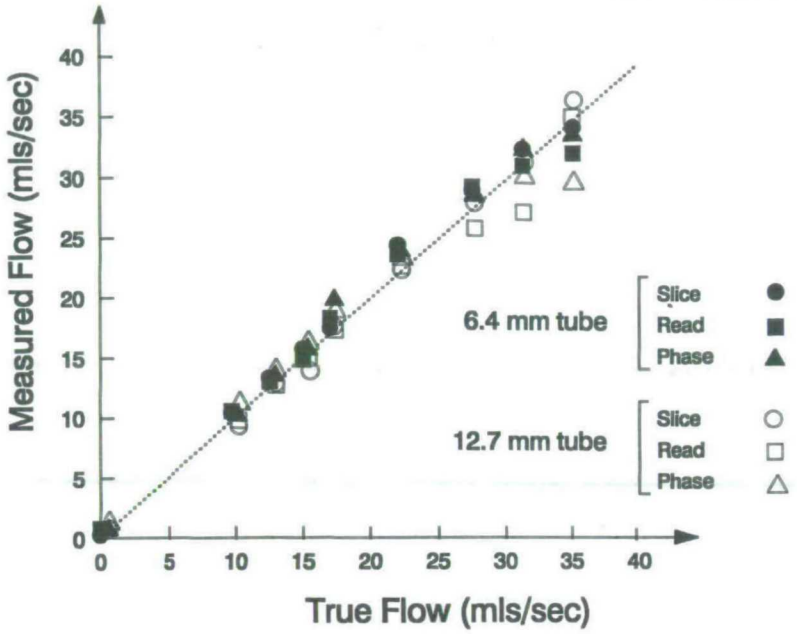


FIG. 4. Plot comparing the measurement of volume flow using the FEER velocity mapping technique and true flow. The measurements were made in the slice select, read, and phase encode directions using both 6.4- and 12.7-mm-diameter tubes in each direction. Many of the measured flow rates exceeded the critical Reynolds number ($Re_{max} = 8000$) indicating that turbulence, while reducing the signal magnitude, does not initially affect the phase velocity measurement when using direct phase mapping techniques.

mm, respectively. Volume flow measurements were made in the slice select, read, and phase encode directions. Nine forward and reverse flow measurements were made in each case, with flows ranging from 0 to 40 ml/s. The results of the comparisons between the true and measured flow are shown in Fig. 4. The correlation coefficients obtained between the true and measured volume flows were 0.994, 0.989, and 0.982 for the slice select, read, and phase encode directions, respectively. The standard errors of the estimates (SEE) were 1.2, 1.6, and 2.0 ml/s, respectively, for the three directions. These results demonstrate the inherent accuracy of the phase mapping method. One point of interest is that many of the measurements were made on flows exceeding the critical Reynolds number ($Re_{max} = 8000$), thus confirming that the accuracy of the measurements is maintained in this situation.

A method of *in vivo* validation has been described previously (*12*). The results showed a very good correlation between the measurement of the stroke volume of the heart carried out by the flow technique and a previously validated multislice volume method.

CONCLUSION

Flow-related phase shifts have been used in a variety of ways to measure blood flow, enabling information to be obtained ranging from bulk flow through vessels to spatial details of the flow velocity profiles or flow distributions. The accuracy and reliability of the methods can be limited by a number of error contributing factors. In this study particular emphasis was placed on those that affect the accuracy of the direct phase mapping method; however, the effect on other methods has also been

considered. The extent of the errors often depends on the specific application involved; however, by prior consideration the techniques can be carried out in such a way that the errors are minimized, in which case the methods have proven particularly reliable and accurate.

ACKNOWLEDGMENTS

We thank the staff of the Magnetic Resonance Unit, National Heart and Chest Hospitals, and Picker International for their helpful advice and discussions. Thanks are also due to Dr. Clipson for proofreading the final manuscript. The work was made possible by financial support from the Halley Stewart Trust, the Maurice Laing Trust, the Lloyds Tercentenary Foundation, the Coronary Artery Disease Research Association (CORDA), and the Governors of the National Heart and Chest Hospitals.

REFERENCES

1. H. Y. Carr and E. M. Purcell, *Phys. Rev.* **94**, 630 (1954).
2. E. L. Hahn, *Geophys. Res.* **65**, 776 (1960).
3. E. O. Stejskal and J. E. Tanner, *J. Chem. Phys.* **42**, 288 (1965).
4. D. J. Bryant, J. A. Payne, D. N. Firmin, and D. B. Longmore, *J. Comput. Assist. Tomogr.* **8**, 588 (1984).
5. T. Grover and J. R. Singer, *J. Appl. Phys.* **42**, 938 (1971).
6. A. N. Garroway, *J. Phys. D* **7**, L159 (1974).
7. P. R. Moran, *Magn. Reson. Imaging* **1**, 197 (1982).
8. P. Van Dijk, *J. Comput. Assist. Tomogr.* **8**, 429 (1984).
9. I. R. Young, G. M. Bydder, and J. A. Payne, *Magn. Reson. Med.* **3**, 175 (1986).
10. J. P. Ridgway and M. A. Smith, *Brit. J. Radiol.* **59**, 603 (1986).
11. G. L. Nayler, D. N. Firmin, and D. B. Longmore, *J. Comput. Assist. Tomogr.* **10**, 715 (1986).
12. D. N. Firmin, G. L. Nayler, R. H. Klipstein, S. R. Underwood, R. S. O. Rees, and D. B. Longmore, *J. Comput. Assist. Tomogr.* **11**, 751 (1987).
13. S. R. Underwood, D. N. Firmin, R. H. Klipstein, R. S. O. Rees, and D. B. Longmore, *Brit. Heart J.* **57**, 404 (1987).
14. R. H. Klipstein, D. N. Firmin, S. R. Underwood, R. S. O. Rees, and D. B. Longmore, *Brit. Heart J.* **58**, 316 (1987).
15. T. W. Redpath, D. G. Norris, R. A. Jones, and M. S. Hutchinson, *Phys. Med. Biol.* **29**, 891 (1984).
16. D. A. Feinberg, L. E. Crooks, P. Sheldon, J. Hoenninger III, J. Watts, and M. Arakawa, *Magn. Reson. Med.* **2**, 555 (1985).
17. J. Hennig, M. Mueri, P. Brunner, and H. Friedburg, *Radiology* **166**, 237 (1988).
18. H. Van As, T. J. Schaafsma, P. A. De Jager, and J. M. Kleijn, *Ann. Radiol.* **27**, 405 (1985).
19. C. L. Dumoulin and H. R. Hart, *Radiology* **161**, 717 (1986).
20. I. R. Young, A. S. Hall, D. J. Bryant, D. G. T. Thomas, S. S. Gill, L. M. S. Dubowitz, F. Cowan, J. M. Pennock, and G. M. Bydder, *J. Comput. Assist. Tomogr.* **12**, 721 (1988).
21. D. N. Firmin, P. J. Kilner, D. J. Pennell, S. R. Underwood, R. H. Mohiaddin, R. S. O. Rees, and D. B. Longmore, in "Proceedings, 8th Ann. Meeting Soc. Magn. Reson. Mod.," Vol. 2, p. 888, Soc. Magn. Reson. Med., Berkeley, 1989.
22. P. J. Kilner, D. N. Firmin, R. H. Mohiaddin, S. R. Underwood, R. S. O. Rees, and D. B. Longmore, in "Proceedings, 8th Ann. Meeting Soc. Magn. Reson. Med.," Vol. 1, p. 320, Soc. Magn. Reson. Med., Berkeley, 1989.
23. P. M. Pattany, J. J. Phillips, L. C. Chiu, J. D. Lipcamon, J. L. Dverk, J. M. McNally, and S. N. Mohapatra, *J. Comput Assist. Tomogr.* **11**, 369 (1987).

Helical and Retrograde Secondary Flow Patterns in the Aortic Arch Studied by Three-Directional Magnetic Resonance Velocity Mapping

Philip J. Kilner, MD; Guang Z. Yang, PhD; Raad H. Mohiaddin, MD; David N. Firmin, PhD; Donald B. Longmore, FRCS

Background. **Helical and retrograde secondary flows have been recorded in the aorta, but their origins and movements in relation to the arch have not been clarified. We set out to do this using magnetic resonance velocity mapping.**

Methods and Results. **Three-directional phase contrast cine magnetic resonance velocity mapping was used to map multidirectional flow velocities in the aortas of 10 healthy volunteers. Computer processing was used to visualize flow vector patterns in selected planes. Right-handed helical flows predominated in the upper aortic arch in late systole, being clearly recognizable in 9 of the 10 subjects. Nonaxial components of velocity in this region reached 0.29 m/s (±0.05 m/s) as axial velocities declined from a peak of 1.0 m/s (±0.1 m/s). Helical flow patterns in the upper descending aorta varied between subjects, apparently depending on arch curvature. End-systolic retrograde flow originated from regions of blood with low momentum, usually along inner wall curvatures. Flow studies in a curved tubular phantom showed right-handed helical flow in the upper "arch" when the inflow section was positioned to simulate ascending aortic curvature, and retrograde flow occurred along the inner wall at end systole during pulsatile flow.**

Conclusions. **Helical and retrograde streams are consistent features of intra-aortic flow in healthy subjects that result, at least in part, from the curvature of the arch and the pulsatility of flow in it. They may have significance in relation to circulatory dynamics and the pathogenesis of atheroma in the arch.** (*Circulation.* **1993;88[part 1]:2235-2247.**)

KEY WORDS • **flow** • **mapping** • **aorta**

In this study, we used magnetic resonance phase shift velocity mapping,[1-5] which has unrivaled capacities for noninvasive acquisition of multidirectional blood velocity data,[6-9] to investigate the distribution of secondary flow patterns in the aortic arch in healthy subjects. Computer image processing was used to combine information from pairs of velocity maps to produce vector maps of flow distributions in planes aligned with and transecting the aortic arch.[10,11] Finally, a tubular phantom was devised to study, also using magnetic resonance velocity mapping, relationships between tube curvature, flow pulsatility, and patterns of helical and retrograde flow. Our aim was to answer questions regarding the nature and origins of secondary flow patterns in the aorta that do not appear to have been addressed by previous studies.[12,16]

The presence of helical flow patterns in the aortic arch must have been suspected by many observers contemplating the right-handed twist of the great arteries. Anyone who experiments with visualization of flow in curved tubes or channels is likely to find that secondary flows, meaning flows with relatively stable components running oblique or counter to the main forward stream, are almost unavoidable. Twisting streamlines occur frequently,[17] and symmetrically paired, counter-rotating helices tend to develop at simple pipe bends.[18] Transparent models have been made that simulate, as far as possible, the morphology of curved arteries so that patterns of flow could be visualized in vitro.[17,19] Even when helical flows can be seen, however, accurate mapping of velocity distributions in pulsatile, twisting streams presents major difficulties. The problem is not only three-dimensional or even four-dimensional (space and time) but effectively seven-dimensional, with three separate velocity components required to specify the flow vector for each point in space-time.[6,9]

This complexity helps to explain the relative lack of data on helical flow patterns in the aortic arch in humans. Some evidence of a rotational component to flow at certain locations in the aorta has been recorded.[12,20] One study used transesophageal color Doppler ultrasonography to image nonaxial blood movements in the descending aorta in humans.[16,21] The authors found evidence of helical flows in the majority of subjects, with variability between individuals. The method did not allow in vivo measurement flow in the arch, but part of the study recorded right-handed helical flow in the upper arch of an aortic model.

Retrograde aortic flows, meaning blood movements running counter to the main forward stream, have been

Received February 9, 1993; revision accepted June 21, 1993.

From the Royal Brompton National Heart and Lung Hospital and the National Heart and Lung Institute, London.

Correspondence to Dr Philip J. Kilner, Magnetic Resonance Unit, Royal Brompton National Heart and Lung Hospital, Sydney Street, London SW3 6NP, UK.

more convincingly demonstrated,[14 15,22] but the origins and distribution of the retrograde streams have not been mapped in relation to the curved geometry of the arch. The present study aims toward filling this gap.

We believed that mapping of all three orthogonal velocity components in an oblique sagittal plane aligned with the upper arch would allow us to observe the distributions of helical and retrograde flows around a significant part of the arch. Depending on what the first velocity maps revealed, we planned to acquire velocity data in additional planes in selected subjects for clarification of initial findings.

The in vitro flow studies were intended to further clarify the flow findings and to give insight into causative factors that may underlie them. The experiments using a curved tubular phantom were carried out after the studies in humans and were devised specifically to throw light on the relationships among secondary flow structures, arch curvature, and flow pulsatility.

Methods

Subjects

Ten healthy volunteers were studied (7 men and 3 women), ages ranging from 24 to 43 years (mean, 34 years). One flow study, mapping velocity distributions through the aortic valve, was included, recorded in an additional healthy 32-year-old man. All studies were at rest, with subjects lying supine in the magnet.

Magnetic Resonance Imaging and Velocity Mapping

We used a Picker magnetic resonance machine operating at 0.5 T with modified gradient coils and a surface receiver coil. Cardiac gated transaxial multislice spin echo images were acquired, covering the region between the left ventricular outflow tract and the aortic arch. Then, an oblique spin echo image was acquired in the aortic arch plane, located by three points: one at the top of the arch and one each in the centre of the ascending and descending aorta at about right pulmonary artery level.

Three-directional cine velocity mapping[6] was performed using a gradient echo sequence with an echo time of 14 milliseconds.[2,3,5 14] Slice thickness was 8 to 10 mm, 40-cm field of view, with two averages of 128 phase encoding steps for each of four interleaved acquisitions: one velocity compensated, for background phase reference, and one each for measurement of velocity-dependent phase shifts in the slice select gradient, read gradient, and phase encode gradient directions. Three-directional cine velocity mapping in a given plane took 16 to 24 minutes, depending on heart rate, velocity maps then being produced by subtraction of reference from respective velocity encoded phase images so as to retain only velocity-related phase shifts. Each directional velocity map consisted of 16 cine frames gated from the R wave of the ECG and distributed through systole and most of diastole, successive cine frames being at 40- to 60-millisecond intervals.

Velocity Mapping Planes

The plane used for three-directional velocity mapping in all 10 subjects was the oblique sagittal plane aligned with the aortic arch (Figs 1, 2, and 3).

Velocity mapping in each of five additional planes was performed in one or more subjects, these planes being (1) a transaxial plane transecting the ascending and descending arch at the right pulmonary artery level (see lines drawn on Fig 3d), (2) a coronal plane tilted forward to transect the upper ascending arch (Figs 3d and 4), (3) a transaxial plane transecting the descending thoracic aorta at mitral valve level (Fig 3d), (4) an oblique plane through the two coronary sinuses of the aortic valve (in the additional subject: Fig 5), and (5) an oblique coronal plane through the left ventricular outflow tract and ascending aorta (Fig 6).

Velocity Vector Map Reconstruction

Software was written to combine the vertically and horizontally encoded velocity map data to produce cine vector maps displaying the distribution of flow in the image plane. (Figs 2 through 6). Local vectors were depicted as tapered streaks, the thick end pointing in the direction of flow, extending from multiple points in a rectangular matrix. The length and direction of each streak represents in-plane velocity at the point of origin.

Data Analysis

The anatomic and flow data were stored and studied in four forms.

Original magnetic resonance image format. Maps of velocity in each direction were displayed as gray-scale images (as in Fig 1). These were viewed at the console in cine mode, or analyzed frame by frame, using a cursor to interrogate pixel values in different regions. Standard software allowed profiles of velocity along any chosen line to be drawn automatically.

Velocity maps. With velocity profiles superimposed, maps were transferred to film hard copy, a convenient form for comparison of findings during the process evaluation.

Cine vector maps. Maps were viewed at a computer console.

Numeric records of peak velocity. Records measured by drawing velocity profiles across the arch, but avoiding exceptionally high or low pixel values, were used to compare flow at different gating delays, at different locations and in different directions (Table).

In Vitro Flow Model

A single flexible plastic tube, 3 cm in diameter and 80 cm in length, was used. It was of the type with wall corrugations that allow relatively tight curvature without kinking. The corrugations, at 3-mm intervals, were small in relation to tube diameter. Part of the tube (the arch) was secured with curvature in a single plane simulating that of the upper aortic arch. Proximal to this, a 30-cm length of the tube was secured either in plane with the arch, aligned with its ascending limb (the flat arch), or arranged so as to curve into the arch plane from its "left" side, simulating entry from the aortic root (the twisted arch). Water, with dissolved copper sulfate, was propelled through the tube by a centrifugal pump delivering continuous flow. Pulsatility could be induced in the tube section by intermittent compression of a flexible chamber connected to a side opening at the tube's proximal end. Compression of the chamber was achieved by a lever mechanism, moved to and fro by a line to the rotating arm of a motor located outside the

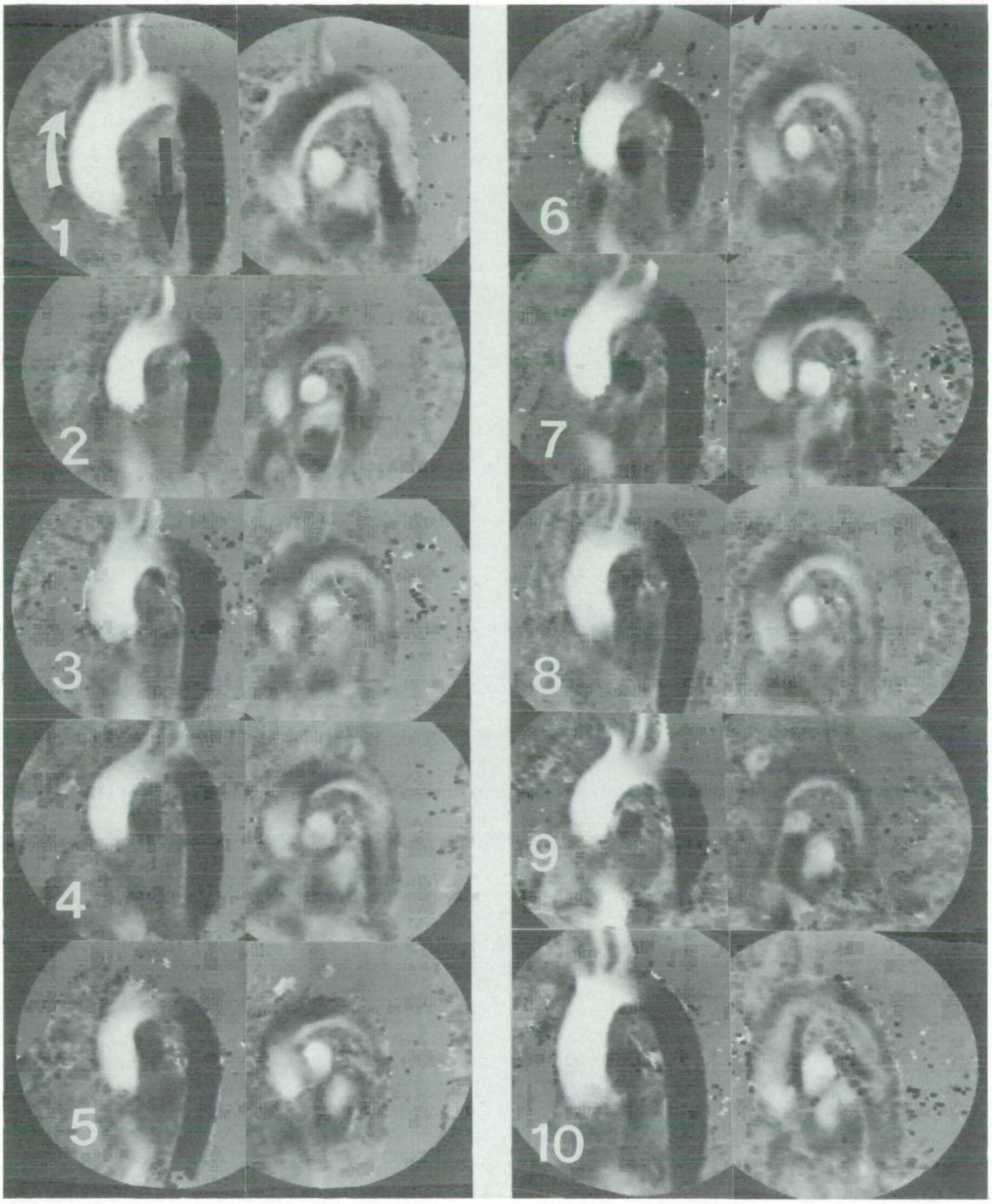


FIG 1. Vertical and through-plane velocity map frames from all 10 subjects. The planes are aligned with the aortic arch, viewed from the left. Images on the left of each pair show peak axial flow (early to mid systole), white representing velocity up the image and black down. Images on the right of each pair show peak through-plane flow in mid to late systole, light gray representing movement away from the viewer and dark toward. Flow entering the plane from the aortic root and flow in the right pulmonary artery are light as they move away from the viewer. A light strip against the inner wall of the upper arch with a broader dark region above it is a consistent finding, clearly identifiable in 9 subjects, less so in patient 10. This pattern indicates the clockwise rotation (viewed in the direction of forward flow) of a right-handed helical flow pattern. Notice variations in arch curvature. Size variations depend on body size; subjects 2, 3, and 5 are women.

magnet. A second flexible capacitance chamber connected to a side opening at the distal end of the arch tube allowed pulsatility of flow in the test section to be induced, free of the inertial damping effect of fluid in several meters of tubing leading back to the pump, which also had to be located outside the magnet. Mean flow rate was adjusted by a gate valve, and the frequency and amplitude of flow pulsatility were adjusted by setting the rotation rate and length of the rotor arm and by adjustment of the tension in the connecting line.

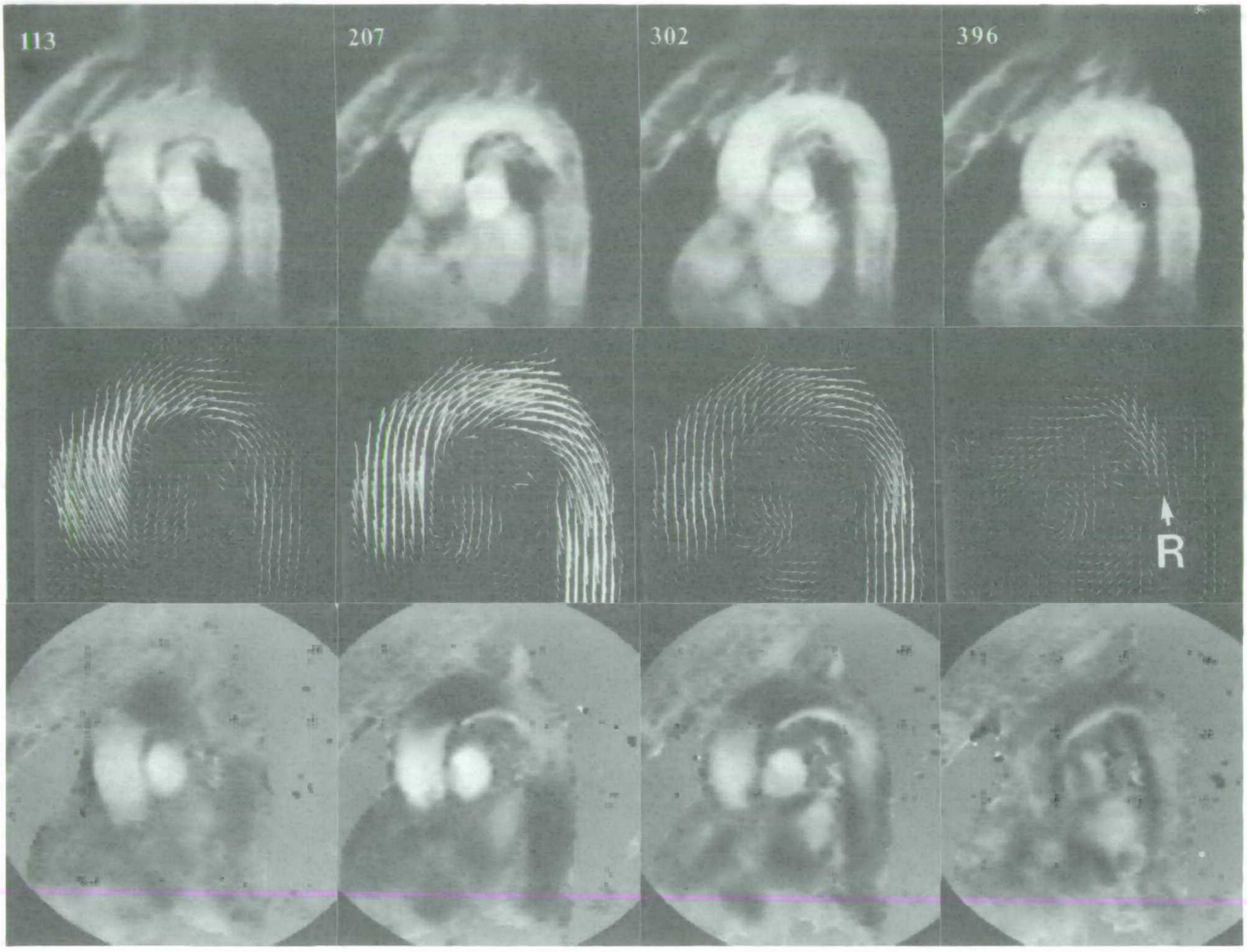


FIG 2. Temporal development of flow depicted by three different types of cine image. The four images in each line span the systolic period in subject 4, the numbers representing the gating delay in milliseconds from the R wave. Upper row, Cine images in which brightness is proportional to signal intensity. Brightest signal is seen where fresh blood moves into the slice. There is only slight local signal loss in the region of inflow from the aortic root in early systole and after peak systole in regions with steep velocity gradients in the upper and distal arch. Middle row, Velocity vector maps, which display combined data from vertical and horizontal velocity maps. Highest axial flow velocities first appear close to the inner curvature (left-hand frame), but they migrate outward through the course of systole, until at end systole, a retrograde stream (labeled "R") arises from relatively slow blood close to the inner curvature. Right-handed rotational flow can be identified in late systole in the right pulmonary artery. Bottom row, Through-plane velocity maps show that helical flow in the upper arch begins after forward flow and persists after it has ceased. In the descending aorta, the third (late systolic) frame shows a central region of flow away from the viewer (light) with darker regions on either side, toward the viewer, indicating paired, counter-rotating helices. The inner helical movement must arise through blood curling forward from the farther wall to fill the space left by separation of streamlines from the inner curvature. By the end of systole, this inner helix has come to dominate, resulting in slight anticlockwise (from above) rotation in the descending aorta.

Flow vector components in planes aligned with and transecting the upper arch were mapped by magnetic resonance, as described above. Both continuous flow and pulsatile flow experiments were performed through flat and twisted arrangements of the arch. For cine imaging of the cycle of pulsatile flow, gating (equivalent to cardiac gating) was achieved through an electric circuit closed at each contact of the driving rotor arm with a second conductor. Sixteen frames were acquired per cycle.

Continuous flow was maintained at a rate of 12 L/min. Pulsation was superimposed at a rate of 30 beats per minute, adjusted to give a peak of forward flow rising to 28 L/min (flat arch experiment) and 22 L/min (twisted arch experiment), with a slight reversal of net flow in the diastolic phase. Peak axial velocities during the systolic phase of pulsatile flow reached 0.5 m/s.

Results

The images in Figs 1 through 6 have been selected to illustrate the principle in vivo flow findings, some of which are schematically drawn in Fig 7. Before we describe them, however, we will draw attention to certain anatomic features and define the terms that we use to describe arch anatomy and patterns of flow.

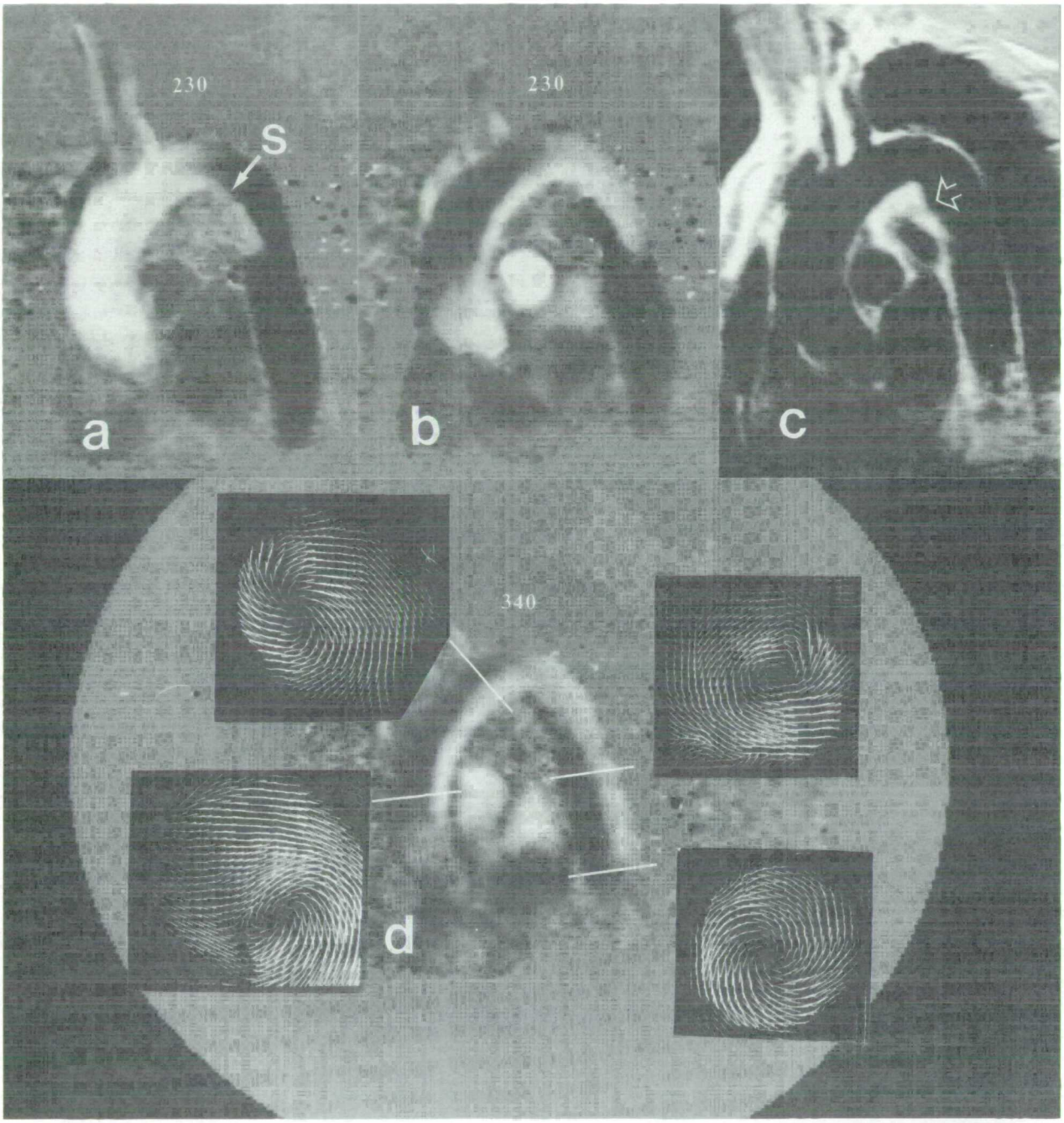


FIG 3. Transition from right-handed to left-handed rotation (in subject 1, a subject with relatively acute distal arch curvature). Numbers indicate gating delays, in milliseconds from R wave. a, Vertically encoded velocity map, mid-systolic frame, showing flow separation (labeled "s") and local retrograde flow in the distal arch. b, Corresponding through-plane velocity map (dark toward viewer, light away). The velocity distribution indicates right-handed helical flow in the ascending and upper arch, but left-handed rotation (with respect to forward flow) is beginning to develop in the distal arch. c, The spin echo image shows the slight dilatation of the ductus diverticulum (arrowed). d, A late systolic through-plane velocity map, 110 ms later than b, showing that at this stage, as axial flow declines, there is right-handed rotation in the ascending and upper arch, but left-handed rotation in the descending arch. The four vector maps show nonaxial blood movements in planes transecting the arch at levels indicated by the lines on the velocity map. The vector maps are all viewed as if looking in the direction of forward flow, ie, from below on the ascending side and from above on the descending side and are orientated with the subject's right side to the right of the vector map.

Arch Anatomy

The extent to which the aortic arch was found to lie in a single plane can be judged from the images in Fig 1. The ascending aorta entered this plane, which we call the arch plane, from its left side, at a level just below that of the right pulmonary artery. We refer to the ascending aorta from this point up to the origin of the first (right) brachiocephalic artery as the ascending

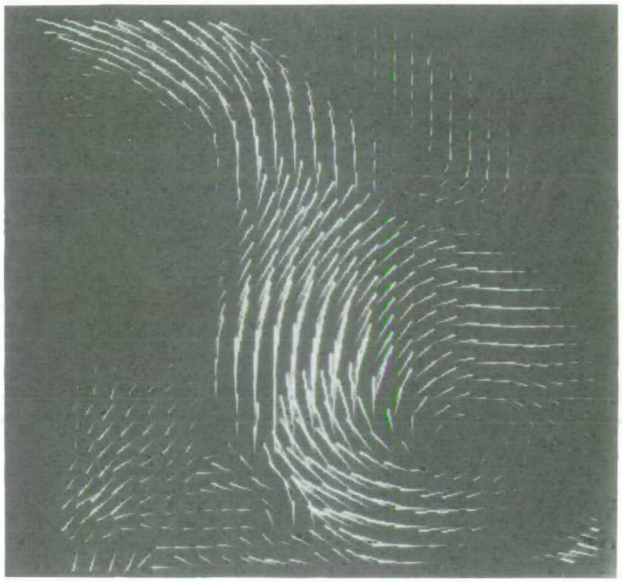


FIG 4. Flow into the first branch of the arch. This vector map obliquely transects the ascending arch of subject 7, showing systolic flow into the right brachiocephalic artery.

arch. The region from the first branch to the point at which arch curvature begins to straighten to become the descending thoracic aorta, we call the upper arch.

In one subject (subject 10, as numbered in Fig 1), the aorta was unusually flat, with nearly all of the ascending aorta, including part of the sinus of Valsalva, lying in the arch plane.

The upper arch curvature varied between subjects from one that continued to ascend for about 3 cm beyond the left subclavian artery branch before turning fairly tightly downward (subject 1) to more smoothly rounded curves in subjects 7 through 9.

A relatively common anatomic feature was the slight bulge of the aortic wall just distal to the point where the arch turns downward. This bulge is known as the ductus diverticulum. It was identifiable in spin echo or late systolic cine images in subjects 1 through 6 (for example, see upper-right-hand images in Figs 2 and 3). We will refer to this anatomic region, whether a bulge is apparent or not, as the distal arch.

Of the three brachiocephalic branches (innominate, L common carotid, and L subclavian arteries), the origins of at least two of the branches could be identified in 9 of the 10 subjects (see Fig 1). (In subject 5, metal caused local magnetic field distortion and degradation of the top of the velocity map images.) The origins of these branches were angulated in the direction of upward and forward flow.

Flow Terminology

We use the term helical flow to refer to fluid movement in which axial and rotational movements coexist in such a way that streamlines would be found to trace helical paths. Helices are referred to as right handed if their rotation, like that of a corkscrew, is clockwise when viewed in the direction of forward movement. Helical flow was recognized in our study by correlating information on axial and nonaxial velocity distributions in the selected image planes.

When helical flow is also pulsatile, the slope of helical streamlines changes through the cycle. At end systole and after, when axial velocities are low or reversed, rotational movement may dominate; we refer to this as rotational flow (although oblique streamlines, moving in forward and/or reversed directions, may be present).

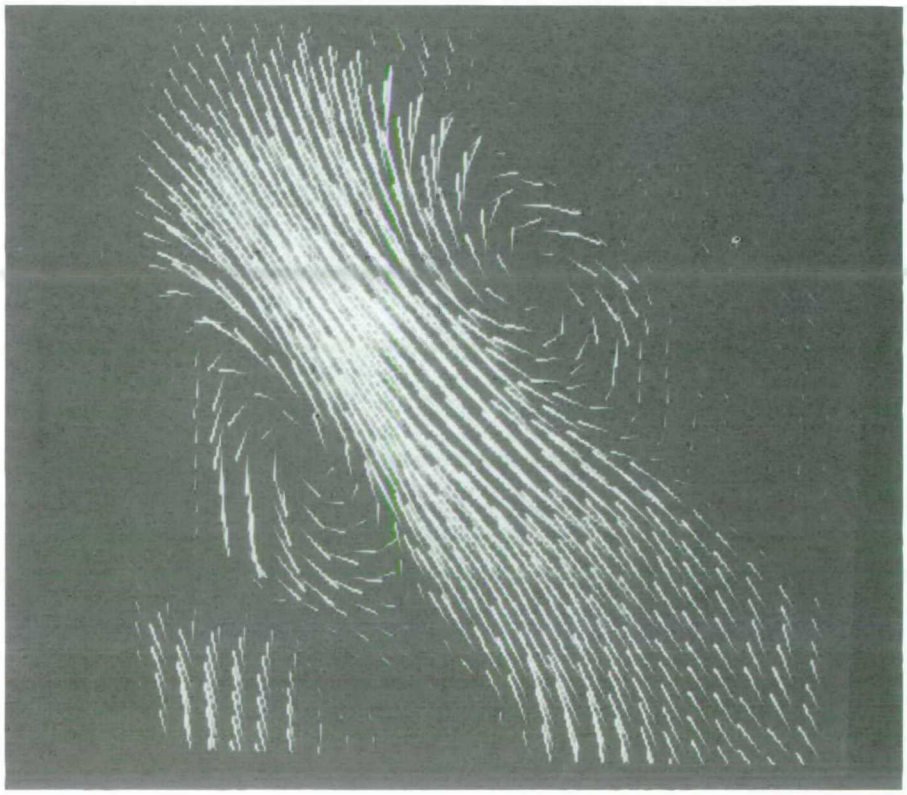


FIG 5. Secondary flow patterns above the aortic valve. This is a late systolic vector map, located through the two coronary cusp sinuses. It shows recirculating flows accommodated by the sinuses that contribute to efficient valve closure at end systole.

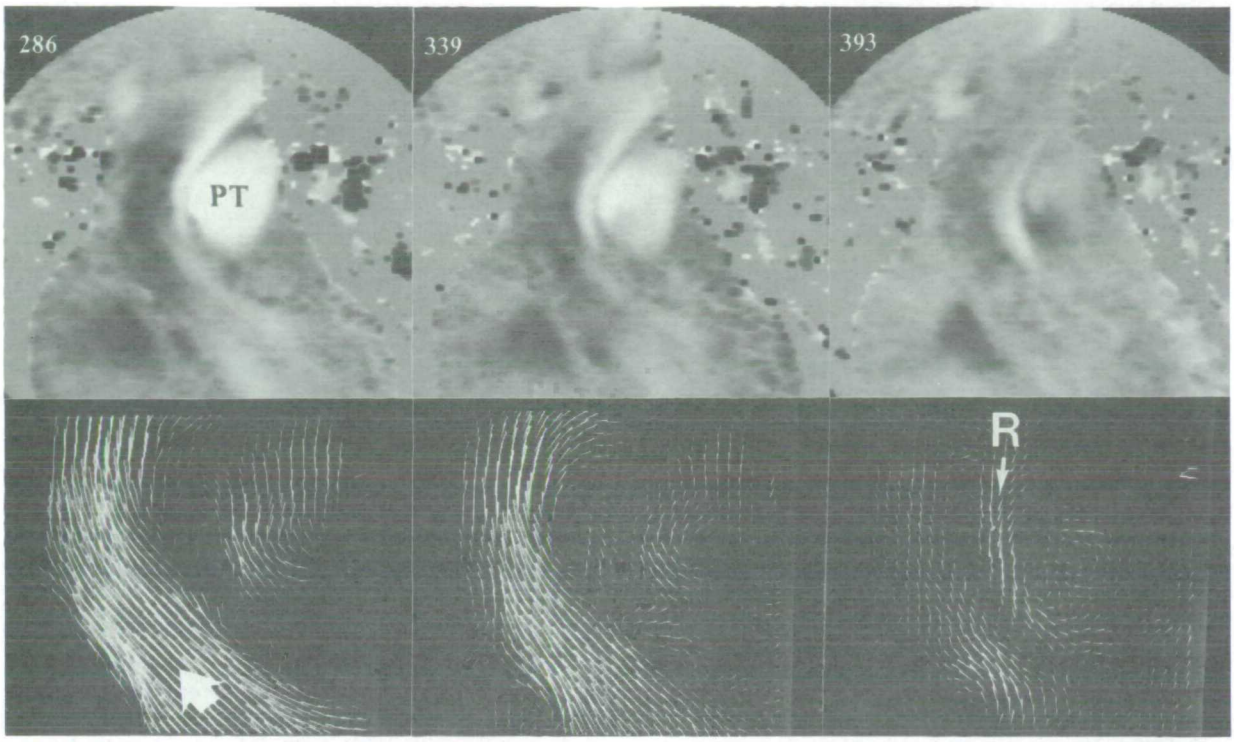


FIG 6. Left ventricular outflow and ascending aorta, viewed from the front (subject 1). Through-plane velocities are shown above (dark toward, light away; PT, pulmonary trunk). In-plane vectors are shown below, in three late to end-systolic frames (numbers represent gating delays in milliseconds from R wave). Through-plane (helical) flow is not obvious in the ventricular outflow tract but develops in the ascending aorta, with a light stream sweeping away from the viewer along the inner curvature. This is also the location of a retrograde movement at end systole (labeled R). Local recirculation can be identified in the left coronary cusp, with the retrograde stream extending down to this cusp in the final frame.

The term skewed will be used to refer to an asymmetric axial velocity profile in which the peak axial velocity is located closer to one wall than the other.

Streamlines are imaginary lines through the flow field at a given moment in time, aligned at all points with the local velocity vector.

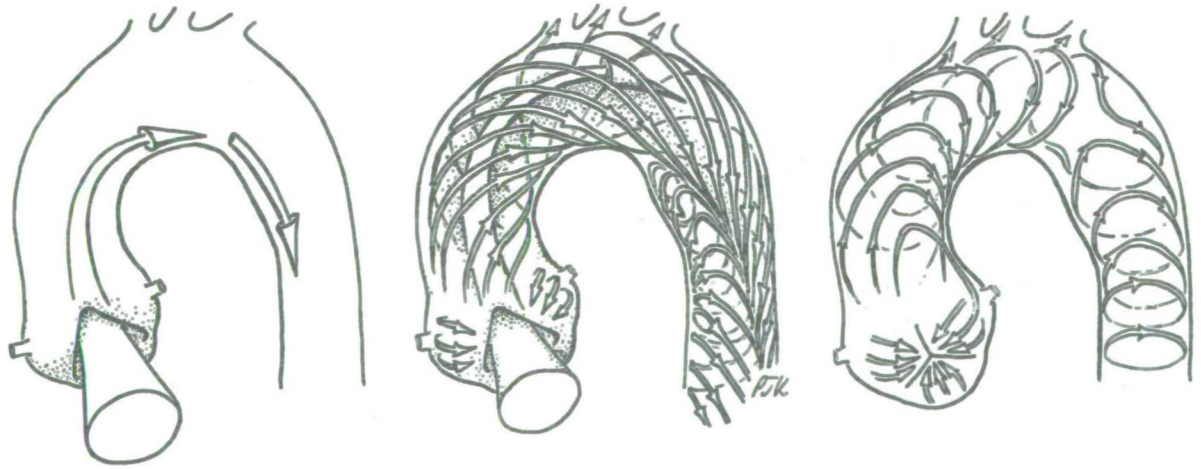


FIG 7. Schematic drawings to illustrate typical aortic arch flow development. a, Early systole. During acceleration, highest axial velocities begin along the shortest flow path, close to the inner curvature (cylindrical arrows). Axially directed flows through the remainder of the arch and its branches have not been drawn. b, Mid to late systole. The highest velocity stream migrates outward, and secondary helical flows develop. Where streamlines separate from the inner wall of the distal arch, the separation zone is filled by oblique retrograde streamlines, curling back toward the viewer from the further wall. c, End systole. Combinations of rotational and recirculating secondary flows persist after aortic valve closure. The drawing is intended to indicate averaged streamlines, although instability of flow and beat-to-beat variation is likely at end systole.

Peak Axial and Nonaxial Blood Flow Velocities in the Aortic Arch Recorded by Velocity Mapping in the Arch Plane

	Peak Axial Velocities			Peak Nonaxial Velocities	
Subject	Ascending	Upper Arch	Descending	Toward Right	Toward Left
1	1.1 (130 ms)	1.1 (180 ms)	0.9 (230 ms)	0.45 (280 ms)	0.4 (280 ms)
2	1.0 (130 ms)	1.1 (130 ms)	1.0 (180 ms)	0.3 (230 ms)	0.25 (230 ms)
3	0.9 (180 ms)	1.0 (180 ms)	0.8 (180 ms)	0.3 (340 ms)	0.2 (340 ms)
4	0.9 (160 ms)	0.9 (160 ms)	0.9 (200 ms)	0.3 (250 ms)	0.3 (250 ms)
5	0.8 (140 ms)	0.8 (140 ms)	0.8 (140 ms)	0.3 (220 ms)	0.3 (220 ms)
6	1.1 (160 ms)	1.0 (160 ms)	1.0 (190 ms)	0.3 (250 ms)	0.25 (250 ms)
7	1.0 (130 ms)	1.0 (130 ms)	1.2 (180 ms)	0.3 (220 ms)	0.3 (220 ms)
8	0.8 (130 ms)	0.9 (170 ms)	1.0 (170 ms)	0.3 (270 ms)	0.25 (270 ms)
9	1.0 (140 ms)	1.2 (140 ms)	1.0 (180 ms)	0.2 (320 ms)	0.3 (280 ms)
10	1.0 (120 ms)	1.2 (160 ms)	1.1 (200 ms)	0.15 (240 ms)	0.2 (240 ms)
Mean	0.96 (141 ms)	1.02 (155 ms)	0.93 (185 ms)	0.29 (252 ms)	0.26 (249 ms)
SD	±0.06	±0.1	±0.1	±0.05	±0.04

Ascending and descending axial velocities were measured on vertically encoded velocity maps, upper arch axial velocities were measured on horizontally encoded velocity maps, and the nonaxial velocities were measured on through-plane velocity maps in the upper arch region where helical flow was most marked. Through-plane velocities directed to the subject's right side were located close to the inner arch curvature, whereas those directed to the left were nearer to the outer curvature.

Values in m/s (followed by the timing, in ms from the R wave).

Turbulence is a region of complex flow containing multiple, small-scale eddies and countereddies whose distribution and movements are chaotic.

Velocity Maps in the Aortic Arch Plane

In Fig 1, pairs of velocity map frames from each of the 10 subjects illustrate the overall similarity of flow patterns between individuals.

Development of arch flow. Fig 2 shows frames spanning the period of systole in subject 4, chosen for illustration because the flow patterns in this subject were reasonably typical, not at one of the extremes of variability. Comparison of the images reveals the sequential development of axial, helical, and retrograde flow. Velocity profiles drawn across selected regions of the arch also changed progressively through the course of systole, showing stages that were broadly similar in all 10 subjects (represented schematically in Fig 7). In early systole (at 100- to 150-millisecond gating delay from the R wave of the ECG), as intra-aortic blood was being accelerated, forward, axial velocities developed across the width of the vessel, but with marked skewing of the profile, with highest velocities close to the inner wall of the arch. In mid systole (150- to 250-millisecond gating delay), the region of maximum axial velocity migrated outward, away from the inner wall, reaching a peak axial velocity of between 0.8 and 1.2 m/s (see Table). An oblique stream moved into the region close to the inner wall of the upper arch, beginning to establish a right-hand helical pattern of flow in this region, with nonaxial velocities reaching their peak after peak axial flow. Separation of the forward stream from the inner wall of the distal arch was seen in all subjects, although it was relatively slight in subject 9, with an unusually rounded arch. Separation was marked by local retrograde flow moving back into the separation zone (marked "s" in Fig 3a). This is the region in which retrograde flow was first seen. In late systole and diastole (250-millisecond gating delay onward), as net forward flow declined, secondary helical and retrograde flows persisted, with relatively low velocities that continued through early diastole, or through the whole of diastole in some cases (subjects 1, 2, 3, and 9).

Helical flows in the upper arch. The through-plane velocity maps in Fig 1 show evidence of helical flows in the arch of all 10 subjects, with right-handed helical flow dominating in the upper arch of all subjects except subject 10. The nonaxial velocities in the upper arch peaked at between 0.15 and 0.4 m/s, with a mean of 0.28 m/s, ie, about one third of peak axial velocity. Because nonaxial, rotational flow reached its peak as axial flow declined, and continued, to a varying extent, after it had ceased, the direction of streamlines must have varied greatly through the cycle, from predominantly axial in early systole to predominantly rotational by end systole.

The core or axis of the helix was generally located eccentrically in the ascending and upper arch lumen, first appearing toward the inner wall, then moving round to the subject's right side (Figs 1 and 3).

In the 10th subject (who was the subject with an unusually flat arch), the helical pattern in the upper arch was barely recognizable in the through-plane velocity map. In the ascending arch of this subject, however, a central white band is flanked by two dark ones. This suggests the presence of paired, counterrotating helices, the central zone moving away from the viewer while both peripheries are moving toward.

Similar dark light dark patterns suggest the presence of paired counterrotating flows in the proximal descending aorta in several of the through-plane velocity map frames in Fig 1, and examination of other cine frames indicated that this pattern occurred, transiently, in all subjects in the distal arch.

Helical flows in the descending arch. There were differences between subjects in the way that helical flow, predominantly right-handed in the upper arch, contin-

ued over into helical flows in the descending aorta. Subject 1, with marked angulation of the distal arch, developed the strongest left-handed rotation in the descending aorta, as viewed in the direction of systolic forward flow (Fig 3). Left-handed rotations also developed in the descending arch of all the remaining subjects except 9 and 10. No net rotation was measurable in the descending aorta of subject 10. Subject 9 (with a smoothly rounded arch) was the only subject in whom the right-handed helical rotation of the upper arch continued to dominate, redirected downward, in the descending limb.

Flow-related signal intensity variations. Gradient echo signal intensity images showed variations of brightness with location and timing. Brightest signal occurred where there was through-plane movement of blood. There was relatively little evidence of signal loss attributable to turbulence (Fig 2, upper row).

Vector maps in transaortic planes. Velocity vector maps acquired in planes transecting the aorta showed evidence of helical or rotational flow, supporting the findings described above. Fig 3d shows the change from right-handed ascending to left-handed descending rotations demonstrated by maps of vectors in planes transecting the arch as well as by maps of velocity components through the arch plane.

Vector maps were also acquired across the descending aorta posterior to mitral valve level in subjects 5 and 9. In both cases, these confirmed the directions of rotation that had been observed in the descending aorta in maps of velocity through the arch plane: left-handed in subject 5, and right-handed in subject 9.

Fig 4 shows a systolic vector map in a slightly oblique cut through the upper ascending aorta, tipped to lie in plane with the origin of the right brachiocephalic artery (subject 7). It illustrates continuity between helical intra-aortic flow and branch flow.

Retrograde streams. End-systolic retrograde flow was visible down the inside curvature of the ascending arch in all cases (seen as downward movement in vertically encoded velocity maps in the arch plane).

Local retrograde flow inside the distal arch separation zone was seen at mid to late systole in all subjects, although it was least marked in subject 9. In most cases, this recirculating region extended back further at end systole to give a retrograde stream round the inner curvature of the upper arch (labeled "R" in Fig 2). There was, however, variability in the upper arch region: in subject 1, retrograde flow appeared on the outside of the bend at the top of the arch, close to the origins of the brachiocephalic branches, and in subjects 2, 7, and 10, there appeared to be a migration of the retrograde stream from the inside to the outside of the upper arch.

Retrograde movements usually coincided with regions of relatively high nonaxial velocity (see Figs 2, 3, and 6), indicating oblique, backward flowing vectors.

Flow entering the ascending aorta. Velocity mapping in an oblique plane cutting through the two coronary cusp sinuses above the aortic valve (in the additional subject, Fig 5) showed secondary recirculating flows in the sinuses toward end systole.

In a slightly different oblique plane, aligned with the ascending aorta as well as left ventricular outflow (in subject 1, Fig 6), velocity mapping demonstrated the onset of both helical and retrograde flows in the proximal ascending aorta. Relatively low levels of through-plane velocity in the left ventricular outflow tract suggest that rotation developing in ascending aorta is not, in this case at least, a continuation of nonaxial movements already present at the ventricular outflow level.

Incidental findings. The principal velocity mapping plane, aligned with the upper arch, also passed through the right pulmonary artery and left atrium in all subjects. In the right pulmonary artery, in-plane velocity maps demonstrated right-handed helical flow in late systole. In the left atrium, through-plane velocity maps showed evidence of a coherent blood movements during atrial filling, with anticlockwise rotation of the blood mass, as viewed from the front of the heart.

In Vitro Flow Studies

The images in Fig 8 have been selected to illustrate the principal in vitro results.

Continuous flow in the flat arch. This led to bilaterally symmetric patterns of secondary flow, with only minimal flow (less than 0.1 m/s) recorded through the central plane (Fig 8a). Where the main forward stream tended to separate from the inside of the arch, the space was filled by oblique, inward flowing streams sweeping round the walls from each side, without retrograde movement.

We found that the symmetry of flow was easily broken. Slight departure of the arch curvature from a single plane resulted in asymmetric patterns.

Continuous flow in the twisted arch. This showed strong, exclusively right-handed helical rotation in the upper arch, with nonaxial velocities through the arch plane up to 0.4 m/s (Fig 8b). A dark light/dark banding is seen where inflow curves into the arch plane. This indicates paired helices, with the right-handed helix coming to dominance as soon as the tube curves into the arch itself.

Pulsatile flow in the flat arch. This demonstrated the progression from axial to secondary flows through the course of systole (Fig 8c). During early systolic acceleration, as in the aorta, axial velocity profiles showed marked skewing, with highest velocities close to the inner wall. As these high axial velocities migrated outward, nonaxial secondary flows curved into the separation zone from each side, leading, by end systole, to secondary movements that resulted in well-developed paired helices and a strongly developed retrograde stream back along the inner curvature (marked "R").

Pulsatile flow in the twisted arch. This also demonstrated development from axial to secondary flows (Fig 8d). In this case, secondary flows began as paired, counterrotating helices with streams moving obliquely into the inner wall region from each side. But, as flow from the twisted ascending limb began to arrive in the upper arch, the right-handed helix came to dominate. At end systole, a retrograde stream was identifiable along the inner curvature of the distal arch. Mapping of axial velocities through a plane transecting the top of the arch showed that the retrograde stream, less strongly developed than in the flat arch, was itself deflected by the helical, rotational movement. This accounts for the absence of retrograde flow in the upper arch region of the vector map located in the central arch plane.

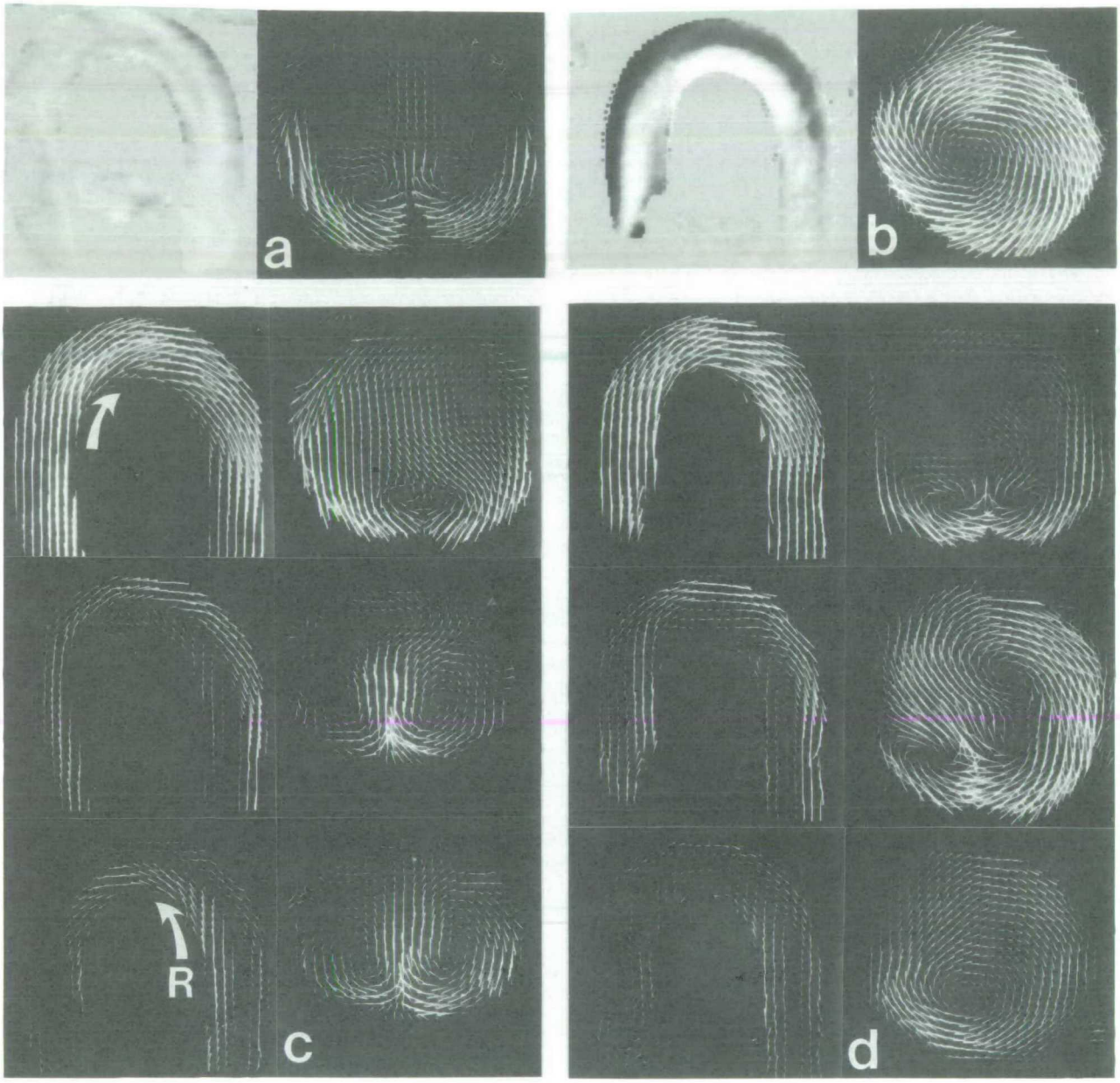


FIG 8. In vitro flow experiments. All the images show flow in the curved tube phantom mapped by magnetic resonance. The left image of each pair is aligned with the arch plane, and the right image of each pair shows flow vectors in a plane transecting the top of the arch, viewed in the direction of forward flow. The images have been grouped in four sections to distinguish four sets of conditions: Images above (a and b) were made during continuous flow, the two gray-scale velocity maps showing through-plane velocities (light away, dark toward). Images below (c and d) were made during pulsatile flow—systolic to early diastolic phases ordered from above downward. Images on the left (a and c) were made with the tube curved in a "flat" arch. Images on the right (b and d) were made with the inflow tube curving into the arch plane from the viewer's side, simulating the twist of human ascending arch. Symmetrically paired helical flow patterns arise in the flat arch (a and c), whereas a single right-handed helical flow pattern develops in the twisted arch (b and d). Retrograde flow (labeled R) develops most strongly along the inner curvature of the flat arch at end systole. It also develops in the distal limb of the twisted arch at end systole.

Discussion

The development of intra-aortic flow patterns can be appreciated through study and comparison of images in the figures, which have had to be selected from the very large number of cine frames acquired. But static illustration is a limitation as some flow findings are more readily appreciated when the data are viewed in cine mode. The schematic drawings of Fig 7 are intended as a guide to recognition of typical flow features.

The velocity maps show evidence of coherent patterns of flow, with general conformity to vessel contours, and development from axial to secondary patterns of flow through the course of systole. These results are, in a sense, self-validating. Methodologic errors or artifacts could not be expected to give such orderly

patterns. Artifacts caused by background noise and non–velocity-related phase shifts occurred in peripheral parts of images, but they did not significantly degrade data from regions of blood flow, which gave reliable levels of magnetic resonance signal. The accuracy of magnetic resonance phase shift velocity measurements is now well established, and as long as sources of error are minimized[23,24] velocity in medium to large blood vessels can be measured with at least 90% accuracy.[3,4]

We limited the main study to 10 healthy subjects, and this meant that sample images from all could be presented together, without exclusions (Fig 1). Mapping of velocity components in and through the arch plane allowed comparison of flows in different arch regions, including the principal inner curvature where we had expected that flow separation and the origins of retrograde flow might be observed. The velocity maps demonstrated right-handed helical flow in the upper arch in mid to late systole. We believe that this is the only reasonable interpretation of the combinations of axial and nonaxial velocity patterns recorded, especially as studies in transaortic planes (Figs 3 and 4) corroborated findings in the arch plane.

Helical patterns in the descending aorta showed variability, and adequate assessment of the prevalence of different variants would require a larger series. Frazin et al[16] did study larger numbers, but using the more limited technique of color Doppler ultrasound, capable only of recording flow directed to and from the intraesophageal transducer. Our findings in the upper part of the descending arch are generally in accordance with theirs. We agree with them that there is variability between subjects, and, on the basis of our observations, we suggest that differences in eventual rotational direction are related to the degree of flow separation in the distal arch, dependent, in turn, on the acuteness of distal arch curvature and the presence of a ductus diverticulum. Separation of streamlines that are themselves moving helically appears to give rise to quite a complex recirculating movement in the separation zone, with reversal of rotation as well as axial direction (compare Figs 2, 3, and 7b).

Causal connections between flow separation and the bulge of the ductus diverticulum may work both ways. Diameter increase immediately beyond a bend can be expected to predispose to flow separation, and, conversely, it may be that the distributions of wall shear stresses and pressure fluctuations associated with unstable, separated flow contribute to the molding of contours in the distal arch region.

In Vitro Model

Helical flow. The in vitro studies confirmed our view that twisted curvature might lead to dominance of a single helix. Continuous flow gave rise to a right-handed helical flow field in the upper curvature of the "anatomically" twisted arch, and during pulsatile flow, a right-handed helix came to dominate during systole. The flat arch, on the other hand, contained bilaterally symmetric patterns.

Deviation from flow symmetry resulted when overall pipe symmetry was broken by lateral displacement of the inflow. Right-handed helical flow dominated when *the tube itself traced part of a right-handed helical path. This principle also applies to the curve of the pulmonary trunk leading into the right pulmonary artery,* where right-handed helical flow was observed.

Retrograde flow. Pulsatility of flow in both the flat and the twisted arch led to retrograde movement along the inner curvature, but this was more strongly apparent in the flat arch. The weakness of recorded retrograde flow in the upper part of the twisted arch can be explained by the more uniform distribution of forward momentum where helical flow is established. Furthermore, helical movement leads to lateral displacement of any retrograde stream to one side of the arch plane.

Limitations and strengths of the model. The plastic tube that we used had no significant compliance, it had no branches, and was of uniform diameter. In these respects it did not simulate the aortic arch, but the advantage was that we could explore the effects of vessel curvature and pulsatility without the influence of additional variables. The corrugations were very small in relation to pipe diameter, and although it is likely that very small vortices were formed and trapped in the corrugations during flow experiments, we do not believe that these significantly influenced larger-scale secondary flow patterns.

Changes of parameters such as flow rate, pulsatility, and curvature might have given different results, but what we aimed for was a system with appropriate relative dimensions and a peak Reynolds number falling within the range of those in the aorta between rest and exercise. (Peak in vitro velocity of 0.5 m/s was half that in the resting aorta, but the vessel diameter was about 50% greater, and the viscosity of the solution used was about 35% of that of blood; this implies that peak Reynolds number rose to about twice that in the resting aorta.)

The results we obtained demonstrate that twisted curvature and pulsatility of flow in the curve lead to helical and retrograde flow, respectively, but we cannot comment on the possible influence of other factors such as the presence of branch vessels, wall compliance, and wave reflection in the peripheral vascular bed. And we cannot exclude the possibility that rotational momentum originating in the left ventricle is carried forward into the aorta, although our one study that recorded nonaxial velocities in the left ventricular outflow tract (Fig 6) showed that these were small compared with the nonaxial velocities arising in the curve of the ascending aorta.

Skewed Axial Flow Profile and Retrograde Flows

The in vitro studies helped us to recognize and understand the sequence of axial flow development in the arch, and the following discussion applies to flow in both the phantom and the aortic arch. First, in early systole, axial flow quickly develops a skewed profile, with higher velocities close to the inner curvature. This pattern has been recognized in a range of earlier aortic flow studies,[12-15] and skewing has been predicted by a mathematical model of curved tube flow.[13] A way to understand it is to imagine axial streamlines, or stream "tubes," in the incompressible fluid around the bend. Those round the inner curvature have a shorter length, and relatively smaller inertial mass, and so are accelerated more readily in early systole. But they also decel*erate more readily in late systole, a factor that contributes to the genesis of retrograde flow.*

Axial velocities in a bend have a centrifugal tendency, local momentum always being tangential to the fluid's curved path. This, combined with relatively low velocities of the boundary layer adjacent to the walls, leads to migration of peak axial flow away from the inner curvature and movement of relatively low velocity secondary flows toward the low-pressure inner wall region. The resulting low momentum of fluid close to the inner wall compared with the high forward momentum of outer streams explains the onset of retrograde flow along the inner wall as net flow is interrupted at end systole.

At no point in the cardiac cycle does flow in the arch have the flat velocity profile of "plug" flow. This is significant because it implies that attempts to deduce cardiac output from local velocity and cross-sectional area measurements may be subject to error, with overestimation likely if high-velocity regions are sampled.[25]

Secondary flows in the aortic sinus. The trapped vortical flows developing during systole in the sinuses the aortic valve cusps (Fig 5) may be regarded as a special case of flow separation and local retrograde flows, more closely related to flows through other cardiac and venous valves than to the secondary flows of the aortic arch. We include the illustration to record their presence and to distinguish them from the retrograde streams of the aortic arch. In the early 16th century, Leonardo da Vinci, apparently on the basis of his own anatomic and flow studies, sketched aortic sinus flow patterns with remarkable accuracy,[26] and their fluid dynamic significance has been investigated.[27]

The stability of helical flow. Flow separation, which occurs readily in a pulsatile, curved system, predisposes to turbulence (flow through cardiovascular valves, with cusp tissue averting collision between forward and recirculating streams, may represent an exception to this rule). A significant aspect of helical flow in the upper arch may be that it minimizes flow separation and turbulence. In a fully developed helical flow, fluid moves obliquely into the potential separation zone from one side only, and carries on round without separation from the inner wall. Momentum is tangential to the curved path, and the helical path makes it possible for the vectors of fluid momentum to not pull away from the inner curvature at any point. This may delay flow separation and minimize turbulence.

In all of our studies, velocity data were averaged over many heartbeats. This means that the chaotic velocity fluctuations of any turbulent regions were not recorded, although regular cyclic variations were captured by cardiac gating. The fact that secondary flow patterns remained clearly recognizable under these conditions indicates that coherent streams were present. But the additional presence of chaotic velocity fluctuations cannot be excluded.

Turbulence, above a relatively low level of intensity, is detectable on cine magnetic resonance imaging, using an echo time of 14 milliseconds, because it results in signal loss.[3,28,29] Complete signal loss did not occur in our studies, although certain arch regions, localized in space and time, did show relative loss of signal (see Fig 2, upper row). These included the core of the helix in the upper arch and the inner edge of the separated stream in the distal arch. In the latter case, where the recirculating stream is shearing against the forward stream, local turbulence probably occurs. But in both cases velocity gradients between regions of through-plane flow, which give enhanced signal, could account for the relative signal loss. The evidence of this study suggests that turbulence remains localized, transient, and of low intensity in the aortic arch at rest, with the distal arch being a particularly susceptible region.

Flow Patterns and the Pathophysiology of Atheroma

The sites of deposition of atherosclerotic plaque are considered to be influenced by flow patterns that cause regions of altered shear stress on the aortic wall.[30,31] Farthing and Perroneau[13] reviewed studies of the distribution of atheroma and of regions of uptake of various markers in the aortic arch in animals. Their evidence suggests susceptibility of the distal arch region to atheroma.

We have had little success in attempting to trace original studies of the distribution of atheroma in the aortic arch in humans. According to Gould,[32] there is a tendency for plaques to form on the posterior wall of the descending aorta, which he attributes to the splinting effect of the vertebral column, whereas the more mobile parts of the ascending and upper arch tend to be spared. If this distribution is indeed typical, we would propose a fluid dynamic explanation that the relative stability of helical flow in upper arch spares this region, whereas more unstable flow patterns impinging on the posterior wall of the descending aorta predispose to atherogenesis.

We have found that patterns of flow in the distal arch vary significantly between individuals. A future study of distribution of atheroma in the aortic arch, which seems to be called for, should take into account individual variations of arch geometry and flow. Magnetic resonance is well suited for this; in addition to its anatomic and flow-imaging capacities it is able to localize and characterize atheromatous plaques in arterial walls.[33]

The Dynamic Significance of Arch Curvature and Helical Flows

The ability of helical flow to minimize turbulence in the upper arch has been discussed. That the blood moves round such a steeply curved arch in the first place has its own dynamic consequences. Rate of change of momentum is proportional to, and in the direction of, the force acting on it (Newton's second law of motion). Within fluids, the forces associated with momentum changes manifest as pressures and pressure gradients. Flow round a steeply curved arch is associated with a raised dynamic pressure on the outside of the bend, ie, at the top of the aortic arch, where the brachiocephalic arteries take their origin. We estimate that convective acceleration resulting from flow at 1 m/s completely changing direction in the span of the arch (a velocity change of 2 m/s in 0.15 second, the arch span being about 15 cm in length) is about 1.35 times the acceleration of free fall in gravity. This suggests dynamic pressures toward the top of the arch of the order of several centimeters of blood, or a few millimeters of mercury, enhancing flow into the brachiocephalic branches.

This applies to resting peak systole. A comparable effect may be extended in time by the late systolic helical spin of blood in the upper arch, where tangential velocities are lower, but the radius of curvature is

smaller. Calculation suggests that the late systolic acceleration due to helical spin is also of the order of gravitational acceleration. A sense that this spin of blood can work to the benefit of branch filling can be gained from study of the vector map in Fig 4.

The significance of the beneficial dynamic gradients, on the one hand, and of the avoidance of detrimental turbulence, on the other, would increase greatly during exercise, each tending to climb with the square of flow velocity. And it is worth remembering that we are considering a system that has to operate unceasingly for a lifetime.

Flow Direction Changes in the Heart

This study has demonstrated the nature of flow direction changes in the aortic arch, and some fluid dynamic implications have been discussed. We would like to close by drawing attention to the direction changes of blood movement through the heart itself.

The vertebrate heart, from its very beginnings, develops a tortuous, S-shaped form, and this basic pattern is retained through all vertebrate species, perhaps because it facilitates efficient, directional exchanges of energy between muscle and blood. The nature and dynamic significance of multidirectional intracardiac flow patterns in health, and their alterations through disease or surgery, remain relatively unexplored. Magnetic resonance velocity mapping opens new possibilities for investigation of the "morphodynamics" of blood movement through heart cavities as well as large vessels.

Acknowledgments

Supported by grants from the Medical Research Council and CORDA (Coronary Artery Disease Research Association), London. We acknowledge the cooperation of our colleagues whose flows were featured in this study. And we thank Professor Ray Gosling, PhD, and Professor Hugo Bogren, MD, for stimulus toward it.

References

1. Moran PR. A flow velocity zeugmatographic interlace for NMR imaging in humans. *Magn Reson Imaging.* 1982;1:197-203.
2. Nayler GL, Firmin DN, Longmore DB. Blood flow imaging by cine magnetic resonance *J Comput Assist Tomogr.* 1986;10:715-722.
3. Underwood SR, Firmin DN. *Magnetic Resonance of the Cardiovascular System.* Oxford: Blackwell Scientific Publications; 1991.
4. Mostbeck GH, Caputo GR, Higgins CB. MR measurement of blood flow in the cardiovascular system. *Am J Radiol.* 1992;159: 453-461.
5. Kilner PJ, Manzara CC, Mohiaddin RH, Pennell DJ, Sutton MStJ, Firmin DN, Underwood SR, Longmore DB. Magnetic resonance jet velocity mapping in mitral and aortic valve stenosis. *Circulation.* 1993;87:1239-1248.
6. Kilner PJ, Wann LS, Firmin DN, Longmore DB. Three directional magnetic resonance flow imaging of the human heart. *Dynamic Cardiovasc Imag.* 1989;2:104-109.
7. Napel S, Lee DH, Frayne R, Rutt BK. Visualizing three-dimensional flow with simulated streamlines and three-dimensional phase-contrast MR imaging. *J Magn Reson Imag.* 1992;2:143-153.
8. Mohiaddin RH, Yang GZ, Burger P, Firmin DN, Longmore DB. Automatic enhancement, animation and segmentation of flow in the peripheral arteries from magnetic resonance phase-shift velocity mapping. *J Comput Assist Tomogr.* 1992;16:176-181.
9. Firmin DN, Gatehouse PD, Yang GZ, Kilner PJ, Longmore DB. Rapid 7-dimensional imaging of pulsatile flow. *Soc Magn Reson Med.* 1992;11:212. Abstract.
10. Yang GZ, Burger P, Kilner PJ, Mohiaddin RH. In vivo blood flow visualization with magnetic resonance imaging. *Proceedings of Visualisation 91, Institute of Electrical and Electronics Engineers.* 1991:202-209.
11. Mohiaddin RH, Yang GZ, Kilner PJ, Longmore DB. Visualisation of flow by multidirectional magnetic resonance velocity mapping: technique and applications. *J Magn Reson Imag.* 1993. In press.
12. Seed WA, Wood NB. Velocity patterns in the aorta. *Cardiovasc Res.* 1971;5:319-330.
13. Farthing S, Peronneau P. Flow in the thoracic aorta. *Cardiovasc Res.* 1979;13:607-620.
14. Klipstein RH, Firmin DN, Underwood SR, Rees RSO, Longmore DB. Blood flow patterns in the human aorta studied by magnetic resonance. *Br Heart J.* 1987;58:316-323.
15. Bogren HG, Klipstein RH, Firmin DN, Underwood SR, Longmore DB. Quantitation of antegrade and retrograde blood flow in the human aorta by magnetic resonance. *Am Heart J.* 1989;117:1214-1222.
16. Frazin LJ, Lanza G, Vonesh M, Khasho F, Spitzzeri C, McGee S, Mehlmann D, Chandran KB, Talano J, McPherson D. Functional chiral asymmetry in the descending thoracic aorta. *Circulation.* 1990;82:1985-1994.
17. Nichols WW, O'Rourke MF. *McDonald's Blood Flow in Arteries.* Edward Arnold; 1989:67-68.
18. Massey BS. *Mechanics of Fluids.* UK: Van Nostrand Reinhold; 1983:222-224.
19. Yearwood TL, Chandran KB. Physiological pulsatile flow experiments in a model of the human aortic arch. *J Biomech.* 1982;15: 683-784.
20. Segadal L, Matre K. Blood velocity distribution in the human ascending aorta. *Circulation.* 1987;36:90-100.
21. Thomas JD. Flow in the descending aorta: a turn of the screw or a sideways glance? *Circulation.* 1990;82:2263-2265.
22. Mathison M, Furuse A, Asano K. Doppler analysis of flow velocity profile at the aortic root. *J Am Coll Cardiol.* 1988;12:947-954.
23. Buoncore MH, Bogren H. Factors influencing the accuracy and precision of velocity-encoded phase imaging. *Magn Reson Med.* 1992;26:141-154.
24. Firmin DN, Nayler GL, Kilner PJ, Longmore DB. The applications of phase shifts in NMR for flow measurement. *Magn Reson Med.* 1990;11:230-241.
25. Fischer DC, Sahn DJ, Friedmann MJ, Larson D, Valdez-Cruz LM, Horowitz S, Goldberg SJ, Allen HD. The effect of variations of pulsed Doppler sampling site on calculation of cardiac output: an experimental study in open-chest dogs. *Circulation.* 1983;67:370.
26. Keele KD. *Leonardo da Vinci on Movement of the Heart and Blood.* London: Harvey and Blythe; 1952:81-87.
27. Bellhouse BJ, Bellhouse FH. Fluid mechanics of model normal and stenosed aortic valves. *Circ Res.* 1969;25:693-704.
28. Sechtem U, Pflugfelder PW, Cassidy MM, White RD, Cheitlin MD, Schiller MB, Higgins CB. Mitral or aortic regurgitation: quantification of regurgitant volumes with cine MR imaging. *Radiology.* 1988;167:425-430.
29. Kilner PJ, Firmin DN, Rees RSO, Martinez JE, Pennell DJ, Mohiaddin RH, Underwood SR, Longmore DB. Valve and great vessel stenosis: assessment with MR jet velocity mapping. *Radiology.* 1991;178:229-235.
30. Caro CG, Fitz-Gerald JM, Scroter RC. Atheroma and arterial wall shear observation: correlation and proposal of a shear dependent mass transfer mechanism for atherogenesis. *Proc R Soc Lond (Biol).* 1971;177:109-159.
31. Rodkiewicz CM. Localization of early atherosclerotic lesions in the aortic arch in the light of fluid flow. *J Biomech.* 1975;8:149-156.
32. Gould SE. *Pathology of the Heart and Blood Vessels.* Illinois: Charles & Thomas; 1968.953-960.
33. Mohiaddin RH, Sampson C, Firmin DN, Longmore DB. Magnetic resonance morphological, chemical shift and flow imaging in peripheral vascular disease. *Eur J Vasc Surg.* 1991;5:383-396.

Computation of Flow Pressure Fields from Magnetic Resonance Velocity Mapping

Guang-Zhong Yang, Philip J. Kilner, Nigel B. Wood, S. Richard Underwood, David N. Firmin

Magnetic resonance phase velocity mapping has unrivalled capacities for acquiring *in vivo* multi-directional blood flow information. In this study, the authors set out to derive both spatial and temporal components of acceleration, and hence differences of pressure in a flow field using cine magnetic resonance velocity data. An efficient numerical algorithm based on the Navier-Stokes equations for incompressible Newtonian fluid was used. The computational approach was validated with *in vitro* flow phantoms. This work aims to contribute to a better understanding of cardiovascular dynamics and to serve as a basis for investigating pulsatile pressure/flow relationships associated with normal and impaired cardiovascular function.

Key words: hemodynamics; pressure distributions; MR velocity imaging.

INTRODUCTION

The dynamics of blood flow through arteries are complex. Several distinct but interacting fluid mechanical factors contribute to pressures of blood at given locations and instants in the system. According to Newton's laws of motion, wherever fluid is subjected to momentum change, forces must be involved, which manifest as gradients of pressure. It is with this aspect of pressure, which we refer to as *flow pressure*, that we are concerned principally in this study. Regions of acceleration and deceleration of blood are associated with gradients of flow pressure. The magnitudes and spatio-temporal distributions of differences in flow pressure across blood masses contained by heart chambers and large vessels still have to be determined, both in healthy subjects and in patients with abnormal cardiovascular function. The proposed noninvasive approach provides access to this relatively unexplored aspect of pathophysiology.

In clinical cardiology, a modification of Bernoulli's equation has been used widely for estimation of pressure differences across stenotic orifices from one-dimensional (1D) velocity data acquired by Doppler ultrasound (1, 2, 3, 4). While a reasonably good correlation has been achieved between the estimated results and actual measurements of pressure difference across stenoses, extension of the technique to other situations is limited by the inapplicability of Bernoulli's equation to unsteady flow. This limitation motivated us to approach the problem through the Navier-Stokes equations as they are recognized as a complete description of the mechanics of simple fluids.

The basic form of the Navier-Stokes equations, which are derived from considering the conservation of momentum in a control volume, can be represented as:

$$-\frac{\partial p}{\partial x_i} = \rho\frac{\partial u_i}{\partial t} + \rho\left(u_1\frac{\partial u_i}{\partial x_1} + u_2\frac{\partial u_i}{\partial x_2} + u_3\frac{\partial u_i}{\partial x_3}\right) - \mu\left(\frac{\partial^2}{\partial x_1^2} + \frac{\partial^2}{\partial x_2^2} + \frac{\partial^2}{\partial x_3^2}\right)u_i - f_i \quad (i = 1, 2, 3) \qquad [1]$$

with x_i $(i = 1, 2, 3)$ representing the three orthogonal axes in space and u_i their corresponding velocity components. In Eq. [1], μ is the coefficient of viscosity, and ρ is the density of the fluid. Variables f_i $(i = 1, 2, 3)$ represent the body force components along x_i. The above equations in fact represent the contribution to the momentum balance of the pressure force, transient and convective inertia, viscous resistance, and body force, i.e.,

Pressure Force = Transient Inertia + Convective Inertia − Viscous Resistance − Body Force.

The term *body force* refers to forces, such as gravity, acting directly on the fluid mass. Use of Eq. [1] for an incompressible fluid is commonly coupled with the divergence-free condition that provides local continuity or conservation of mass within the fluid region, and with the compatibility condition that ensures the global conservation of mass to obviate the effects of incremental errors introduced by numerical algorithms (5). Given velocity distribution $\boldsymbol{u} = (u_1, u_2, u_3)$ and body force $\boldsymbol{f} = (f_1, f_2, f_3)$ (notice that within the fluid the only body force present is gravity), the pressure gradient and thus the pressure, relative to an integration constant, can be calculated. The SI unit for pressure is pascal (Pa), which corresponds to newtons per square meter (N/m^2). In clinical settings, however, millimeters of mercury (mm Hg) are commonly used for recording pressure values.

MRM 36:520–526 (1996)

From the Magnetic Resonance Unit, Royal Brompton Hospital, London, United Kingdom.

Address correspondence to: G. Z Yang, Ph D., Magnetic Resonance Unit, Royal Bromptom Hospital, 30 Britten Street, London SW3 6NP, United Kingdom.

Received August 14, 1995; revised November 30, 1995; accepted January 3, 1996.

1996 SMR Young Investigators' Rabi Award Winner

This work was supported by the Coronary Artery Disease Research Association (CORDA) and the British Heart Foundation.

0740-3194/96 $3.00

Copyright © 1996 by Williams & Wilkins
All rights of reproduction in any form reserved.

MATERIALS AND METHODS

MR Flow Data Acquisition

The velocity data used for this study were acquired using a Picker International Vista MR machine operating at 0.5 T with modified gradient coils and driven by a SMIS (Surrey Medical Imaging Systems, Ltd.) imaging console. Cine phase shift velocity mapping was performed using a gradient echo velocity sequence with an echo time of 14 ms. The slice thickness used was 10 mm and the field of view was 30 or 40 cm. The images were reconstructed on a 256 × 256 matrix from the average of 2 × 128 phase-encoding steps. For *in vivo* studies, 16 cine frames were acquired for each directional velocity map and were gated from the onset of the ECG (electrocardiogram) R wave.

Image Segmentation

Before pressure distribution calculation, velocity image segmentation was required to delineate the flow region and its corresponding boundaries. This process was performed interactively using the magnitude images associated with the velocity data to recognize anatomical structures. This step created a region mask, which was then used to register with the flow images so that the fluid region, denoted as Ω_F, and its corresponding boundary, denoted as $\partial\Omega_F$, required for pressure calculation, could be defined. A fully automatic segmentation approach was attempted, but with limited success for complicated regions.

Pressure Distribution Calculation

It can be seen from Eq. [1] that the pressure gradient $\nabla p = (p_{x_1}, p_{x_2}, p_{x_3})$, where $p_{x_i} \equiv \partial p/\partial x_i$ can be calculated directly from the given velocity data. Thereafter, an integration step is required to derive pressure from ∇p within the flow region. Given a reference pressure at position $(x_{1(0)}, x_{2(0)}, x_{3(0)})$, one can recover the relative pressure $p(x_1, x_2, x_3)$ by integrating along an arbitrary path such that

$$p(x_1,x_2,x_3) = p(x_{1\,0}, x_{2\,0}), x_{3(0)}) + \int_{x_{1(0)},x_{2(0)},x_{3(0)}}^{x_1,x_2,x_3} (p_x\,dx_1 + p_{x_2}dx_2 + p_{x_3}dx_3). \quad [2]$$

In practice, however, this integration step can be troublesome because of noise presented within the original flow signal and the result might depend on the path chosen. A more practical solution to the problem is to take the least-squares method (6) and use the pressure Poisson equation to derive a consistent pressure distribution from ∇p. This is the approach that we have taken. A comparable approach to pressure estimation was used by Song *et al.* (7), who derived velocity information from analysis of ultrafast computed tomography (CT) images. In this paper, however, we adopt a simple yet effective iterative method for deriving pressure by which certain difficulties of the numerical methods described in (7) can be avoided.

Denote p_c as the final pressure distribution that is to be found. We seek to solve for p so that the gradient of p_c within Ω_F is as close as possible to the pressure gradient ∇p derived directly from the original velocity data. The problem can thus be formulated as follows and we aim to find p_c so that the error

$$\iiint_{\Omega_F} \sum_{i\ 1}^{3} \left(\frac{\partial p}{\partial x_i} - p_x \right)^2 dx_1 dx_2 dx_3 \quad [3]$$

is minimized. According to the theory of calculus of variations (8), the Euler equation corresponding to the above integral is in the form of:

$$\nabla^2 p = \sum_{i\ 1}^{3} \left(\frac{\partial p_{x_i}}{\partial x_i} \right), \quad within \quad \Omega_F \quad [4]$$

In Eq. [4] the term ∇^2 is the Laplacian operator.

Before we proceed, however, we also need to know what to do about the boundary $\partial\Omega_F$ of Ω_F over which Eq. [4] is to be solved. The natural boundary condition (5) for an integral of the form shown in Eq. [3] is

$$\nabla p_c \cdot \boldsymbol{n} = \nabla p \cdot \boldsymbol{n}, \quad on \quad \partial\Omega_F \quad [5]$$

in which $\boldsymbol{n}$ is the outward normal vector on $\partial\Omega_F$. It, in essence, states that the normal derivative of the desired pressure distribution must equal the estimate of the normal derivative obtained from the data.

Numerical Algorithm

The Poisson equation described in Eq. [4] can be solved in many ways. For irregular flow region Ω_F, one of the most common approaches is to use lexicographic ordering, and the desired pressure distribution is solved through matrix manipulations. Although the matrices are mainly band-limited, their size can become extremely large and the amount of calculation involved is formidable, and thus impractical in our case. To circumvent this problem, an iterative scheme that incorporates a special property of the discretized Laplacian operator was used (9). In discrete form, the Laplacian operator can be represented as

$$\nabla^2 p_{a,b} = \lambda(\bar{p}_{a} - p_{a,b}) \quad [6]$$

where λ is a constant depending on the differential mask that is used, and $\bar{p}$ is the local average of p. The calculation of local averages will be dependent upon the chosen discretization scheme, and for a 3 × 3 area when only neighbors in the x_1 and x_2 directions are considered (four-neighborhood) it becomes

$$\bar{p} \quad -\frac{1}{4}(p \quad , + p \quad , + p_{a} \quad + p_{a} \quad). \quad [7]$$

When all eight neighbors are considered we have:

$$\bar{p} \quad = \frac{1}{5}(p \quad + p \quad + p \quad + p \quad) + \frac{1}{20}(p \quad ,_{1,+} + p \quad ,_{1} \quad + p \quad + p \quad) \quad [8]$$

In this study, however, only Eq. [7] was used in the calculation. The final iterative process can now be formulated as follows:

$$p_c^{(k+1)} = \bar{p}_c^{(k)} - \frac{1}{\lambda}\sum_{i=1}^{3}\left(\frac{\partial p_{x_i}}{\partial x_i}\right) \quad [9]$$

in which k and $k + 1$ are two successive iteration steps. Initial values of p_c can be generated by a simple integrating scheme and the boundary condition stated in Eq. [5] should be observed throughout the iterative process. The completion of this iterative process is determined by the absolute difference between two successive iteration steps. It terminates if this difference is less than a predefined threshold.

EXPERIMENTAL SETUP AND RESULTS

In Vitro Flow Phantom Validation

Before applying the above process to *in vivo* studies, two *in vitro* experiments were performed to provide appropriate validation of the proposed technique. The first one consisted of an open-topped rotating cylinder containing water, as illustrated in Fig. 1a. The steady angular velocity of the cylinder was controlled by a high precision rotary motor, and the fluid within had reached hydraulic equilibrium (*solid body rotation*). In this case, the pressure value at any given point within the fluid should be proportional to its vertical distance below the surface. In other words, if we measure the pressure distribution within a horizontal cross section of the cylinder, the result expressed in millimeters of water (mm H_2O) should match the surface shape of the fluid. This relationship was used to evaluate the accuracy of our proposed numerical method. Figure 1b, shows the calculated relative pressure distribution within the image plane, and Fig. 1c shows the central horizontal pressure profile of the calculated result and its correlation with the surface shape of the fluid. An encouragingly close match was achieved. Slight discrepancies may reflect minor inaccuracies in the velocity data, particularly in voxels spanning the fluid boundary.

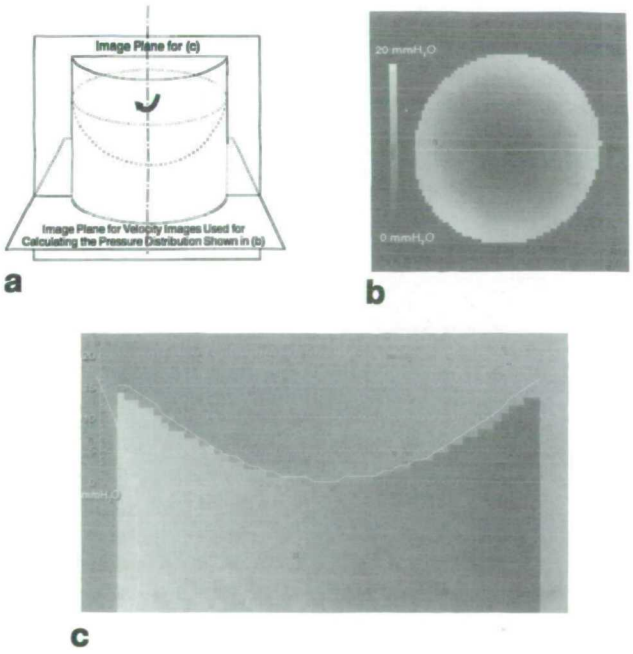


FIG. 1. (a) Schematic drawing of a phantom that contains water in a steadily rotating open-topped cylinder. (b) The calculated relative pressure distribution expressed in millimeters of water (mm H_2O) within a horizontal image plane as shown in Fig. 1a. (c) The central horizontal pressure profile of Fig. 1b and its correlation with the surface shape of the fluid determined by a through-plane velocity encoded image aligned with the axis of the phantom. Because the fluid had reached hydraulic equilibrium, a match between the surface shape of the fluid and the pressure profile (expressed in mmH_2O) should be expected. The imaging field of view used for this experiment was 30 cm.

Although the rotating cylinder phantom provided a convenient way of assessing pressure results calculated from MR data, it should be noted that its velocity field, and hence the calculation, involved spatial but not temporal acceleration. As the fluid had reached hydraulic equilibrium, i.e., $\partial u_i/\partial t = 0$, transient inertia played no part in balancing Eq. [1]. We therefore devised a phantom with transient motion. It consisted of a glass tank filled with water in which a relatively large scale standing wave was induced, as shown in Fig. 2. A pivoted flap, located at an antinode of the wave approximately a quarter wavelength from one end of the tank and driven by a motor located outside of the magnet, was used to generate wave motion. By preliminary testing, the natural frequency of the single standing wave, and a readily achieved wave amplitude were determined, were recorded, and were reproduced in subsequent experiments in and out of the magnet. Because the total length of the tank exceeded the extent of linearity of magnetic field gradients in the z direction, there was spatial displacement of image data close to each end of the tank. This artifact did not affect data in the central 30-cm field, which were used for analysis. A gating circuit was attached to the arm of the motor to allow for interleaved data acquisition similar to that of *in vivo* studies. A total of 24 time frames were collected for each cycle, the time interval between frames being 35 ms.

Figures 3a–3d show the calculated pressure at four different time instances positioned at 105, 245, 385, and 525 ms after the onset of the gating pulse. Within each subfigure, the top picture shows the overall pressure distribution with white for high pressure and black for low pressure. In the bottom subfigure, the pressure values are wrapped around at 1 mm Hg intervals, each occupying a complete gray scale range, so that a semiquantitative visual assessment can be made. In this display scheme, the pressure gradient is proportional to the number of 1 mm Hg bands crossed in a given spatial distance.

During the calculations, the viscous terms in Eq. [1] were neglected, and this is justified as follows. The thickness of the unsteady viscous (Stokes) boundary layer in the fluid in contact with the wall may be estimated from the result of Stokes' second problem (10). This refers to the boundary layer above a harmonically oscillating plate, but a fluid oscillating parallel to a stationary plate is equivalent, and it results from an exact solution of the

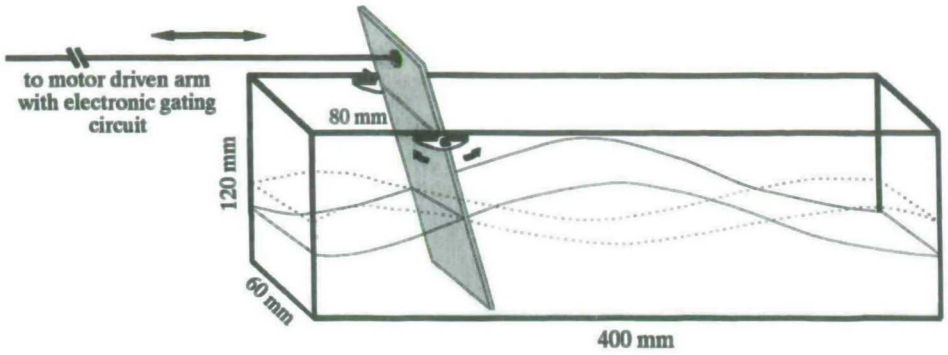


FIG. 2. A schematic diagram showing the configuration of the wave phantom. The glass tank is 400 mm in width, 120 mm in height, and 60 mm in depth. The water was filled to a level of 50 mm. A motor driven pivoted flap was used to generate large scale standing waves. A gating circuit was attached to the arm of the motor to allow acquisition of cine velocity data.

Navier-Stokes equation, which is valid for this case. The thickness of the layer depends on $\sqrt{\nu/\omega}$, in which ν is the kinematic viscosity of the fluid and ω the characteristic frequency. Boundary layers decay asymptotically with distance perpendicular to the wall, so thicknesses are defined arbitrarily. For pulsatile flow, they vary with time through the cycle; the fluid velocity is zero at the wall and reaches at least 99% of the undisturbed velocity when the distance from the wall is $8\sqrt{\nu/\omega}$. The frequency in the wave tank was approximately 1.7 Hz and, taking the kinematic viscosity of water as 0.01 cm^2/s, gives a boundary layer thickness of some 2 to 3 mm. Therefore, viscosity may be neglected over most of the depth of water in the tank. During image segmentation the boundary layer is excluded from the flow region Ω_F.

This neglect of viscous force is, in fact, advantageous for the numerical stability of the algorithm. The calculation of the viscous force involves taking the second-order derivatives of the original velocity data. This process is highly noise sensitive and may cause an undesirable effect on the accuracy of the pressure gradient, and this error will be propagated further during the final pressure calculation.

The actual pressures within the wave phantom were subsequently measured using a 2F Millar SPR-524 catheter-tip pressure transducer, which provides high-fidelity pressure readings. The transducer of the probe was set parallel to the main direction of fluid motion. Possible errors caused by deflection of the flow around the probe are likely to have been negligible, given the small size of the catheter and minute flow disturbance directed across its length.

Figure 4a shows the absolute temporal pressure variations measured at points A and B as marked in Fig. 3. In Fig. 4b, the temporal pressure difference between A and B is plotted as a solid line, whereas the corresponding pressure difference calculated from MR velocity data is delineated as a dotted line. Because these curves represent the pressure difference between two points, the unknown integration constant cancels out after subtraction. It can be seen that a good correspondence between the measured and calculated results was achieved. Some underestimation of the pressure difference, however, is evident for results derived from the MR velocity data. This can be attributed to a number of factors but the

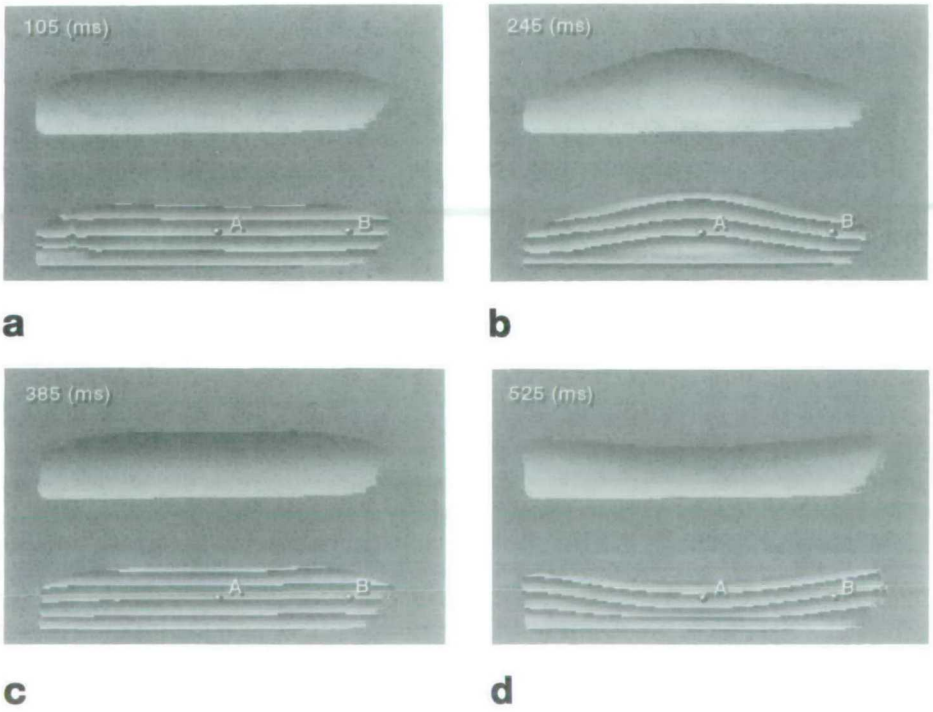


FIG. 3. The reconstructed pressure distribution for an *in vitro* flow phantom. The wave timed at (a) 105 ms, (b) 245 ms, (c) 385 ms, and (d) 525 ms after the onset of the electronic gating pulse. The top picture in each subfigure shows the overall pressure distribution with white for high pressure and black for low pressure. In the bottom subfigure the pressure values are wrapped around at 1 mm Hg intervals to provide a convenient visual assessment of pressure, pressure gradient, and isopressure contours. Catheter-tip pressure measurements were performed at positions marked as A and B, and the results were used to compare with MR measurements. Distortion of the wave tank outside the central 30-cm region of the field of view in image data was caused by nonlinearity of magnetic gradients.

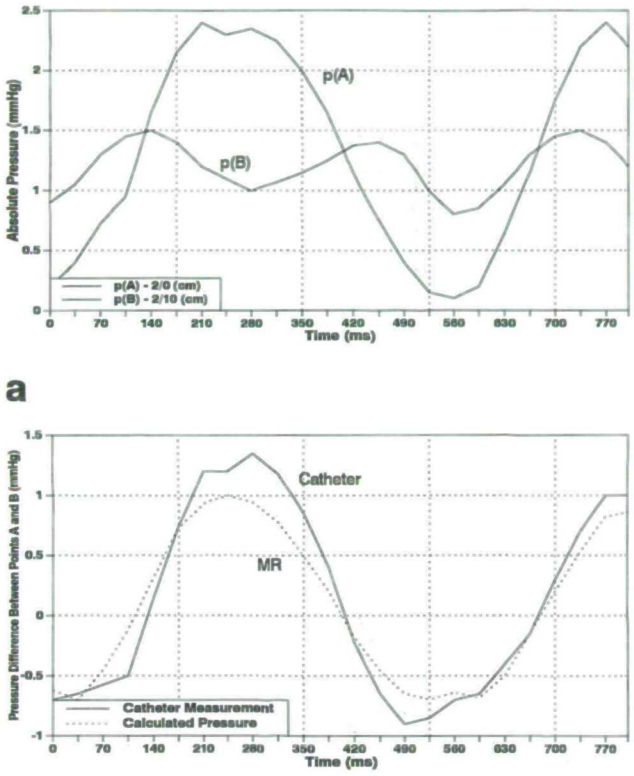


FIG. 4. (a) The pressure measured at positions A and B of Fig. 3 using a high-fidelity catheter-tip pressure transducer. (b) A comparison of the pressure difference curves calculated from the catheter measurements (solid line) and that derived from the MR technique (dotted line).

following two are considered to be the primary causes:

1. The catheter measurement records the instantaneous pressure changes within the fluid, whereas the pressure calculated from the gated MR velocity data represents pressure variation derived from data acquired over many cycles. The averaging effect tends to smooth out small pressure fluctuations.
2. Although the time interval between successive frames was set to be 35 ms, this still may not be adequate for deriving temporal acceleration during peak acceleration or deceleration. Generally, the larger the time interval between successive sampling points, the more the underestimation of transient inertia, thus causing the rounding off of sharp pressure variations.

In Vivo Results

For illustration of *in vivo* application of the method described above we have chosen to analyze a study of blood flow velocity in the aortic arch of a healthy volunteer at rest (11). Figure 5 shows the time curve of mean flow velocity recorded in the ascending aorta. Solid circular markers indicate the times of calculated pressure distributions, which are to be shown in Figure 6. The position at which the mean flow velocity was measured is indicated by the arrow in Figure 6a. A total of 16 time frames

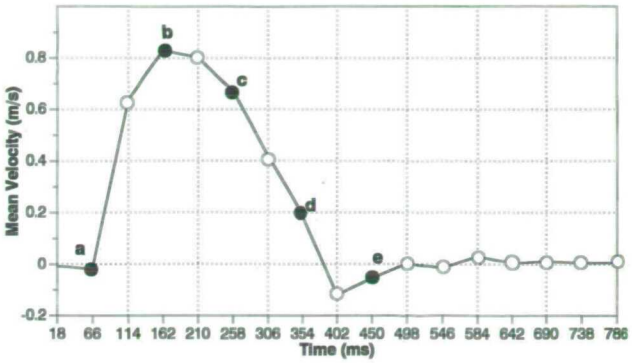


FIG. 5. The mean velocity in the ascending aorta measured at a position indicated by the arrow in Fig. 6a, with solid circular markers representing the time frames at which the pressure distributions were calculated. A total number of 16 time frames were acquired to cover evenly through systole and most of diastole. The time interval between slices was 48 ms.

were acquired to cover systole and most of diastole, and the time interval between frames was 48 ms. Acquisition was in a single slice aligned with the axis of the aortic arch.

Figures 6a–6e illustrate the calculated pressure distributions within the ascending/descending aorta timed at 66, 162, 258, 354, and 450 ms after the onset of the ECG R wave. To assist visualization, they have been superimposed on the magnitude images that show surrounding anatomic structures. The subject was studied in a supine position, and the force of gravity was neglected in our computation. As in the *in vitro* study, the top image of each subfigure shows the overall pressure distribution whereas the lower one uses 1 mm Hg pressure bands to provide a semi-quantitative representation of the pressure distribution.

In Figure 6, changing flow pressure gradients associated with pulsatile flow are apparent. The mass of fluid is almost at rest at the start of the cardiac cycle. In early systole (Fig. 6a), acceleration of blood is associated with a pressure gradient with relatively tightly packed 1 mm Hg pressure bands in the ascending aorta, and high pressure proximally. Toward peak systole, Fig. 6b, the driving pressure gradient declines, and by Fig. 6c, the direction of the gradient has started to reverse, retarding the blood flow. Maximum deceleration is evident in Fig. 6d, in which the higher pressure is located distally, in the descending aorta. It can also be seen that during peak flow, Fig. 6b, there is relatively high pressure toward the outer curvature of the aortic arch as a result of a centrifugal pressure gradient. At the end of systole, the aortic valve closes. The negative pressure gradient does not cause complete flow reversal, but restores flow to a steady state with almost zero velocity and a corresponding zero pressure gradient through diastole (Fig. 6e).

As with our wave tank study, the effects of viscosity were neglected. The Stokes layer in the aorta may be conveniently estimated from the Womersley parameter,

$$\alpha = \frac{D}{2}\sqrt{\left(\frac{\omega}{\nu}\right)}, \qquad [10]$$

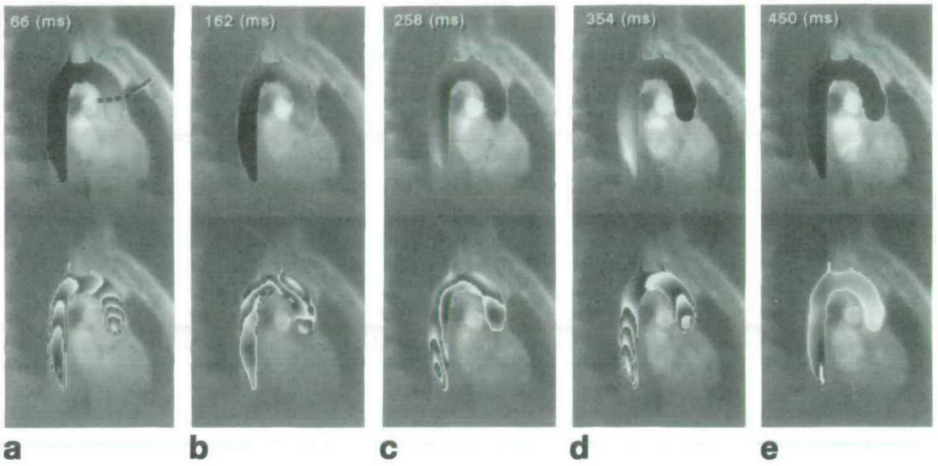


FIG. 6. The reconstructed pressure distribution for flow around the aortic arch. Five of sixteen time frames, corresponding to solid circular marker positions shown in Fig. 5, are displayed here. They illustrate pressure distributions at (a) 66 ms, (b) 162 ms, (c) 258 ms, (d) 354 ms, and (e) 450 ms after the onset of the ECG R wave. The top image of each subfigure shows the overall pressure distribution whereas the lower one uses 1 mm Hg pressure bands to provide a semi-quantitative representation of the pressure distribution.

with D being the blood vessel diameter. As mentioned earlier, ω is the characteristic frequency, and ν the kinematic viscosity of the fluid. The Womersley parameter represents the ratio of the radius of the pipe or artery to the unsteady boundary layer thickness. In this study, α was approximately 12.5 ($D \approx 2.0$ cm, pulsatile frequency ≈ 1 Hz, and assuming $\nu = 0.04$ cm^2/s) so the boundary layer thickness was less than 1 mm; i.e., viscous effects are confined to a thin region near the wall.

DISCUSSION AND CONCLUSION

In this paper, we have presented an approach to the problem of computing flow pressure variations from MR velocity data. Our approach is based on use of the Navier-Stokes equations, which allow computation of pressure/flow relations in the region studied. Our aim was to map intravascular flow pressure distributions, contributing toward a better understanding of cardiovascular physiology and to provide a basis for investigation of abnormal blood flow dynamics. It must be emphasized that not absolute blood pressures but relative pressures within flow fields were sought by this technique. Conventional approaches to blood pressure measurement usually record pressure changes at limited locations without registering spatial variations of pressure. We have set out to visualize spatial distributions of flow pressure related to momentum changes. Altered distributions of flow pressure in the heart and great vessels are to be expected in a range of conditions, for example where there is impaired ventricular function, where there has been surgical reconstruction of the heart, and, in diseases such as atheroma, where there is altered compliance of arterial walls. The nature and significance of abnormal flow pressure distributions will require thorough investigation. This field of investigation should enhance understanding and clinical evaluation in a range of diseases of the heart and circulation.

There are, however, several limiting factors that should be considered. The multidirectional velocity mapping technique used has a relatively long data acquisition time, thus restricting the number of slices that can be imaged in a given time. This may be surmounted by using recently developed rapid volume flow imaging techniques (12) with improved spatio-temporal resolutions. Also, attention should be paid to factors that affect the accuracy of the velocity phase mapping technique. These include partial volume averaging, misregistration effects, and phase errors introduced where there are higher orders of motion (13). Because transient inertia plays a dominant part in the Navier-Stokes equation, attempts are being made to reduce the time interval between successive image frames so that the smoothing effect described earlier can be minimized.

For the aortic arch study, acquisition of data in only one plane meant that any convective acceleration directed through the plane is overlooked. Our previous study of normal aortic flow (11) showed that the nonaxial component of velocity peaked at less than 30% of axial velocity and occurred during late systolic deceleration, during which transient rather than convective components of acceleration would dominate the balance of the Navier-Stokes equations. Through-plane convective acceleration can be expected therefore to play little part in the calculation of pressure gradients. Multiple plane or volume acquisition might be required, however, for the computation of flow pressure distributions in the presence of pathological distortions of the aorta.

In the present study, we have neglected viscous forces, and have given a justification for doing so. In the future, particularly if smaller blood vessels are to be investigated, it may be necessary to introduce the viscosity terms that we have omitted. There are further considerations that deserve attention. First, we have mentioned the problem of noise in the signal. One approach to dealing with this would be to smooth the data in a controlled way, probably using the continuity equation, which would impose internal consistency on the measurements and improve the results of subsequent analysis. A further problem is raised by the large time intervals between the cine frames, reducing the accuracy of the treatment of discretized equations involving time derivatives and integrations. This has made it difficult to relate pressure between time intervals, and we have been restricted to deriving differences of instantaneous pressure within the system. The possibility of reducing the time intervals has been mentioned. This would be particularly beneficial during phases of rapid change of momentum such as early systole. Further, suitable curve fitting procedures might be introduced to improve the

accuracy of arithmetic operations involving time. Linking the spatial and temporal progression of the pressure wave via knowledge of its speed of propagation in the aorta has been used in the past for investigating ventricular contraction efficiency (14, 15), and we believe this should be investigated further in the present context.

In conclusion, our results show the potential suitability of the proposed method for providing information on flow pressure fields associated with blood momentum change in the heart and large vessels. We believe that this approach will provide important new information on cardiovascular physiology and pathophysiology.

ACKNOWLEDGMENTS

The authors thank their colleagues in the Magnetic Resonance Unit and the Department of Paediatrics of Royal Brompton Hospital for their advice and critical suggestions. In particular, we wish to thank Dr. R. R. Chaturvedi and Mr. P. A. White for their assistance with catheter pressure measurement, Drs. P. Burger and D. G. Gibson for their helpful comments, and Mr. R. L. Hughes for designing the electronic gating circuit for the wave phantom.

REFERENCES

1. L. Hatle, A. Brubakk, A. Tromsdal, B. Angelsen, Noninvasive assessment of pressure drop in mitral stenosis by Doppler ultrasound. *Br. Heart J.* **40**, 131–140 (1978).
2. C. Chen, L. Rodriguez, J. L. Guerrero, S. Marshall, R. A. Levine, A. E. Weyman, J. D. Thomas, Noninvasive estimation of the instantaneous first derivative of left ventricular pressure using continuous-wave Doppler echocardiography. *Circulation* **83**, 2101–2110 (1991).
3. R. A. Nishimura, A. J. Tajik, Determination of left-sided pressure gradients by utilizing Doppler aortic and mitral regurgitant signals: validation by simultaneous dual catheter and Doppler studies. *J. Am. Coll. Cardiol.* **11**, 317–332 (1988).
4. H. B. Xiao, X. Y. Jin, D. G. Gibson, Doppler reconstruction of left ventricular pressure from functional mitral regurgitation: potential importance of varying orifice geometry. *Br. Heart J.* **73**, 53–60 (1995).
5. Y. C. Fung, "Biodynamics: Circulation," Springer-Verlag, New York, 1984.
6. S. L. Sobolev, *in* "Partial differential equations of mathematical physics," Pergamon Press, Oxford, 1964.
7. S. M. Song, R. M. Leahy, D. P. Boyd, B. H. Brundage, S. Napel, Determining cardiac velocity fields and intraventricular pressure distribution from a sequence of ultrafast CT cardiac images. *IEEE Tran. Med. Imag.* **13**, 386–397 (1994).
8. R. Weinstock, *in* "Calculus of variations: With applications to physics and engineering," Dover Publications, New York, 1974.
9. E. Kreyszig, *in* "Advanced engineering mathematics," 7th ed, John Wiley and Sons, New York, 1993.
10. H. Schlichting, *in* "Boundary layer theory," 7th ed, McGraw Hill, New York, 1979.
11. P. J. Kilner, G. Z. Yang, R. H. Mohiaddin, D. N. Firmin, D. B. Longmore, Helical and retrograde secondary flow patterns in the aortic arch studied by three-directional magnetic resonance velocity mapping. *Circulation*, **88** (part 1), 2235–2247 (1993).
12. D. N. Firmin, P. D. Gatehouse, J. P. Konrad, G. Z. Yang, P. J. Kilner, D. B. Longmore, Rapid 7-dimensional imaging of pulsatile flow, in "Proc., Computers in Cardiology, London, 1993," p. 353–356.
13. D. N. Firmin, G. L. Nayler, P. J. Kilner, D. B. Longmore, The application of phase shifts in NMR for flow measurement. *Magn. Res. Med.* **14**, 230–241 (1990).
14. S. Senda, M. Sugawara, Y. Matsumoto, T. Kan, H. Matsuo, A noninvasive method of measuring Max (dP/dt) of the left ventricle by doppler echocardiography. *J. Biomechanical Engineering* **114**, 15–19 (1992).
15. S. N. Urchuk, D. B. Plewes, An MR method for non-invasive blood pressure measurement, *in* "Proc., SMRM, 12th Annual Meeting, New York, 1993," p. 149.

Originals

Heart and Vessels
© Springer-Verlag 1997
Heart Vessels (1997) 12: 103–110

Our tortuous heart in dynamic mode – an echocardiographic study of mitral flow and movement in exercising subjects

Philip J. Kilner[1], Michael Y. Henein[2], and Derek G. Gibson[2]

[1] Magnetic Resonance Unit and [2] Department of Cardiology, Royal Brompton Hospital, Sydney Street, London SW3 6NP, United Kingdom

Summary. Blood traces tortuous paths of flow through the heart. We postulate that momentum changes associated with direction changes optimize dynamic coupling between ventricular and atrial function, particularly on exercise. Traces of pulsed Doppler mitral flow and M-mode long-axis mitral ring movement were recorded before and during exercise, increased in 25-W steps to strenuous levels (146 ± 30 W), in 16 healthy volunteers, aged 38 ± 10 years. R-R intervals fell from 821 ± 151 to 437 ± 51 ms, and diastole from 458 ± 134 to 169 ± 33 ms. Peak mitral flow velocities rose from 0.68 ± 0.17 to 1.27 ± 0.16 m/s, and mitral valve ring displacements from 13.8 ± 3.3 to 19.3 ± 3.4 mm. Biphasic diastolic curves of flow and movement became monophasic as R-R fell below 500 ms, with atrial systole apparently coming to coincide with elastic ventricular recoil to give a single elevated peak of mitral flow. The increased slope and amplitude of Doppler curves indicate increased rates of change of momentum, which imply enhanced inertial forces. The illustrated patterns of flow and movement on exercise accord with the postulated "dynamic" mode of function, in which forces between atria, ventricles, and passing blood masses become tightly coupled to achieve a sling-like redirection of momentum through tortuous paths of flow, but more extensive data are needed to adequately model and quantify inertial force exchanges of the exercising heart.

Kew words: Exercise – Echocardiography – Mitral – Physiology – Hemodynamics

Address correspondence to: P. Kilner
Received August 9, 1997; accepted September 9, 1997

Introduction

The echocardiographic studies of mitral long-axis movement and mitral flow reported in this paper reflect changing interactions, with exercise, between the left atrium, the left ventricle, and the blood moving through them. The findings are intended to be considered in relation to a hypothesis regarding the overall shape and dynamic function of the human heart, which, as an organ of flow, has a remarkable shape. During embryonic development, its form loops to take on a twisted S-shaped curvature [1]. Passing blood is, thus, made to change direction, particularly at ventricular level, but also at the levels of the atria and great arteries (Fig. 1). Sinuous intracardiac flow paths occur not only in humans, but in species throughout the vertebrate line [2, 3]. Looped curvature of the heart appears to have been retained and refined through the course of vertebrate evolution. This being so, it seems likely that changes in flow direction have functional significance. We are not aware, however, that functional advantages of loops (as opposed to less tortuous arrangements of heart cavities found in a range of invertebrate species) have been explained satisfactorily, or even investigated.

Our principal hypothesis is that changes in flow direction help to optimize dynamic coupling, *particularly on exercise*, between ventricular and atrial function. Change in direction at the ventricular level is important for the following reason: if systolic ejection is to become "dynamic", with appreciable momentum imparted to out-flowing blood, then, according to Newton's laws, the ejecting chamber must recoil in the opposite direction. If systolic recoil pushed back towards the atrium, it would tend to impair, or even reverse, motion of the atrioventricular valve, with consequent impairment of atrial filling. The direction change at ventricular level allows inertial recoil of a contracting ventricle to pull, rather than push, on the atrium, thus enhancing atrial filling.

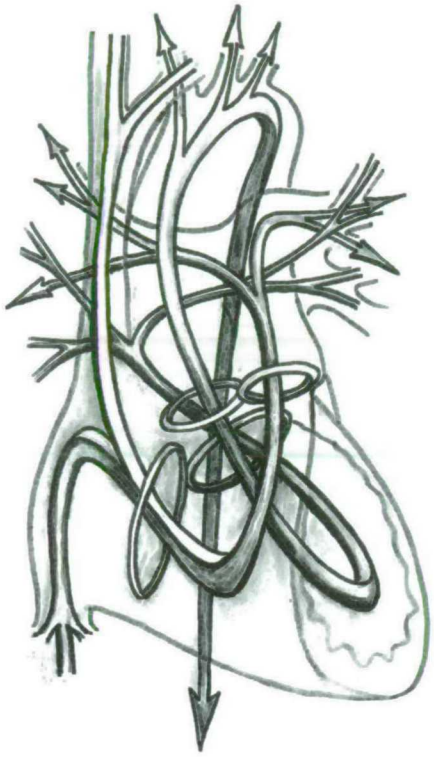


Fig. 1. Tortuous paths of flow through the human heart. The drawing is based on anatomical and flow information from post-mortem casts and magnetic resonance flow studies. For clarity, principal flow paths are represented by *continuous bands*; no attempt is made to depict the vorticity and phasic variability of flow through chambers and valves

That paths of flow through hearts are not inevitably tortuous can be appreciated from study of heart shapes of invertebrate species [3]. One example is the heart of a snail, such as *Helix pomatia* [4]. Although thought to have evolved independently of vertebrate hearts [5], this particular molluscan heart shows major components surprisingly similar to those of vertebrate hearts, with atrial and ventricular cavities juxtaposed in a pericardial space. In distinction from vertebrate equivalents, however, the cavities and main vessels are linearly arranged. Atrium, ventricle, and aorta lie in-line, so inertial recoil of the contracting ventricle, were it to occur, would push back on blood in the atrial cavity. Snails, though, are not noted for dynamic vigour.

Vertebrate species, on the other hand, achieve unrivalled combinations of size, complexity, and sustained dynamic movement. When a terrestrial vertebrate runs, the mechanics of the whole body operate in a distinct dynamic mode. Rapid locmotion is achieved through cycles of force and energy exchange that differ from the statics-dominated mechanics of walking. Inertial forces increase to match and overcome gravitational forces, with powerful, transient interactions between myo-contractile, inertial, and elastic forces.

We propose that the heart of a vertebrate undergoes transition to dynamic mode during exercise, functioning as a flexible, pulsatile, tortuous, *kinetic* pump, for which there is no close mechanical equivalent. In this state, there could be tight coupling between contractile, inertial, and elastic forces of atria, ventricles, great vessels, and their passing blood masses, the whole heart functioning as a unit to achieve sinuous, sling-like redirection and enhancement of fluid momentum. An aspect of this dynamically coupled state, amenable to investigation by echocardiography, would be the patterns and timings of atrio-ventricular interactions.

Pulsed Doppler and M-mode echocardiography are well suited to investigation during exercise, displaying flow and movement of selected cardiac regions. We chose to focus attention mainly on the mitral valve region. Although studies of mitral flow during exercise have been published [6, 7], we could not find data presented in ways that revealed the progress, timing, and extent of changes in atrio-ventricular interaction from rest to strenuous exercise. We have therefore recorded mitral flow by pulsed Doppler, and long-axis mitral ring motion by M-mode echocardiography, from rest to strenuous exercise in healthy volunteers. As stress echocardiography is gaining importance in clinical investigation [8, 9], we documented measurements of indices relevant to the evaluation of patients, but our principal aim is to present normal exercise echocardiographic findings in relation to the hypothesis we have outlined.

Subjects and methods

Subjects

We studied 16 volunteers, 15 men and 1 woman, aged 24–57 years (mean ± SD, 38 ± 10 years), without symptoms or a history of cardiovascular disease.

Exercise

Echocardiographic studies were performed before and during exercise on a semi-recumbent exercise cycle, starting at 75 W, increased in steps of 25 W at 2-min intervals. The final work levels achieved varied with the strength and tolerance of the subjects. Peak work rates between 100 and 225 W were reached (146 ± 30 W). The aim was to record echocardiographic traces at rest, during at least one intermediate stage of exercise, and during strenuous exercise. Subject 1 (Fig. 2) went through a more extended exercise protocol than the other subjects: exercise was commenced at 25 W, and increased in 25-W steps to 175 W over a period of 25 min. This allowed investigation at a series of stages of exercise, four of which are illustrated in Figs. 2, 4, and 5.

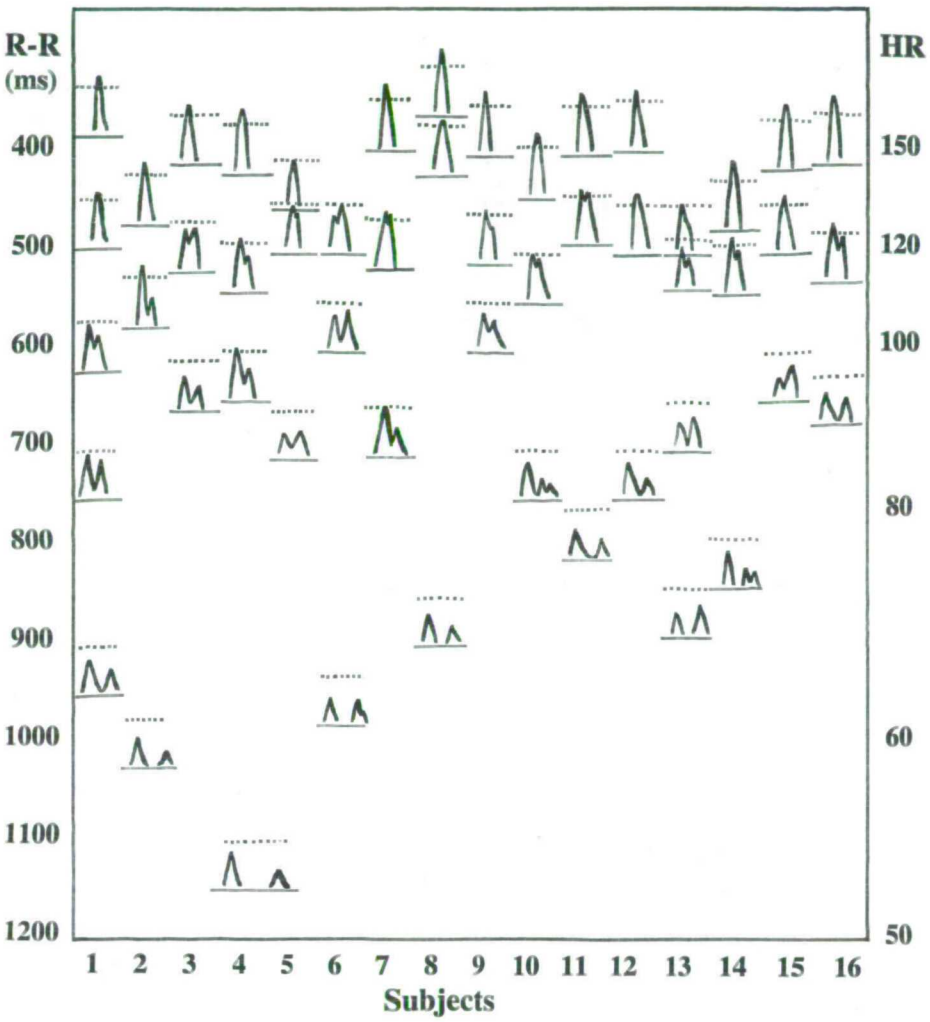


Fig. 2. Doppler mitral flow curves in all subjects, from rest to strenuous exercise, displayed with respect to R-R interval and heart rate (*HR*, in beats per min). *Dotted lines* mark 1 m/s levels. Transition to single-peak mitral inflow occurred at approximately 120 beats/min. *Y-axis values* should be read off at the baseline under each curve

No subject reported chest pain or other unexpected symptoms during the investigation. The subjects varied in physical fitness. Subjects 1, 2, and 4 had exercised regularly over a number of years, subjects 2 and 4 being competitive athletes. None of the other subjects were in the habit of exercising regularly, and subjects 6, 14, and 15 were overweight for their height. Subject 11 was the only woman.

Echocardiography

A Hewlett Packard 77020 Sonos 1000 system (Andover, MA, USA) was used with a 2 MHz transducer. Electrocardiographic and phonocardiographic traces were recorded.

Mitral flow velocities were recorded from the apical four-chamber view by pulsed Doppler echocardiography with frequency shift calibration [10]. In addition to mitral studies, left ventricular outflow tract (LVOT) flow velocities were recorded at rest in ten subjects, at intermediate exercise in six of these, and at strenuous exercise in four.

M-mode echocardiograms showing long-axis movements of the atrioventricular valve plane were recorded in all subjects from an apical window using the same equipment [11]. Movements of left lateral and septal regions of the mitral ring, and of the tricuspid ring, to the right of the valve, were recorded. M-mode traces shown in Figs. 3 and 4 are from the septal region of the mitral ring.

Doppler and M mode studies were recorded at a paper speed of 100 mm/s. Measurements were made either directly from the paper recording, or by analysis of a digitized record traced from the original. Measurements made from the traces were as follows: the R-R interval was measured as an average of five electrocardiogram (ECG) cycles. The systolic period was measured from the ECG Q wave to the onset of A2, the aortic component of the second heart sound identified on the phonocardiographic trace. The diastolic period was taken as the R-R interval minus the systolic period. The isovolumic relaxation time was measured from the onset of A2 to the onset of mitral flow, located by linear extrapolation of the early diastolic upstroke back to the

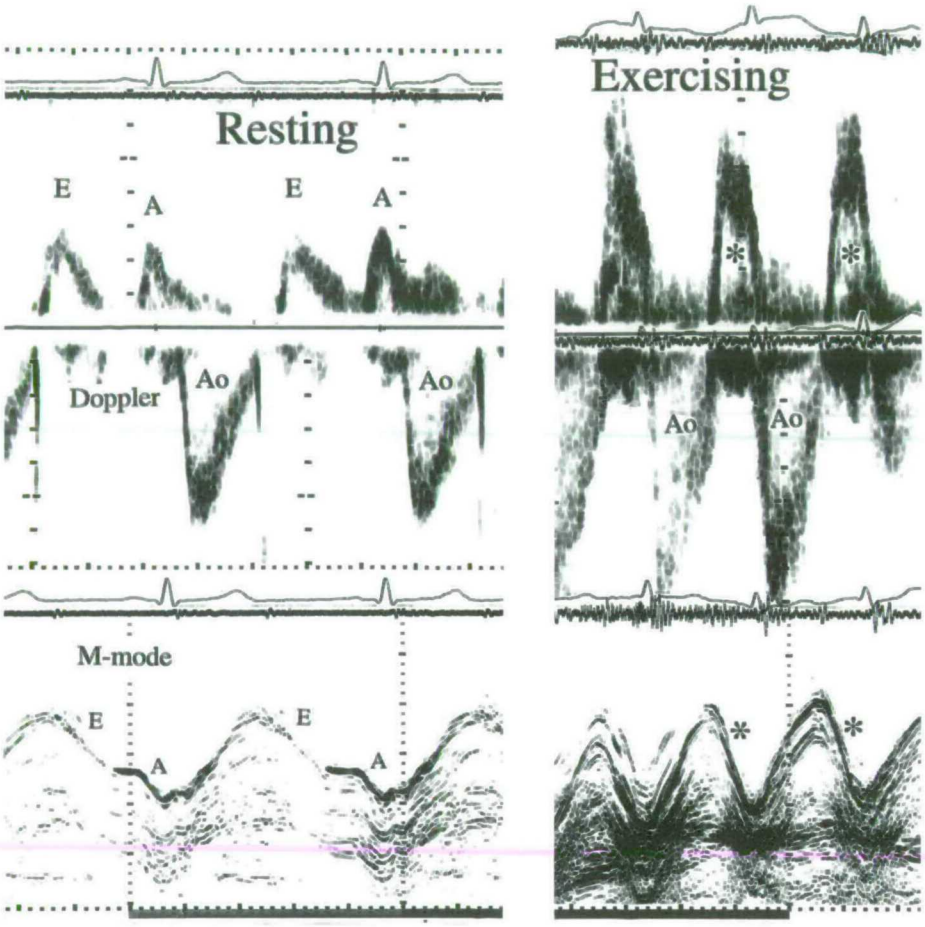


Fig. 3. Pulsed Doppler traces of mitral and aortic flow, M-mode traces of long-axis movement of the septal part of the mitral ring, and corresponding electro cardiogram (ECG) traces, at rest (*left*) and during exercise (*right* – subject 11 exercising at 125 W). Phases of corresponding traces are temporally registered, as far as possible, although they were not recorded simultaneously. Upward deflexions of Doppler and M-mode traces represent velocities or displacements towards the apically located transducer. On exercise, notice the short diastolic period with a single, elevated peak of mitral filling, reaching about 1.3 m/s, coinciding with a single, rapid downstroke on the M-mode trace, to which elastic ventricular recoil and atrial systole presumably contribute, simultaneously (*asterisks*). *Ao*, Aorta; *E*, E-wave; *A*, atrial systolic wave

base-line. Total valve ring excursion and, at lower heart rates, its late diastolic, atrial systolic component, and peak rates of systolic shortening and diastolic lengthening were measured from the digitized traces, as were times to peak shortening and peak lengthening, from the Q-wave and A2, respectively.

Results

Figures 2–5 display the patterns and amplitudes of Doppler and M-mode curves at rest and during exercise. Figure 2 gives an overview of mitral flow curves in all 16 subjects. Figure 3 correlates mitral and LVOT Doppler and mitral M-mode traces at rest and exercise in subject 11. Figure 4 shows progressive changes of Doppler and M-mode mitral curves from rest through intermediate stages to peak exercise in subject 1. Outlines of these are traced and superimposed, using the R wave of the ECG for temporal registration, in Fig. 5. Table 1 presents values of selected measurements.

There was a striking increase in peak mitral flow velocity, in the region of 100%, from rest to exercise – a greater proportional increase than that recorded at the aortic valve. This was associated with marked shortening of the diastolic period, which, although longer than systole at rest, was shorter than systole in all subjects at peak exercise. At rest and through the initial stages of exercise, two peaks of mitral flow, the early diastolic E-wave and late diastolic (atrial systolic) A-wave, were distinct, but they progressively merged with rising heart rate, and fused to a single elevated peak at heart rates above 120 beats per min, as the R-R interval fell below 500 ms (Figs. 2–5).

Progressive summation of mitral Doppler E and A waves with increasing heart rate was accompanied by corresponding changes in M-mode traces of long-axis valve ring motion (Figs. 2, 4, and 5). Whereas at rest the diastolic phase contained two distinct periods of movement, these merged to one rapid, continuous diastolic movement on exercise, at the same time as the single peak of mitral flow appeared. Peak lengthening rate was consistently greater than the maximum early diastolic value at rest.

There was relatively little difference between M-mode trace changes recorded in the lateral and septal mitral positions. The extent of long-axis motion of the

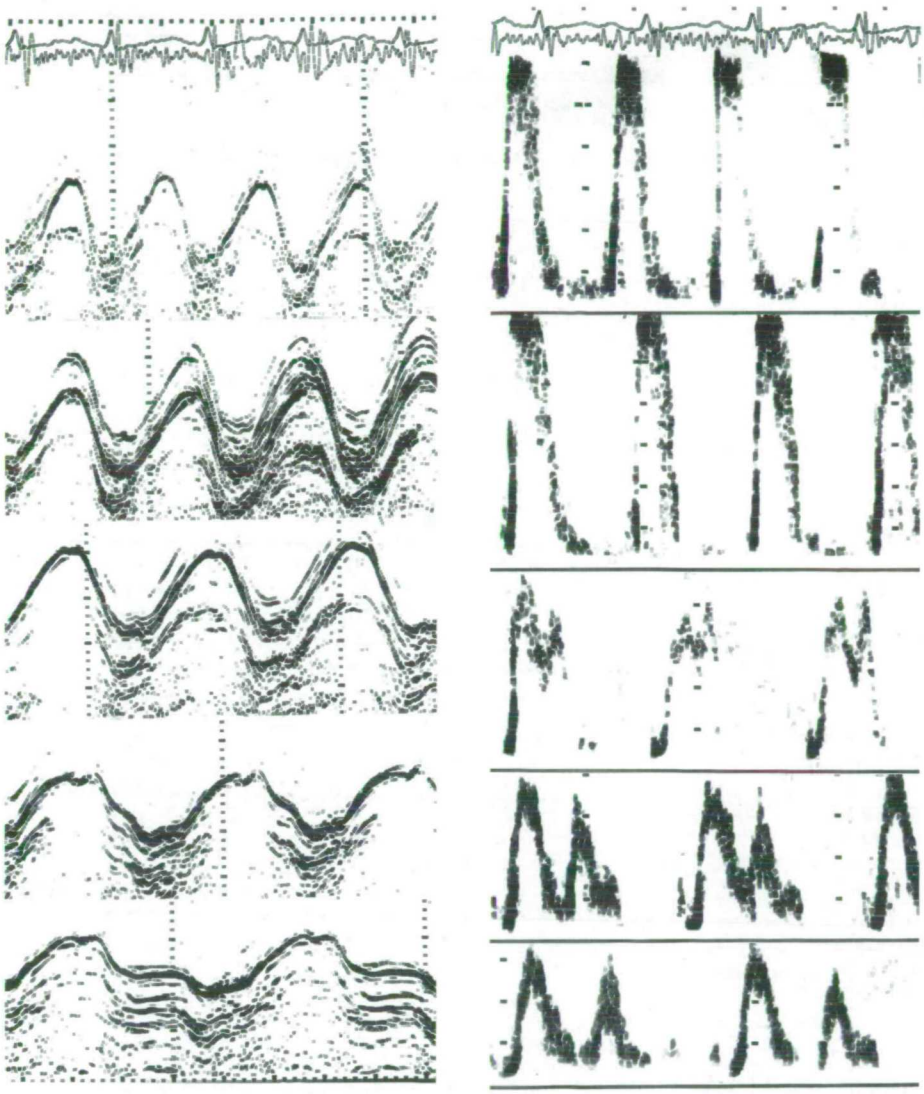


Fig. 4. Progressive changes from rest (*below*) to strenuous exercise (*above*) of M-mode long-axis mitral ring motion (*left*) and Doppler mitral flow (*right*) in subject 1

tricuspid valve ring was greater than that of the mitral ring at rest, but the long-axis motion of the tricuspid valve ring showed little increase with exercise in the few subjects studied.

The isovolumic relaxation time progressively shortened, and at peak exercise was effectively eliminated.

Discussion

The patterns and timing of mitral flow and movement change progressively, as illustrated by the traces displayed in the Figures. In the much shortened diastolic period of exercise, the entire stroke volume, possibly greater than that of the resting heart [12–14], has to pass through the atrioventricular valve. This is accomplished by rapid apical flow of blood, coinciding with rapid basal movement of the valve. Correlation of echocardiographic and ECG traces (Fig. 5) shows that elastic ventricular recoil, considered to be the principal cause of the early diastolic peak of flow and movement at rest, must come to coincide with atrial systole in the short diastolic phase of exercise. So, in contrast to the relatively prolonged, biphasic diastolic interactions of the resting heart, the exercising heart develops one-to-one coupling of atrial systolic with ventricular diastolic function (and *vice versa*).

Although these observations of transmitral velocity and ring motion, up to strenuous exercise, may come as no surprise to cardiologists familiar with stress echocardiography, we had not been able to find them clearly recorded and displayed. We set out to do this, with the aim of considering the changes in relation to momentum changes of blood as it moves through the curvatures of the heart. We believe that the way in which the atria, ventricles, and arterial trunks are connected in space gains particular importance on exercise. To appreciate this, the roles of static and dynamic force

Table 1. Measurements from Doppler and M-mode echocardiographic traces

	Rest	Moderate exercise	Peak exercise
Work rate (W)	–	75–125 (103 ± 19)	100–225 (146 ± 30)
R-R interval (ms)	600–1160 (821 ± 151)	420–620 (527 ± 51)	355–530 (437 ± 51)
Systolic period (ms)	320–405 (362 ± 27)	255–340 (294 ± 28)	240–320 (268 ± 22)
Diastolic period (ms)	310–780 (458 ± 134)	190–310 (233 ± 48)	115 230 (169 ± 33)
Isovolumic relaxation time (ms)	65–90 (71 ± 11)	10–55 (29 ± 10)	0–35 (12 ± 10)
Mitral flow velocities (m/s)			
E peak	0.4–1.0 (0.68 ± 0.17)		
Summation peak		0.9–1.3 (1.09 ± 0.15)	1.0–1.50 (1.27 ± 0.16)
A peak	0.4–0.8 (0.54 ± 0.13)		
LVOT velocity (m/s)			
Peak velocity	0.8–1.1 (n = 10)	1.2–1.5 (n = 6)	1.4–2.0 (n = 4)
Displacements of valve rings (mm)			
Lateral mitral	9–20 (13.8 ± 3.3)	13–24 (18 ± 2.8)	15–24 (19.3 ± 3.4)
Septal mitral	11 18 (13.7 ± 2)	15–20 (17.4 ± 2.2)	14–25 (18.6 ± 3.6)
Tricuspid	20–32 (23.8 ± 3.9) (n = 13)	22–34 (n = 4)	20–32 (n = 3)
Peak shortening rate (mm/s) and time to peak shortening from Q wave of ECG (ms)			
Lateral mitral	50–100 (73 ± 13)	70–130 (99 ± 20)	70–170 (125 ± 24)
Q-PS	60–230 (157 ± 47)	50–200 (127 ± 47)	50–200 (96 ± 33)
Septal mitral	50–100 (70 ± 13)	60–120 (87 ± 19)	60–170 (109 ± 35)
Q-PS	100–150 (137 ± 33)	100–180 (137 ± 40)	70–170 (108 ± 32)
Tricuspid	70–170 (115 ± 30) (n = 13)	110–200 (n = 4)	120–210 (n = 3)
Q-PS	80–170 (134 ± 28) (n = 13)	70–130 (n = 4)	60–110 (n = 3)
Peak lengthening rate (mm/s) and time to peak lengthening from A2 heart sound (ms)			
Lateral mitral	50–140 (92 ± 27)	120–210 (154 ± 30)	90–230 (170 ± 42)
A2-PL	80–150 (122 + 18)	90–230 (102 + 17)	70–130 (86 + 16)
Septal mitral	50–120 (81 ± 20)	80–190 (135 + 38)	90–220 (163 ± 56)
A2-PL	90–180 (119 ± 20)	80–180 (99 ± 27)	60–180 (82 ± 20)
Tricuspid	80–170 (106 ± 30) (n = 13)	140–220 (n − 4)	140–380 (n = 3)
A2-PL	80–200 (134 ± 46) (n = 13)	80–100 (n = 4)	50–80 (n = 3)

Subjects: n = 16 (except where fewer indicated), 15 men and 1 woman; age, 24–57 (38 ± 10) Years: Range (mean ± SD)
LVOT, Left ventricular outflow tract; ECG, electrocardiogram

exchanges between the atria and ventricles need to be recognized.

Stresses associated with tension of elastic and muscle fibers, hydrostatic pressures in blood and pericardial fluid, plus any gravitational influences on these, can be considered as static forces or counter-forces. Atrial and ventricular function are coupled through these static forces at rest and during activity, even in a snail [15]. Dynamic force exchanges, on the other hand, only gain significance with increasing rates of change of momentum. When this happens, flow direction-change has a twofold bearing on atrioventricular coupling. Firstly, it determines the direction in which inertial recoil (away from ventricular ejection) acts. Recoil from rapid ventriculo-arterial ejection would hinder statics-mediated atrioventricular coupling in a linearly arranged heart, but can act as a bonus in the looped vertebrate heart, contributing to increased mitral ring motion during exercise. Secondly, reversal of direction between inflow and outflow means that momentum changes of decelerating inflow and of accelerating outflow are summated. They act in the same direction, swiftly following one another, on exercise, without an intervening pause. The rapidity with which mitral inflow turns to become left ventricular outflow can be appreciated upon examination of the exercise Doppler traces in Fig. 3. Flow into the exercising heart does not need to come to rest (it does not need to be stopped by valve closure, given excursions of valve rings and swirling of blood in the cavities), but may be redirected from one direction to another in a swift, fluent movement.

We propose that the exercising heart operates as a coordinated unit, propelling blood kinetically as well as by occlusive displacement, through redirection and enhancement of momentum via sinuous paths of flow. It is the combination of looped curvature with alternating contractility of atrial and ventricular loops that makes possible the sling-like action and counter-action of the heart's dynamic mode.

The echocardiographic changes reported in this paper are in accord with this description, but do not, on their own, enable proof or quantitative analysis of it.

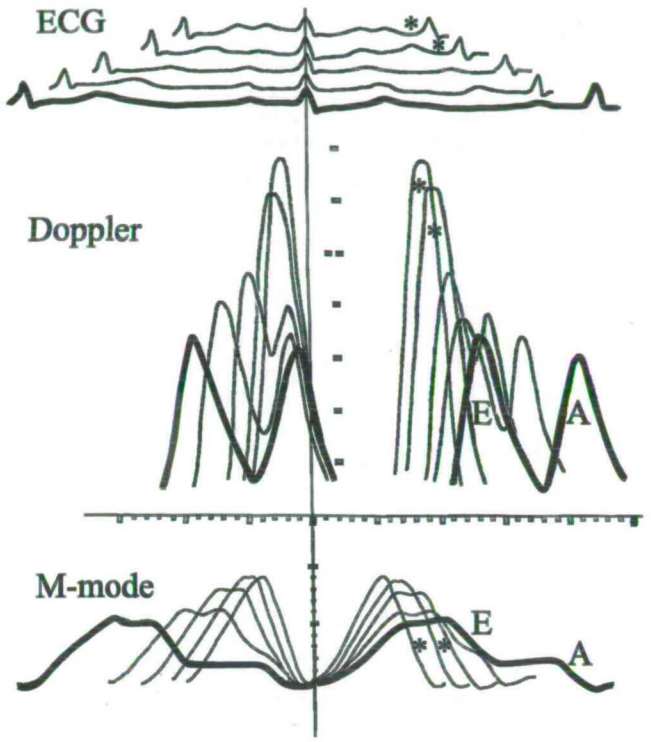


Fig. 5. Superimposed outlines of Doppler and M-mode traces (from *Fig. 4*), showing progressive changes from rest to strenuous exercise, together with corresponding ECG traces. All Doppler curves share the same base line and velocity scale. *Asterisks* mark atrial systole on two sets of exercise traces

Since the postulated dynamics involve fluid-structure interactions extending across the heart chambers and vessels, echocardiographic data remain, on their own, too limited for quantification of the role of inertial force exchanges in relation to other components of cardiovascular mechanics. There is, as yet, no technique that provides sufficiently comprehensive information on changing cardiovascular geometries, velocity fields, and wall mechanics. Magnetic resonance techniques offer relatively comprehensive anatomic and flow information [16–18], but are not well suited to investigation during exercise. Development of computational models, incorporating structural and functional information from multiple sources, may provide an indirect approach to the subject, although, even for single heart chambers and valves, such computation is complex [19], and basic input data are lacking. We draw attention to the possibility of computer simulation of large-scale dynamic interactions across the exercising heart, and present data that could contribute towards appropriate computer simulation.

Clinically, our findings and interpretation may have bearing on the management of physically active patients who require reconstructive heart surgery, or who have rhythm or conduction disturbances needing intervention by drugs or pacing. Better understanding of the morphodynamic function of the exercising heart could lead to refinement of surgical, pharmacological, or electrophysiological approaches, with a view to maintenance of optimal heart function during exercise as well as at rest.

Acknowledgments. Philip Kilner is supported by the British Heart Foundation.

References

1. Icardo JM (1996) Developmental biology of the vertebrate heart. J Exp Zool 275:144–161
2. Johansen K, Burggren W (1980) Cardiovascular function in the lower vertebrates. In: Bourne GH (ed) Hearts and heart-like organs. Academic, New York, pp 61–117
3. Robb JS (1965) Comparative basic cardiology. Grune and Stratton, New York
4. Somerville BA (1973) The circulatory physiology of *Helix pomatia*. J Exp Biol 59:275–303
5. Nielsen C (1995) Animal evolution – interrelationships of the living phyla. Oxford University Press, Oxford
6. Rassi A Jr, Crawford MH, Richards KL, Miller JF (1988) Differing mechanisms of exercise flow augmentation at the mitral and aortic valves. Circulation 77:543–551
7. Turkevich D, Micco A, Reeves JT (1988) Noninvasive measurement of the decrease in left ventricular filling time during maximal exercise in normal subjects. Am J Cardiol 62:650–652
8. Armstrong WF (1991) Stress echocardiography for detection of coronary artery disease. Circulation 84:143–149
9. Marwick TH (1995) Recent advances in stress echocardiography. Curr Opin Cardiol 10:619–625
10. Henein MY, Gibson DG (1995) Suppression of left ventricular early diastolic filling by long axis asynchrony. Br Heart J 73:151–157
11. Jones CJ, Song GJ, Gibson DG (1991) An echocardiographic assessment of atrial mechanical behaviour. Br Heart J 65:31–36
12. Higginbotham MB, Morris KG, Williams RS, McHale PA, Coleman RE, Cobb FR (1986) Regulation of stroke volume during submaximal and maximal upright exercise in normal man. Circ Res 58:281–291
13. Nonogi H, Hess OM, Ritter M, Krayenbuehl HP (1988) Diastolic properties of the normal left ventricle during supine exercise. Br Heart J 60:30–38
14. Salmasi AM, Salmasi SN, Dore C, Nicolaides AN (1987) Non-invasive assessment of changes in aortic blood velocity and its derivatives with exercise in normal subjects by Doppler ultrasound. J Cardiovasc Surg (Torino) 38:321–327
15. Dale B (1973) Blood pressure and its hydraulic functions in *Helix pomatia* L. J Exp Biol 59:477–490
16. Kilner PJ, Wann LS, Firmin DN, Longmore DB (1989) Three-directional magnetic resonance flow imaging of the human heart. Dynamic Cardiovasc Imaging 2:104–109

17. Kilner PJ, Yang GZ, Mohiaddin RH, Firmin DN, Longmore DB (1993) Helical and retrograde secondary flow patterns in the aortic arch studied by three-directional magnetic resonance velocity mapping. Circulation 88:2235 2247
18. Kim WY, Walker PG, Pedersen EM, Poulsen JK, Oyre S, Houlind K, Yoganathan AP (1995) Left ventricular blood flow patterns in normal subjects: A quantitative analysis by three-dimensional magnetic resonance velocity mapping. J Am Coll Cardiol 26:224–238
19. Peskin CS, McQueen DM (1995) A general method for the computer simulation of biological systems interacting with fluids. Symp Soc Exp Biol 49:265–276

References

Abraham, R. (1985) *On morphodynamics*, pp 65-68, Santa Cruz: Aerial Press.

Ambrosi, C., Starr I (1965) Incoordination of cardiac contraction as judged by the force ballistocardiogram and the carotic pulse derivative. *Am Heart J* **70**, 761.

Appleton, C.P., Hatle, L.K. and Popp, R.L. (1987) Superior vena cava and hepatic vein Doppler echocardiography in healthy adults. *J Am. Coll. Cardiol.* **10**, 1032-1039.

Appleton, C.P., Hatle, L.K. and Popp, R.L. (1988) Relation of transmitral flow velocity patterns to left ventricular diastolic function: new insights from a combined hemodynamic and Doppler echocardiographic study. *J Am. Coll. Cardiol.* **12**, 426-440.

Bellhouse, B.J., Bellhouse, F.H. and Reid, K.G. (1968) Fluid mechanics of the aortic root with application to coronary flow. *Nature* **219**, 1059-1061.

Bellhouse, B.J. and Bellhouse, F.H. (1968) Mechanism of closure of the aortic valve. *Nature* **217**, 86-87.

Bellhouse, B.J. and Bellhouse, F.H. (1969) Fluid mechanics of the mitral valve. *Nature* **224**, 615-616.

Bellhouse, B.J. (1972) Fluid mechanics of a model mitral valve and left ventricle. *Cardiovasc. Res.* **6**, 199-210.

Boucaud-Camou, E. and Boucher-Rodini, R. (1983) Feeding and digestion in cephalopods. In: Saleuddin ASM and Wilbur KM, (Eds.) *Physiology Part 2*, pp. 149-188. New York: Academic Press

Bourne, G.H. (1980) *Hearts and heart like organs: comparative anatomy and development*, pp. 1-39, 61-169, 259-600. New York: Academic Press.

Buonocore, M.H. and Bogren, H. (1992) Factors Influencing the Accuracy and Precision of Velocity-Encoded Phase Imaging. *Mag. Reson. in Med.* **1**, 141-154.

Burton, A.C. (1965) *Physiology and biophysics of the circulation*,pp 95-104, Chicago: Year Book Medical Publishers.

Clarke, K.U. (1979) Visceral anatomy and arthropod phylogeny. In: Gupta AP, (Ed.) *Arthropod phylogeny*, pp. 467-549. New York: Van Nostrand Reinhold

Dale B (1973) Blood pressure and its hydraulic functions in Helix pomatia L. *J Exp Biol* **59**, 477-490.

Daley, P.J., Sagar, K.B., Collier, B.D., Kalbfleisch, J. and Wann, L.S. (1987) Detection of exercise induced changes in left ventricular performance by Doppler echocardiography. *Br. Heart J* **58**, 447-454.

Daley, P.J., Sagar, K.B. and Wann, L.S. (1985) Doppler echocardiographic measurement of flow velocity in the ascending aorta during supine and upright exercise. *Br. Heart J* **54**, 562-567.

Firmin, D.N., Nayler, G.L., Klipstein, R.H., Underwood, S.R., Rees, R.S.O. and Longmore, D.B. (1987) In vivo validation of MR velocity imaging. *J. Comput. Assist. Tomogr.* **11**, 751-756.

Firmin, D.N., Nayler, G.L., Kilner, P.J. and Longmore, D.B. (1990) The application of phase shifts in NMR for flow measurement. *Mag. Reson. in Med.* **14**, 230-241.

Fujimoto, S., Parker, K., H, Xiao, H., B, Inge, K., K and Gibson, D., G (1995) Early diastolic left ventricular inflow pressures in normal subjects and patients with dilated cardiomyopathy. Reconstruction from pulsed Doppler echocardiography. *British. Heart Journal* **74**, 419-425.

Garitey, V., Gandelheid, T., Fuseri, J., Pelissier, R. and Rieu, R. (1995) Ventricular flow dynamic past bileaflet prosthetic heart valves. *International. Journal of Artificial. Organs* **18.** 380-391.

Goodwin, B. (1995) *How the leopard changed its spots*, pxi. New York: Wiedenfeld and Nicholson.

Hamlett, W.C., and Munoz-Chapuli, R. (1996) Comparative Cardiovascular Biology of Lower Vertebrates (Symposium). *Journal of Experimental Zoology* **275**.

Hamlett, W.C., Schwartz, F.J., Schmeinda, R. and Cuevas, E. (1996) Anatomy, histology, and development of the cardiac valvular system in elasmobranchs. . *J Exp. Zool.* **275**, 83-94.

Harrison, F.W. (1990-1998) *Microscopic anatomy of invertebrates*. 1-15. New York: Wiley-Liss:

Crustacea. 1992.
Onychophora, Chilopoda and Lesser Protostomata. 1993.
Echinodermata. 1994.
Mollusca I and II. 1996.
Annelida. 1997.
Insecta. 1997.
Lopophorates. 1997.
Hemichordata, Chaetagnatha and the Invertebrate Chordates. 1997.
Chelicerate Arthropoda. 1998.
Decapod Crustacea. 1998.

Harrison, F.W., Woollacott, R.M. (1994) *Lopophorates, Entoprocta and Cyliophora.* New York: Wiley-Liss

Harrison, F.W., Chia, F.S. (1994) *Echinodermata*. New York: Wiley-Liss

Harvey, W. (1976) *The movement of the heart and blood* (original latin text 1628) pp 38-73, Oxford: Blackwell.

Harvey, R.P. (1996) NK-2 homeobox genes and heart development. *Developmental Biology* **178**, 203-216.

Higginbotham, M.B., Morris, K.G., Williams, R.S., McHale, P.A., Coleman, R.E. and Cobb, F.R. (1986) Regulation of stroke volume during submaximal and maximal upright exercise in normal man. *Circ. Res.* **58**, 281-291.

Hildebrandt, G. (1991) Reactive modifications of the autonomous time structure in the human organism. *J Physiol Pharmacol.* **42**, 5-27.

Holbrook, E.L. (1984) *Design of pneumatic and fluidic control systems*, New York: Pech Publishing.

Icardo, J.M. (1996) Development biology of the vertebrate heart. *Journal of Experimental Zoology* **275**, 144-161.

Johansen, K., and Burggren, W. (1980) Cardiovascular function in lower vertebrates. In: Bourne GH, (Ed.) *Hearts and heart-like organs 1*, pp. 61-117. New York: Academic Press.

Jones, C.J., Raposo, L., and Gibson, D.G. (1990) Functional importance of the long axis dynamics of the human left ventricle. *Br. Heart J* **63**, 215-220.

Jones, H.D. (1983) Circulatory systems in gastropods and bivalves. In: Saleuddin ASM and Wilbur KM, (Eds.) *The Mollusca, Volume 5, Part 2*, pp. 189-239. New York: Academic Press.

Kamm, R.D., Pedley, T.J. (1989) Flow in collapsible tubes. *J Biomech Eng* **111**, 177-179.

Keele, K.D. (1952) *Leonardo da Vinci on movement of the heart and blood*, pp 60-87 London: Harvey and Blythe.

Kilner, P.J., Ho, S.Y. and Anderson, R.H. (1988) Cardiovascular cavities cast in silicone rubber as an adjunct to post-mortem examination of the heart. *Intern. J. Cardiol.* **22**, 99-107.

Kilner, P.J., Wann, L.S., Firmin, D.N. and Longmore, D.B. (1989) Three directional magnetic resonance flow imaging of the human heart. *Dynamic Cardiovascular Imaging* **2**, 104-109.

Kilner, P.J., Firmin, D.N., Rees, R.S.O., Martinez, J., Pennell, D.J., Mohiaddin, R.H., Underwood, S.R. and Longmore, D.B. (1991) Valve and great vessel stenosis: Assessment with MR jet velocity mapping. *Radiology* **178**, 229-235.

Kilner, P.J., Manzara, C.C., Mohiaddin, R.H., Pennell, D.J., Sutton, M.G.S., Firmin, D.N., Underwood, S.R. and Longmore, D.B. (1993) Magnetic resonance jet velocity mapping in mitral and aortic valve stenosis. *Circulation* **4**, 1239-1248.

Kilner, P.J., Yang, G.Z., Mohiaddin, R.H., Firmin, D.N. and Longmore, D.B. (1993) Helical and retrograde secondary flow patterns in the aortic arch studied by three-directional magnetic resonance velocity mapping. *Circulation* **88**, 2235-2247.

Kilner, P.J., Shinohara, T., Sampson, C.S., Mohiaddin, R.H., Firmin, D.N. and Somerville, J. (1996) Repaired coarctation in adults - magnetic resonance imaging with velocity mapping shows distortions of anatomy and flow. *Cardiol Young* **6**, 20-27

Kilner, P.J., Henein, M.Y. and Gibson, D.G. (1997) Our tortuous heart in dynamic mode - an echocardiographic study of mitral flow and movement in exercising subjects. *Heart and Vessels* **12**, 103-110.

Kim, W.Y., Bisgaard, T., Nielsen, S.L., Poulsen, J.K., Pedersen, E.M., Hasenkam, J.M. and Yoganathan, A.P. (1994) Two-dimensional mitral flow velocity profiles in pig models using epicardial Doppler echocardiography. *Journal of the American. College. of Cardiology* **24**. 532-545.

Kim, W.Y., Walker, P.G., Pedersen, E.M., Poulsen, J.K., Oyre, S., Houlind, K. and Yoganathan, A.P. (1995) Left ventricular blood flow patterns in normal subjects: a quantitative analysis by three-dimensional magnetic resonance velocity mapping *J Am. Coll. Cardiol.* **26**, 224-238.

Laniado, S., Yellin, E.L., Miller, H. and Frater, R.W. (1973) Temporal relation of the first heart sound to closure of the mitral valve. *Circulation* **47**, 1006-1014.

Laniado, S., Yellin, E., Kotler, M., Levy, L., Stadler, J. and Terdiman, R. (1975) A study of the dynamic relations between the mitral valve echogram and phasic mitral flow. *Circulation* **51**, 104-113.

Lauboeck, H. (1980) The conditions of closure of the mitral valve. *Journal of Biomedical Engineering* **2**, 93-96

Macrae J M, Sun Y H, Isaac DL, Dobson G M, Cheng C P, Little WC, Parker KH and Tyberg JV (1997) Wave-intensity analysis: A new approach to left ventricular filling dynamics. *Heart and Vessels* **12**. 53-59.

Malcolm, J.E.(1960) Korotkov sounds: action of the heart. *Nature* **186**: 723-724

Malcolm, J.E.(1961) Oscillatory flow in a fluid-filled elastic system. *Nature* **190**: 88-89

Malcolm, J.E. (1962) An analogue model of the heart. *Proceedings of the Physiological Society*. **24-25**: 2-5

Manteuffel-Szoege, L. (1960) Energy sources of blood circulation and the mechanical action of the heart. *Thorax* **15**: 47-53

Martin, A.W. (1980) Some invertebrate myogenic hearts: the hearts of worms and molluscs. In: Bourne GH, (Ed.) *Hearts and heart-like organs 1*, pp. 1-39. New York: Academic Press.

Martin, A.W. (1983) Excretion. In: Saleuddin ASM and Wilbur KM, (Eds.) *The Mollusca, volume 5, part 2.* pp. 353-405. New York: Academic Press

Matsunaga, N., Hayashi, K., Sakamoto, I., Ogawa, Y., Matsuoka, Y., Imamura, T. and Kuriya, T. (1993) Coronary-to-pulmonary artery shunts via the bronchial artery: analysis of cineangiographic studies. *Radiology* **186**, 877-882.

Miyatake, K., Izumi, S., Shimizu, A., Kinoshita, N., Okamoto, M., Sakakibara, H. and Nimura, Y. (1986) Right atrial flow topography in healthy subjects studied with real-time two-dimensional Doppler flow imaging technique. *J Am. Coll. Cardiol.* **7**, 425-431.

Mohiaddin, R.H., Amanuma, M., Kilner, P.J., Pennell, D.J., Manzara, C. and Longmore, D.B. (1991) MR phase-shift velocity mapping of mitral and pulmonary venous flow. *J Comput. Assist. Tomogr.* **15**, 237-243.

Nayler, G.L., Firmin, D.N. and Longmore, D.B. (1986) Blood flow imaging by cine magnetic resonance. *J. Comput. Assist. Tomogr.* **10**, 715-722.

Nielsen, C. (1995) *Animal Evolution - interrelationships of the living phyla*, Oxford: Oxford University Press.

Nielsen, C. (1994) Larval and adult characters in animal phylogeny. *American Zoologist* **34**, 492-501.

Nielsen, C., Scharff, N. and Eibye Jacobsen, D. (1996) Cladistic analyses of the animal kingdom. *Biological Journal of the Linnean Society* **57**, 385-410.

Noble, M.I. (1968) The contribution of blood momentum to left ventricular ejection in the dog. *Circ. Res.* **23**, 663-670.

Noble, M.I. (1978) The Frank-Starling curve. *Clin. Sci Mol. Med.* **54**, 1-7.

Noble, M.I. (1979) Left ventricular load, arterial impedance and their interrelationship. *Cardiovasc Res* **13**, 183-198.

Nonogi, H., Hess, O.M., Ritter, M. and Krayenbuehl, H.P. (1988) Diastolic properties of the normal left ventricle during supine exercise. . *Br. Heart J* **60**, 30-38.

Nylund, A., Ruhberg, H., Tjonnelund, A., and Meidell, B. (1988) Heart ultrastructure in four species of Onychophora (Peripatopsidae and Peripatidae) and phylogenetic implications. *Zool. Beitr.* **32**, 17-30.

Olson, E., N and Srivastava, D. (1996) Molecular pathways controlling heart development. *Science (Washington. D. C).* **272.** 671-676.

Pedley, T.J. (1980) *Fluid mechanics of large blood vessels*, pp 335-368. Cambridge, UK: Cambridge University Press.

Pendleton, J.W., Nagai, B.K., Murtha, M.T. and Ruddle, F.H. (1993) Expansion of the Hox gene family and the evolution of chordates. *Proc. Natl. Acad. Sci U. S. A* **90**, 6300-6304.

Peskin, C.S. and McQueen, D.M. (1995) A general method for the computer simulation of biological systems interacting with fluids. *Symp. Soc. Exp. Biol.* **49**, 265-276.

Rahr, H. (1979) The circulatory system of amphioxus (Branchiostoma lanceolatum). *Acta zool. (Stockh.)* **60**, 1-18.

Randall, D.J. and Davie, P.S. (1980) The hearts of urochordates and cephalochordates. In: Bourne GH, (Ed.) *Hearts and heart-like organs 1*, pp. 41-59. New York: Academic Press]

Rassi, A., Jr., Crawford, M.H., Richards, K.L. and Miller, J.F. (1988) Differing mechanisms of exercise flow augmentation at the mitral and aortic valves. *Circulation* **77**, 543-551.

Reynolds, O. (1883) An experimental investigation of the circumstances which determine whether motion of water shall be direct or sinuous, and the law of resistance in parallel channels. *Philosophical Transactions of the Royal Society* 935-982.

Reynolds, T. and Appleton, C.P. (1991) Doppler flow velocity patterns of the superior vena cava, inferior vena cava, hepatic vein, coronary sinus, and atrial septal defect: a guide for the echocardiographer. *J Am. Soc. Echocardiogr.* **4**, 503-512.

Robb, J.S. (1965) *Comparartive basic cardiology*, New York: Grune and Stratton.

Robinson, T.F., Factor, S.M. and Sonnenblick, E.H. (1986) The heart as a suction pump. *Sci Am.* **254**, 84-91.

Rockwell, D., Naudascher, E. (1978) Self sustaining oscillations of flow past cavities. *Journal of fluids engineering* **100**, 152-165.

Rowlatt, U. (1980) Functional and non-functional determinants of mammalian cardiac anatomy. In: Bourne GH, (Ed.) *Hearts and heart-like organs 1*, pp. 259-300. New York: Academic press.

Ruppert, E.E., and Carle, K.J. (1983) Morphology of matazoan circulatory systems. *Zoomorphology* **103**, 193-208.

Ruppert, E.E., and Barnes, R.D. (1994) *Invertebrate Zoology*, 6th edn. Philadelphia: Saunders College Publ.

Ruppert, E.E. (1997) Cephalochordata (Acrania). In: Harrison FW and Ruppert EE, (Eds.) *Hemichordata, Chaetognatha, and the Invertebrate Chordates*, New York: Wiley-Liss.

Rushmer, R. (1964) Initial ventricular impulse. A potential key to cardiac evaluation. *Circulation* **29**, 268

Salmasi, A.M., Salmasi, S.N., Dore, C. and Nicolaides, A.N. (1987) Non-invasive assessment of changes in aortic blood velocity and its derivatives with exercise in normal subjects by Doppler ultrasound. *J Cardiovasc. Surg. Torino.* **28**, 321-327.

Satchell, G.H. (1971) *Circulation in fishes*, pp 1-7 Cambridge: Cambridge University Press.

Satoh, Y., and Nitatori, T. (1980) On the fine structure of lymph hearts in amphibia and reptiles. In: Bourne GH, (Ed.) *Hearts and heart-like organs 1*, pp. 149-169. New York: Academic Press.

Schmid, K. (1892) Uber Herzstoss und Pulskurven. *Wiener medizinische Wochenschrift* 578-622.

Schwenk, T. (1962) *Das sensible Chaos*, Stuttgart: Verlag Freies Geistesleben.

Schwenk, T. (1996) *Sensitive chaos*, New York: Anthroposophic Press.

Scram, F.R. (1986) *Crustacea*, Oxford: Oxford University Press.

Shinn GL. (1993) The existence of a hemal system in chaetognaths In Moreno I (ed): *Proceedings of the II international workshop of Chaetognatha.* pp17-18 Universitat de les Illes Belears, Palma,

Shinn GL. (1997) Chaetognatha. In: Harrison FW (Ed) *Hemichordata, Chaetagnatha and the Invertebrate Chordates.* pp103-220. New York, Wiley-Liss.

Skelton, P. (1993) *Evolution - a Biological and Palaentological Approach*, Wokingham, England: Addison-Wesley.

Somerville, B.A. (1973) The circulatory physiology of Helix pomatia. *J Exp Biol* **59**, 275-282.

Sonnenblick, E.H. (1980) The structural basis and importance of restoring forces and elastic recoil for the filling of the heart. *Eur. Heart J* **Suppl A**, 107-110.

Spencer, M. and Greiss, F. (1962) Dynamics of ventricular ejection. *Circulation Research* **10**, 274

Starr, I., Horwitz, O., Maycock, R.L. and Krumbhaar, E.B. (1950) Standardization of the ballistocardiogram by simulation of the heart's function at necropsy; with a clinical method for estimation of cardiac strength and normal standards for it. *Circulation* **1**, 1073-1096.

Starr, I., Schnabel, T.G., and Maycock, R.L. (1953) Studies made by simulating systole at necropsy II. *Circulation* **8**, 44-61.

Steen, T. and Steen, S. (1994) Filling of a model left ventricle studied by colour M mode Doppler. *Cardiovascular. Research.* **28**: 1821-1827.

Steiner, R. (1976) *Geisteswissenschaft und medizin (1922)*, Dornach Swizerland: Rudolf Steiner Verlag.

Strobeck, J.E. and Sonnenblick, E.H. (1981) Myocardial and ventricular function. Part II: Intact heart. *Herz* **6**, 275-287.

Sugawara, M., Uchida, K., Kondoh, Y., Magosaki, N., Niki, K., Jones, C.J., Sugimachi, M. and Sunagawa, K. (1997) Aortic blood momentum - the more the better for the ejecting heart in vivo? *Cardiovasc. Res.* **33**, 433-446.

Taylor, D.E. and Wade, J.D. (1973) Pattern of blood flow within the heart: a stable system. *Cardiovasc. Res.* **7**, 14-21.

Taylor, D.E. and Whamond, J.S. (1977) Computation and modelling of resistive inertive and turbulent contribution across heart valves [proceedings]. *J Physiol Lond.* **273**, 24P-25P.

Taylor, T.W.and Yamaguchi, T. (1995) Flow patterns in three-dimensional left ventricular systolic and diastolic flows determined from computational fluid dynamics. *Biorheology.* **32**: 61-71.

Tjonneland, A., Okland, S. and Nylund, A. (1987) Evolutionary aspects of the arthropod heart. *Zool Scr* **16**, 167-175.

Tompsett, D.H. (1970) *Anatomical Techniques*, Edinburgh: Livingstone.

Turbeville, J.M., Schulz, J.R. and Raff, R.A. (1994) Deuterostome phylogeny and the sister group of the chordates: evidence from molecules and morphology. *Mol. Biol. Evol.* **11**, 648-655.

Turkevich, D., Micco, A. and Reeves, J.T. (1988) Noninvasive measurement of the decrease in left ventricular filling time during maximal exercise in normal subjects. *Am. J Cardiol.* **62**, 650-652.

Valentine, J.W. (1994) Late Precambrian bilaterians: Grades and clades. *Proceedings of the National Academy of Sciences of the United States of America* **91**, 6751-6757.

Victor, S. and Nayak, V.M. (1994) The tricuspid valve is bicuspid. *Journal of Heart Valve Disease* **3**, 27-36.

Victor, S. and Nayak, V.M. (1995) Bicuspid evolution of arterial and venous atrioventricular valves. *Journal of Heart Valve Disease* **4**, 78-87.

Wada, H. and Satoh, N. (1994) Details of the evolutionary history from invertebrates to vertebrates, as deduced from the sequences of 18S rDNA. *Proceedings of the National Academy of Sciences of the United States of America* **91**, 1801-1804.

Wells, M.J. (1983) Circulation in cephalopods. In: Saleuddin ASM and Wilbur KM, (Eds.) *The Mollusca, volume 5, part 2*, pp. 240-290. New York: Academic Press.

Wilbur, K.M. (1983) *The Mollusca*, New York: Academic Press.

Wilkes, A.J., inventor (1977) Method and apparatus for treating liquid. United Kingdom. 1: 482-527.

Williams, N. (1997) Biologists cut reductionist approach to size. *Science* **277**, 476-477.

Xiao, S., Zhang, Y. and Knoll, A.H. (1998) Three-dimensional preservation of algae and animal embryos in a Neoproterozoic phosphorite. *Nature* **391**, 553-558.

Yamauchi, A. (1980) Fine structure of the fish heart. In: Bourne GH, (Ed.) *Hearts and heart-like organs 1*, pp. 119-148. New York: Academic Press

Yang, G.Z., Kilner, P.J., Wood, N.B., Underwood, S.R., and Firmin, D.N. (1996) Computation of flow pressure fields from magnetic resonance velocity mapping. *Magnetic Resonance in Medicine* **36**, 520-526.

Yellin, E.L., Peskin, C., Yoran, C., Koenigsberg, M., Matsumoto, M., Laniado, S., McQueen, D., Shore, D. and Frater, R.W. (1981) Mechanisms of mitral valve motion during diastole. *Am. J Physiol* **241**, H389-400.

Young, J.Z. (1981) *The life of vertebrates*, pp 40, 82, 134-136, 348-249. 3rd edn. Oxford: Clarendon.